Using Positron Annihilation as a Method to Characterise Epoxy Networks with Regards to Chemical Resistance

Alec SD Shackleford

Thesis submitted in partial fulfillment for the degree of Doctor of Philosophy

The University of Sheffield,
Faculty of Engineering,
Department of Mechanical Engineering

2019

Acknowledgements

I'd like to firstly thank my supervisor Professor Patrick Fairclough, a man with a ridiculous brain. On several occasions, he will suggest an incredible way to do some research and I will be sat there, nodding and thinking "There is no way I can actually do what he is saying". Initially, he scared me and he still does at times but that's usually because he is the busiest man on the planet or his hungry. He's given me a great deal advice regarding research but also advice in general life with a view that your personal well being should always come first. That is something I have massively appreciated. Thank you for allowing me to do science and giving me the opportunity to go on some awesome trips, it has been a (stressful) pleasure.

Next, I'd like to thank my homies from the office and members of Ruud van Adium FC. Ste Knox, the hero, the legend, the founder of the club. We have worked side-by-side for a large portion of my PhD and I think I would have seriously struggled without your knowledge. You're also just a top top man who has been there when times get crappy. RJAM, The man who fell. Some people think you're grumpy but you're actually such a nice person who is potentially one of the funniest people I've met. Stupid dry humour and your reference game is on point. Thanks for all you're help throughout. Foxy, the big timer, club sponsor, massive head. A very slow man with vast knowledge of obscure sports and random crap. A true gent who is always up for a pint and helpful when it comes to work. So bad at FIFA but its great playing with you. Seabright, the man mountain. Probably the most competent man on the planet. Could probably solve global warming and I'd back him to fix a boiler. Always there to make you feel inferior without meaning to. I'll never forget to wish you a Happy Mothers Seabright. p.s TOTS TOTS TOTS. Legend has it that there was once a sixth member of the team called Browndog who disappeared long long ago. He had such such silky technique on the pitch, could spin a ping pong ball like no other and fuelled entirely by tea & custard creams. His legacy lives on...

I'm sure to miss some people but who's actually going to read my thesis anyway. But I'd like to thank Christine for her positivity and knowledge in many group meetings. Wendy who has helped me several times with 3D printing and sorting secret Santa out every year. Kurt, you're ridiculous but nice. Thanks to Andy Parnell for general advice and taking me abroad for experiments. Some great food and drink in Holland. Thanks to John McMillan, Rob Hanson, Babs, Prykey and Rod for support throughout my PhD. A special mention to Candice who is going to pay me to do some science for a bit and for general useful chats in addition to numerous muggings off.

Not to forget Morg. The absolute Garg who gave me a kick up the arse all those years ago. There's no doubt that without you intervening back in the day, my life would be going down a completely different route. Still fat though. Si gets a mention for coming up with Kevin Melon. Julian, thank you for being my weird German friend.

To my bro Rashid, although we aren't as close as I'd like any more, you were the first one to get me into space and science. This started with you and I hope I'm doing you proud. My sister Natalie, who's older but I feel like she's my little sister. You've always been supportive of what I'm doing and I'm so proud of what you've done. My Mum, thank you for being supportive in every way and believing in me even though you have no idea what I'm doing. You struggled and worked so hard whilst we were young and I hope I can make you proud. You always put your kids first no matter the consequence. I don't see you as much as I should but that will change. I love you lots and always.

Finally, the poet, the "real" doctor to be, A future Shackleford, a co-ruler of the Bread empire, Dami. I'm punching well above my weight in this relationship. You're better looking than me, smarter and I hate to admit it funnier than me. But there must be something wrong with you as I don't have ANY money and you've stuck around for quite a while now. As cringe as it sounds, the best thing to come out of this PhD is meeting you. You are perfect. The last few months of my PhD you really helped me through some tough times and I can't wait to spend the rest of my life with you.

Abstract

Free volume is a topic of great discussion in the field of polymers and whilst there are a number of techniques available to measure such a property, positron annihilation lifetime spectroscopy (PALS) is seen as the preferred choice. Free volume has been shown in several studies to highly influence properties concerning permeability and diffusion. The work presented in this research concerns chemically resistant protective coatings based on DGEBF epoxy resins and as such, free volume is an important property to study.

Positron beam techniques were utilised in order to measure free volume properties such as Doppler broadened annihilation energies using variable energy positron spectroscopy (VEPS). Whilst VEPS indicated free volume defects, mono energetic positron spectroscopy yields a direct measure of free volume. This latter technique was used to measure free volume as a function of implantation depth in epoxy networks.

In addition positron beam studies, a digital PALS system was successfully constructed for the study of free volume at the University of Sheffield. The system is based on fast plastic scintillators and a timing resolution of 470 $\pm$ 26 ps was achieved. This system was then ultimately used throughout this research.

Both PALS and positron beams studies showed that when similar chemistries are probed for free volume, only minimal changes are witness regardless of the preparation method. However, changes in chemistry see significant changes in free volume with PALS and MEPS showing similar free volume trends

A wide range of diffusion studies were performed on epoxy resins by means of methanol ingression. Studies concerning the production of epoxies were carried out in addition to varying the chemical formulations. Industrial applicability was considered with pigmentation and solvation of epoxies employed.

Ultimately, this research compared the glass transition temperature (T_g) to free volume and the effects on the diffusive nature of methanol in epoxy networks were observed. Overall findings showed that whilst both free volume and T_g are sensitive to changes in diffusion on many occasions, it is free volume which can detect changes in free volume between chemistries and due to strong correlations, indicate properties of diffusion.

Contents

List of Figures

List of Tables

1

Introduction

1.1 Background

1.1.1 Polymer coatings

Generally, we paint or coat objects either to decorate or to protect. The most widely used decorative paints are wall and artistic paints(i.e oil, acrylic, watercolour etc.). While wall paints provide basic protection, when referring to protective coatings this concerns more specialist coatings such as anti-corrosive or chemically resistant coatings. The research presented here, concerns the latter protective coating. When chemical cargoes are transported worldwide on chemical shipping tankers, the cargo is stored inside a number of individual cargo tanks. The interior walls are coated with a protective coating to prevent degradation of the container walls. A materials ability to resist this degradation due to aggressive chemicals is known as its chemical resistance. Chemically resistant coatings are generally polymer based and as such it is important to first consider the fundamentals of polymeric materials. Polymers, also referred to as macromolecules, are molecules, which comprise of several units of small molecules called monomers. If all the monomers are the same, then the polymer is referred to as a homopolymer (Figure 1.1.1). If there are more than one monomer then the polymer is called a copolymer[1]. To produce a polymer, a polymerisation reaction must take place. There are two mechanisms by which a polymer is formed; chain and step growth polymerisations.

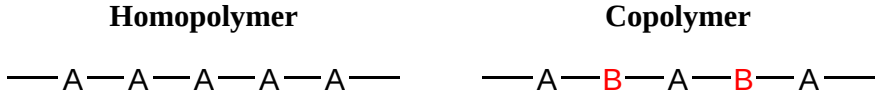

Figure 1.1.1: *The structure of a homopolymer compared to that of a copolymer. The letters A & B represent two different monomer units whilst solid lines are the bonds connecting the monomers.*

Polymerisation in which chain growth is achieved only by the reaction of a monomer with a reactive end group on a polymer chain is known as chain-growth polymerisation. Generally, an initiator is reacted with the monomer to begin chain growth. At low monomer conversion a high degree of polymerisation is achieved and the monomer is reacted at a constant, steady rate. After the initial chain growth, polymer chains form rapidly by a succession of molecule addition to the functional chain end. Step growth polymerisations refers to chain growth in a step-wise manner due to reactions between any two molecular components. In contrast to chain growth, the monomer is heavily consumed in the initial stages of reaction with the degree of polymerisation increasing steadily throughout the reaction. Chain growth continues throughout as the conversion of functional groups to chain links increases. Table 1.1 depicts the differences bewteen step and chain growth.[2]

Table 1.1: *Polymer chain growth for chain and step polymerisations where I is an initiator and O refers to monomer units.*

Oligomer	Chain polymerisation	Step polymerisation
Dimer	I + O ⟶ I-O I-O + O ⟶ I-O-O	O + O ⟶ O-O
Trimer	I-O-O + O ⟶ I-O-O-O	O-O + O ⟶ O-O-O
Tetramer	I-O-O-O + O ⟶ I-O-O-O-O	O-O-O + O ⟶ O-O-O-O O-O + O-O ⟶ O-O-O-O
Pentamer	I-O-O-O-O + O ⟶ I-O-O-O-O-O	O-O-O-O + O ⟶ O-O-O-O-O O-O + O-O-O ⟶ O-O-O-O-O

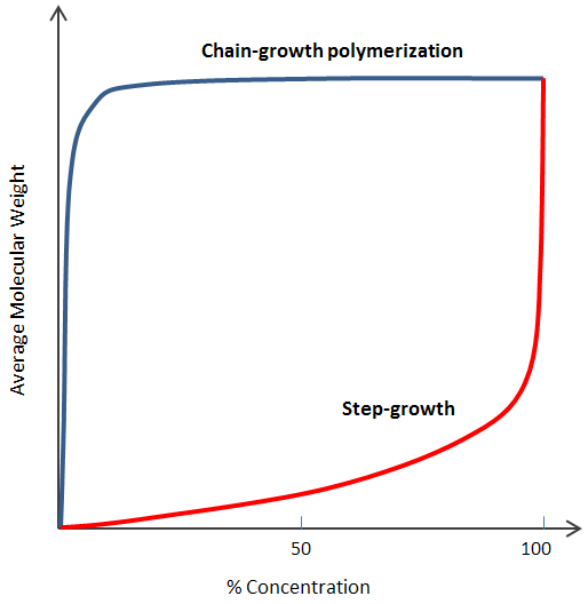

Figure 1.1.2: *The comparison of molecular weight evolution for step and chain growth polymerisations. Image obtained from polymerdatabase.com*

1.1.2 Thermoplastics and thermosets

Polymers can be classified into two categories; thermoplastics and thermosets. These categories are based on a polymeric materials response to temperature variation. Monomers which produce branched and linear polymers are generally classified as thermoplastics. Above certain temperatures, the polymer will break up into small molecules, which causes the material to flow. This is known as the melt temperature and occurs due to weak Van der Waals forces binding the monomers. On cooling, the smaller molecules will solidify and retains its previous mechanical properties. This behaviour makes thermoplastics ideal for many manufacturing processes including; extrusions, post-die processing, forming and injection moulding.[3] Some common thermoplastics are high & low density polyethylene (HDPE & LDPE), poly-amides and polyvinyl-chloride (PVC). Monomers which produce crosslinking structures are generally thermosets. Unlike thermosets, they do not flow at any temperature. However, at high temperatures, the polymer will break down by disintegration. This is because the monomers form one large molecular structure by means of chemical reaction. As such, this structure effectively has infinite molecular weight. In the initial stages of polymerisation , the structure is in a fluid state called the "sol" phase. As the reaction progresses, the monomers functional groups are converted. At a certain conversion level, gelation occurs i.e. a large structure which moves through the sol forms. The point of conversion at which this structure forms can be roughly calculated using equation 1.1.1.[4,5]

$$P_{gel} = \left[\frac{m_a f_a}{m_e f_e (f_a - 1)(f_e - 1)}\right]^{1/2} \tag{1.1.1}$$

Where m is the number of moles, f is the functionality. In this case, subscripts a and e refer to amine and epoxy components respectively. The functionality is the number of times which a molecule can react. This model assumes that the reactivity of each functional group is equal, all possible reactions between components occur and finally there are no intramolecular interactions. As the reaction progresses, more monomer is converted until the sol fraction diminishes. At this point a final crosslinked network is produced. Thermosets are used in a wide range of applications due to their strong mechanical properties and ability to resist chemical degradation. An example of a thermoset is produced by the reaction of an epoxy and an amine.[6]

1.1.3 Epoxy - amine reaction

Epoxy resins are polymers, which contain an epoxide group, (Figure 1.1.3). This epoxy group is the reactive component of the resin and opens upon reaction. Even though this product no longer contains an epoxy group, it is still referred to as an epoxy resin.[7]

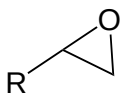

Figure 1.1.3: *The chemical structure of an epoxy functional group. R refers to the rest of the molecule which the epoxy is attached to.*

When an epoxy resin is combined with a hardener, a crosslinked polymer will eventually be produced. A crosslinked polymer is a network of polymer chains, bonded together at sites of reactive functional groups. They have infinite continuation in three possible directions.[6] The graphic shown (Figure 1.1.4) depicts the difference between linear, branched and crosslinked polymers where the red dots represent junctions at which individual polymers have combined.

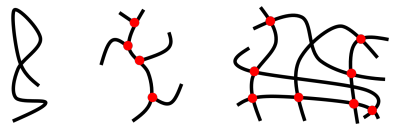

Figure 1.1.4: *Graphical representation linear, branched and crosslinked polymer networks. The red dots represent fixed reaction junctions.*

The reaction begins with the primary amine group reacting with an epoxide group. This produces a secondary amine group which is also free to react with other epoxide groups in the mixture (Figure 1.1.5). The ring opening mechanism also results in hydroxyl groups which can cause auto-catalysis which causes the rate of reaction to increase. As the reaction progresses and the number of crosslinks increases, the molecular weight and therefore the viscosity increases. This causes a reduction in mobility and hence the rate at which crosslinks are produced decreases. Eventually, the mobility is negligible and this gives rise to dangling chain ends which do not contribute to the mechanical properties of the network. It is suggested that at these ends, free space occurs called free volume due to the constant motion of the chain end.[2,8]

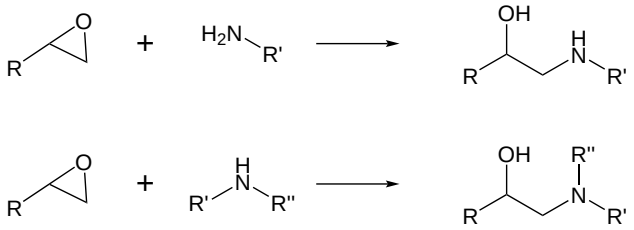

Figure 1.1.5: *The reaction mechanism for an epoxy amine reaction. The bi-functionality results in a secondary and tertiary amine forming. Eventually, a single molecule consisting of connected tertiary amines is produced.*

1.2 Free volume

This section will introduce a fundamental property present in polymeric materials called free volume. The factors which affect free volume and methods of to measure it will be discussed.

1.2.1 Introduction

Origins

The works of Van der Waals and then later Fowler and Glasstone *et al* are probably account for the origin of free volume theory.[9–11] A liquid is imagined to be a group of molecules moving within a confined space. Other molecules of liquid surround the molecular group.

The molecules occupy an intrinsic volume, V_O and the space needed for molecular group thermal motion is the free volume, FV. For a liquid, the total specific volume and fractional free volume are calculated by equations 1.2.1 and 1.2.2.[12] These are the most common ways of simply calculating free volume properties. V_O is equal to the reciprocal of the polymer density ($1/\rho$ in g/cm^3).

$$V = V_O + FV \tag{1.2.1}$$

$$FFV = \frac{FV}{V} = 1 - \frac{V_O}{V} \tag{1.2.2}$$

Basic definition

Free volume in polymers can be thought of as defects, on a nanosacale. It occurs in polymers, due to the random arrangement of polymer chains during polymerisation. This random arrangement produces free "gaps" throughout the polymer matrix.[13] Free volume has been shown to have a great affect on a molecules ability to diffuse through a material.[14] If the van der Waals volume of the diffusing molecule is similar to the average free volume of the material, then its mobility will become hindered.[15,16]

1.2.2 Properties affecting free volume

The glass transition temperature

The glass transition temperature (T_g) is defined as the temperature at which a polymer transitions from a rubbery to a glass and more brittle state.[17] Studies have shown[18,19] free volume increases when a polymer is above it glass transition temperature. In particular, Duda *et al*[18] showed the variation in free volume with increasing temperature for polystyrene (PS)/Toluene mixtures. It was shown that as the temperature increases, FV gradually increases. In pure PS, the FV increases rapidly above its glass transition temperature whereas a mixture of toluene and PS exhibited two stages in which the FV increase rate changed. The first stage corresponded to the T_g of the combined mixture and the second stage occurred at the T_g for pure PS. Their free volume measurements were based on thermal expansion coefficients of the polymer and concluded that this coefficient is history dependant. This suggest that the same material may exhibit differing thermal expansion coefficients and therefore differing free volumes. A study of gas separating polymer membranes by Recio *et al*[20], showed an increase in segmental mobility in terms of T_g, corresponded to an increase in inter-segmental spacing with regards to free volume.

Factors affecting the measured T_g

The measured Tg can be affects by a number of factors which include Humidity/moisture content, heating rates, sample thickness and the addition of plasticisers to name a few as shown by the studies of Drake, Yang and Yong et al in addition to the review by Jadhav et al.[21–24]

An increasing amount of moisture has been shown to cause the T_g to decrease considerably.[22,25–27] In particular the study by Yang *et al*[22] focussed on how moisture effects the

T_g in polyurethanes filled with nano-carbon powder. It was found that the absorption of moisture causes a reduction in the T_g until saturation occurs due to water interacting with polymer chains which leads to improved mobility. They also noted how the reduction in T_g can be reversed by the removal of moisture by heating cycles due to the physical nature of the process.

Patial *et al*[23,28], used DSC and DMA respectively to study the effects of heating rate on the measured T_g. Both showed that that increasing the heating rate leads to a higher measured T_g. Furthermore, Yong *et al*[23] showed that as the rate of heating increased during DMA measurements, the measured glass transition temperature increased. They also showed how this effect is more prominent when the sample is thicker. For the thickest sample (3.5 mm), a high heating rate resulted in a much higher measured T_g than the thinnest (0.25 mm).

A study by Honary *et al*[29] concerned the addition of the plasticiser hydroxypropylmethylcellulose (HPMC) to polyethlene glycol (PEG). Increasing the amount of plasticiser caused the Tg to decrease. The plasticiser increases the distance between polymer chains which increases the free volume and in turn increases the polymer mobility[24].

Thermal history

A number of papers[30–32] have shown that the thermal history can affect the free volume of polymers. A study by Cheng and Sun[30] showed that the thermal history affects the free volume measured using PALS in semi-crystalline membranes. Samples were melted at 170 °C before being compression moulded and cooled by three different methods: 1) Rapid cooling – quenched to 0 °C in an ice box; 2) step cooling – cooled to 120 °C in a period of 30 minutes and then cooled to ambient in 10 minutes; and 3) slow cooling – cooled to ambient temperature at an average rate of 0.3 °C min^{-1}. Each sample was then tested using PALS over a temperature range of 25 – 90 °C. The fractional free volume (FFV) was shown to increase with PALS measurement temperature. Rapidly cooling samples generally resulted in the largest FFV whilst slow cooling samples had the lowest. The high level of fractional free volume when cooled rapidly can be explained due to trapping of excess free volume. Over time, this would decrease due to physical ageing.[33] Figure 1.2.1 illustrates the kinetic effects and the process of physical ageing[16]

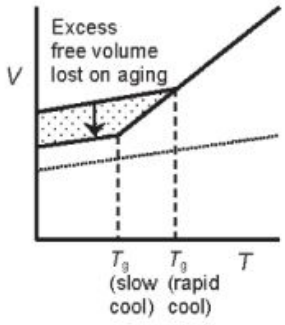

Figure 1.2.1: *Figure reproduced from the work of Budd et al[16]. An illustration on kinetic effects and the process of physical aging in a polymer.*

Crosslink density

The crosslink density is defined as the density of chains or segments that connect two infinite parts of the polymer network[34]. As a crosslinking reaction progresses, the number of crosslinks increases. A higher crosslink density will result in a stronger polymer network which corresponds to an increase in the glass transition temperature[35–39] and hence why the T_g is a good indication of reaction conversion.

Pressure

Studies have shown[40,41], increasing pressure will cause a decrease in free volume. Dlubek *et al*[41] showed this by performing positron annihilation lifetime spectroscopy (PALS) under pressure on a number of polymer materials. Free volume was found to decrease in an exponential manner with increasing pressure. As PALS has been mentioned, it is worth briefly introducing this measurement technique along with other measurement types.

1.2.3 Measuring free volume

Positron annihilation lifetime spectroscopy

Positron annihilation lifetime spectroscopy (PALS) is the most used technique for determining free volume properties[42–47] This technique utilises the annihilation event between a positron and an electron inside a free volume void. Effectively, the time between positron implantation and annihilation with an electron is measured by fast timing detection[48,49]. The positron's lifetime is related to the size of free volume defects in matter[50,51]. A detailed overview of this technique is given in Section 1.4. and examples of the measurement are found in Chapter 4 in which the construction of the instrument used is shown.

Xenon NMR Spectroscopy

The shift in Xe NMR spectroscopy is highly sensitive the free volume in materials where xenon gas is absorbed. Essentially a large free volume element (FVE), the smaller the shift Xe chemical shift relative to the chemical shift characteristic of the gas phase[52].

Inverse gas chromatography

This technique compares the rate at which carrier gases (commonly helium, argon and nitrogen) pass through a sample of interest which is attached to a solid porous substrate. The retention times of the gas through the materials can can yield information on various properties such as free volume.[52,53]. Results using IGC are in fairly good agreement with PALS as shown in Figure 1.2.2

Lipson *et al*[54] brought attention to the many definitions of free volume and how they are confusingly interchanged throughout the literature. In the research presented here, free volume is determined using the Tao-Eldrup model[50,51] which involves positron annihilation theory and voids are considered spherical. This model is detailed in 1.4.4. Before moving on to positron annihilation, it is a good idea to introduce diffusion as this is a key focus of the work presented in this thesis.

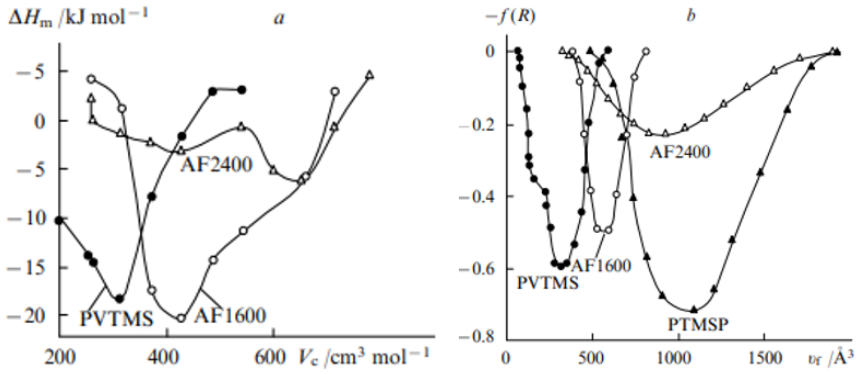

Figure 1.2.2: *Free volume results compared between (a) inverse gas chromatography and (b) positron annihilation lifetime spectroscopy. This figure was reproduced from the publication by Yampolskii et al*[52]*.*

1.3 Diffusion

1.3.1 Introduction

As this research is focussed on diffusion in polymer networks and how it relates to free volume, some fundamental concepts of diffusion will be introduced. The properties which affect diffusion will be discussed and some experimental techniques will be described.

1.3.2 Fickian diffusion

Diffusion is the movement of particles from a region of high concentration to regions of low concentration.[55] Where research concerns diffusion, Fick's laws of diffusion are considered (equations 1.3.1 and 1.3.2).

$$J = -D\frac{\delta c}{\delta x} \tag{1.3.1}$$

$$\frac{\delta c}{\delta t} = \frac{\delta J}{\delta x} \tag{1.3.2}$$

In other words, the flux (J) of matter through a system is proportional to the concentration (c) gradient measured normal to the system with a known proportionality constant called the diffusion coefficient (D). The flux measures the amount of matter that will flow through a unit area during a period of time. The diffusion coefficient or diffusivity is defined as the magnitude of flux through a surface per unit concentration gradient. The diffusion coefficient will increase with increasing temperature as shown in other studies[56–58]. Fick's second law (equation 1.3.2) relates the concentration at a time, (t) to the flux relative to position. This model is an example of positive diffusion but negative diffusion can also occur. In this instance the particles move from regions of low concentrations to high concentrations.[59] Spinodal decomposition is an example where negative diffusion occurs.[60]

1.3.3 Solvent diffusion in polymers

A key area of study is diffusion in polymers and in particular, the ability to prevent the ingression of solvents. The diffusion of small molecules in polymers is a complex process which is not perfectly described by any single theory[61]. This is due to the fact that on ingression, polymer chains will rearrange and swelling can occur. This can ultimately cause the T_g to decrease and polymers become rubbery and leads to large parts of the polymer to rearrange through chain rotations, translations and vibrations.[61] Whilst polymers are in a glass like state (below T_g), ingression is hindered because the polymer will be hard and brittle. In this state free volume is smaller in comparison to the rubbery phase.

Figure 1.3.1 shows the mass uptake profiles for four types of diffusion which are; (a)classical Fickian, (b) sigmoidal, (c) two-step and (d) Case II. These terms are generally used to describe absorption which is (a) linear with the square root of time, (b) has an S-shape with the square root of time, (c) is initially linear before an S-shape profile occurs or (d) is linear with linear time.[62]

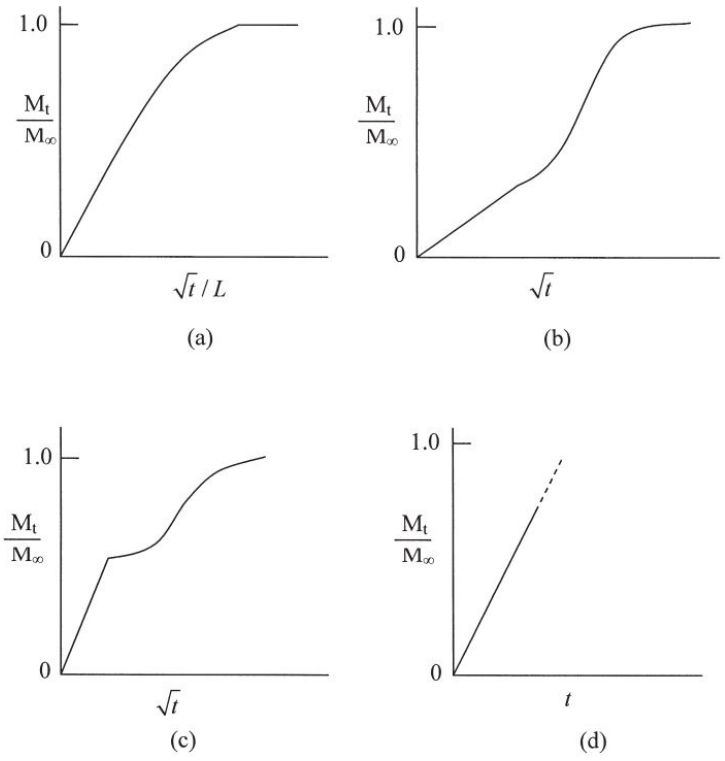

Figure 1.3.1: *Four different types of diffusion: (a) Fickian, (b) sigmoidal, (c) two-step and (d) case II.*[63]

Crank's computations showed that an exponentially increasing surface concentration gives rise to sigmoidal diffusion profiles[64] whilst other researchers showed this behaviour experimentally.[65–67] Rossi *et al* determined that Fick's laws can still be used as a simple diffusion model for sigmoidal diffusion.[61,68–70] Two-step occurs when a system consisting of two regimes is present such as in a polymer blend. The heterogeneous structure provides regions with differing accessibility for penetrants.[71] Case II is an interesting scenario, as the typical decrease in rate of diffusion is not observed. This mechanism is dependent on the mechanical response of the polymer due to swelling of the penetrant. Plasticisation of the polymer due to sorption of the penetrant causes a decrease in relaxation times which causes a glassy polymer to behave in a rubbery manner which in turn drives diffusion.[63,72,73]

1.3.4 Properties affecting diffusion

Temperature

Increasing the temperature of the system containing a solvent and polymer can result in a large increase in diffusion. This was demonstrated by Billing *et al*[58] in which the study of MEK passing through viton/chlorobutyl rubber and also the diffusion of methylene chloride through a Teflon/Nomex composite. Hajiagha *et al* also showed the effects of increasing temperature for water passing through TFX. Increasing the temperature to 40°C saw a slight increase in the rates of diffusion (i.e. the diffusion coefficient) and when exceeding the glass transition temperature, diffusion was greatly enhanced.[57]

Solubility

In terms of diffusion, the solubility concerns the miscibility of the polymer network with the penetrant. Generally, this is governed by the polarity similarities of the ingressor and the polymer network . Solubility can be quantified in terms of solubility parameters such as Hansen solubility parameters. These are physiochemical parameters used to estimate the type of interactive forces responsible for the compatibility between materials.[74,75] It fundamentally assumes that the cohesive energy can be divided into three distinct components which concern molecular interactions. The first component is the atomic dispersion, the second is the molecular dipole interactions and the third is hydrogen bonding. The solubility can similarly be divided into three solubility parameters, one for each component. The total cohesive energy(E) and solubility(δ_T^2) are shown in Equations 1.3.3 and 1.3.4 respectively. Where E_{d-h} and δ_{d-h} correspond to the individual components of cohesive energy and solubility respectively.[74,75]

$$E = E_d + E_p + E_h \tag{1.3.3}$$

$$\delta_T^2 = \delta_d^2 + \delta_p^2 + \delta_h^2 \tag{1.3.4}$$

When materials have similar solubility parameters, mixing is favourable and diffusion enhanced. Whilst' solubility is mainly governed by polarity, it will increase when the temperature of the environment increases. Another key factor which affects diffusion is the free volume along with molecular size.

Free volume and molecular size

The size of free volume in polymers has be shown in several instances to enhance the diffusion in polymers[15,20]. Recio *et al* showed an increase the diffusion of gas (except in CO_2) which corresponded to an increase in fractional free volume[20]. Jackson *et al* also showed that as the size of the ingressing molecule approaches the size of the free volume, the diffusion will become hindered.[15]

1.3.5 Measuring diffusion

Solvent ingression

Solvent uptake is a simple way of obtaining information relevant to a materials chemical performance. A traditional gravimetric technique determines solvent uptake over time for a substance of interest. Immersing the sample in a liquid/gas for a long period (days to years) results in solvent uptake. Recording the mass of the sample as a function of time and comparing to the dry sample mass, the solvent percentage uptake is determined. Shen and Springer's[76] analytical work led to the derivation of a simple model for mass uptake at short immersion times.

$$\frac{M_t}{M_\infty} = \frac{4}{L}\sqrt{\frac{Dt}{\pi}} \tag{1.3.5}$$

Where (M_t), is the mass uptake at a time (t), M_∞ is the ultimate uptake, (L) is the sample thickness and (D) is the diffusion coefficient. The ultimate uptake is the mass at which no further ingression occurs. The diffusion coefficient has two values, one concerning desorption $(D_{EGR})$and the other absorption (D_{ING}). Desorption describes the rate at which solvent is released from the material whereas absorption concerns rate of solvent ingression. Figure 1.3.2 is an example of how ingression and egression curves might appear. At short times, a linear fit is applied and the gradient is used to determine (D) in Equation 1.3.5.

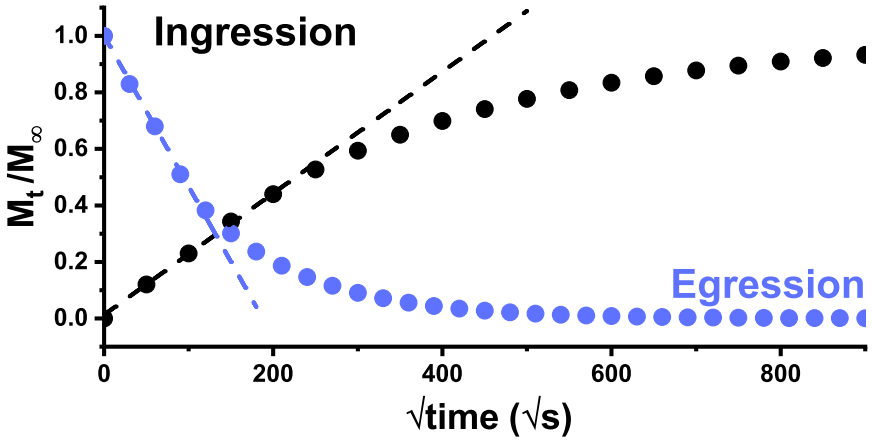

Figure 1.3.2: *An example of how absorption and desorption curves appear. At short times a linear fit is used to determine diffusion coefficients. This graph was produced in origin and does not represent any experimental data.*

Ultimately, diffusion in polymers has a number of contributing factors to its behaviour which also affect one another. Changes in crosslink density corresponds to changes in T_g which in turn affects the ability to prevent ingression. On ingression, this leads to plastisication which reduces T_g and promotes ingression. Additionally, studies at temperatures above T_g accelerate the rate of diffusion and so on. Experimentation throughout the work will involve traditional gravimetric studies, the glass transition temperature and free volume. The latter being the fundamental measurement which will be determined using positron annihilation lifetime spectroscopy (PALS). As such, the theory of positron annihilation techniques must be presented.

1.4 Positron annihilation

This sections covers the fundamental theory regarding positron annihilation studies. Background theory and experimental techniques will be introduced followed by an assessment of literature.

1.4.1 Introduction

Discovery of the positron

The positron is an elementary particle,which is the anti-matter counterpart to the electron; it has an intrinsic spin of $\frac{1}{2}$ and is therefore a fermion. Properties such as the mass, magnitude of charge and gyromagnetic ratio are equivalent to that of an electron however, the positron is positively charged, hence the name.[77] Anderson discovered it in 1933 whilst capturing images of cosmic-ray tracks in a vertical Wilson chamber. Whilst capturing these images, Dr. Anderson noticed a strange curvature to some of the tracks (Figure 1.4.1). He deduced that this could only be characteristic of a particle which has a positive charge with mass equal to that of an electron[78]. It was later confirmed the following year by Blackett and Occialina[79].

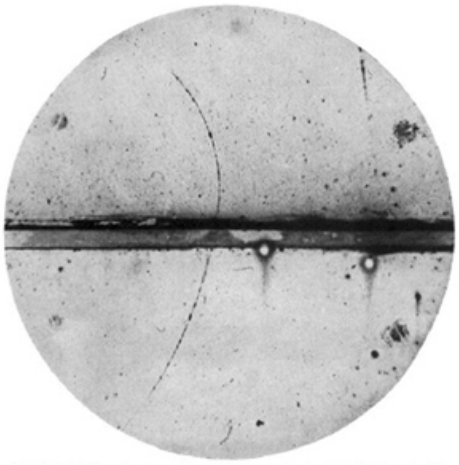

Figure 1.4.1: *Anderson's cloud chamber picture of cosmic radiation from 1932 showing the existence of the "anti-electron" for the first time.[78] (Copyright permission granted by the American Physical Society 2019).*

Positronium

When a positron interacts with an electron, a quasi-stable bound system called Positronium (Ps) may form (Figure 1.4.2). It is similar to a hydrogen atom but with a much lower mass due to the substitution of a proton for a positron. This results in a binding energy of 6.8 eV[80]. Its existence was proposed in 1934[81] and given the name positronium in 1945[82]. Several years later, Ps was experimentally discovered in 1951.[83] It can exist in two spin states; one where S = 1 and another where S = 0[84]. The singlet state (S = 0) involves the spins of the electron and positron which are anti-parallel; this state is called parapositronium(pPs). The triplet state involves spins which are parallel; this is called orthopositronium(oPs)[50]. Positrons are present in cosmic radiation as Anderson discovered but positrons can be produced artificially and utilised in a number of ways.

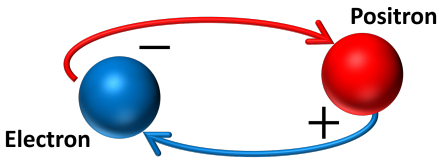

Figure 1.4.2: *Depiction of a positronium atom. The electron and positron orbit about their combined centre of mass before an annihilation event occurs.*

1.4.2 Positron sources

Positrons (e^+) are produced in the form of positron beams, or from point sources. Positron beams are usually the product bombarding a target, such as graphite with protons or deuteron. Positrons are emitted as a by-product and are guided using magnetic fields to a sample target chamber. Point sources emit positrons radially from the centre of the source.[48,85,86] Radioisotopes are generally utilised in positron studies and the majority produce positrons as a by product of a decaying element.[15,87–89]. Some commonly used radioisotopes are listed in Table 4.1.

Table 1.2: *Half-life decays of commonly used isotopes for positron annihilation studies.*[90]

Isotope	Half-Life
^{22}Na	2.6 years
^{68}Ge	271 days
^{58}Co	70.86 days
^{64}Cu	12.7 hours

Sodium-22 (^{22}Na) is normally the preferred choice as it is easy to manufacture in the laboratory and economically favourable. ^{22}Na comes in the form of salt solutions such as sodium chloride (NaCl) and sodium carbonate ($NaCO_3$), which allows for easy handling capabilities.[91] In the case of ^{22}Na, it decays to form Neon (Ne) alongside a positron (Figure 1.4.3).

Decay Type	Reaction Mechanism
Positron Decay	$^{22}Na \rightarrow {}^{22*}Ne + \beta^+ + \nu_e$ $\searrow$ $^{22}Ne + \gamma_{1.27\ MeV}$
Instantaneous Positron Decay	$^{22}Na \rightarrow {}^{22}Ne + \beta^+ + \nu_e + \gamma_{HE}$
Electron Capture	$^{22}Na + e^- \rightarrow {}^{22*}Ne + \nu_e + \gamma_{1.27\ MeV}$

Figure 1.4.3: *The three reaction mechanisms of sodium-22 (^{22}Na) decaying to Neon-22 (^{22}Ne). Two of which result in the emission of a positron.*

The most probable decay is positron decay, which occurs 90.4% of the time. The emission of a positron and electron neutrino leaves an unstable neon atom. Rapidly (3.7 ps), Ne stabilizes by releasing a gamma photon of approximately 1.27 MeV. It is possible, although unlikely (0.1% of the time), that the Na atom will directly decay to Ne releasing a high-energy gamma photon in the process. Finally, electron capture occurs 9.5% of the time. During the decay, an electron is picked up by the Na nucleus and an electron neutrino is emitted. A characteristic gamma photon of 1.27 MeV is produced.

1.4.3 Implantation and annihilation

When a positron is implanted into a microporous material, it quickly reaches a thermalised state due to energy loss during inelastic collisions with molecules[43]. When sufficient energy is lost, the positron will become trapped due to repulsion of nuclei and subsequently annihilate with a localized electron. During thermalisation, ionisation of the media will produce secondary electrons. These electrons can then form the bound state atom positronium of either singlet or triplet state (pPs or oPs)[92]. The rate of annihilation is dependent on the electron density of the local region. Free annihilation between positrons and electrons typically have lifetimes of between 0.1 – 0.5 ns. In a vacuum, pPs and oPs have lifetimes of 0.125 ns and 142 ns respectively. In matter, the pPs lifetime remains relatively unchanged due to self-annihilation. oPs on the other hand does not experience self-annihilation. Instead, it annihilates through collisions in the local environment, which drastically reduces the lifetime (1-5 ns). This mechanism is referred to as pick-off annihilation and the reduction in lifetime is dependent on the void size in which the oPs resides in.[93]Figure 1.4.4 is a representation of these three annihilation types. The annihilation event predominantly translates the momentum of the annihilating pair into two gamma photons travelling in opposite directions with energies of 0.511 MeV. Positrons and Ps atoms will 'seek out' voids in the material as they are more stable in the vacuum than the bulk. This is due to the positive nuclei repelling the positively charged positron or the highly polarisable positronium.[94]

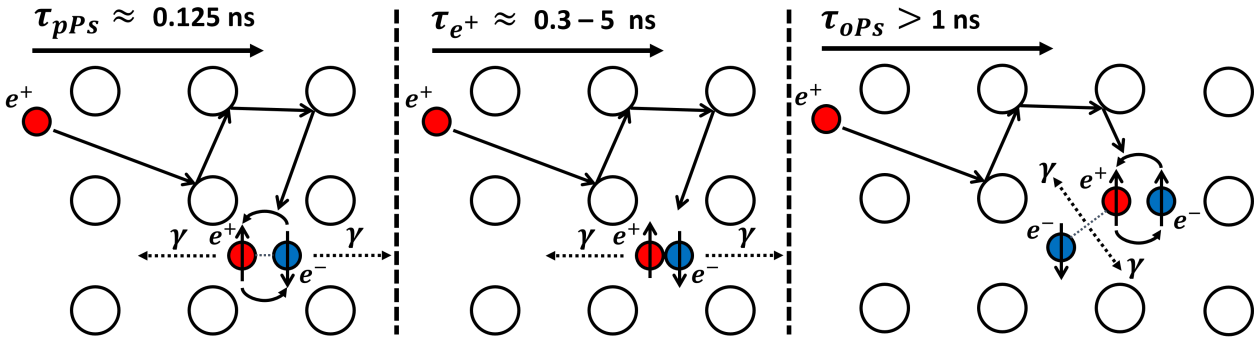

Figure 1.4.4: *The three annihilation types which can occur when a positron is implanted into a material. oPs annihilation occurs inside free volume voids.*

The oPs annihilation component concerns annihilations which occur in free volume voids. The size of the voids can be determined using the Tao-Eldrup model.

1.4.4 Tao-Eldrup bubble model

The Tao-Eldrup model is a quantum mechanical model which relates the lifetime of oPs to the size of the void in which it annihilates.[50,51] The voids are assumed spherical and as such the model considers oPs to become trapped inside an infinite potential well with spherical symmetry. In order for oPs to interact with the surrounding electrons and annihilate, the wave-function of oPs and the electrons must overlap (Figure 1.4.5).

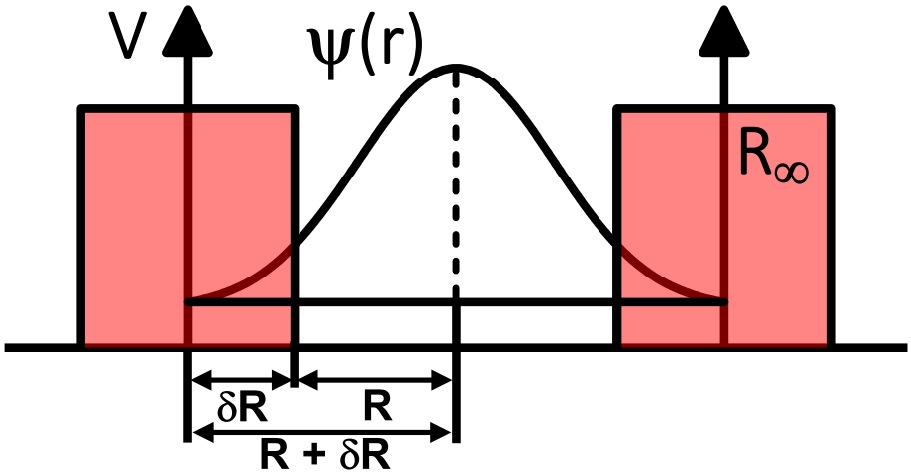

Figure 1.4.5: *The wave function of positronium in a infinitely deep spherical potential well. δR is the electron layer thickness and R is the free volume radius of the void in which the annihilation has occurred.*

The overlapping electron layer has a thickness δR. The radius in which the oPs atom can probe is R. This is the free volume radius. The rate of annihilation of oPs , τ_{oPs} is proportional to the overlapping integral of the oPs and electron layer wave-functions. The model assumes the electron density at this overlapping layer is the same as the bulk of the material. This means the annihilation rate in the layer and the bulk are also proportional. With these assumptions in mind, the relation for the annihilation rate and the free volume radius is derived (Equations 1.4.1 - 1.4.3). The value of δR is generally accepted to be 1.66 nm based on experimental data and the value for λ_{Bulk} is set to 2 ns^{-1} based on the average rates of decay of oPs and pPs.[50 ,51]

$$\psi(0 \leq r \leq R_\infty) = \frac{sin\left(\frac{\pi r}{R_\infty}\right)}{\sqrt{2\pi R_\infty r}}, \qquad \psi(r \geq R_\infty) = 0 \tag{1.4.1}$$

$$\lambda_{oPs} = \lambda_{Bulk} \int_R^{R_\infty} \left|\psi(r)\right|^2 4\pi R^2 dr \tag{1.4.2}$$

$$\frac{1}{\tau_{oPs}} = 2\left[1 - \frac{R}{R+1.66} + \frac{1}{2\pi} sin\left(\frac{2\pi R}{R+1.66}\right)\right] \tag{1.4.3}$$

The relationship is shown in Figure 1.4.6 for the range relevant for the epoxy resins studied in this research. Generally, a larger free volume results in a longer lifetime. This relationship diminishes at much higher void sizes (>100 nm).

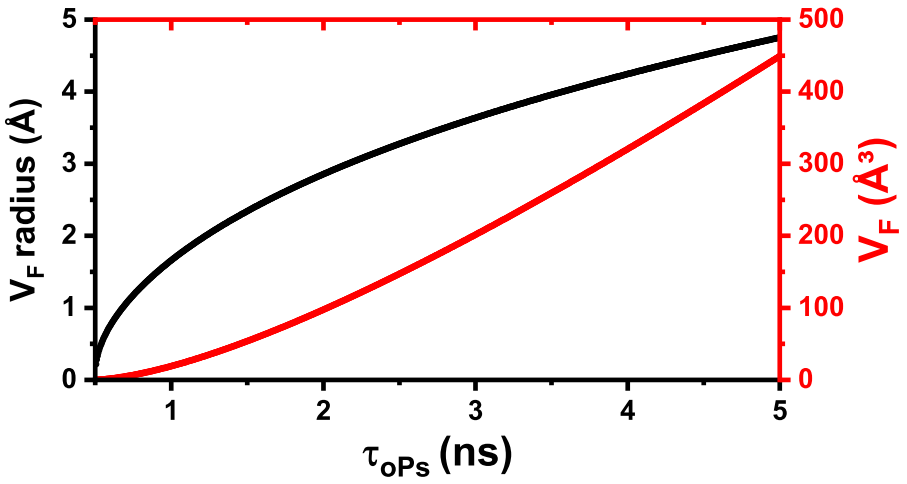

Figure 1.4.6: *The relationship between average oPs lifetime, free volume radius and free volume. An increase in lifetime results in a higher free volume although this is not a linear relationship.*

1.5 Annihilation techniques

This section will describe the positron annihilation techniques which are used in this research. The first concerns free volume measurements by positron annihilation lifetime spectroscopy (PALS), the second is based on Doppler broadening spectroscopy (DBS) which measures annihilation energies and finally mono energetic positron spectroscopy (MEPS) which is a combination of both lifetime and energy measurements.

1.5.1 Positron annihilation lifetime spectroscopy

Positron annihilation lifetime spectroscopy (PALS) utilizes the "birth" gamma photon, produced in the decay mechanism of ^{22}Na to ^{22}Ne, and the subsequent "annihilation" gamma photon, which is a consequence of an electron-positron interaction. As we know, the ^{22}Na source emits a positron effectively simultaneously ($\approx$ 3ps delay) with a gamma photon of 1.27 MeV. On implantation, the positron undergoes thermalisation through inelastic collisions. During thermalisation, the positron may form orthopositronium which can become trapped inside a free volume void. The positron in the oPs atom can interact with a valence electron with an opposing spin and annihilate in the form of two gamma photons of 0.511 MeV in opposite directions (Figure 1.5.1). By measuring the time between the emission photon and either of the annihilation photons, the positron lifetime is determined.[93,95,96]

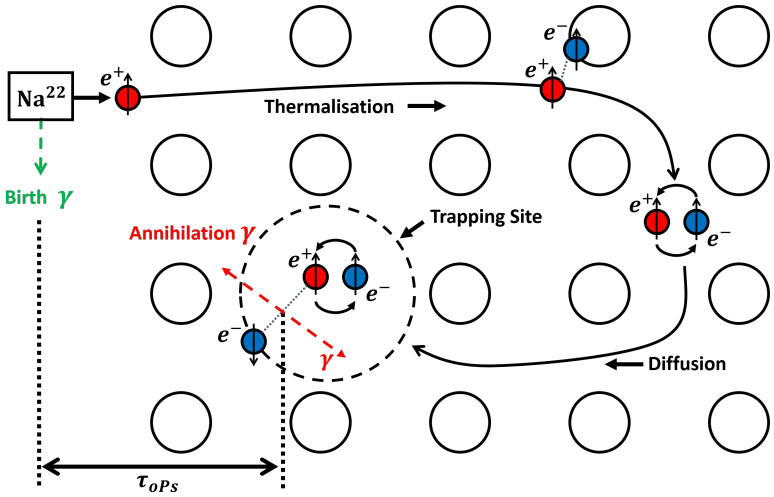

Figure 1.5.1: *After implantation, the positron is repelled by positive nuclei and can become trapped in regions of free volume. An annihilation event occurs in the form of two gamma photons as a result of the interaction of an electron and positron.*

The reason the gamma photons produced have an energy of 0.511 MeV can be shown using Einstein's famous equation from his theory of special relativity (Equation 1.5.1);

$$\begin{aligned} E &= mc^2 \\ &= (9.11 \times 10^{-31} kg)(3.00 \times 10^{8} ms^{-1})^2 \\ &= 8.14 \times 10^{-14} J \approx 511 keV \end{aligned} \tag{1.5.1}$$

To measure the positrons lifetime, two gamma detectors are implemented. Figure 1.5.2 shows the equipment configuration used for this research. A detailed description of the individual components can be found in Section 4.2.

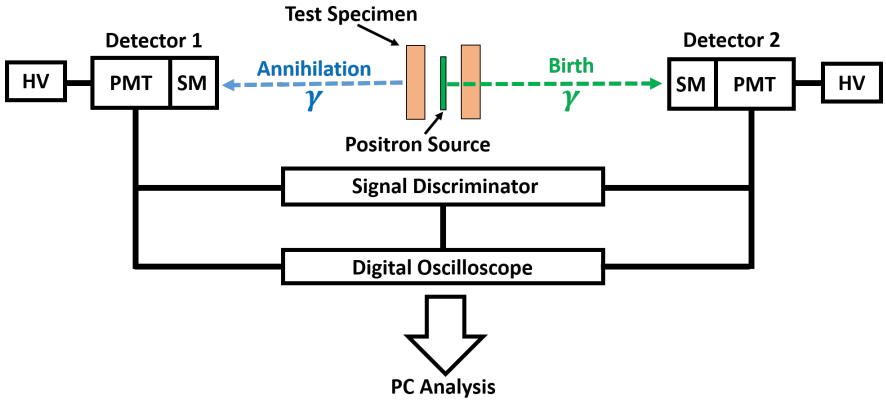

Figure 1.5.2: *The setup of a digital PALS system. Consisting of; photomultiplier tubes (PMTs) powered by high voltage power supplies (HV); scintillation materials (SM) coupled to PMTs; A positron source, sandwiched between two test sample; a discriminator unit and; a digital oscilloscope which transfers relevant signals to a PC for analysis.*

Effectively, the photomultiplier tube and scintillation material combine to function as a gamma radiation detector. One detector will detect the initial gamma photon and transmit an electrical pulse to the coincidence unit. This electrical pulse indicates the start time. The other detector will detect either of the corresponding annihilation photons and transmit an electrical signal to the coincidence unit. This pulse indicates the stop time. The time between these two values is the positron lifetime (an example measurement can be found in Section 4.3.2. Repeating this lifetime measurement results in a positron lifetime distribution (example in Figure 1.5.3). It is necessary to record at least one million measurements to obtain reasonable statistics. Each spectrum consists of a number of exponential decay components corresponding to each annihilation type.

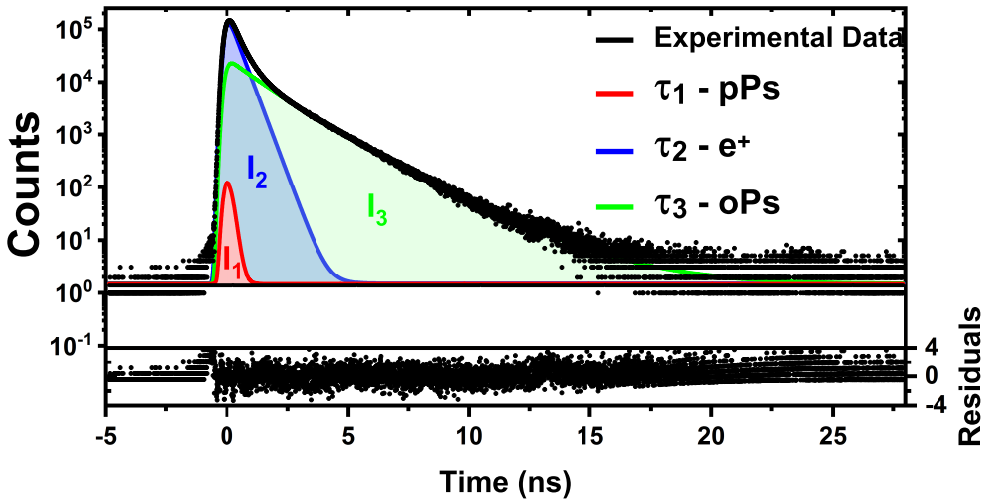

Figure 1.5.3: *PALS spectrum for a polymeric material. The experimental data is fitted using an exponential model containing three components corresponding to each annihilation type. (This data was obtained during a beam line experiment at HZDR, Dresden. Further details of this experiment is found in Chapter 3).*

The distribution can be described by Equation 1.5.2. Where A,B and C are y intercepts at a time, $t = 0$ and correspond to the annihilations due to pPs, free e^+ and oPs respectively. λ_i is the annihilation rate with respect to the three annihilation components.

$$y(t) = Ae^{-(\lambda_1 t)} + Be^{-(\lambda_2 t)} + Ce^{-(\lambda_3 t)} \tag{1.5.2}$$

The third exponential decay component corresponds to the formation of oPs inside a free volume void. The reciprocal of the annihilation rate λ_3 gives the average lifetime τ_3 of the component in question (Equation 1.5.3)

$$\tau_3 = \frac{1}{\lambda_3} \tag{1.5.3}$$

The free volume radius which is determined as previously discussed (Equation 1.4.3) is used to calculate the free volume with the assumption the void is spherical (Equation 1.5.4). By multiplying FV by the intensity I_3, the fractional free volume, FFV is calculated (Equation 1.5.5). This gives an indication of the total free volume present in the test specimen[97]. The intensity is a relative measure of the amount of annihilations occurring from each annihilation component.

$$FV = \frac{4}{3}\pi R^3 \tag{1.5.4}$$

$$FFV = I_3 \times FV \tag{1.5.5}$$

Whilst PALS concerns lifetime measurements used to determine free volume and vacancy defects, Doppler broadening spectroscopy (DBS) measures the energy of the annihilation which yields useful information with regards to the annihilation site.

1.5.2 Doppler broadening spectroscopy

Doppler broadening spectroscopy (DBS) involves a magnetically guided positron beam bombarding a sample material. The material is surrounding by a number (at least two) of highly sensitive gamma radiation detectors, which obtain an energy spectrum of the subsequent annihilations. A schematic of this setup is shown in Figure 1.5.4.

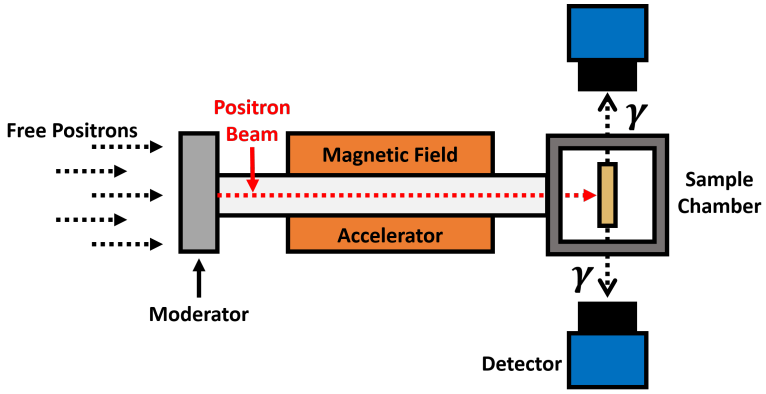

Figure 1.5.4: *DBS instrument set-up. Magnetic fields produced by copper solenoids accelerate and guide positrons towards a test sample. Highly sensitive gamma detectors surround the sample chamber to measure annihilation energies. The energy distribution produced can be analysed to give information on the annihilation environment.*

The central peak of the spectrum corresponds to the 511 keV annihilation with the spectrum deviating from this peak by a few eV. The reason for this spectral broadening is the Doppler Effect. In the rest frame, the annihilations occur in opposite directions with energies of 511 keV. However, in the laboratory frame the annihilation energies are Doppler shifted due to the centre-of-mass motion of the electron-positron pair relative to the direction of annihilation[98]. Motion directed towards the detector will result in a higher energy due to wavelength reduction (Figure 1.5.5). This is shown by the equation for the energy of a photon (Equation 1.5.6).

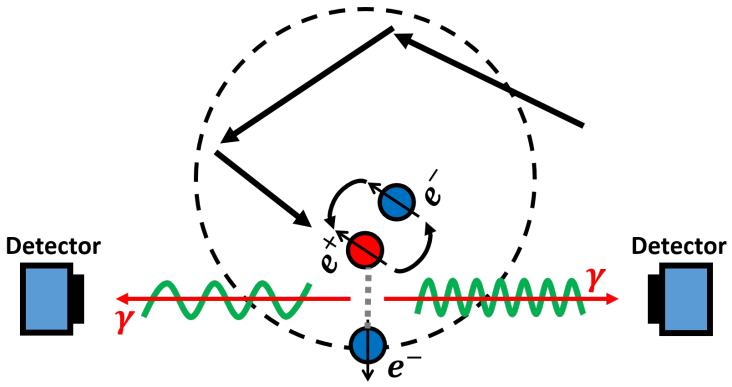

Figure 1.5.5: *An oPs atom entering a void and annihilating with a surrounding electron. The direction of motion of the annihilating pair causes the energy of the gamma photons to be Doppler shifted.*

$$E = \frac{hc}{\lambda} \tag{1.5.6}$$

The energy distribution varies depending on the number of high or low momentum electrons that are available. Core electrons have a relatively high momentum in comparison to valence electrons which have a lower momentum. If a material is microporous, then it is likely that a positron will become trapped inside a pore and interact with a valence electron. If a material is completely free of defects, then only high momentum events occur. This produces a very broad and shallow distribution. If a material is microporous, then predominantly low momentum events will occur. This produces a sharp peak. It can be shown that valence electrons have lower momentums by considering the orbit of the electrons as that of the Bohr model. Equating the centripetal force of an electron in orbit to the Coulomb force between the orbiting electron and proton in the nucleus (equation 1.5.7). Rearranging the equation such that momentum, P (where $P = mv$) is the subject shows the inverse square root relationship between momentum and orbital radius (equations 1.5.8 & 1.5.9).

$$F = \frac{mv^2}{r} = \frac{k_e q^2}{r^2} \tag{1.5.7}$$

$$P = \sqrt{\frac{k_e q^2 m}{r}} \tag{1.5.8}$$

$$P \propto \frac{1}{\sqrt{r}} \tag{1.5.9}$$

An example of the measured energy distribution is shown in Figure 1.5.6. Region 1 is due to Compton scattered photons which are produced alongside the emission of the positron(1.27 MeV). There is then a decrease in counts called the Compton edge. Region 2 involves a combination of Compton scattered photons from outside the detector volume i.e. inside the test samples, sample chamber and detector casing. The final region shows the photo-peak which is due to the annihilation photons with energies of 0.511 MeV.

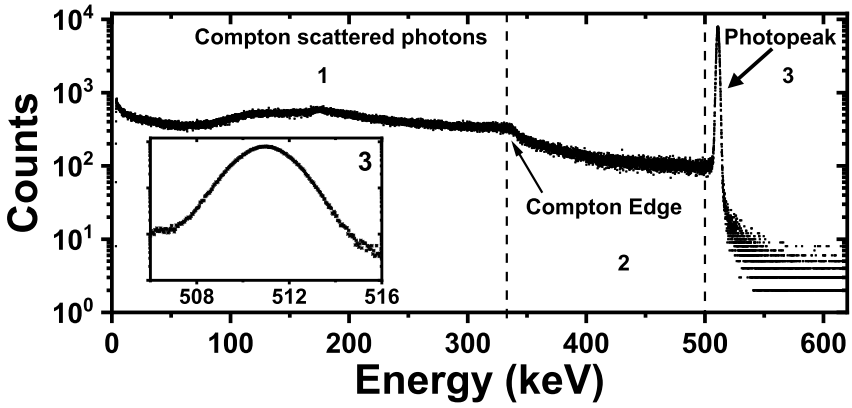

Figure 1.5.6: *A positron energy spectrum corresponding to detected gamma photons. Regions 1 and 2 are due to Compton scattered photons. The sharp peak present in region 3 is a consequence of electron-positron annihilations and as such is centred about 511 keV. The inset image shows this peak in more detail. (The data obtained during positron beam experiment at HZDR, Dresden).*

To quantify the Doppler broadening energy distribution, S and W parameters are commonly used. The S parameter emphasises the number of low momentum annihilation events. The W parameter concerns the number of high momentum annihilation events. Equations 1.5.10 and 1.5.11 show how to calculate the S and W parameters. Figure 1.5.7 helps to understand these calculations more clearly.

$$S = \frac{A_s}{A_{tot}} \tag{1.5.10}$$

$$W = \frac{A_{W1} + A_{W2}}{A_{tot}} \tag{1.5.11}$$

Where, A_s is the area of the small window centred on 511 keV, A_{W1+2} are areas of the wing regions of the distribution and A_{tot} is the total area of the distribution.

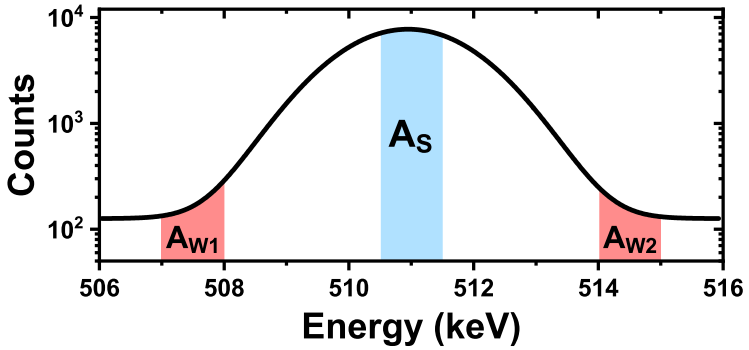

Figure 1.5.7: *Analysis of a Doppler broadened peak. The regions of the distribution used to determine S and W parameters are highlighted blue and red respectively.*

The S and W parameters are essentially ratios of low and high momentum events with respect to all the annihilation events in the distribution. If the number of voids in a material increases, this will result in a higher S value. A decrease in voids leads to more high momentum interactions and therefore W increases. The choice of parameter windows differ from researcher to researcher. These regions should be consistent when directly comparing spectra of different materials.

A relatively new technique based on a variable energy positron beam called mono energetic positron spectroscopy (MEPS) has the advantage of measuring both free volume and Doppler broadened energies as a function of depth. It is likely the first instrument of its type and Chapter 3, details experiments carried out using this instrument.

1.5.3 Closing remarks

The key annihilation techniques used in this work have been introduced and described, Studies presented in literature with a relevance to free volume and epoxies will now be discussed.

1.6 Some relevant studies in epoxy resins

1.6.1 Introduction

1.6.2 Free volume and diffusion

As mentioned previously, Recio *et al* studied permeability of gas vapours through polymer membranes. It was shown that the fractional free volume (FFV), correlated with permeability in that an increase in FFV corresponded to an increased permeability. Interestingly, they showed that the glass transition temperature (T_g) also increased with FFV.

Masoumi and Valipour[99] studied the effects of moisture exposure on crosslinked epoxy networks which comprised of DGEBA and the amine hardener, Jeffamine. They calculated the free volume based on segragational analysis and it was seen that water molecules tended to reside in large hydrophilic voids. They showed that increasing the water content increases the number of voids but void sizes on average decreased. Further increasing water content causes the T_g to decrease and concluded that this was due to hydrogen bonds breaking which ultimately increase network mobility.

Patil *et al*[36] compared T_g, crosslink density , diffusion and free volume in DGEBA-Jeffamine based epoxies. They showed that T_g decreased with decreased crosslink density and free volume, measured using PALS, increased. The increase in free volume and fractional free volume also corresponds somewhat with the chain length of the curing amine. When comparing free volume and FFV with the water content after 48 hours, it was shown that water content increases with increased free volume properties. This was by no means in a linear fashion (as seen in Figure 1.6.1) and it was concluded that not only free volume influences the uptake of water but also the chemical structure and segmental relaxation between chains.

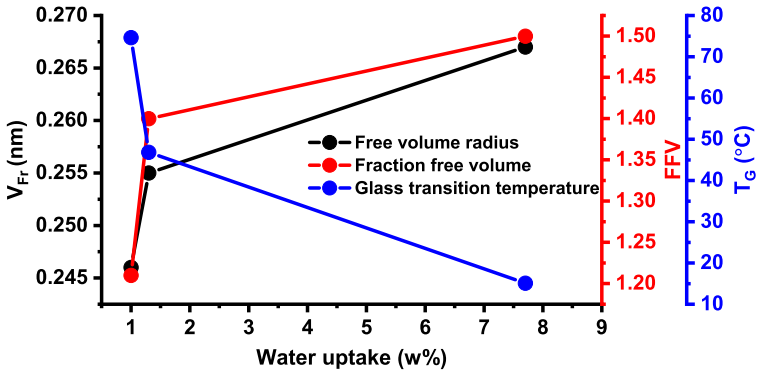

Figure 1.6.1: *Study of water uptake by Patil et al[36]. Connecting solid lines are present as a guide for the reader only. The graph produced is based on data included in the publication[36].*

Jackson *et al* carried out experiments which is probably the closest in relation to the work presented in this thesis. They performed ingression studies on epoxy samples consisting of DGEBA, DGEBF and TGDDM which were cure with amine isomers 3,3 and 4,4 DDS. The profiles of diffusion were compared to free volume measurements made by PALS. They concluded that when the size of the ingression molecule becomes similar to the average free volume, diffusion becomes hindered. The summary of results is depicted in Figure 1.6.2

where light grey curves correspond to ingression where the Van der Waals (VdW) radius is greater than free volume. The darker curves correspond to solvents in which VdW volume is lower than the average hole size.

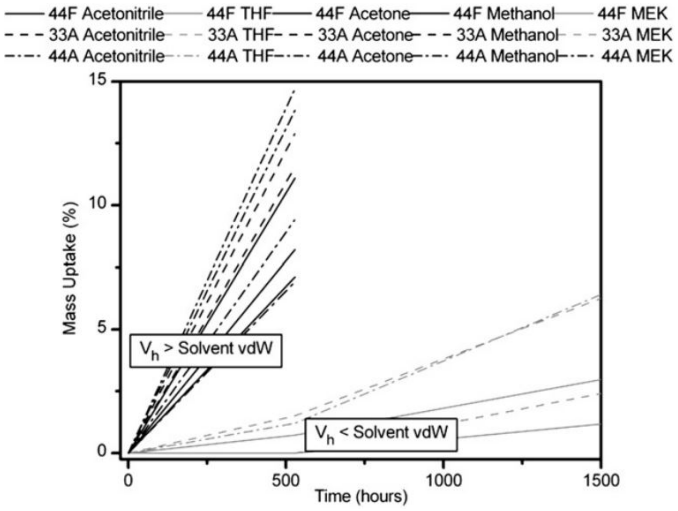

Figure 1.6.2: *The uptake data for various solvents in a number of epoxy materials by Jackson et al*[15]*.*

1.6.3 General observations

A number of traditional PALS studies have been carried out involving epoxy resins, generally DGEBA based resins. Lifetime measurements range from 1.5 to 2 ns at room temperature.[36,100,101] Suzuki[102] showed that as a monomer is consumed, the intensity of annihilation increases and τ_3 decreases. When both intensity and lifetime are constant the polymerisation is assumed to be completed. This is expected when considering that as monomer is consumed, the gel increases and more crosslinks are formed. This reduces free volume. It was also shown that when heating the sample after curing, the lifetime increases rapidly at a specific temperature. This temperature is assumed to be the glass transition but was shown to be lower than that obtained by other methods.[102] Methods such as DMA generally report tanδ values as the point of T_g[103–106]. This value generally occurs later than measurements made which use the point at which short relaxations occur on a molecular level such as the loss modulus (Section 2.4.1). As PALS is a direct measure of defects on a molecular level, it could be argued that one would expect T_g to occur earlier than that measured by a tanδ response.

1.6.4 Positron beam studies

There are few positron beam studies on neat epoxy resins. Where epoxy resins are concerned, they are generally thin films on a substrate. A study which involved epoxies on steel surfaces was carried out by Galindo *et al.* The resin used in this study is assumed to be a DGEBA based resin as the EEW quoted is 190 and referred to as 'type 828'. This matches the DGEBA based resin Epikote828. The epoxy was dissolved in acetone and reacted with MDEA. The liquid was spin coated onto steel before curing. The S values of pure steel and epoxy coated

steel were made over a range of implantation energies. The S values of coated steel increase initially before decreasing to a value similar to that of pure steel. The W values obtained are then plotted against the S values (Figure 1.6.3). A data clump is observed in the bottom right of the graph which is attributed to pure epoxy. S then decreases with increasing W which is attributed to an inter-facial region between steel and epoxy. A slight change in gradient indicates the beginning of the substrate.

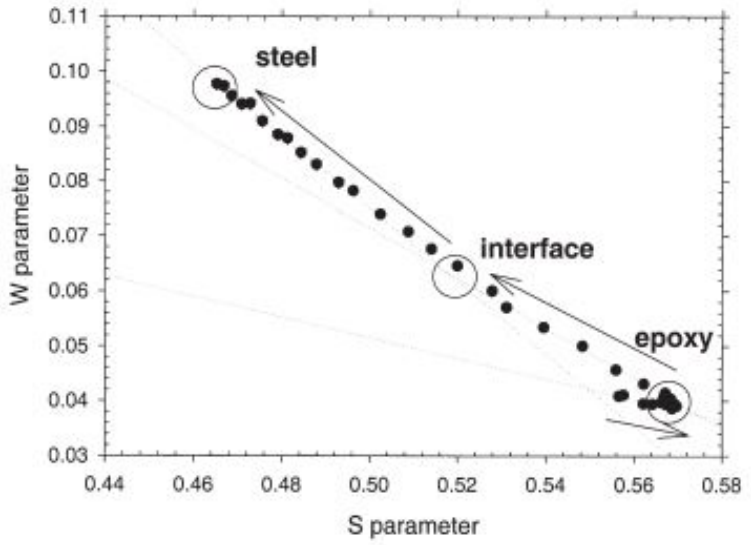

Figure 1.6.3: *The SW plot from Doppler broadening spectroscopy as measured by Galindo et al for epoxy resin on a steel substrate. Arrows show the direction corresponding to deeper implantation of positrons and therefore deeper probing. Lines added represent liner fits which emphasise changes in gradients. This change corresponds to a change in annihilation type which ultimate indicates a change in environment.*

1.6.5 Closing remarks

Now that some of the relevant literature has been discussed, the outline of the thesis will be presented before moving on to some methodological details required for other researchers to repeat the work carried out in this thesis.

1.7 Thesis structure

1.7.1 General aims and objectives

Construction of a PALS system

The first objective, it the construction of a positron annihilation lifetime spectroscopy (PALS) system in order to study free volume on polymer networks. The quality of instrumentation, safety and financial constraints must be considered. The second overall objective is to study diffusion of methanol in epoxy network and compare to free volume.

1.7.2 Thesis outline

Chapter 1: Introduction to the project covering relevant literature and basic concepts.

Chapter 2: Detailed information on the various techniques, instrumentation and sample preparation used through this work. This section includes all information necessary for researchers to perform the same investigations as presented in this work.

Chapter 3: This chapter presents the results and conclusions based on two positron beam studies. DBS and PALS data are obtained as a function of implantation depth for a number of epoxy resin samples.

Chapter 4: This chapter concerns solely the construction of the PALS system used in this work. Decisions made such as equipment selection are discussed and initial testing shown. The finances of producing PALS are also outlined in detail.

Chapter 5: This chapter presents the results and discussion of diffusion and free volume experiments. Correlations are shown for several studies in which the chemistry and production methods of epoxies are varied.

Chapter 6: The final chapter which summarises the findings in this work. Potential future work is also discussed.

2

Methodology and experimental techniques

2.1 Introduction to chapter

This chapter describes the range of methods and techniques used throughout this work. This includes details of the materials used, sample production, and techniques used. This chapter intends to give enough detail such that the reader could reproduce samples and perform experiments in the same manner.

2.2 Sample production

2.2.1 Materials

The key materials used in this research are epoxy resins and amine hardeners which produce a cross-linked network. The epoxy and amines will be described and suppliers listed. Other materials which were used throughout this research will also be listed.

Epoxy resins

The majority of epoxy resins used in this research are listed in Table 2.1. The epoxies referred to as "diluent" are not intended to be reacted solely with an amine hardener but are incorporated into the formulation to reduce the viscosity of the mixture without reducing chemical resistivity. This reduction in viscosity is necessary for coating applications such as spray coating.

Table 2.1: *List of epoxy resins used in this research along with their suppliers. (*supplied by AkzoNobel).*

Name	Epoxy	Supplier
DER354	Diglycidyl ether of bisphenol F (DGEBF)	The Olin Corporation
BDDGE	Diluent 1,4-butanediol diglycidyl ether	Original supplier unknown*
PGE	Diluent phenyl glycidyl ether	Original supplier unknown*
DEN431 Novalac	polyglycidyl-2-methylphenyl ether (PGMP)	The Dow Chemical Company
Epikote 828	Diglycidyl ether of bisphenol A (DGEBA)	Delta Resins

Hardeners

The curing hardeners used in this work are listed in Table 2.2 along with their suppliers.

Table 2.2: *List of hardeners used in this research along with their suppliers. (*supplied by AkzoNobel).*

Name	Amine	Supplier
MXDA	m - xylylene diamine	Sigma Aldrich
1,3-BAC	1,3 -bis (amino methyl) cyclohexane	Sigma Aldrich
1,4-BAC	1,4 -bis (amino methyl) cyclohexane	Tokyo Chemical Industry Ltd
PACM	4,4-Methylenebis(cyclohexylamine)	Original supplier unknown*
DMP30	2,4,6-Tris ((dimethyl amino) methyl) phenol	The Dow Chemical Company
DMPDA	3-(diethylamino)-1-propylamine	Delta Resins
IPD	Isophorone diamine	Delta Resins

Other materials

Several other materials were used in various parts of this research. Cleaning grade xylene was used as a diluent for DER354 in the solvated epoxy study (Section 5.4). Methanol was used in all ingression studies described in Chapter 5. N_2 gas is used in sample preparation to produce an inert atmosphere during cure as described in Section 2.2.2. Octamethyl trisilazane (OMTS) and deuterated chloroform were used for NMR sample preparation. Barytes was used as the pigment which was incorporated into epoxy networks as presented in Section 5.3.

2.2.2 General sample preparation

Determination of stoichiometry

A typical sample produced in this work comprises of an epoxy and an amine hardener in which there is an equivalent number of amine hydrogens and epoxide groups. This is a stoichiometric ratio of 100 %. To determine how much amine needs to be added to the epoxy to reach a stoichiometry of 100 % Equation 2.2.1 can be used.

$$A_{SM} = \frac{AHEW}{EEW} \tag{2.2.1}$$

Where A_{SM} is the amine stochiometric multiplier, AHEW is the amine hydrogen equivalent weight and EEW is the epoxide equivalent weight. The AHEW and EEW are determined using the molecular weights (M_W) and the component functionality (Equations 2.2.2 and 2.2.3 respectively).

$$AHEW = \frac{M_W}{Amine\ functionality} \tag{2.2.2}$$

$$EEW = \frac{M_W}{Amine\ functionality} \tag{2.2.3}$$

They mass of the epoxy (M_{epoxy}) is then multiplied by the A_{SM} value to give the amount of amine to be added (A_{mass}) in order to achieve a stoichiometric ratio of 1:1 between the amine hydrogens and epoxide groups (Equation 2.2.4).

$$A_{mass} = A_{SM} \times M_{epoxy} \tag{2.2.4}$$

Mixing of epoxy and amine

Approximately 30g of epoxy is poured from a glass decanter into a sample tube. The liquid amine is added via a pasteur pipette until until a stoichiometric ratio is reached. The epoxy-amine mixture is stirred thoroughly by hand for 5 minutes using a glass stirring rod. The sample tube is covered with parafilm with the stirring rod still in the mixture. Parafilm is used to prevent contamination from dust and to reduce carbamation and oxidation effects. The stirring rod remains as to not remove material which reduces stoichiometric errors. The mixture is stirred 3 more times at 15 minute intervals to prevent separation of epoxy and amine and encourage maximum cross-linking. This persistent mixing inevitably induces air bubbles. As samples will be used for solvent ingression studies, it is necessary to remove these bubbles. Ultrasonication is performed at this stage using a Fisherbrand FB15051 on degas mode for 20 minutes. After sonication, the mixture is left at room temperature for

45 minutes before stirring again. At this point, stirring should be gentle as to avoid large bubbles forming. The mixture is left at room temperature for a further 45 minutes before being transferred to a PTFE mould. However, the time between the final stir and transfer to mould is dependent on the laboratory temperature. At temperatures of $\approx$ 30 °C, this time can be reduced to as low as 15 minutes. At cooler temperatures (12 °C) the time may increase to 1 hour 30 minutes. This is due to the rate of reaction being increased and the gel point shifting as a consequence. Following sample preparation, the moulds are placed in an oven to cure. The reason for a seemingly lengthy mixing time is to allow for some initial crosslinking to occur which should reduce amine evaporation because of an increase in molecular weight.

Cure regime

The oven is preheated to 60 °C and the samples placed inside. Before commencing a temperature ramp, the oven is purged with nitrogen gas to create an inert atmosphere to reduce oxidation and carbamation[71]. The oven is ramped up in temperature to 160 °C at a rate of 1 °C min^{-1}. Once the target temperature is reached, it remains constant for 3 hours. The samples are then removed from the oven and allowed to cool before being removed from the moulds. Samples are typically contained inside a desiccator over phosphorous pentoxide. The oven used for the majority of this work was a Vacucell vacuum drying oven line comfort 22L model supplied by MMM Group.

2.2.3 Pigmented epoxy networks

In many applications, pigments are added to epoxy resins for reasons such as aesthetics or mechanical reinforcement. The pigment added to the epoxy networks in this work is barium sulphate which is also known as barytes or barites. This was supplied by AkzoNobel.

Preparation adjustment

The ratio of epoxy to amine in the formulation of pigmented epoxy networks is kept at 1:1. The pigment is incorporated into the epoxy before adding the amine hardener using a VM1-DETZMANN Dispermat mixer. Approximately 60 g of epoxy is added to an empty paint tin and mixed for 15 minutes. Approximately 96 g of pigment is added slowly whilst the mixing continues. After 5 minutes, a further 30 g of epoxy resin is added and stirring continues for 15 minutes. The amount of pigment added is dependent on the desired weight percentage of pigment to total mass (inclusive of amine). The amine hardener is added and the typical sample preparation and cure regime are carried out as described in Section 2.2.2.

2.2.4 Epoxy blends

Several epoxy blends were are studied in this work. The blends were formulated in terms of epoxide equivalent weight (EEW%) rather than weight percentage. The ratio of epoxide functionality and amine functionality remained at 1:1 for all cases.

DGEBF-DGEBA blends

DER354 (DGEBF) was added to Epikote828 (DGEBA) and then heated to 50 °C. This was done to reduce the viscosity of Epikote828 and promote good mixing between the two resins. The mixture is continually stirred and cooled to room temperature. The amine hardener is

added until a stoichiometric ratio is reached. Following this, the typical sample preparation and cure regime are carried out as described in Section 2.2.2.

Diluent epoxies
Diluent epoxies are used in industry to reduce viscosity depending on the application method such as spray coating. The epoxies used here were butanediol digycdyl ether (BDDGE) and phenyl glycidyl ether (PGE). The diluent epoxies were added to DER354 in ratios depending on EEW. The amine is added and the general sample preparation outlined in Section 2.2.2 is carried out. The final pot-time was left at an hour regardless of lab conditions as the fluid nature of the epoxies made viscosity a poor judgement of reaction progression.

2.2.5 Solvated epoxy networks

Where epoxy diluents are unwanted, solvents maybe incorporated to adjust viscosity as desired. Once the coating is applied, the solvent is expected to evaporate. However, the industrial sponsor of this research (AkzoNobel) suggest that solvent will remain locked in the coating once dry. As such, solvent is purposely locked into epoxy networks and ingression and free volume studies carried out.

Preparation adjustment
In this work, cleaning grade xylene is added to DER354 at 20 w% and mixed well. The amine is added and mixed as per Section 2.2.2. However, the rate of reaction was hindered greatly and as such the mixture was kept in a refrigerator for 14 hours. Once the mixture reached room temperature, it is poured into PTFE moulds and placed into an oven.

Cure adjustment
The typical cure regime outlined in Section 2.2.2 was attempted but samples produced were discoloured and cracked. This is most likely due to the cure temperature being higher than the boiling point of xylene. The boiling point of xylene is 138 °C therefore the cure regime was changed to a ramp from ° 60 to 135 °C at 1 °C min^{-1}.

2.2.6 Industrial cure

The typical cure used in this work is not practical in real-world scenarios. The materials produced are intended to coat the inside of large chemical storage tanks and it is unlikely that they would be heated to 160 °C. As such, a comparison of an industrial cure regime to an "ideal" cure regime is studied in Chapter 5.

Cure adjustment
Epoxy amine samples are mixed as stated in Section 2.2.2 but are poured into moulds instantly. The samples were then left in a nitrogen environment for 24 hours at room temperature. The samples are then put in an oven for 16 hours at 80 °C.

2.3 Sample processing

2.3.1 Dynamic mechanical analysis

Samples used for dynamic mechanical analysis (DMA) were in the form of resin sealed in aluminium material pouches supplied by Perkin Elmer. Approximately 1g of uncured resin is deposited in the centre of the pouch and spread across the crease. The pouch is sealed and cured according to the type of sample that is being produced. For each measurement, a minimum of two samples were prepared.

2.3.2 Positron annihilation lifetime spectroscopy

Samples used for positron annihilation lifetime spectroscopy (PALS) studies can effectively be any dimension provided that the thickness is at least 1 mm to absorb a large amount of positrons. In this work, samples were produced in PTFE moulds with dimensions of 40 x 20 mm with a minimum 2 mm thickness. The sample is then cut in half using a circular water saw. The samples are left in a desiccator for one week to dry. The samples are combined using Kapton tape and the positron source is placed in between the samples. The source-sample sandwich is then positioned with tweezers between detectors.

2.3.3 Diffusion study

Samples used for diffusion studies were polished to a thickness of approximately 0.9 mm using a rotational grinder/polisher (ECOMET brand). As water is used as a coolant, samples were left in a desiccator for one week before diffusion studies commenced. For each sample, three samples were prepared.

2.3.4 Nuclear magnetic resonance

Nuclear magnetic resonance (NMR) was used in the determination of EEW for the epoxy resins used in this work. The EEW is an important property to determine especially when isomers are present in the material used. Samples used for NMR studies consisted of 0.02 g of octamethyltrisilazane (OMTS), 2 g of deuterated chloroform (d-chloro) and 0.05 g of epoxy resin. The OMTS and d-chloro were added to the resin in a sample tube and sonicated for 10 minutes on sweep mode (Fisherbrand FB15051) to ensure good mixing. The solution was transferred to an NMR vial via a plastic pipette. For each sample, three solutions were prepared.

2.4 Sample characterisation

2.4.1 Dynamic mechanical analysis

Dynamic mechanical analysis (DMA) is commonly used to determine the glass transition temperature (T_g) of polymers. The T_g is a key property of polymers which affects how a material can be effectively used in it final form. The T_g is defined as the temperature at which a transition from a glassy to a rubbery state occurs or vice versa. Above this temperature, materials are more flexible due to increased molecular mobility. DMA works by applying a constant sinusoidal force to a material whilst the sample is heated. The stiffness or modulus (E') and the damping (tan δ) are measured and large changes in these two components signal the T_g.

T_g determination

To determine Tg, DMA measurements were performed using a Pyris Diamond DMA by Perkin Elmer in single cantilever mode. Samples were cooled to 0 °C using liquid nitrogen and then heated from 0 to 180 °C at a rate of 3 °C per min whilst a constant sinusoidal force is applied at a frequency of 1 Hz. The T_g is determined by two analytical methods in this work;

1. *The peak of the tan δ profile*

This is the ratio of the loss modulus to the storage modulus. It is measure of the energy dissipation of a material.

2. *The onset of the storage loss*

This is calculated by the intersection of the two linear regions before and after a large drop in storage modulus.

The calculation of both methods are shown in Figure 2.4.1. Generally, the peak of the tanδ is used as the point at which the glass transition occurs but it could be argued that a more accurate representation of T_g is the onset of the drop in storage modulus as this is when short range relaxations of bonds occurs and effectively the material become rubbery. In this work both the Tan δ and E' are reported. The peak measurement was determined using the Gaussian fit function in Origin software. The onset of the drop in storage modulus was determined by equating the two linear equations of the dashed lines and calculating the value for X which corresponds to the temperature at the intersection. For each material, two DMA samples were tested and the result averaged.

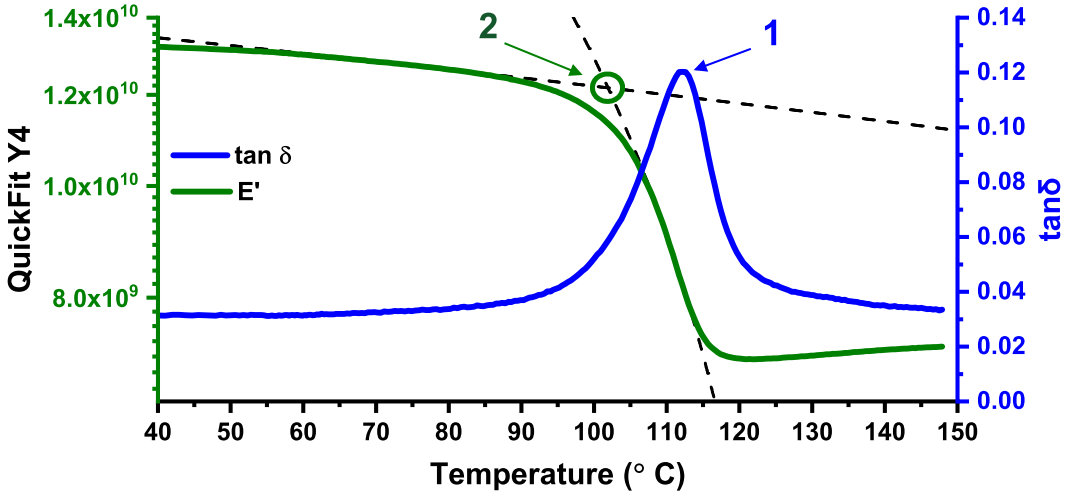

Figure 2.4.1: *The storage modulus and tan δ profiles for an epoxy material. Both profiles can be used to determine the glass transition temperature of a material with the storage modulus usually yielding a much lower value.*

2.4.2 Nuclear magnetic resonance

Topspin NMR sofware was used for data analysis. The signal peaks recorded were compared to that of the OMTS reference.

2.4.3 Density measurement

The density of materials were determined using helium pycnometry. This technique works by pressurising two chambers with helium gas; one empty and one chamber which contains the sample. The pressure differential is then used in conjunction with the ideal gas law to determine the true density of the sample. In this work, a MicrometricsAccupye1330 was used. Approximately 0.5 g of material (powder or bulk) were added to the sample chamber of 1 cm^3 volume. For each sample, 10 density measurements were made which were then averaged. Standard deviation is used to determine the standard error.

2.5 Experimental

This section describe how some of the key experiments were carried out including instruments and materials used.

2.5.1 Diffusion studies

Diffusion studies were carried out on several epoxy samples using traditional gravimetric techniques. These were performed to give a measure of chemical resistance of each material.

Ingression

For the study of ingression diffusion, samples prepared as described in Section 2.3.3 were placed in glass staining jars. Slots inside the jars ensure samples remain separated and upright. The slot position was used as an identifier of the samples to prevent the need of marking the sample itself and subsequently effecting measurements. The masses and thickness of each sample were measured before HPLC grade methanol is added such that the samples are completely submerged. Over time, the samples are removed and weighed. Masses were frequently monitored in the first week before measurements were taken less frequently as diffusion rate decreased. For each mass measurement, a sample is removed, placed on paper towel and patted down until touch dry. After weighing, the sample is immersed once again. This is repeated until the mass uptaken becomes constant which signals that the maximum amount of methanol has been uptake by the sample. This is referred to as the ultimate uptake/ingression throughout this work. Once the ultimate uptake is reached, egression studies can commence.

Egression

Egression studies concern the rate at which the methanol is released from the sample once removed from the jars. The initial mass is measured once removed and the sample is then placed in a dry clean staining jar. The mass is monitored over time in the same manner as ingression studies. Studies were performed at room temperature unless specified otherwise. Some studies which saw the egression mass stabilise were re-immersed for a second ingression cycle.

2.5.2 Variable energy positron spectroscopy

Variable energy positron spectroscopy (VEPS) was used for Doppler broadening spectroscopy (DBS) studies. Experiments were carried out at the Reactor institute in Delft, Netherlands. The instrument details are listed in Table 2.3.

Table 2.3: *Instrument details for the variable energy positron spectrometer used at The Reactor Institute, Delft.*

Specification	Information
Positron source	^{22}Na isotope (1Gbq activity) magnetostatic beam transport
Beam intenisty	1×10^5 e^+ s^{-1}
Beam diameter at target	8 mm
Maximum beam energy	30 keV
Detectors	High purity Ge solid-state detector (resolution of 1.8 keV)
Temperature range	20 - 1700 K

This study compares the Doppler broadened annihilation energies of two epoxy samples prepared as described in Section 2.2.2 with one of the samples being cured at 120 °C and the other at the standard cure temperature of 160 °C. Energies from 0 - 25 keV were probed for each sample and 6 million annihilation events recorded. Data was analysed using the program "SP".

2.5.3 Mono energetic positron spectroscopy

Mono energetic positron spectroscopy (MEPS) was used for positron annihilation lifetime spectroscopy (PALS) as well as simultaneous Doppler broadening spectroscopy (DBS) studies. Experiments were carried out at the Helmholtz Zentrum in Dresden-Rossendorf, Germany. The instrument details are listed in Table 2.4.

Table 2.4: *Instrument details for the mono energetic positron spectrometer used at Helmholtz Zentrum in Dresden-Rossendorf.*

Specification	Information
Positron source	Pair production by electron bombardment of tungsten target
Beam intensity	10×10^5 e^+ s^{-1}
Beam diameter at target	4 mm
Maximum beam energy	15 keV
Detectors	High purity Ge solid-state detector (resolution of 1.09 keV)
Temperature range	Unknown

Several epoxy samples were studied as described in Chapter 6. Energies of 1 - 10, 12 and 15 keV were probed. At each energy, 5 million counts were collected. A further 25 million counts were collected at energies of 2, 5 and 10 keV for high statistics.

2.5.4 Positron annihilation lifetime spectroscopy

Positron annihilation lifetime spectroscopy (PALS) was performed using a digital system which was constructed as part of this research. It consists of two EJ232 fast plastic scintillators, two H1919-X Hammatsu photomultiplier tubes, a four-fold coincidence unit (supplied by Rehberg Technology) and a DRS4 evaluation board. Full details of this instrument are presented in Chapter 4. For each measurement, a minimum of 1 million counts were acquired in approximately 10 hours. Two identical sample pieces surround the source and are placed between both detectors. A combination of MATLAB code and QTPALS software were used for data acquisition. The analysis of lifetime spectra was performed in the fitting software "LTPOLYMERS" with lifetime distributions determined using the MELT MATLAB program.

2.6 Summary

This chapter has given information for the various techniques and methods required to perform the research which is outlined in the following chapters. From this point on, this chapter will be referred to where necessary but methods and techniques will be reintroduced where deemed necessary for ease of the reader.

3

Positron beam studies of epoxies

3.1 Introduction to chapter

This chapter concerns studies of epoxy resins using positron beam instruments. Section 3.2 discusses experiments performed using The Variable Energy Positron (VEP) Beam at the Reactor Institute, TU Delft. This instrument is used for Doppler broadening spectroscopy (DBS) which measures the energy produced in the annihilation event between positrons and electrons. This produces a broadened spectrum as described in Section 1.5.2. This data can then be used to indicate free volume as a function of depth. This experiment was an initial small scale test to see whether a change in cure temperature affects the free volume which can be indicated by measuring S values.

Section 3.3 is themed around experiments carried out at the Helmholtz-Zentrum Dresden-Rossendorf (HZDR), ELBE center for high-power radiation sources. This involved the use of a positron beam which is used for mono energetic positron spectroscopy (MEPS). This instrument measures positron lifetime measurements whilst DBS measurements can be collected simultaneously. The key aim of this experiment is to measure the free volume as a function of implantation depth for several epoxy samples. Different sample production methods and chemical compositions were studied and are discussed.

3.2 Doppler Broadening Spectroscopy at TU Delft

3.2.1 Experimental brief

Doppler broadening spectroscopy (DBS) was performed on two epoxy samples consisting of Diglycidyl ether of bisphenol F (DGEBF) cured with the amine hardener m-xylyldiamine (MXDA). These samples were produced as described in Section 2.2.2. but with one sample being cured at a higher temperature of 160 °C (labelled 160 °C cure) and the other cured at a lower of 120 °C (labelled 120 °C cure). S and W parameters are determined using the program "*SP*" for implantation energies up to 25 keV. The data is presented as a function of mean implantation depth which is calculated as per Section 3.3.2.

3.2.2 S and W implantation profiles

Figure 3.2.1 shows the S and W parameters as a function of Depth. S increases as positron implantation increases in both samples. The sample cured at 120 °C plateaued at a lower S value than the 160 °C. This is depicted by coloured dashed lines corresponding to the colour of their respective data points.

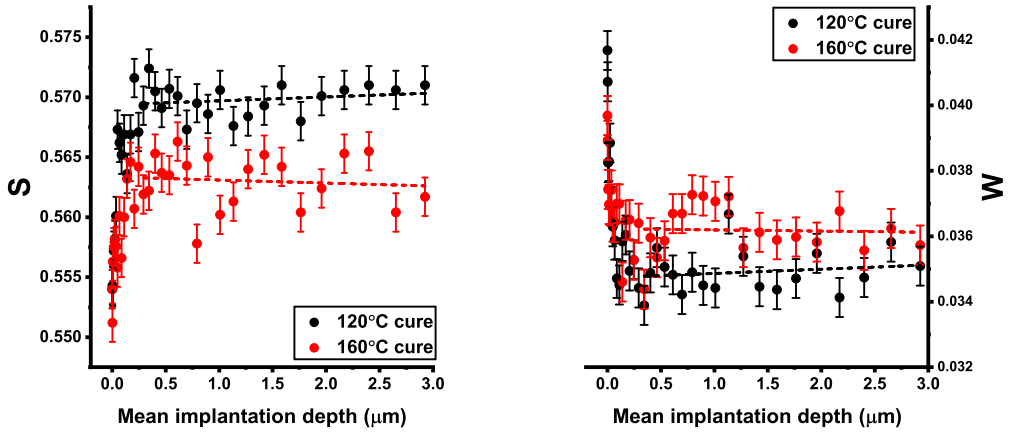

(a) *S values* ***(b)*** *W values*

Figure 3.2.1: *S and W values as a function of mean implantation depth for two samples of DGEBF-MXDA which were cured at temperatures of 160 °C and 120 °C. Linear fits emphasise the difference between in S and W between the two samples in the plateau region (0.5 - 3μm). Standard error is shown using error bars.*

W decreases from the surface to a depth of $\approx 0.4\mu$m for both 160 °C and 120 °C cures. The 120 °C plateaus at a lower level than 160 °C. The 160 °C appears to increase in W from 0.5 μm but in general, the 160 °C sample has a higher W. Again, linear fits are shown to depict the difference in W. The higher S parameter in the 120 °C means that a higher number of the total annihilations were due to valence electron interactions than in the 160 °C sample. This implies that curing at a lower temperature causes a higher number of free volume (FV) voids or larger amount of FV in general. This could be explained by the nature of the reaction between the resin (DGEBF) and amine harderner (MXDA). As the reaction progresses, viscosity increases as monomer is used up as crosslinks form. During the latter stages of reaction, the mobility of molecules becomes hindered and a fraction of functional groups will not react ($< 1\%$ as shown by NIR[71]). A higher temperature increases the mobility and therefore allows a higher percentage of functional groups to react. This increases the number of cross links and theoretically reduces free volume[36] which in turn decreases the S value.

Positron implantation issue and repeat experiment

A calibration check was performed due to the small peak in W for the 160 °C sample. During the calibration/adjustment, a strange effect was observed. Figure 3.2.2 represents the rate of positron annihilations at low energies (< 1 keV) for both samples. The 120 °C samples required a higher energy before a considerable number annihilations were recorded. Given that, each count corresponds to a positron implanting into the material and annihilating with an electron, this implies that positrons in the 120 °C sample are being re-emitted or deflected and hence the annihilation event is not recorded. This behaviour is seen in potential barriers where particles are repelled by repulsive forces, such as coulomb forces and therefore this may have been due to static charge.

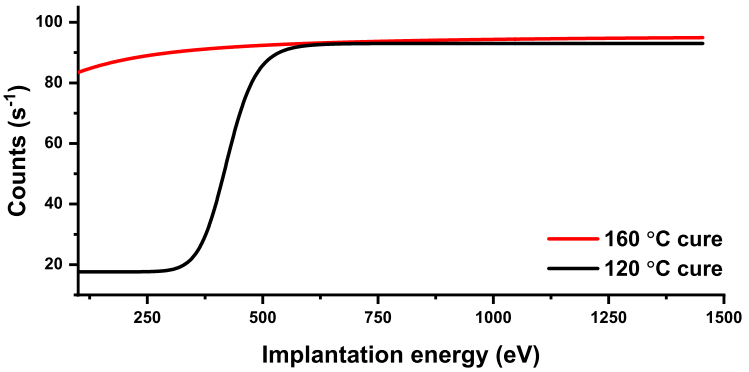

Figure 3.2.2: *The rate of positrons detected at low beam energies for the 160 °C and 120 °C samples. In the sample cured at a lower temperature, positrons required a higher energy before implanting and subsequently annihilating in the material. This is for visual purposes only and values shown are not accurate.*

The samples were grounded, and the effect was reduced but still remained in some capacity. No conclusion could be reached about this barrier effect. S and W measurements were repeated following the instrument adjustment and the results are shown in Figure 3.2.3. The small peak previously seen in 160 °C sample is no longer present but in general the results are similar with respect to one another. Average values of S and W were calculated from data beyond 1 μm for both experiments as shown in Figure 3.2.4. Both samples showed the same changes in S and W after the instrument calibration and the difference between the two was unchanged.

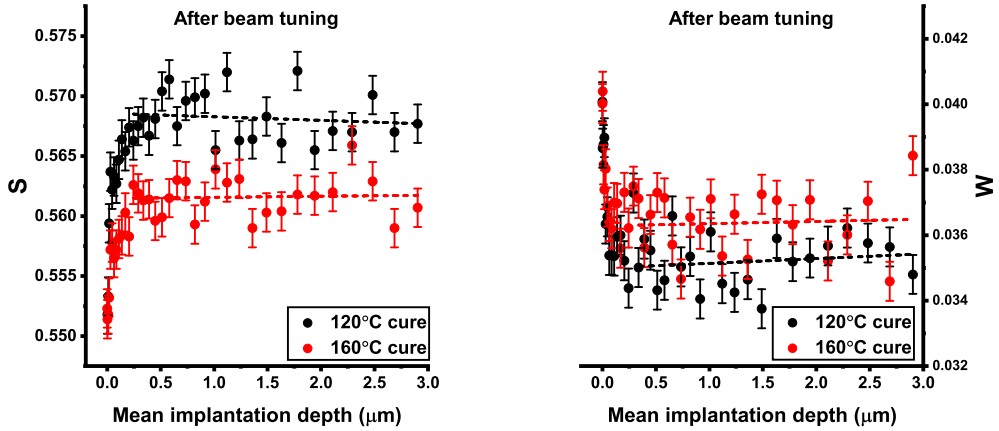

(a) *S values* ***(b)*** *W values*

Figure 3.2.3: *The repeated Doppler broadening spectroscopy measurement after beam calibration. Similar results were recorded for S and W as a function of mean implantation depth. Linear fits are shown from the point of plateau to clearly show the difference in S and W between the two samples. Standard error bars are shown.*

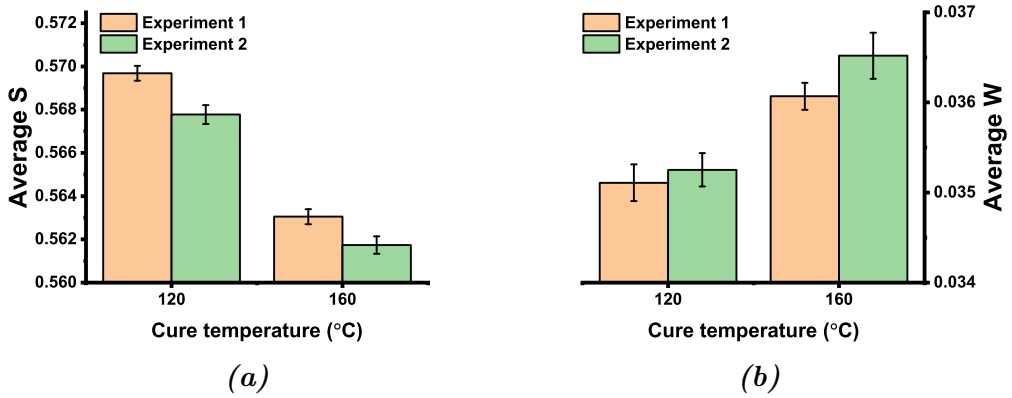

Figure 3.2.4: *Average values in S and W from 1 μm onwards. Experiments 1 and 2 refer to measurements made before and after the instrument was adjusted. Standard errors are shown.*

3.2.3 SW plot

S-W plots can be used to determine layer thickness (if layers are present) and the depth of transitional phases from one layer to the next. The S-W plot for the two epoxy samples is shown in Figure 3.2.5. There is no definition of layers here which implies free volume sites are similar. If layers were present, a change in gradient of S vs W would be seen and data points would shift in a continuous fashion[107]. This is an expected result as the samples have effectively identical chemistry and only the production method varies. The linear fits show that where S is high, W is generally lower which is also expected.

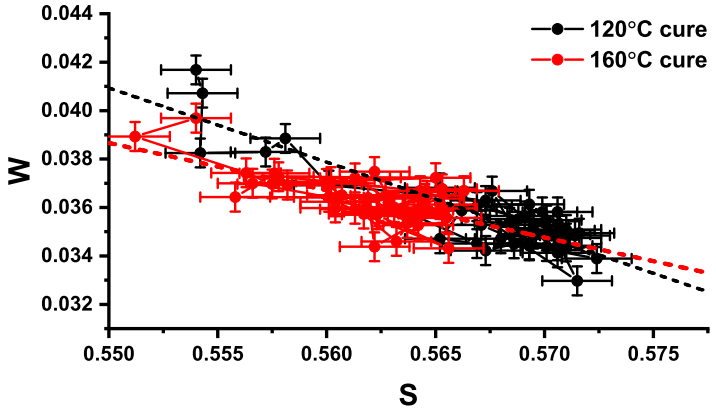

Figure 3.2.5: *The S-W plot for DGEBF-MXDA epoxies cured at 120 °C and 160 °C. Both show a similar downward trend overall but there is no trend as a function of implantation depth. Linear fits are included to emphasise the downward trend and standard errors are shown.*

Conclusion

The key conclusion from DBS measurements using the VEP beam is that differences in S and W were observed between samples cured at different temperatures. Before and after

an instrumental adjustment, W was determined to be lower in the 120 °C cure sample. S was found to be higher in the 120 °C cure sample which suggests that curing at lower temperatures increases the free volume or the total number of free volume voids present. Table 3.1 summarises the results of this study.

Table 3.1: *Average S and W values determined by Doppler broadening spectroscopy. The numbers 1 and 2 refer to measurements made before and after instrumental adjustment respectively.*

Sample	S1	W1	S2	W2
120° C	0.5697 ± 0.0003	0.0351 ± 0.0002	0.5678 ± 0.0004	0.0353 ± 0.0002
160° C	0.5631 ± 0.0003	0.0361 ± 0.0001	0.5617 ± 0.0004	0.0365 ± 0.0003

3.3 Mono energetic positron spectroscopy

This section presents results obtained using the mono energetic positron spectroscopy (MEPS) instrument at the ELBE centre, HZDR in Dresden. Doppler broadening spectroscopy (DBS) and positron annihilation lifetime spectroscopy (PALS) measurements were made simultaneously for implantation energies up to 15 keV on several epoxy (DGEBF) based resins. The results are grouped into different studies which will be described at the beginning of each subsection. To begin, a "defect-free" (i.e. lack of free volume) reference sample is compared to a sample of DER354-MXDA (produced as described in Section 2.2.2. The defect free sample is based on yttria-stabilized zirconia supplied by the user facility. In this first study, each aspect of DBS and PALS data are introduced and discussed. For the following studies, only figures concerning S, W , free volume and fractional free volume are presented.

3.3.1 Introductory results

Positron lifetime spectrum

Figure 3.3.1 illustrates the difference in lifetime spectra between DER354-MXDA (labelled MXDA) and yttria-stabilized zirconia (labelled YSZ) for an implantation energy (E) of 5 keV. As expected, YSZ has a much narrower lifetime distribution than MXDA due to the lack of oPs annihilations occurring in free volume (FV) voids.

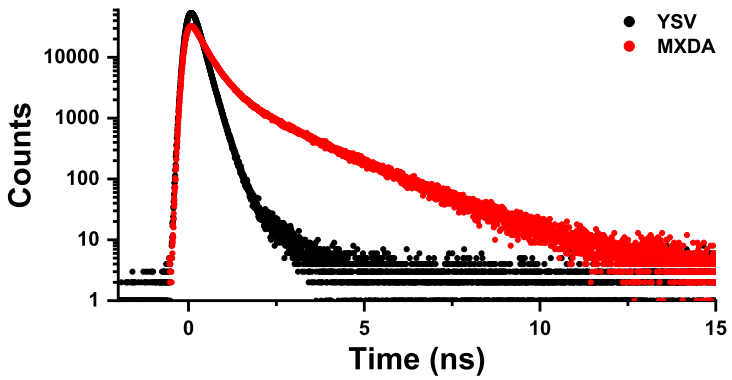

Figure 3.3.1: *Positron lifetime spectra for yttria-stabilized zirconia (YSZ) and an epoxy resin comprising of DGEBF and MXDA sample. The epoxy has a much shallower decay than YSZ due to the presence of orthopositronium annihilations which occur inside free volume.*

Doppler broadened spectrum

In addition to PALS measurements, DBS measurements were made simultaneously using this instrument. An example distribution for an implantation energy of 5 keV for both MXDA and YSZ is shown in Figure 3.3.2. Taking into account the central area and the wing regions (A_S and A_w respectively), this broadening follows theory described in Section 1.5.2. In brief, YSZ has a lower S value due to a smaller fraction of counts corresponding to valence electron interactions whilst W is high as a higher fraction of annihilations are resultant of core electron interactions. The region used for determining S is shaded in blue whilst the regions used for the calculating W is shaded black and red for YSZ and MXDA respectively.

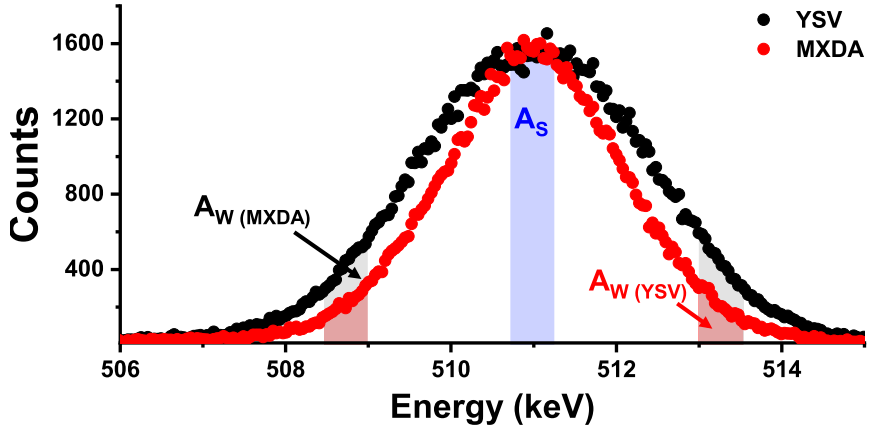

Figure 3.3.2: *Doppler broadened energy distributions for DGEBF-MXDA epoxy (MXDA) and the reference sample, yttria-stabilised zirconia (YSZ). The region highlighted in blue shows the area used in the calculation to determine S. The regions highlighted black and red show the areas used to determine W for YSZ and MXDA respectively.*

Comparison of results

The values for S and W in addition to the lifetimes of parapositronium, free positron and orthopositonium (τ_{pPs}, τ_{e+} and τ_{oPs} respectively) are shown in Table 3.2. Lifetime results

were determined using the program "*LTPOLYMERS*". A three component model was used for fitting analysis of MXDA with (τ_{pPs}) fixed to 0.125 ns which is a common fitting constraint.[108,46] YSZ was fitted using a two component method with τ_{pPs} also fixed to 0.125 ns. YSZ has been shown to be freely fitted in other studies[109] but here for a direct comparison, τ_{pPs} was constrained.

Table 3.2: *S and W values for the YSZ reference sample and a DGEBF epoxy cured with MXDA. Standard errors in S and W were produced by the program SP. Standard error of positron lifetimes were produced by the program "LTPOLYMERS".*

Sample	S	W	$\tau_{pPs}(ns)$	$\tau_{e+}(ns)$	$\tau_{oPs}(ns)$
MXDA	0.57 ± 0.003	0.0016 ± 0.0005	0.125 (fixed)	0.369 ± 0.002	1.58 ± 0.02
YSZ	0.48 ± 0.002	0.0032 ± 0.0006	0.125 (fixed)	0.234 ± 0.002	N/A

S and W implantation energy profiles

S and W values for MXDA and YSZ are shown in Figure 3.3.3 as a function of positron implantation energy. As expected, S is significantly higher in the MXDA sample. In both samples, the S value is relatively unstable throughout. Usually, DBS results are seen to show some form or continuity[110,111] and often stabilise once the bulk of the material is reached.[47,112] The same inconsistency is seen for W which is highlighted by the sharp rise in W at 4 keV in the YSZ sample. A high W value is expected in the defect free samples with a higher fraction of high momentum annihilations (i.e. core versus valence electron interactions).

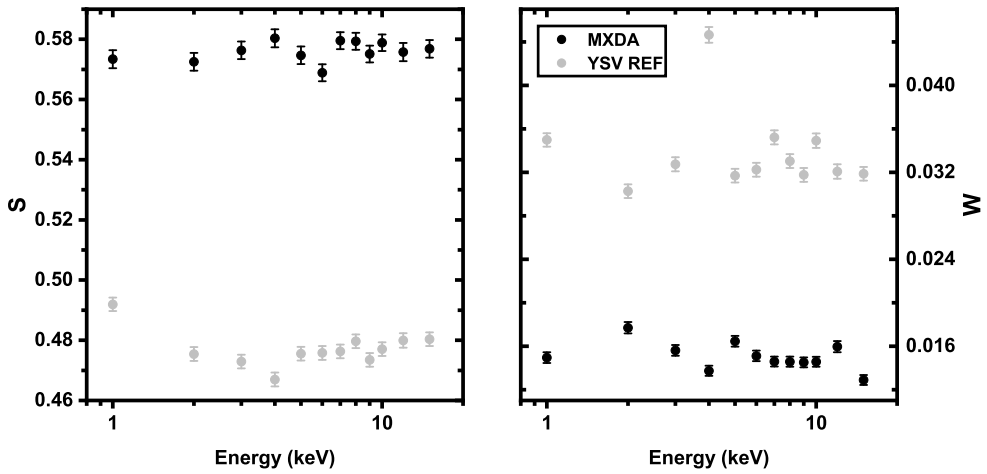

(a) *S values* ***(b)*** *W values*

Figure 3.3.3: *S and W values as a function of positron implantation energy obtained by Doppler broadening spectroscopy for DGEBF-MXDA epoxy resin and yttria-stabilised zirconia (YSZ). Standard error is shown using error bars.*

SW plot

By plotting S against W, information regarding the annihilation site can be obtained. Generally, S should increase with a decrease in W and where a change in gradient occurs, this indicates a transition between layers.[44,107] Where a transition between layers is not the case, then there should be a direction of change in SW which is fairly continuous, such as increasing fatigue test cycles.[113] This was not seen in either YSZ or MXDA as shown in Figure 3.3.4 where connecting lines emphasise the randomness of direction. Red dotted lines represent linear fits which show that the expected downward trend of W with S is present but poor as suggested by R^2 values. The lack of trend here begins to cast doubt over the reliability and usefulness of this data.

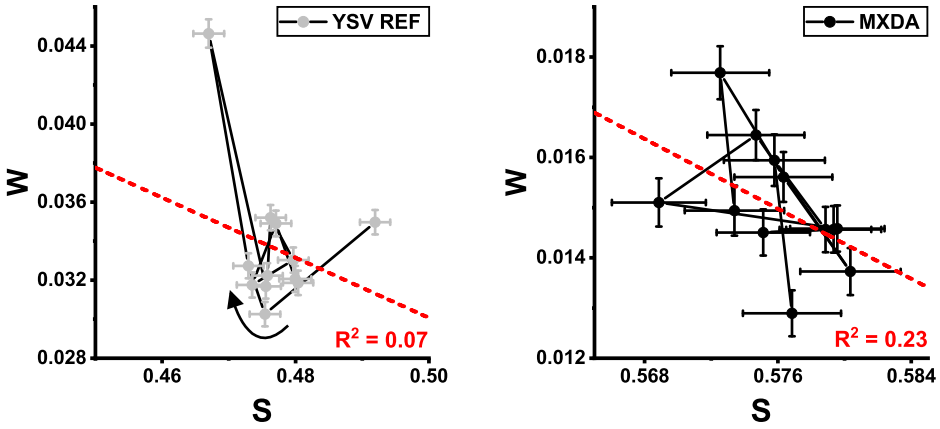

(a) YSZ *(b) MXDA*

Figure 3.3.4: *The S-W plots for yttria-stabilised zirconia (YSZ) and DGEBF-MXDA epoxy (MXDA). The red dashed lines represent linear fits which show that overall as W decreases, S increases. However, the low R^2 values highlight that the correlation is poor. Connected lines show how the data varies with changing energy. The arrow is intended to guide the reader in the direction of increasing implantation energy. This was not possible for MXDA.*

However, a study by Galindo *et al.*[107] which showed the transition from a layer of epoxy to steel in terms of S vs W did show that measurements in the pure epoxy resulted in a data clump. As implantation energy was increased and therefore implantation depth, the SW value shifted to the top left of the plot in a smooth manner due to a combination of epoxy steel measurements.

Figure 3.3.5 shows Galindo's results along side an SW plot which contains both the MXDA and YSZ samples collected with MEPS. Measurements are made with increasing positron energies which corresponds to an increased implantation depth. The increase in energy is indicated by an arrow for YSZ but this was not possible for the MXDA sample as the data overlaps considerably.

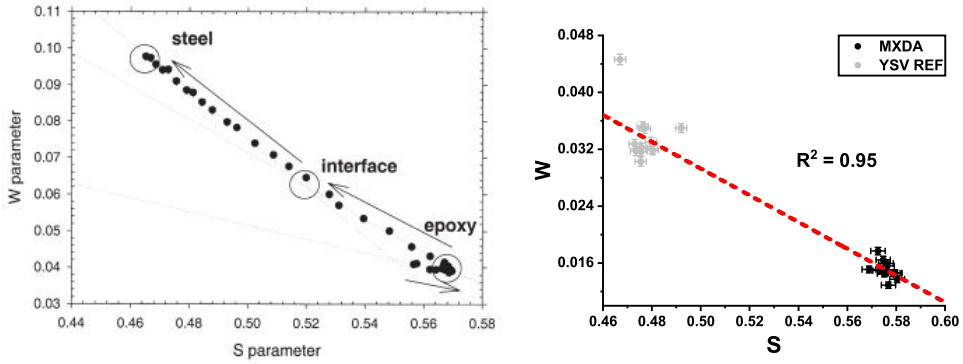

(a) *SW plot presented by Galindo et al.* ***(b)*** *SW plot for MXDA and YSZ*

Figure 3.3.5: *A comparison of SW plots produced by Galindo et al. and those obtained using MEPS for MXDA and YSZ. The dashed red line in Figure (b) shows a good linear fit for all data points present. Error bars in Figure (b) represent standard errors of three samples.*

A data clump for the epoxy in the bottom right is similar to that of Galindo's. The spread of data points for YSZ are most likely attributed to the fact that there is no epoxy contribution here (i.e no layers). To conclude, the expected relationship between S and W is seen when comparing all the data for each sample (i.e two data clusters). However, as a function of implantation energy, this trend is not observed and the relationship is random. This shows that there are no significant differences in void annihilations with increasing implantation energy or that the measurement is insensitive to changes in a single component material without any changes to the environment (temperature and humidity).

Lifetime and annihilation intensity implantation energy profiles

As discussed in previous chapters, the positron lifetime yields information which is related to the site in which the annihilation occurs. In polymers, at least three annihilation types are present; parapositronium (pPs), free positron (e^+) and orthopositronium (oPs) annihilation. Each component has a respective annihilation intensity which is a measure of how frequent a specific annihilation occurs. All three lifetimes and their respective annihilation intensities are shown in Figure 3.3.6 as a function of implantation energy for the MXDA sample.

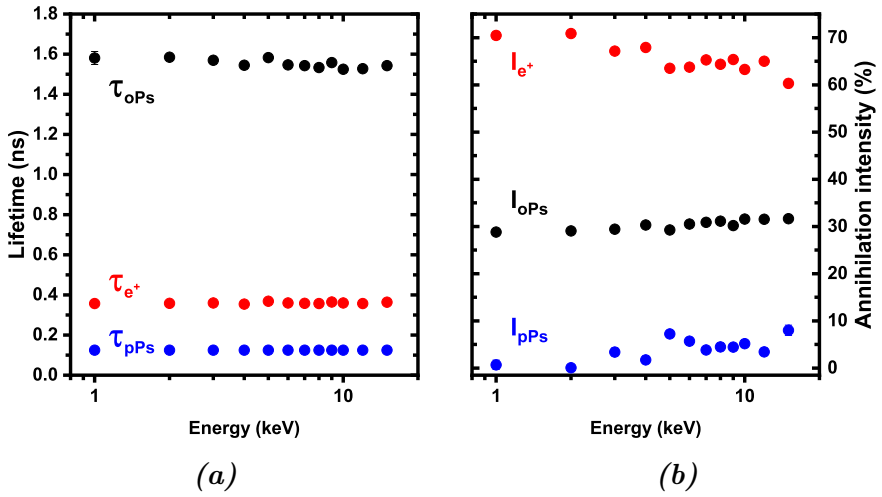

Figure 3.3.6: *The average lifetimes of each annihilation component (a) alongside their respective annihilation intensities (b) for a DGEBF-MXDA epoxy sample. Standard error bars are included but are smaller than the data point on this scale. The lifetime of τ_{pPs} was fixed to 0.125 ns.*

Annihilations due to oPs concern free volume annihilations, e^+ is due to positron trapping in the bulk or mono-vacancy defects and pPs is due to bulk anihillations.[94,114] Near the surface, pPs intensity is almost 0% before increasing to levels around 6% as you move deeper into the sample. Backscattering of pPs at the surface may account for this. Changes in I_{pPs} are mirrored by I_{e+} whilst I_{oPs} is relatively stable. By plotting the intensities against one another, it can be determined whether the correct number of components have been chosen for fitting analysis. If two components correlate well ($R^2 > 0.9$) then it is probable that the two components could be described by a single component instead. Figure 3.3.7 shows the I_{e+} plotted against I_{pPs} and I_{oPs}.

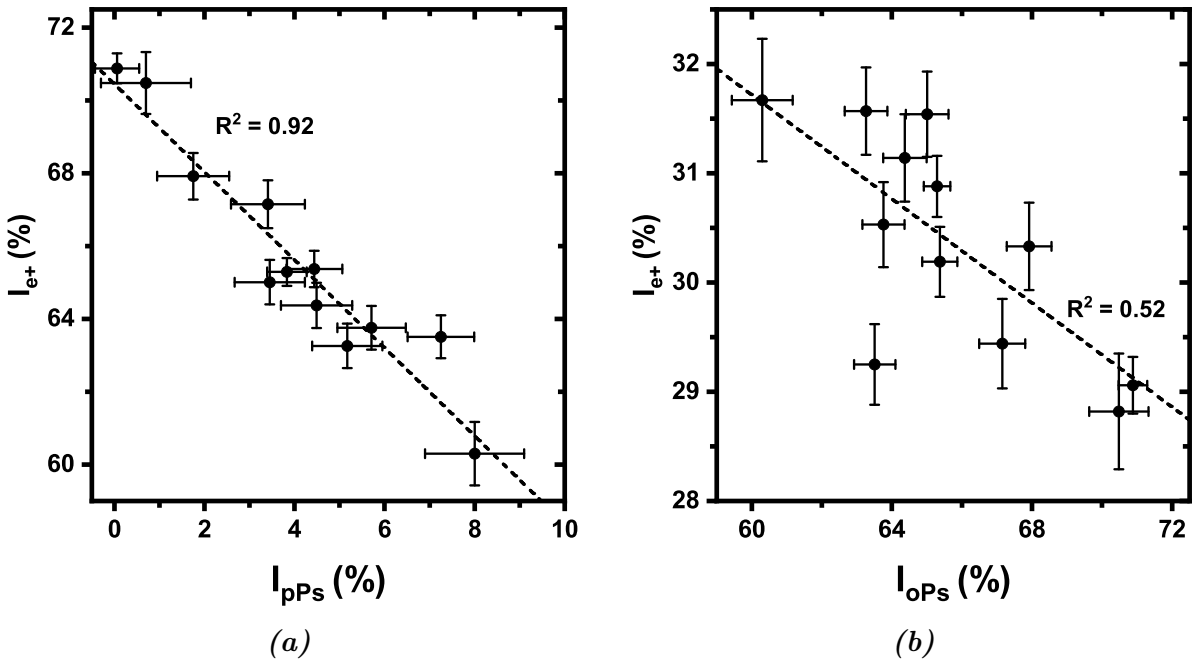

Figure 3.3.7: *The comparison of intensities over the full range of implantation energies for MXDA. A good correlation is seen when comparing (a) I_{e^+} and I_{pPs} which implies that pPs is not only due to bulk annihilations but also positron trapping. We can conclude this as pPs and e^+ generally concern annihilations due to bulk annihilations and defect trapping respectively. Therefore, as the intensity of e^+ changes in an opposing manner to pPs then they must not be independent of one another. The correlation between (b) I_{e^+} and I_{oPs} is poor which means I_{oPs} is mainly due to free volume annihilations as changes in I_{oPs} do not change in tandem with I_{e^+}*

.

The relationship between I_{e+} and I_{pPs} is linear which implies that the short lifetime intensity is not only due to bulk annihilations but actually has a proportion which are due to positron trapping in the bulk or mono vacancy defects. There is no true trend between I_{e+} and I_{oPs} which implies that that changes in I_{oPs} are associated with the number of free volume annihilations only. There is a potential case to fit lifetime data with only one short component which would combine both intensities but in this research, the three component model suffices as the main focus is free volume annihilation i.e oPs annihilations.

Figure 3.3.8 shows the lifetimes τ_{e^+} and τ_{oPs} as a function of implantation energy for MXDA on a scale which allows small difference to be observed. It can be seen that a small decrease in τ_3 is observed as a function of energy. This implies that free volume is larger near the surface of the material. τ_2 shows a small increase as a function of implantation energy which means that there is a small decrease in electron density.

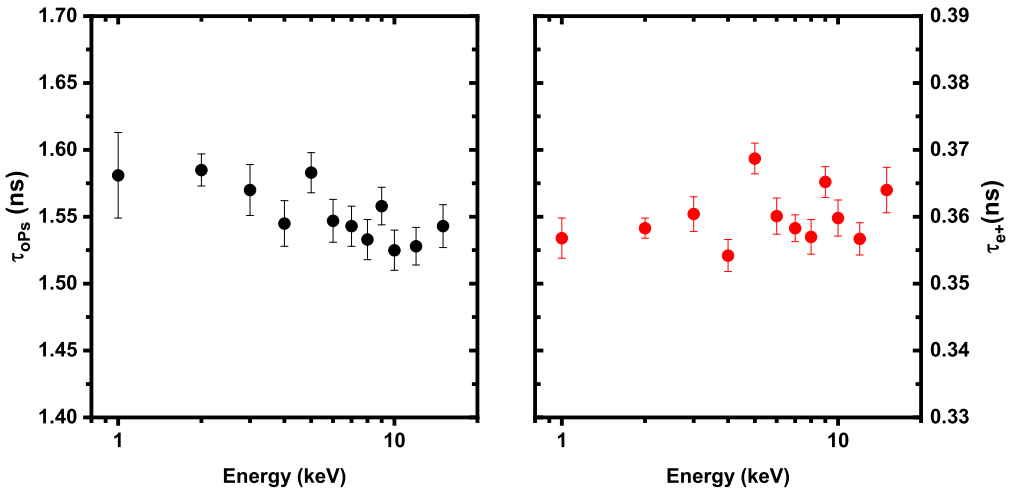

(a) *Orthopositronium lifetimes* ***(b)*** *Free positron annihilation*

Figure 3.3.8: *The measured lifetimes of orthopositronium (a) and free positron (b) in the DGEBF-MXDA sample as a function of implantation energy. Standard errors are shown which were generated in the program "LTPOLYMER".*

Free volume and fractional free volume

For this research, the key component is the the oPs lifetime, τ_3. As mentioned previously, oPs resides in FV before annihilating and the duration from positron birth to annihilation is related to the size of the void. For these reasons, only the oPs lifetime will be considered from this point on and will also be converted to average free volume. The average free volume is the free space between polymer chains and has been shown to effect the rates of solvent diffusion in epoxies[15]. In this work, the free volume is calculated using the Tao-Eldrup model previously shown in Section 1.4.4. The average free volume can then by multiplied by the oPs annihilation intensity to give the fractional free volume. The fractional free volume gives an indication of the free volume per specific volume of the polymer.[95]

Figure 3.3.9 shows that FV decreases in general over the full range of implantation energies in MXDA. It appears as though there are regions of free volume: 1 - 4 keV, 6 - 8 keV and 10 keV onwards. However this is based on single data points being a transition between reigons. The FFV is seen to show a slight increase with increasing implantation energy.

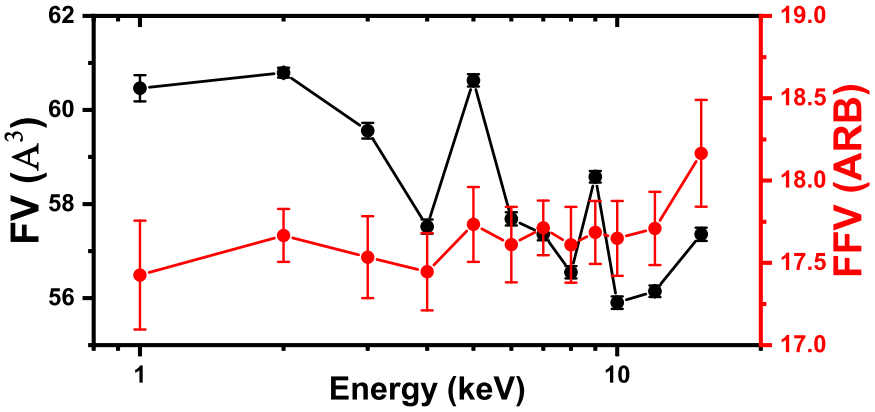

Figure 3.3.9: *Free volume (FV) and fractional free volume (FFV) as a function of positron implantation energy for MXDA. Standard errors are shown and connected lines are intended as a guide for the reader.*

Thus far, free volume and DBS results have been presented as a funtion of implantation energy. However, it is also common to assign a finite implantation depth to each energy.[44,96,115] In addition to this general representation, a novel analytical approach is used in this work. This considers both the probability of a positron annihilating at a depth, Z and the average free volume, FV measured with respect to implantation energy.

3.3.2 Convolution depth profile derivation

This section outlines a novel representation of positron annihilation measurements as a function of depth. The calculation of depth profile distributions will be shown and an example convolution shown.

Positron implantation depth profile

If the positron implantation energy is increased, then it can be expected that the depth of implantation increases. This is generally true, however the depth is not well defined and the energy has an affect on the probability of a positron annihilating at a specific depth. This probability can be described by the Makhov model which is shown by Equations 3.3.1 and 3.3.2.[?,116]

$$P(Z) = \frac{mZ^{m-1}}{Z_0^m} \exp\left[-\frac{Z}{Z_0}^m\right] \tag{3.3.1}$$

$$Z_0 = \frac{AE}{\rho \frac{1}{m} ln2} \tag{3.3.2}$$

Where P is the probability, Z is the implantation depth with Z_0 determined by Equation 3.3.2. m and A are material dependent parameters determined by Monte-Carlo simulations[117], E is the implantation energy of the positrons in eV and ρ is the density of the test material. This work concerns DGEBF based resins, the values for A, m and ρ are 2.17, 2.94 and 1.22 kg m^{-3} respectively. The value of ρ was determined by helium pycnometry as described in Section 2.4.3. Figure 3.3.10 shows how the probability density function becomes

broader with increased implantation energy. One might expect the probability of annihilation to decrease exponentially from the surface as with the Beer-Lambert law. However, due to the thermalisation of the positron, the probability of annihilation at at a depth Z is described by a Gaussian distribution.

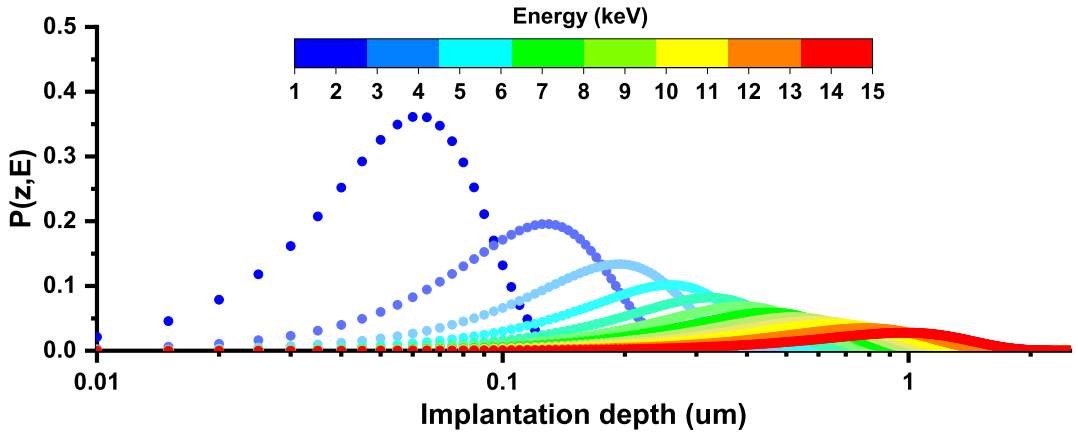

Figure 3.3.10: *The evolution of the implantation depth probability distribution generated using the Makhov model.*

Mean implantation depth and probability density function

The probability of an annihilation occuring at the mean implantation depth does decrease exponentially while the mean implantation depth increase in a linear fashion as shown in Figure 3.3.11.

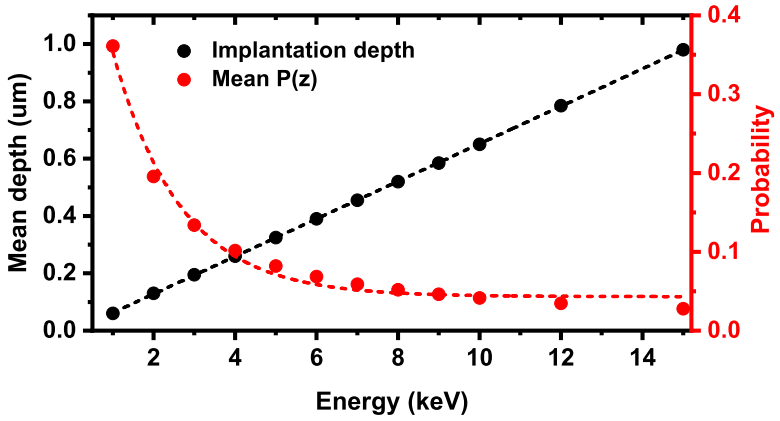

Figure 3.3.11: *The change in mean implantation depth and the corresponding probability of annihilation occurring at said depth. The mean implantation depth increases linearly whereas the probability decays exponentially due to broadening of the distribution.*

Convolution example

The distributions which describe the implantation depth profiles can be used to estimate how free volume or DBS values vary with depth in a continuous fashion. Free volume measurements at all mean implantation depths for a sample of DGEBF cure with MXDA (labelled MXDA) are shown in Figure 3.3.12. Each value of free volume represents the free volume for a distribution of implantation depths.

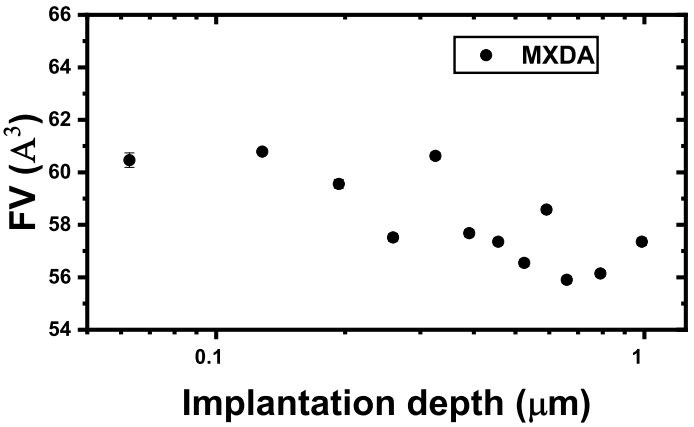

Figure 3.3.12: *Average free volume as a function of implantation depth for MXDA. Standard errors are included but are smaller than the data point size.*

Let us consider the implantation profiles and free volume values which correspond to the implantation depths of 0.06 and 0.29 um . These depths were determined by profiles obtained for implantation energies of 1 and 4 keV respectively. Figure 3.3.13 shows these profiles in blue and turquoise with the average free volume noted for their respective profiles. The profiles overlap which means the free volume measurements which correspond to each profile cannot be mutually exclusive of one another. At each depth, only a fraction of the total annihilations occur. This fraction is dependent on the probability density function, P(z,E). Where two profiles overlap, the fraction of counts at each depth in the overlapping region can be used to determine the average by considering both individual FV values. This combination is shown in red. Either side of the overlapping region, FV is completely attributed to either the 1 keV profile (left) or the 4 keV profile (right). This explains the constant values of convolved FV either side. At the point of intersection, the fraction of annihilations of both profiles are equivalent. Therefore, each profile has a 50% contribution to the actual FV value at this specific depth.

Mathematically, this convolution can be described by Equation 3.3.3;

$$FV(z,E) = \sum \left(\frac{P(z,E) \times FV(E)}{P_{tot}(z,E)} \right) \tag{3.3.3}$$

Where, FV is the average free volume, z is the implantation depth, E is the implantation energy, P is the annihilation probability and P_{tot} is the total annihilation probability. By using this for all energies, a continuous profile of FV can be obtained as shown in Figure 3.3.14. This can also be used for S, W and FFV. From this point onwards, the convolved profile will be presented alongside the original results.

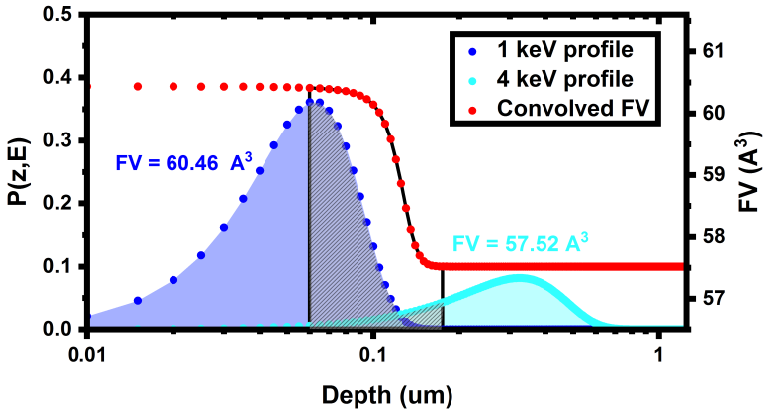

Figure 3.3.13: *An example convolution of free volume measurements made at two different implantation energies. At each energy, the depth of implantation is described by a Makhov distribution. These distributions overlap which means the individual free volumes for each energy must also overlap and a new average is calculated. This overlap is shaded in grey and the convolution of free volumes is shown in red over a range of depths.*

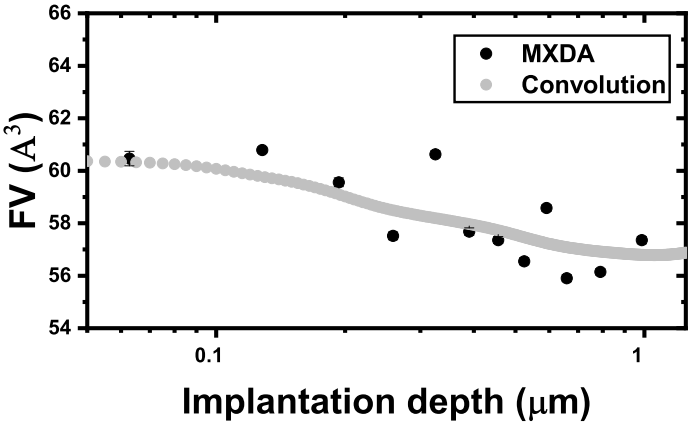

Figure 3.3.14: *The average free volume at each mean implantation depth and the convolution of all free volume measurements. This produces a smooth, continuous curve which takes into account the overlapping implantation depth probabilities at each implantation energy.*

3.3.3 Amine hardener variation

This study considers how DBS measurements and free volume are affected by varying the amine hardener used in an epoxy-amine reaction. Three samples based on the epoxy DGEBF were reacted with the amines MXDA, PACM and 1,3 - BAC.

S and W depth profiles

Figure 3.3.15 shows the S and W values as a function of mean implantation depth for each sample. It is difficult to distinguish between S and W values and therefore lines connecting each value have been included to guide the reader. From the surface to a depth of 0.11 μm implantation depth that PACM has the highest S value, with BAC second and MXDA having the lowest. This implies that nearer the surface there is a lower average free volume in MXDA when compared to BAC and PACM samples. Beyond this point it is difficult to distinguish between S values for each sample especially when taking into consideration the error bars. The W values appear indistinguishable. Statistical analysis can be implemented to determine whether results are significantly different from one another. Tests such as ANOVA or t-tests are common methods.

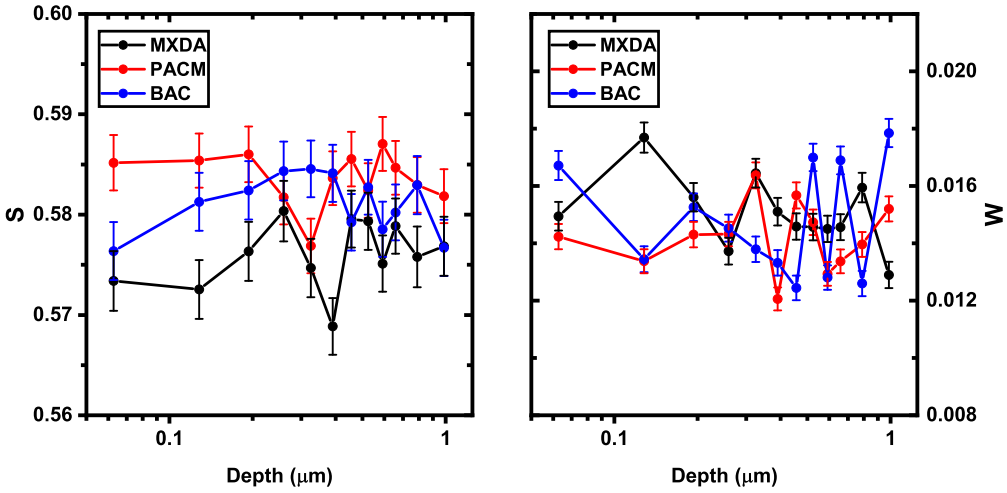

(a) S values *(b) W values*

Figure 3.3.15: *S and W values as a function of mean implantation depth for three DGEBF epoxy samples with differing amine hardeners (MXDA, PACM, 1,3 - BAC). Connecting lines are intended to guide the reader as the results overlap frequently. Standard errors are shown which were given in the program "SP".*

Example ANOVA analysis

Hypothesis tests can be implemented to show whether significant differences between results are present. In this work, an ANOVA one-way test was applied to data using Origin software. If a significant difference is registered between two results the number "1" is returned. As an example of how significance (SIG) values work, the S values over all mean implantation depths are shown in Figure 3.3.16 for MXDA and BAC samples. To give some definition to areas below the surface, the data has been separated into regions which are highlighted.

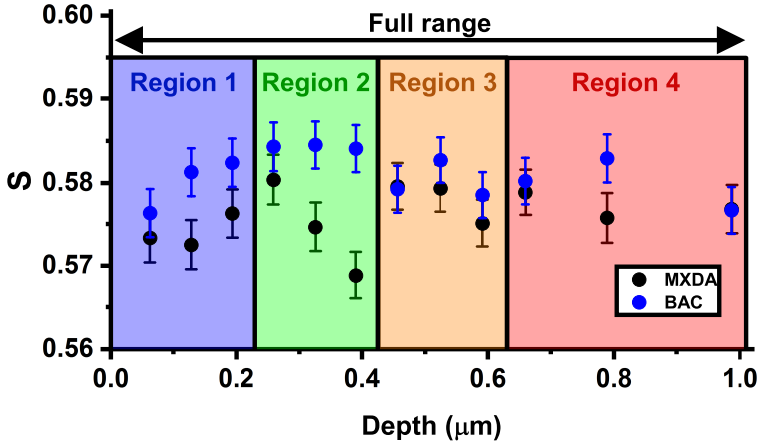

Figure 3.3.16: *S values from DBS measurements for MXDA and BAC. The four regions used for statistical analysis are highlighted. Standard errors in S are shown.*

Average S values for the full range and each region in Figure 3.3.16 were statistically compared using ANOVA. The results are shown in Table 3.3. R1 and 2 both returned a SIG value of 1 whilst both regions 3 and 4 returned a SIG value of 0. Regions 1,2 and 3 are reasonably easy to interpret in terms of whether there is a difference in results. Region 4 is more difficult to assess and this is where the hypothesis test proved to be useful. Significant differences were reported for the full range of depth with BAC having a higher S value than MXDA.

Table 3.3: *Results from one way ANOVA hypothesis testing performed in origin. Each region was analysed for MXDA and BAC samples and compared to one another. The full range of mean implantation depth was also statistically analysed. Where the number "1" features, there is a significant difference between S values.*

Significance values with respect to S values

Comparison	R1	R2	R3	R4	Full range
MXDA - BAC	1	1	0	0	1

S values

To fully demonstrate ANOVA tests, the parameters S, W ,FV and FFV will be presented in their entirety alongside average values and significance results. Figure 3.3.17 shows the S values as a function of mean implantation depth for three epoxy samples each comprising of DGEBF epoxy and one of three amines (MXDA, 1,3BAC and PACM). Over the full range, PACM has the highest S value with MXDA the lowest. As S is a relative measure of the fraction of annihilations occurring with electrons likely to be found in voids (i.e valence), this implies MXDA has the least amount of free volume annihilations whilst PACM has the highest. In R1, PACM has the highest S value near the surface with MXDA showing the lowest. Statistically, S for MXDA was lower in R2 whilst BAC and PACM were similar. The fluctuation of PACM suggests BAC is more stable in R2. R3 sees MXDA increase in S to a value which is similar to BAC. PACM however has a higher S value in this region. In R4, MXDA and BAC are considered to have similar S values with PACM being higher than both. ANOVA results are shown in Table 3.4. These results correlate with diffusion studies carried out in Section 5.8.3. in that PACM and 1,3 BAC do not resist the ingression of methanol as well as MXDA does. With S being lower in MXDA then the ingression characteristics could be explained by a reduction in free volume.

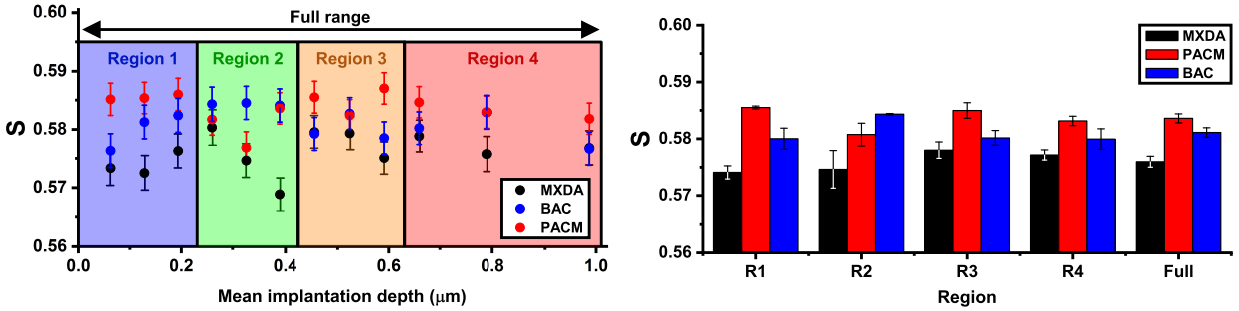

(a) *(b)*

Figure 3.3.17: *(a) S values as a function of mean implantation depth for three DGEBF epoxies containing amines, MXDA, BAC and PACM. (b) Average S values for each region (R1 - R4). Standard errors are shown in both figures.*

Table 3.4: *One-way ANOVA results. Each sample is compared for regions 1 to 4 (R1 - R4). A "1" indicates a significant difference in S between the samples concerned.*

Comparison	R1	R2	R3	R4	Full range
MXDA - BAC	1	1	0	0	1
MXDA - PACM	1	1	1	1	1
PACM - BAC	1	0	1	1	1

W values

The W values are effectively indistinguishable in every aspect as seen in Figure 3.3.18. The only difference (as shown by ANOVA tests) is seen when comparing PACM to MXDA near the surface in which MXDA has a higher W value. Beyond 0.2 μm, the data is similar. Interestingly, BAC exhibits a gradual decrease when transitioning from regions 1 to 3 which signifies a trend of sorts but this could be coincidental. As W represents the relative fraction of annihilation events occurring with core electrons, it implies that in this region of decrease that there is an increase in free volume annihilations but for reasons which will become clear throughout this chapter, this is unlikely. ANOVA results are shown in Table 3.5. As W appears to be of a random nature whereas S shows some sensible results, it suggests that W values are not useful for characterising epoxy systems.

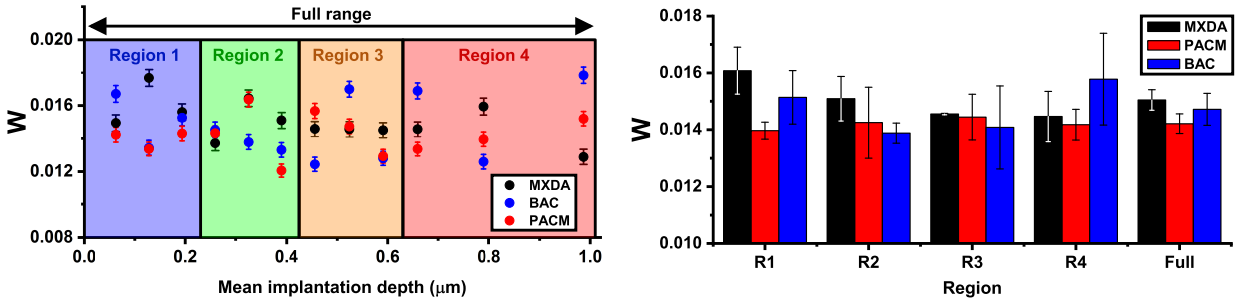

Figure 3.3.18: *(a) W values as a function of mean implantation depth for three DGEBF epoxies containing amines, MXDA, BAC and PACM. (b) Average W values for each region (R1 - R4). Standard errors are shown in both figures.*

Table 3.5: *One-way ANOVA results. Each sample is compared for regions 1 to 4 (R1 - R4). A "1" indicates a significant difference in W between the samples concerned.*

Comparison	R1	R2	R3	R4	Full range
MXDA - BAC	0	0	0	0	0
MXDA - PACM	1	0	0	0	0
PACM - BAC	0	0	0	0	0

Free volume

Free volume measurements as a function of implantation energy are shown in Figure 3.3.19. It is easy to determine that MXDA has the lowest FV over the whole range of depth without ANOVA analysis. When comparing PACM and BAC, the statistics show no significant differences in R1 and R2. R3 and R4 are considered different with PACM showing the highest FV. PACM is shown on average to have the highest FV over the entire data range with BAC marginally lower. When considering each sample individually, its interesting to see a peak for MXDA in R2 and R3. In both cases, this is a single data point which normally would be ignored. However, each individual data point is the result of several million annihilation events. This implies that these spikes in FV could point to some transitional phase. ANOVA results are shown in Table 3.5.

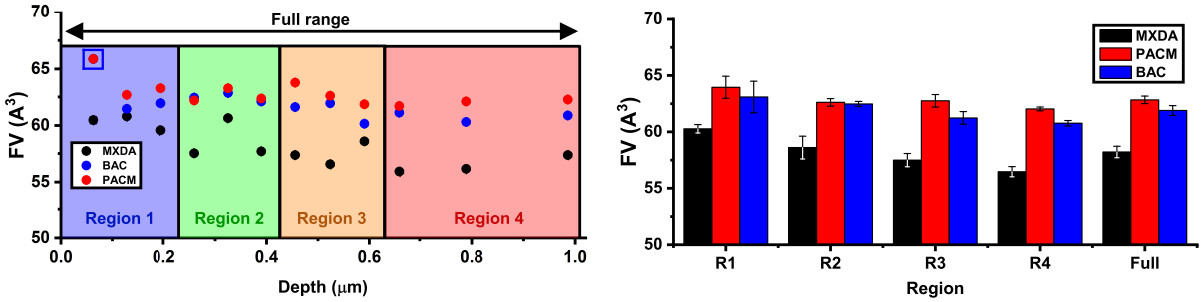

(a) *(b)*

Figure 3.3.19: *(a) FV values as a function of mean implantation depth for three DGEBF epoxies containing amines, MXDA, BAC and PACM. One data point of BAC is fully hidden behind a PACM data point. This is highlighted using a blue box in region 1. (b) Average FV values for each region (R1 - 4). Standard errors are shown in both figures.*

Table 3.6: *One-way ANOVA results. Each sample is compared for regions 1 to 4 (R1 - R4). A "1" indicates a significant difference in FV between the samples concerned.*

Comparison	R1	R2	R3	R4	Full range
MXDA - BAC	1	1	1	1	1
MXDA - PACM	1	1	1	1	1
PACM - BAC	0	0	1	1	1

Fractional free volume

The results for fractional free volumes are easily distinguishable as shown in Figure 3.3.20. PACM shows the highest FFV with BAC marginally lower and MXDA substantially so. FFV is an indication of the total free volume present so it is interesting that while, BAC and PACM could not be distinguished between free volume mesurements, they can for FFV. This suggests that while the average free volume size is similar, the total number of voids is greater in PACM.

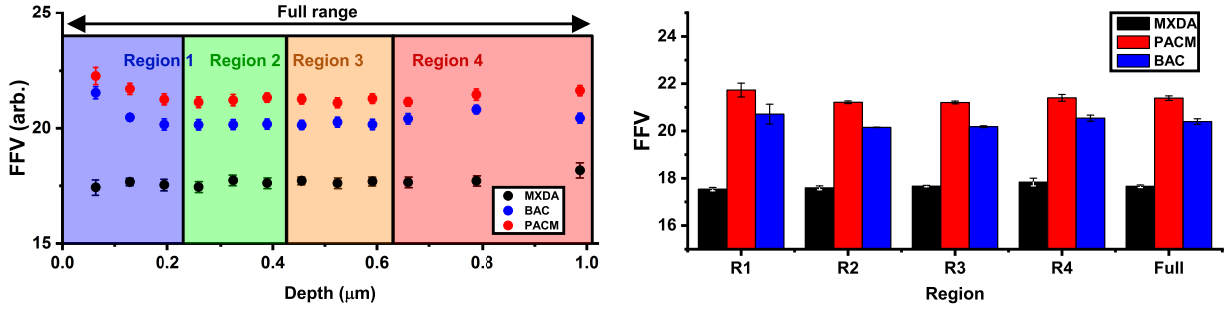

(a) *(b)*

Figure 3.3.20: *(a) FFV values as a function of mean implantation depth for three DGEBF epoxies containing amines, MXDA, BAC and PACM. (b) Average FFV values for each region (R1 - 4). Standard errors are shown in both figures.*

Table 3.7: *One-way ANOVA results. Each sample is compared for regions 1 to 4 (R1 - 4). A "1" indicates a significant difference in FFV between the samples concerned.*

Comparison	R1	R2	R3	R4	Full range
MXDA - BAC	1	1	1	1	1
MXDA - PACM	1	1	1	1	1
PACM - BAC	1	1	1	1	1

Based on the FV and FFV results for the three amine varied epoxies, mass uptake properties (Ultimate ingression, ingression and egression diffusion coefficients) of small molecules such as methanol can be suggested. MXDA would be expected to exhibit the values whilst PACM the highest. This was shown to be correct during diffusion studies which are shown in Section 5.8.3 with the exception of the ingression diffusion coefficient for PACM which was lower than BAC.

DBS and free volume comparisons

Figure 3.3.21 shows the S-W plot for the three samples. The data is effectively the same for all three samples which suggests the same vacancy type. The lack of any layers in the epoxy is the probable cause of the data clumping as was the case for DBS measurements shown in Section 3.2.3.

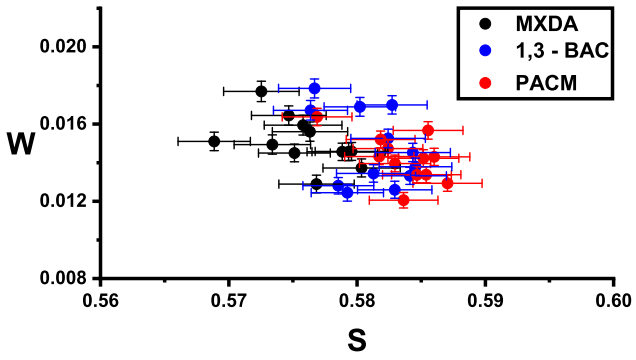

Figure 3.3.21: *Relationship between S and W for three DGEBF based resin samples cured with three different amine hardeners. Errors in S and W are shown.*

The relationship between FV, FFV and S is shown in Figure 3.3.22 for the three epoxy samples. A linear fit has been applied to all data in the graph. Whilst R^2 values were poor (<0.5), there is a small trend which shows FV and FFV increase with an increase in S. This is an expected results as S increases with an increase in the number of valence electron interactions and therefore implies an increase in void annihilations. However, if we were to only consider each epoxy samples results then this trend is not seen. This is shown by solid lines which are linear fits of each data set. This implies that S has a low sensitivity to changes in free volume which is counter intuitive.

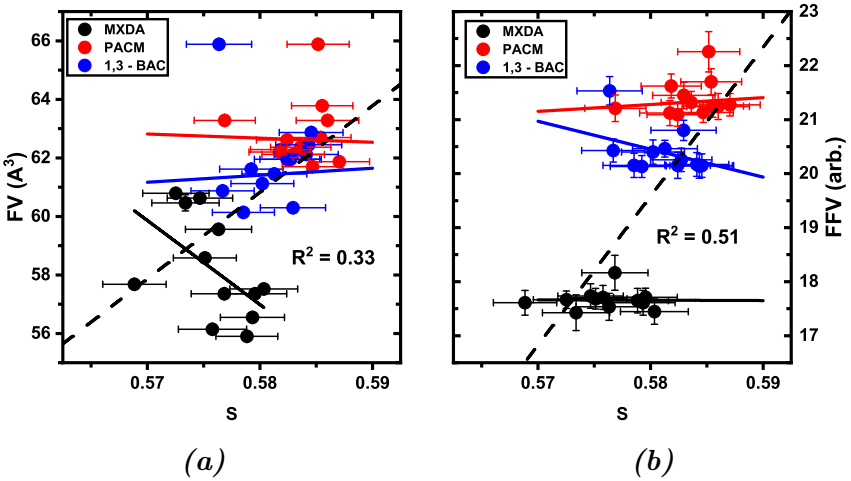

Figure 3.3.22: *(a) Free volume (FV) and (b) fractional free volume (FFV) against S. Dashed lines represent linear fits of all the data whereas solid lines correspond to each data set.*

Convoluted free volume and fractional free volume data

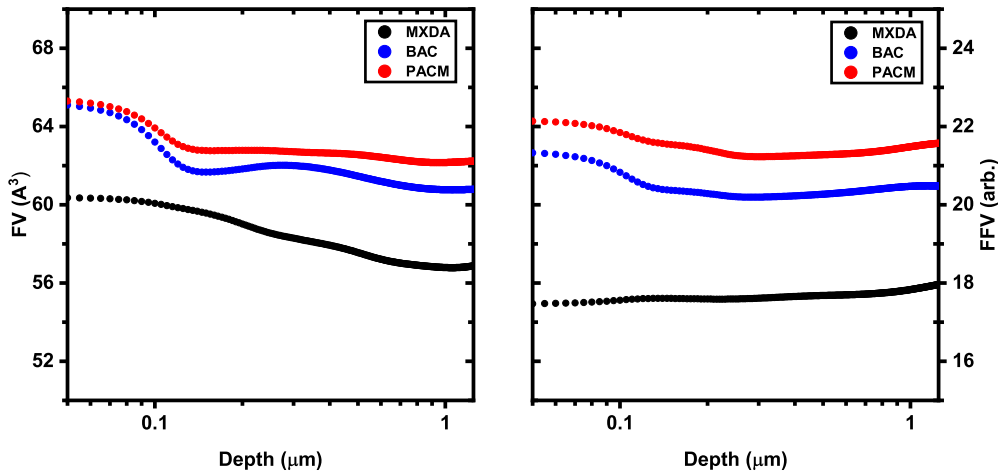

(a) *free volume* ***(b)*** *fractional free volume*

Figure 3.3.23: *Convolved (a) Free volume (FV) and (b) fractional free volume (FFV) as a function of implantation depth for three epoxies consisting of DGEBF and one of the three amines MXDA, 1,3-BAC and PACM.*

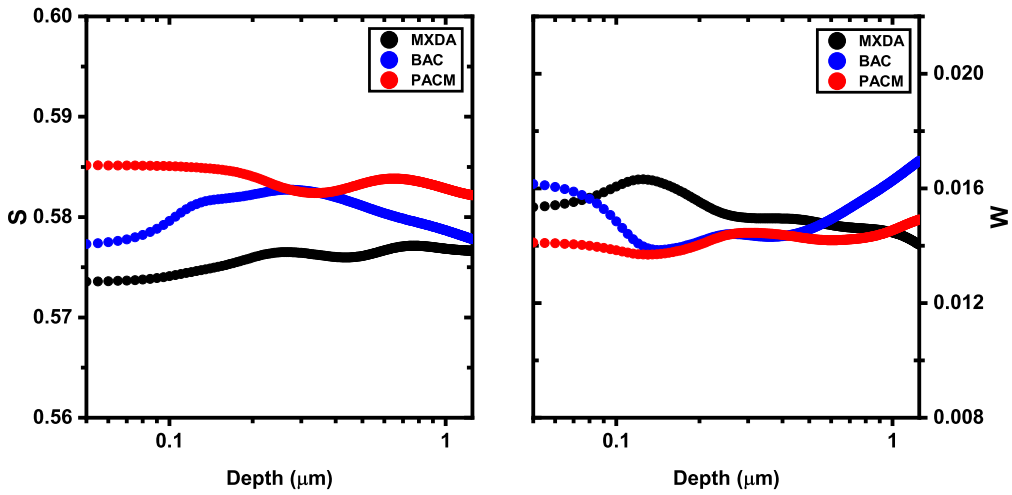

(a) ***(b)***

Figure 3.3.24: *(Convolved (a) S and (b) W as a function of implantation depth for three epoxies consisting of DGEBF and one of the three amines MXDA, 1,3-BAC and PACM.*

The DBS results for the remaining studies also showed insignificant changes and random like data in addition to a lack of trends. After presenting these results to the instrument scientists at the ELBE centre in Dresden, they advised me that an issue with detector geometry may be the cause for the lack of correlations and almost random nature of S and W values. However, lifetime data and therefore free volume data was confirmed to be reliable. This section effectively highlights some issues with the DBS aspect of MEPS and as the instrument is relatively new, this will hopefully aid the facility with future improvements. As such, the remainder of this chapter will only consider free volume and fractional free volume.

3.3.4 Effects of curing conditions

This study concerns how changes to cure schedule, environment and temperature affect the free volume (FV) and fractional free volume (FFV) as a function of positron implantation depth. Table 3.8 shows samples which will be compared here and the sample ID is also given.

Table 3.8: *Table of sample characteristics for the study focussed on curing conditions. Colour coding has been applied to some sample ID's to coincide with graphs which follow.*

ID	T_{RAMP} (°C/min)	T°C	Dwell (hours)	Environment	Amine
R2 MXDA - N	2	160	3	N_2	MXDA
R2 MXDA - A	2	160	3	Air	MXDA
R10 MXDA - A	10	160	3	Air	MXDA
R2 120C - N	2	120	3	N_2	MXDA
R2 BAC - N	2	160	3	N_2	1,3 - BAC
R2 BAC - A	2	160	3	Air	1,3 - BAC
R10 BAC - A	10	160	3	Air	1,3 - BAC

Ramp rate and environment: DGEBF - MXDA

FV and FFV results are shown in Figure 3.3.25. Over the full range, ANOVA determined that there was no significant differences between samples. R2MXDA-N and R10MXDA-A showed insignificant differences in FV for all regions. R2MXDA-A is shown to have the largest FV close to the surface (<0.1 μm) in comparison to R10MXDA-A and R2MXDA-N. The FV in R2MXDA-A decreases rapidly through R1 before further reduction in R2 to the lowest FV level. From this point on R2MXDA-A is significantly lower in average free volume than R10MXDA-A and R2MXDA-N . When comparing R2MXDA-A and R10MXDA-A, FFV is similar over the entire range. R2MXDA-N clearly shows the highest FFV over the entire range. Strangely, ANOVA tests deemed the difference between R2MXDA-A and R10MXDA-A in R1 to be insignificant. I think this could be considered a false result when using common sense. Differences between all three samples for R2 and R3 were recorded as significant with R2MXDA-N having the highest whilst R2MXDA-A has the lowest FFV. While FFV is obviously higher in R2MXDA-N, ANOVA statistics showed R2MXDA-A and R10MXDA-A indistinguishable. Similar trends are shown in the convolved data sets in Figure 3.3.26 but an almost step like phase in free volume is seen near the surface rather than the steep drop shown when using mean depth alone.

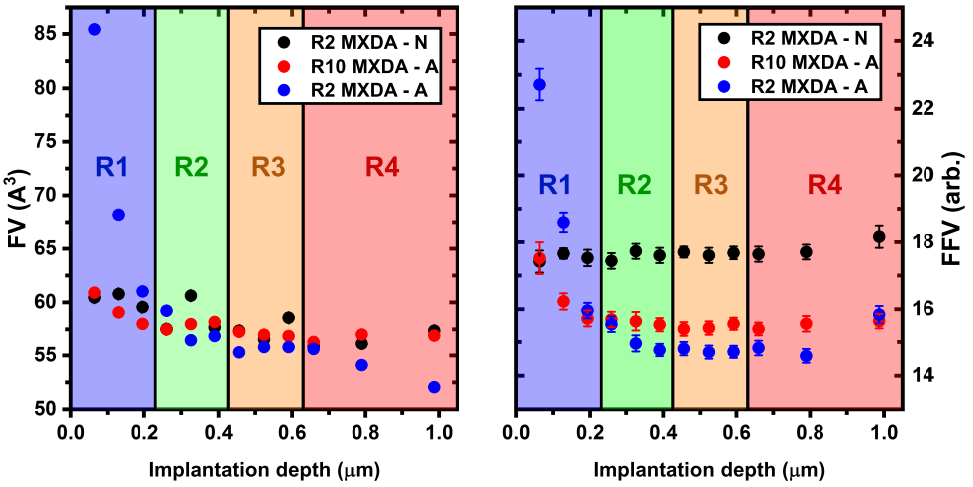

Figure 3.3.25: *FV and FFV as a function of mean implantation depth for three MXDA based epoxy samples.*

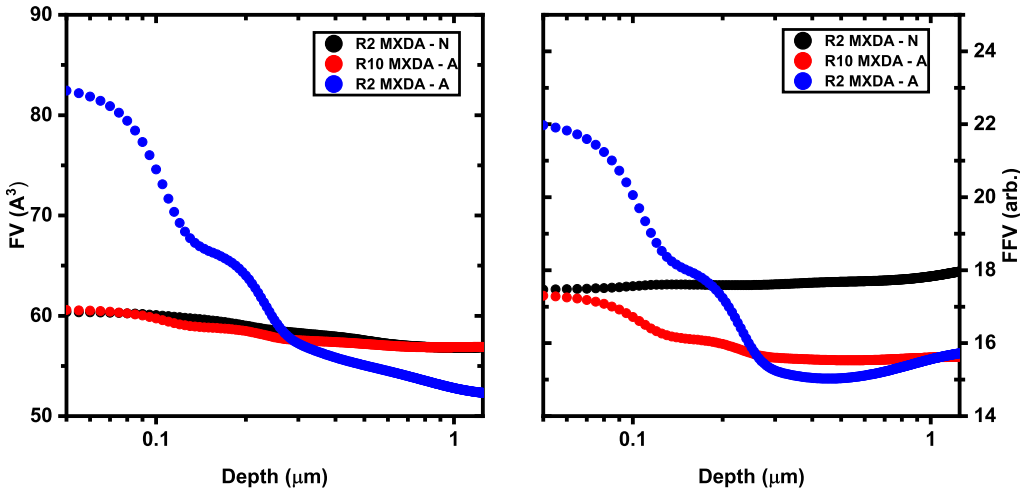

Figure 3.3.26: *The convoluted versions of FV and FFV for the cure condition study of the MXDA based epoxies.*

Ramp rate and environment: DGEBF - 1,3-BAC

The FV and FFV as a function of mean implantation depth is shown in Figure 3.3.27. ANOVA showed that for the full implantation depth range the differences were insignificant between all samples. It also showed insignificant differences for all regions (R1 - R4). The FFV did show significant differences which can be seen clearly without ANOVA analysis. R10BAC-A showed the lowest FFV across the full range and for all individual regions. R2BAC-N was shown to have the highest FFV with R2BAC-A second. This means that although the FV size between the three samples are similar, the number of voids does vary. It is interesting that the highest FFV is seen in the sample cured at a slower rate but in a nitrogen environment as this is expected to be closer to perfect stoichiometry than the other two samples. In fact, the complete opposite result is seen with the sample R10BAC-A having the lowest FFV. This sample is expected to lose the most amine due to evaporation and oxidation due to the air environment. The convolutions do show a distinct difference near the surface before all three samples converge and stabilise. The convoluted FFV show the same distinct differences as with the original data.

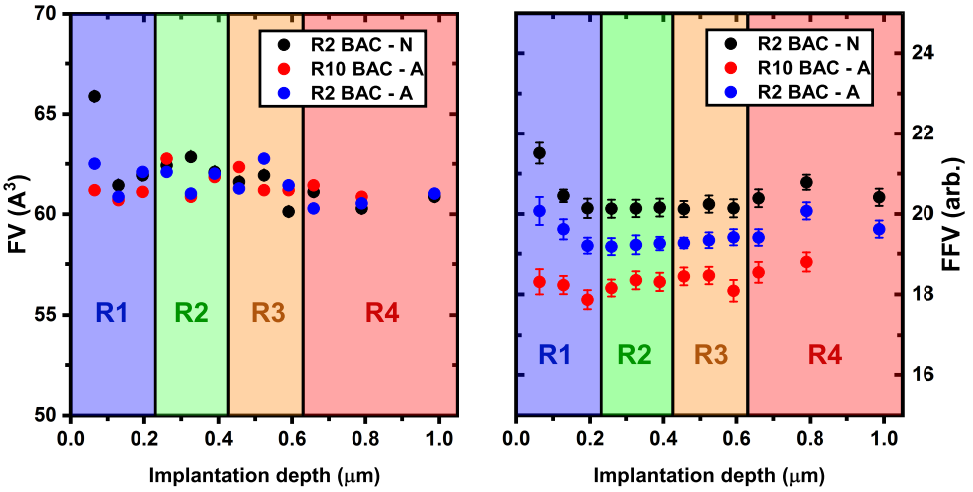

Figure 3.3.27: *FV and FFV as a function of mean implantation depth for three BAC based epoxy samples.*

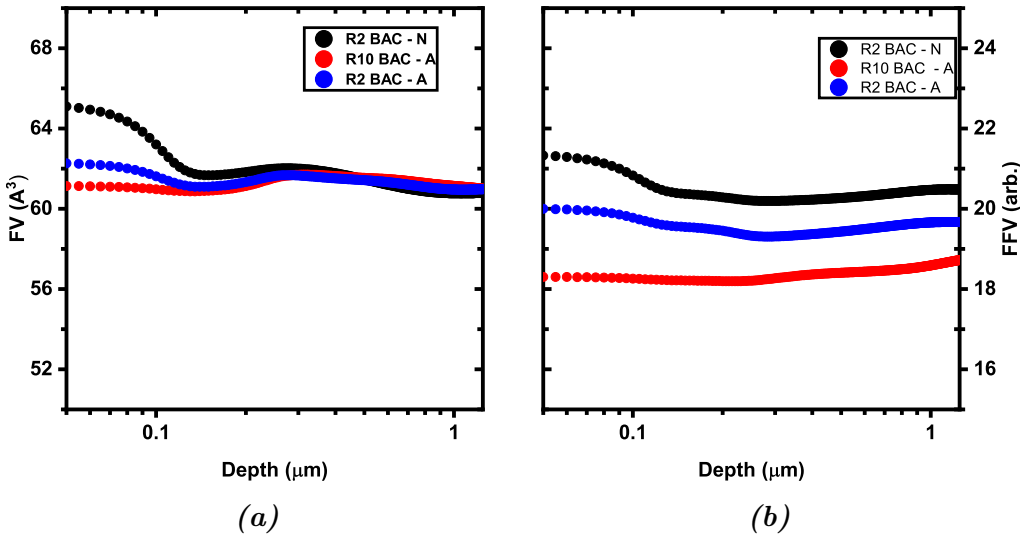

Figure 3.3.28: *The convoluted versions of FV and FFV for the cure condition study of the 1,3 - BAC based epoxies.*

Cure temperature: DGEBF - MXDA

Figure 3.3.29 shows FV and FFV as a function of mean implantation depth for two epoxies cured at different temperatures. FV is high at the surface (R1) for R2MXDA 120C-N and decreases in an exponential fashion down to a similar level to that of R2MXDA-N in R2. Beyond this region, FV is considered similar. Statistically, FV was shown to be significantly different over the full rang of depths but considering the massive drop in FV near the surface for R2MXDA 120C-N, these data sets cannot reliably be compared for the full range of depths, only regionally. FFV shows the same drop-off from R1 to R2. The only true difference is in R4 which shows R2MXDA 120C-N to drop below R2MXDA-N. It was expected that the sample cured at 120 °C would exhibit a higher free volume than the sample cure at 160 °C (R2MXDA-N) but this was only seen near the surface (i.e. R1). In R2, R2 and R3, values are similar which does not coincide with DBS measurements presented in Section refsubsec:SWPROFILESDELF. The results showed that S was lower over the majority of implantation depths for an epoxy cured at a higher temperature. However, the production method of the samples were not identical to those tested in this section and therefore cannot be directly compared.

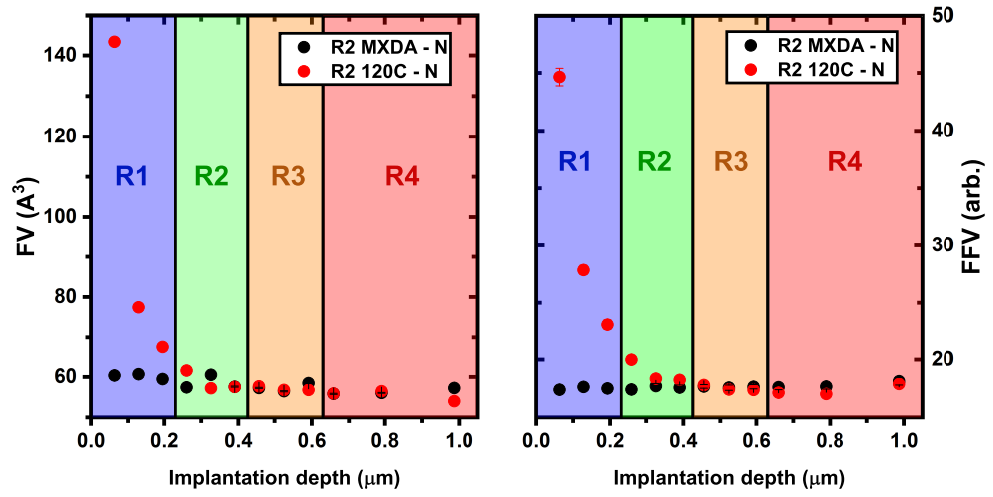

Figure 3.3.29: *The variation in FV and FFV for two DGEBF-MXDA epoxies which were cured at 120 and 160 °C (R2MXDA-N and R2120C-N respectively) in a nitrogen environment with a cure ramp rate of 2 °C min $^{-1}$.*

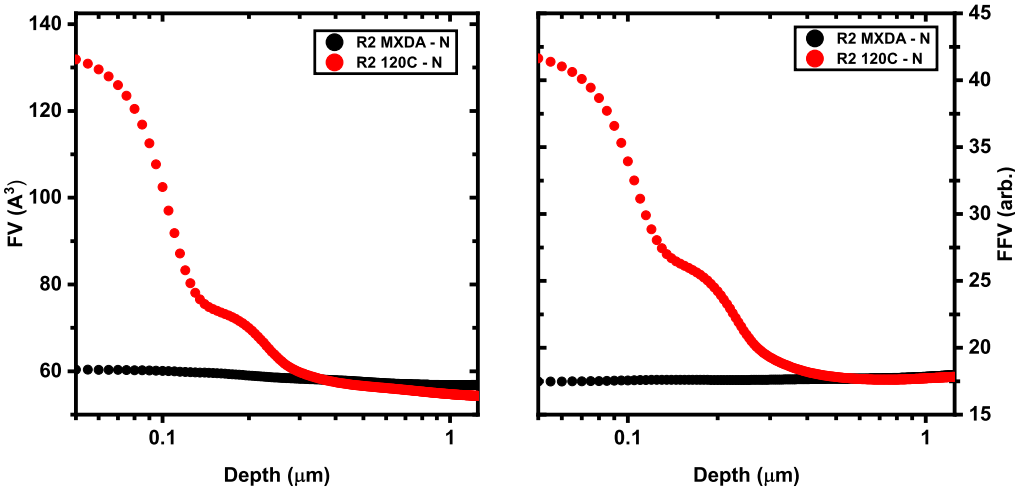

Figure 3.3.30: *The convoluted versions of FV and FFV for two samples cured at different temperatures.*

3.3.5 Epoxy ammoniation

This study compares two samples cured in the same exact cure but contained in different environments post-cure. One was placed in an ammoniated environment for a period of time (labelled AMM). Theoretically, the ammonium gas will permeate through the sample and react with functional groups on dangling chain ends. This should lead to a reduction in void size. The other sample was contained in the standard manner for this research. Figure 3.3.31 shows that , near the surface (R1), AMM has a higher FV than NAMM. R2 and R4 are statistically considered similar. The increase in free volume near the surface for AMM counters the hypothesis previously discussed. Ammonium gas may have affected the surface of the epoxy in a swelling manner but this is merely a speculative assessment. FFV shows a similar trend to FV except both samples exhibit a drop in FFV followed by an increase in R4.

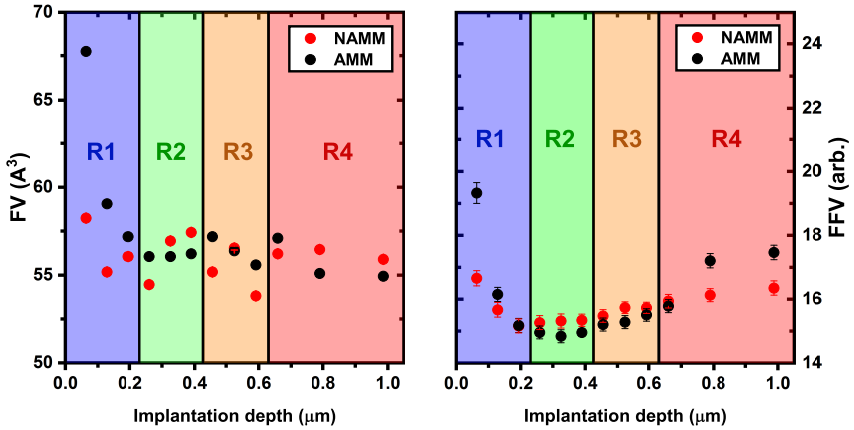

Figure 3.3.31: *FV and FFV as a function of positron implantation depth for the ammoniation study. Standard errors are present but are smaller than the data point.*

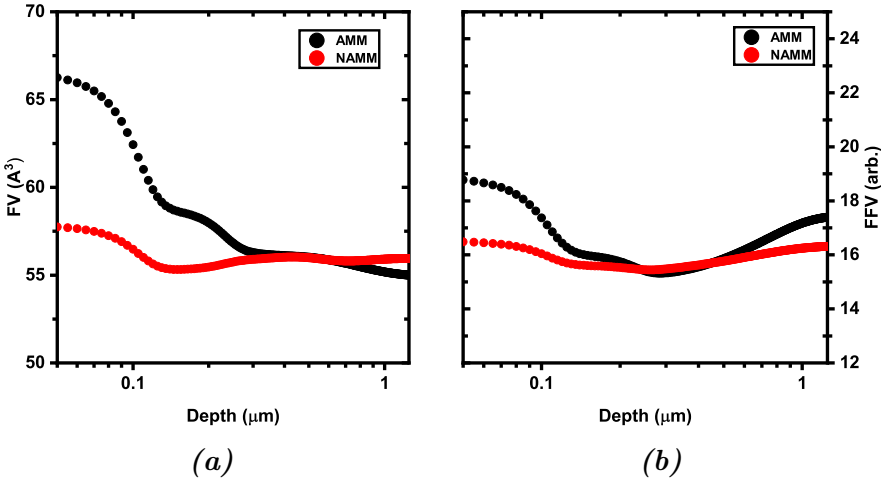

Figure 3.3.32: *The convoluted FV and FFV for the ammoniation study.*

3.3.6 Amine deficiency

This study compares two DGEBF-MXDA samples with differing stoichiometric ratios. Both are cured in the same manner but the sample labelled 80MXDA has 80 % of the amine functionality required for all epoxide groups to be reacted in an ideal scenario. Here, it is expected that FV properties should increase as it is impossible for all epoxy functional groups to react and form cross-links.

FV and FFV as a function of mean depth is shown in Figure 3.3.33. In contrast to expectations, on average 80MXDA has a lower average free volume for the full range. This is also the case for R1 and R2 before results become similar in R3. MXDA does see a decrease in FV to a lower value than that of 80MXDA for the same region. FFV shows that 80MXDA has a higher FV which drops to below that of MXDA. ANOVA showed that the differences in average values for R1 were insignificant. However, the transition to R2 is continuous and therefore, it can be concluded that in R1, this decrease is a real feature. Through R2 and R3, FFV is lower in 80MXDA but is rising in comparison to MXDA. The final region sees both exhibit the same FFV level. The convolutions of both FV and FFV are shown in Figure 3.3.34

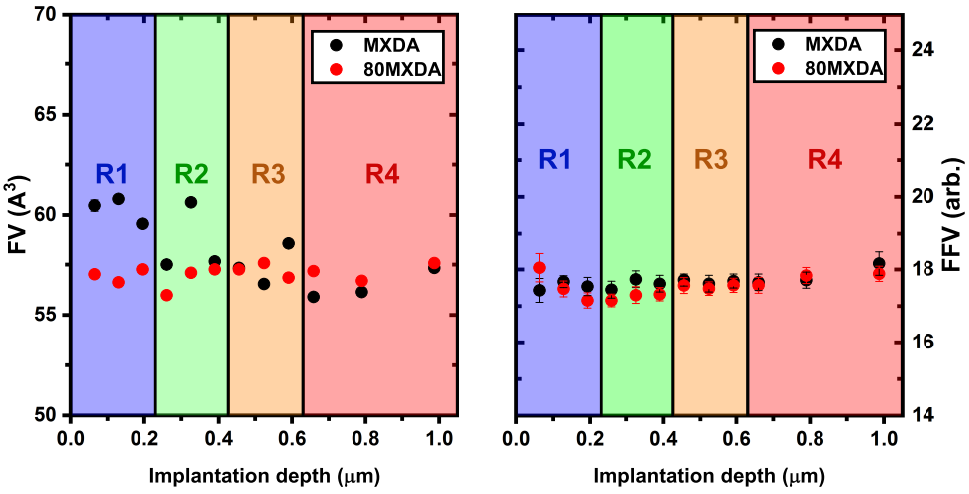

Figure 3.3.33: *Free volume and fractional free volume as a function of positron implantation depth. Dashed lines represent linear fits for regions 3 and 4. This is to emphasise that 80MXDA will most-likely have a high free volume the further into the bulk.*

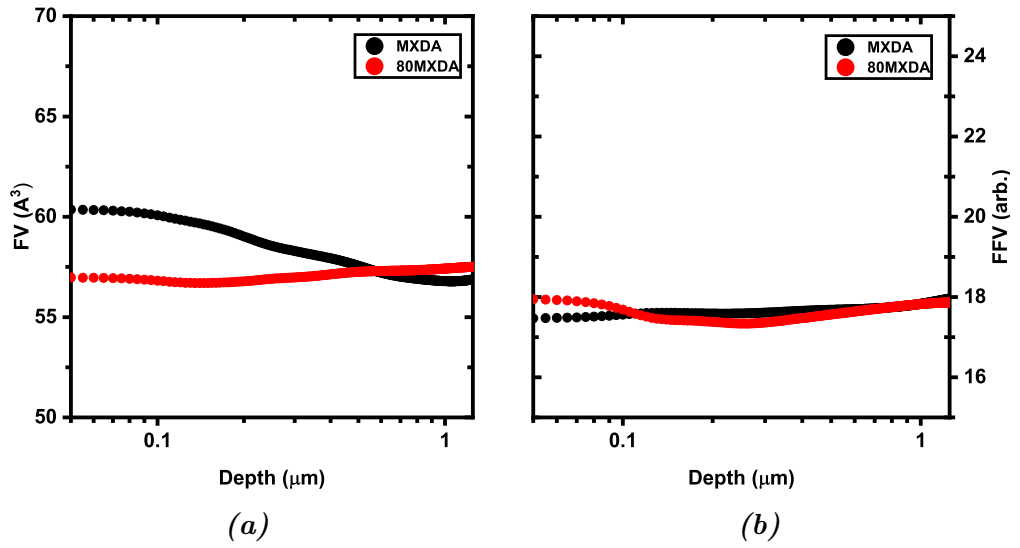

Figure 3.3.34: *The convoluted FV and FFV for two samples of MXDA-DGEBF resins. One sample labelled MXDA has been produced with ideal stoichiometry whereas 80MXDA has only 80% of amine functionality needed.*

3.3.7 Dendrimer

This study concerns the affects on free volume when introducing a dendrimer to the system. In Figure 3.3.35, it can be seen that free volume is lower near the surface in the DEND sample. ANOVA showed that the following three regions were indistinguishable. Over the entire range, the difference in FV is significant with DEND having a lower FV. ANOVA tests showed that for all individual regions and the entire range, significant differences are present. DEND has a higher FFV in each area and the full range also. The larger differences are seen at the surface and even more so in the deepest region. The incorporation of dendrimer into the epoxy network was not ideal and parts of it crashed out during preparation. Large lumps of dendrimer were visible which might mean the free volume measurement might actually be a combination of two different free volumes. As shown in Section 4.4.4., when two materials are measured with PALS together, a free volume measurement will be determined which falls between the FV value for each individual component. If the solid dendrimer has a lower free volume than the pure epoxy then this may account for this decrease in FV in the DEND sample. Unfortunately this was not tested due to limited supply of dendrimer.

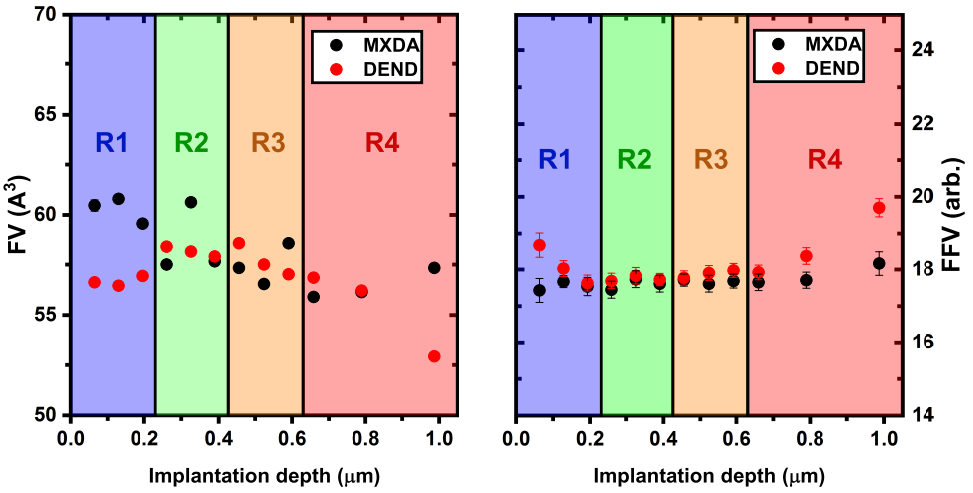

Figure 3.3.35: *FV and FFV as a function of implantation depth for MXDA and the dendrimer containing epoxy, DEND. Standard errors are shown.*

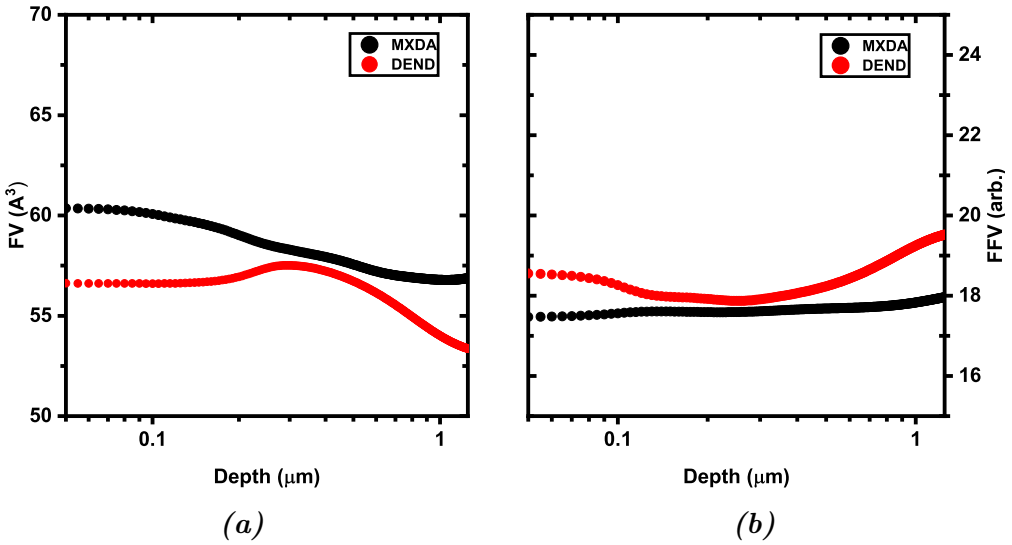

Figure 3.3.36: *The convoluted FV and FFV for MXDA and DEND as a function of implantation depth.*

3.3.8 Epoxy variation

This study compares how a change in epoxy can affect free volume properties. DGEBF-MXDA is the sample labelled MXDA which has been assessed throughout this research. The sample to compare is DEN431-MXDA labelled DEN431 which is used in industrial applications. DEN431 has a similarly high EEW to DER354 but has a lower viscosity and higher functionality. DEN431 is useful when solvents cannot be tolerated or when application temperature is relatively low.

The FV and FFV show a clear difference between MXDA and DEN431 for the full range and individual regions as shown in Figure 3.3.37. This was also confirmed in ANOVA one way testing. FV is higher in MXDA than DEN431 over the full range. At the surface (R1), this difference is the greatest before the FV values converge to a similar level but DEN431 remains lower in R2. Both samples then tend downwards slightly and both exhibit two spikes in FV at roughly the same point but this is less pronounced in DEN431. The first data point in FFV is similar for both samples before DEN431 drops significantly. From R2, FFV is stable for both samples. As DEN431 is a high quality epoxy in terms of chemical resistance, it might be expected to have a lower free volume.

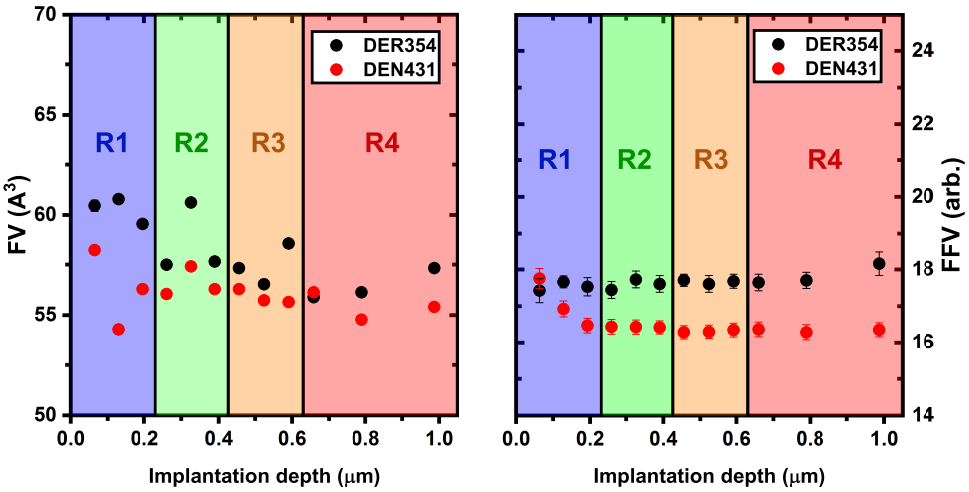

Figure 3.3.37: *FV and FFV as a funciton of implantation depth for two epoxy resins (DER354 and DEN431)*

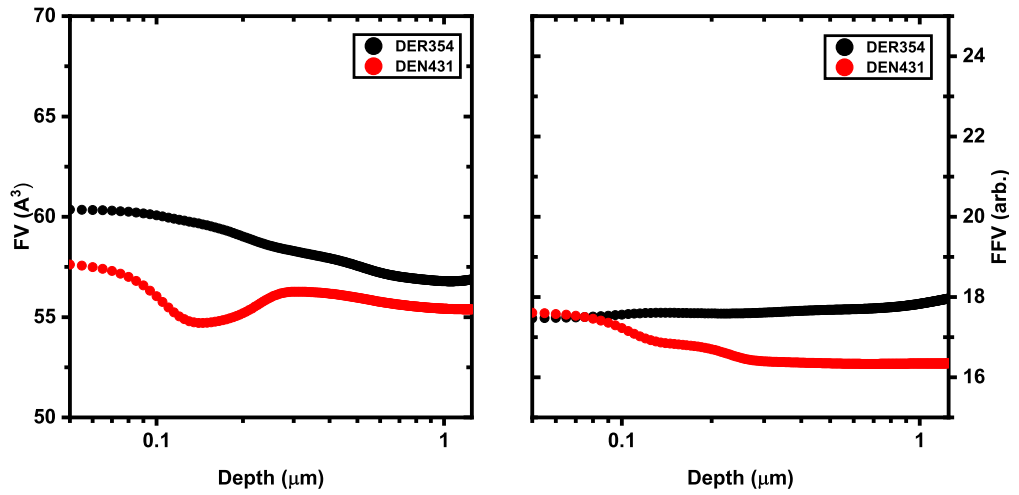

Figure 3.3.38: *The convoluted FV and FFV for MXDA and DEND as a function of implantation depth.*

3.4 Conclusions

3.4.1 Doppler broadening spectroscopy

TU Delft study - cure temperature

Two epoxy samples cured at 120 and 160 °C had S and W values which increased and decreased respectively when going from the surface to the bulk. On average in the bulk, S was higher in the sample cured at 120 °C than the 160 °C cure. This is expected to be a consequence of increased free volume (FV) or fractional free volume (FFV) and can be explained by the nature of the epoxy amine reaction. As the reaction progresses, mobility becomes hindered and dangling chain ends form which induce FV. A higher temperature increases mobility of molecules in the latter stages of reaction and allows for a higher degree of cure which reduces dangling ends and hence reduces FV.

HZDR - Measurement unreliability

The Doppler broadening measurements collected with MEPS showed unexpected results in terms of depth profile patterns when compared with those collected using VEPS. The unreliability of data was realised when comparing free volume (FV) and fractional free volume (FFV) to S values. An increase in FV or FFV should see a rise in S as this represents the relative number of void annihilations. Figure 3.4.1 shows the linear fits of FV against S for all studies which clearly show that effectively no correlations were seen.

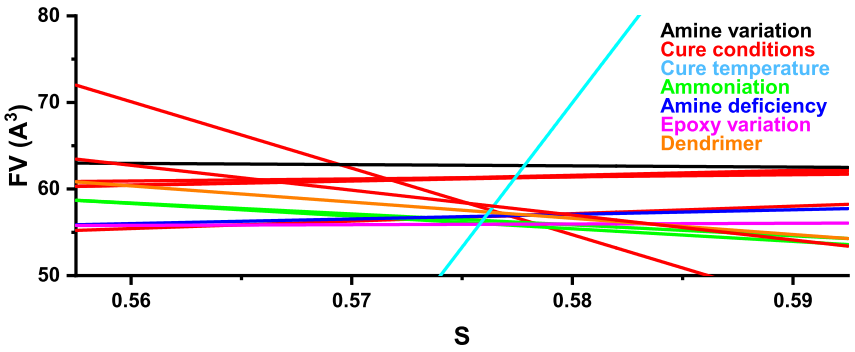

Figure 3.4.1: *The linear fits for all studies for free volume (FV) plotted against S. Normally, an increase in S should correspond to an increase in free volume. This graph emphasises the lack of such trends and confirms that the values for S are unreliable.*

When comparing the S values of different samples, significant differences did occur in a reasonable number of comparisons. Figure 3.4.2 shows how often a significant difference was seen between results for S, W. FV and FFV. As several significant differences were found for the values for S, a full assessment of the data was carried out. Unfortunately, it was recently (August 2019) brought to my attention that the data collected for DBS is unreliable. This was discovered during a conversation about the data with the instrument scientists at HZDR who confirmed that there has been an issue for some time. It is hoped that the information provided from this work will aid the facility in future improvements of the instrument. It should be noted that only the DBS data was deemed unreliable and lifetime (therefore free volume) data is reliable.

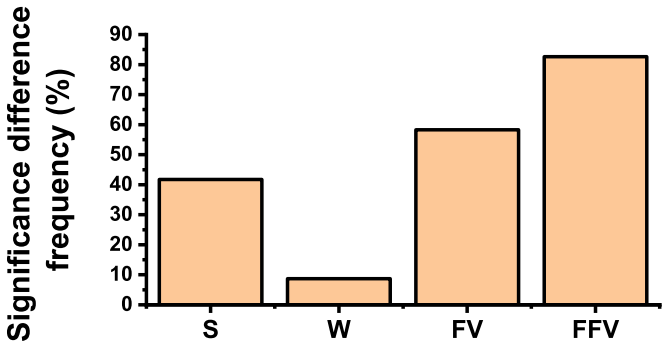

Figure 3.4.2: *The frequency of significant differences for DBS and PALS measurements as determined in ANOVA one way hypothesis testing.*

3.4.2 Lifetime analysis

Positron lifetimes were derived from lifetime spectra as a function of depth. As this research concerns free volume, only the long lifetime component (oPs) was truly considered. The free volume was calculated using the Tao-Eldrup model and was then used in conjunction with the respective annihilation intensity to yield the fractional free volume. The data was interpreted as a whole data set and also split into regions defined in the amine variation study (Section 3.3.3). All data was statistically analysed using ANOVA one way analysis. A novel representation was introduced which convoluted the depth of annihilation proabilty distributions with the average free volume associated with it to give an estimate for how free volume is distributed throughout a material.

Amine variation

In this study, the epoxy produced using the amine curing harderner MXDA resulted in the lowest free volume and fractional free volume when compared to epoxies produced using 1,3-BAC or PACM amines. Free volume was similar between BAC and PACM samples whilst FFV was highest in PACM. This trend was also seen for bulk measurements which are presented in Chapter 2.6.

Curing conditions

The rate at which the sample is heated to maximum temperature had minimal affect on the free volume for both BAC and MXDA with the exception of R2 MXDA-A. This sample which was cured in an air environment at a slow rate of 2 °C min $^{-1}$ showed a large free volume near the surface before dropping to a low value. This trend was not seen for the 1,3BAC counter as shown in Figure 3.4.3.

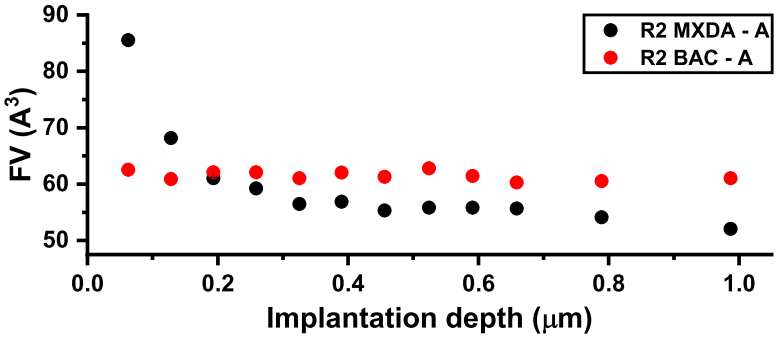

Figure 3.4.3: *Average free volume as a function of implantation depth for MXDA and BAC samples cured in air with a ramp rate of 2 °C min $^{-1}$*

Figure 3.4.4 shows the differences observed in FFV for the MXDA and BAC sample series. When curing in a nitrogen environment at a slow ramp rate (R2MXDA-N and R2BAC-N) the highest amount of FFV occured. This is counter intuitive as curing in a nitrogen environment with a slow ramp rate should minimise oxidation/carbomation effects[71] and also reduce the amine evaporation. This should cause the network to be closer to stoichiometry and therefore maximise the number of cross linked form which reduces free volume. Figure 3.4.3 also shows the inconsistency in trends for differing environments. BAC showed the lowest FFV in the sample cured in air and at a fast rate of 10 °C min^{-1} whereas MXDA did not.

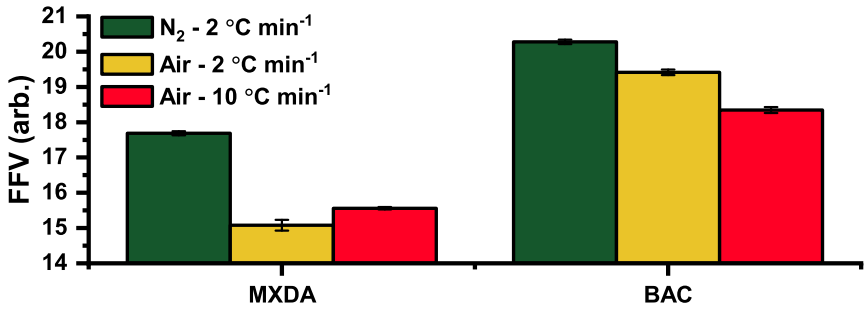

Figure 3.4.4: *The average fractional free volume from an implantation depth of 0.1 μm below the surface for two DGEBF based resins cured with different amines (MXDA and BAC). Each bar corresponds to a different cure condition which is based on the cure environment and the temperature ramp rate.*

Cure temperature

A reduction in cure temperature from 160 to 120 °C showed free volume to be large near the surface of the epoxy. The FV decreased significantly with increased implantation depth. It was expected that free volume would be larger or more prevalent when curing at lower temperatures due to less energy available to overcome steric hindrance. However, this was only seen near the surface and beyond 0.3 um, results were similar in both FV and FFV. These results do not follow the conclusion made with regards to the Delft DBS measurements.

Epoxy ammoniation

Placing samples of DGEBF-MXDA into an ammonium gas environment produced results which opposed those expected. Ammonium gas was expected to permeate through the network and react with dangling chain ends which theoretically would reduce free volume. Near the surface it was shown that ammoniation actually increased at the surface before similar values were seen beyond 3 μm. This may be due to network swelling to a depth of 3 um but cannot be confirmed.

Amine deficiency

In an attempt to purposely increase free volume, an epoxy sample was produced with insufficient amounts of was amine. Free volume was actually seen to decrease near the surface rather than increase. However, as FV measurements were made at deeper implantation, the amine deficient sample showed signs of FV/FFV increasing to levels which were greater than that of a stoichiometric sample.

Dendrimer incorporation

The incorporation of the denrimer PAMAM decreased the FV over the full range on average whilst FFV was seen to be marginally higher than a pure epoxy network. This decrease may be due to a combination of free volume measured in solid dendrimer which crashed out during epoxy production and FV in the epoxy. If the solid parts contain free volume measurements which are lower than that of the pure network then this would cause the collected lifetime spectra to be a combination of two materials and therefore a false calculation of free volume is made.

Epoxy variations

A high quality epoxy DEN431 was compared to DER354. Both were cured with MXDA and it was seen the DEN431 had a lower free volume and fractional free volume.

General conclusions

To conclude, it has been shown that where chemistry is similar, only minor changes in free volume are seen and are most common near the surface. When the chemistry is changed, the change in free volume properties are more pronounced. This is emphasised by high statistical measurements made at implantation energies of 2, 5 and 10 keV.

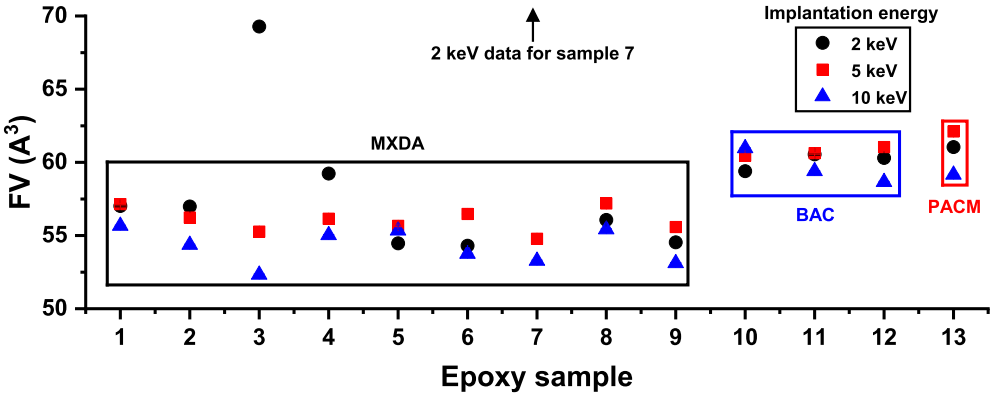

Figure 3.4.5: *Free volume at implantation energies 2, 5 and 10 keV for all epoxy samples. Coloured boxes highlight the amines which correspond to the contained data points.*

For every sample except the amine deficient epoxy, FV was seen to decrease as a function of implantation depth. Figure 3.4.6 shows the linear fit over the full range for all samples. This depicts this general decrease in free volume with implantation depth. Two curves are exponentials as this seemed more appropriate based on the results.

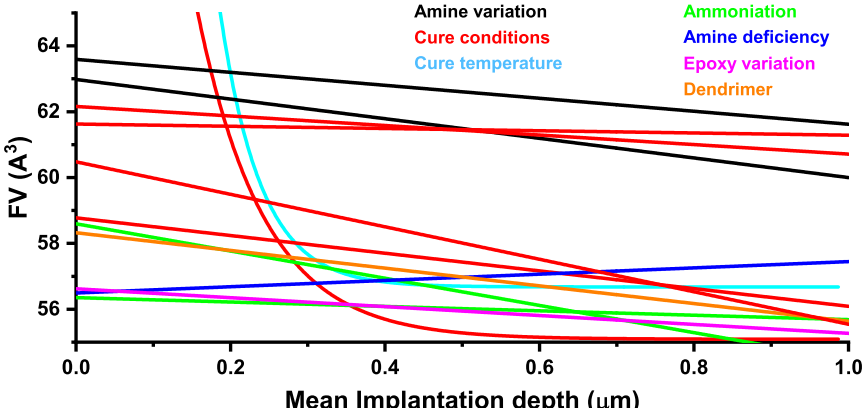

Figure 3.4.6: *Linear and exponential fits of free volume data for all samples. The colours correspond to the study which the sample belongs to. In general, free volume decreases with increase implantation depth with the exception of the amine deficient sample.*

4

Construction and testing of PALS

4.1 Introduction to chapter

This chapter presents information on the PALS system constructed in Sheffield to be used for free volume studies. Details will be given such that the reader could purchase and assemble a similar system if desired. Each component will be discussed in terms of general function, justification of choice and also pricing. The key aim here is to produce a system which is capable of measuring orthopositronium lifetimes in a reliable manner. This lifetime measurement concerns free volume annihilation which is the key feature of this work.

4.2 Equipment selection

This section discusses each component of the Sheffield positron annihilation lifetime spectrometer (SPALS). Each component is introduced such that the functioning of a PALS system can be discussed in a logical order. Equipment used in other studies will be compared to that used in this work and reason for choosing specific equipment will be justified. As this project had a total consumables budget of £21,000, pricing was of utmost importance.

4.2.1 Positron source

The key component of PALS is of course the positron source. The source constantly emits positrons at rate referred to as the activity[118] and is usually given units of Becquerels or Curies. One Becquerel is the equivalent of one emission per second and is a suitable unit for relatively low radioactive sources. One Curie represents 3.7×10^{10} emissions per second and is useful when dealing with high activities[118]. For successful analysis of lifetime spectra, a minimum of 1 million annihilation events are recorded. Therefore the activity needs to be sufficiently high to reduce the lifetime spectral acquisition time. However, this value is limited by the quality of the equipment used and safety concerns. A high activity requires better quality instrumentation in terms of timing, due to a reduced time interval between each positron emitted. For PALS, this is an issue as a birth signal from one annihilation event may be paired with an annihilation signal from a different event which of course is a false measurement. These false measurements increase the amount of background noise. The most important consideration is minimizing the individual dose to the user to prevent radiation illness. The easiest methods for reducing the dose of radiation is shielding in the form of lead bricks or increasing the distance between the source and user. When setting up an experiment, these methods may not be possible. Therefore, minimizing the dose can be achieved by using a less active source which is proportional to the effective dose rate (D_{eff}) as shown in Equation 4.2.1. (A) is the activity, (E) is radiation energy in MeV, (f) is the fraction of emissions for respective energies and (L) is the distance between the centre of the source and any body part.

$$D_{eff} = \frac{AEf}{7L^2} \tag{4.2.1}$$

The radioactive half-life is the time taken for the activity of the source to reach half the initial activity[118]. The half-lives of some commonly used isotopes are shown in Table 4.1. A long half-life is useful as this means the source can be used for a greater length of time. However, with an increased half-life, the routes for disposal become more expensive or it requires a greater amount of time to dispose of cheaply. Germanium - 68 and Colbalt - 58 could be used for some time but would need replacing much sooner than Sodium - 22. They are also less available commercially. Copper - 64 is used in the field of medicine such as Positron Emission Tomography (PET).

Table 4.1: *Half-life values of some commonly used isotopes in positron research.*

Isotope	**Half-Life**
^{22}Na	2.6 years
^{68}Ge	271 days
^{58}Co	70.86 days
^{64}Cu	12.7 hours

Another thing to consider is the ability to handle the source. When using sources for PALS, a dry source consisting of radioactive material sealed by Kapton is commonly used. When making sources for PALS it is helpful to use a ^{22}NaCl salt solution. Sources are prepared by depositing droplets on Kapton layers which dries leaving a radioactive salt.[87] Preparing a custom made positron source was considered but due to a lack of necessary laboratory conditions, this was not possible. The positron source used in this research was purchased from HTSL. Its technical information is listed in Table 4.2 and the cost can be found in Section 4.2.7 .

Table 4.2: *Technical information for the positron source used in this research as given by High Tech solutions Limited.*

Technical Information	
Source Identifier	POSK - 22 - 1.85 MBQ
Activity	1.85 MBq ±15 %
Active dimensions	5.08 mm diameter
Overall dimensions	12.7 mm diameter
Temperature Limits	Up to 200 °C
Other	Not suitable for use in Vacuum

4.2.2 Scintillating material

As previously discussed in Chapter 1, a gamma photon will be emitted a few picoseconds after positron emission and interact with a scintillator. This is a material which undergoes luminescence when ionizing radiation is incident on it. Atoms in the material interact with particulate radiation by absorption which causes the atom to excite and upon relaxation, produces a number of photons. The number of photons produced from a single interaction is related to the energy of the incident radiation.[118]. This process is depicted in Figure 4.2.1.

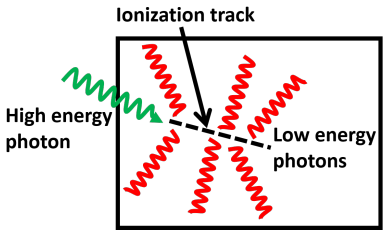

Figure 4.2.1: *Radiation incident on a scintillating material producing low energy photons.*

The emitted photons have a distribution of wavelengths which needs to be taken into account in order to be compatible with the photomultiplier tubes to be used. Each scintillator has its own characteristic distribution of emission wavelengths. Two example distributions are shown in Figure 4.2.2 for a (a) EJ 232 fast plastic and a (b) barium fluoride (BaF_2) crystal scintillator.

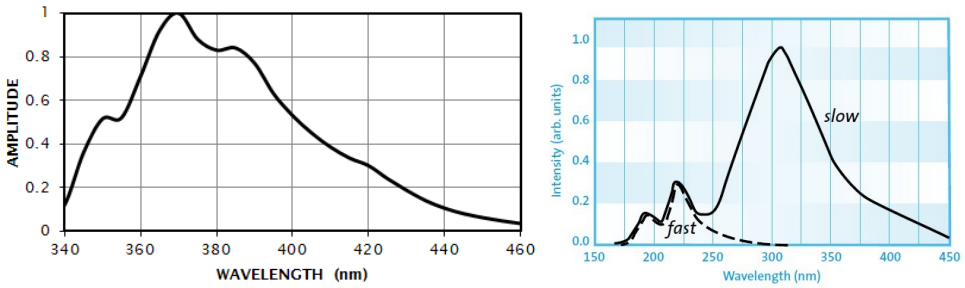

(a) *EJ-232* ***(b)*** *BaF_2*

Figure 4.2.2: *Wavelength emission spectra the commonly used crystal scintillator BaF_2 and the fast plastic scintillator EJ-232 used in this research. Images were reproduced from supplier data sheets which can be found in the following links: (a) https://eljentechnology.com/products/plastic-scintillators/ej-232-ej-232q (b) https://www.crystals.saint-gobain.com/sites/imdf.crystals.com/files/documents/barium-fluoride-data-sheet.pdf*

For these photons to be detected by a coupled PMT, the material of the PMT input window must correspond somewhat to the photon wavelength profile. Depending on the application, the number of PMT's available might be limited. This project concerns fast timing measurements and unfortunately this means suitable PMT's are sparse. The lack of PMT's available also limits the number of suitable scintillators . A large portion of the emission range should be detected by the PMT and ideally with the maximum emission in the centre of this range.

The scintillator efficiency (SE) is also worthy of consideration. The SE is the number of photons produced due to incident radiation and is dependent on the energy of said incident radiation. The SE is usually given as a comparison to a reference material and is called light output[118]. This comparison is generally made to anthracene as it has a high SE[119]. How quickly this process of emission occurs is also of great importance in this project due to fast-timing needs. The decay time of the scintillator is therefore considered. The decay time determines the rate at which the light is emitted following the excitation of the atom. This must be low to avoid light emissions from different annihilation events combining. An overlap of event signals causes false measurements to be recorded and included in the lifetime spectrum. An example scintillation pulse is shown in Figure 4.2.3. This was generated in origin software software using an exponential growth followed by an exponential decay function.

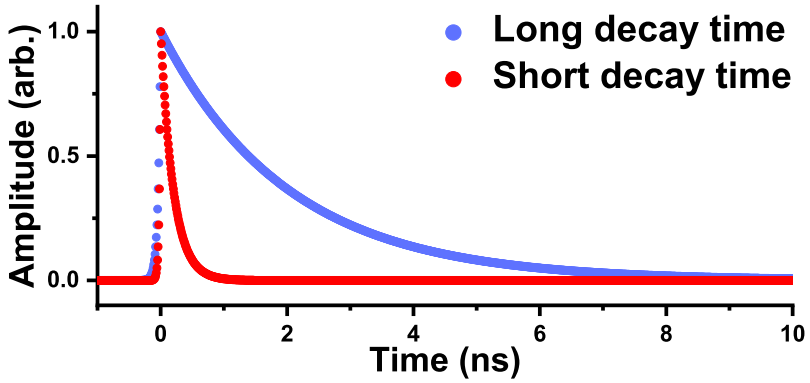

Figure 4.2.3: *An example of how a long and short scintillator decay vary. These curves were generated based on an exponential growth followed by a decay using Origin software.*

Barium flouride (BaF_2) crystal scintillators are commonly used in positron annihilation studies due to their fast time response.[49,120,121] Due to its crystalline structure, backscattering effects are more likely to occur. As such, the size and shape of the scintillator should be considered to reduce this. In recent times, fast plastic scintillators are being utilised.[98,122,123] Due to their non crystalline structure, scattering effects are reduced and therefore larger dimensions can be used. In this research, an EJ232 fast plastic scintillator is used. A comparison between BaF_2 and EJ232 scintillators is shown in Table 4.3 for the key properties which have been discussed in this section.

Table 4.3: *Comparison of some key properties between EJ232 fast plastic and a barium Flouride crystal scintillator. Note: slow and fast refer to the two distributions of wavelength emission in BaF_2 which have different timing characteristics.*

Property	**EJ232**	**BaF2** slow (fast)
Scintillation Efficiency (photons/ keV)	8.4	10 (1.8)
Light output (% Anthracene)	55	36.78 (6.90)
Decay time (ns)	1.6	630 (0.6-0.8)
Wavelength maximum emission (nm)	370	310

4.2.3 Photomultiplier tubes

Photoelectron emission

The photons produced by the scintillating material have relatively low energies. A photomultiplier tube can convert these photons into a detectable electrical current. The photons pass through a window and are incident onto a photocathode. The photon flux produced by the scintillator converts into electron flux via the photoelectric effect[124]. The electrons bound to the photo-cathode absorb the energy from the photons and if the photon energy is higher than the electron's work function energy, electron emission occurs (Figure 4.2.4). Sufficiently high energies can result in multiple electron emission.

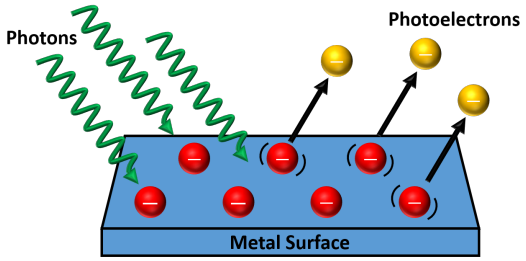

Figure 4.2.4: *Depiction of the photoelectric effect. Surface electrons absorb photon energies and are emitted via the photoelectric effect.*

Electron amplification

The photoelectrons accelerate through a vacuum and are directed towards the first of a series of dynodes by the focusing electrode. These initial photoelectrons bombard the dynode, which causes further electron emission, which then interact with the next dynode. This process continues, with the number of electron emissions increasing, until reaching the final dynode. The amplified number of electrons are emitted from the last dynode, collected by the anode and outputted as an electrical current. This amplification and the fundamental components of a PMT are shown in Figure 4.2.5.

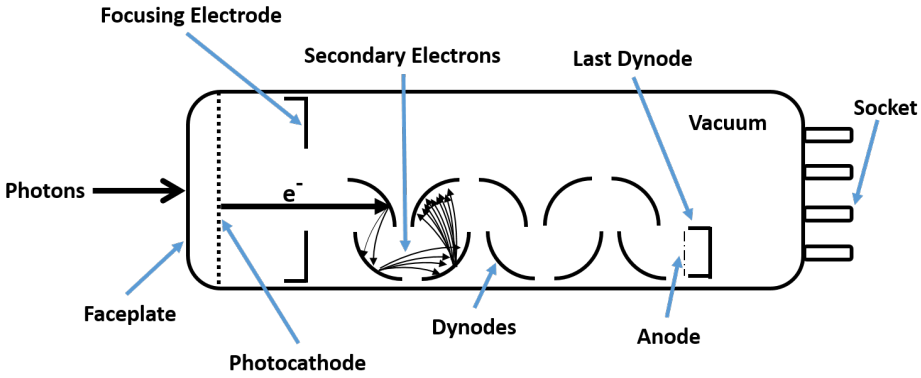

Figure 4.2.5: *The key components of a photomultiplier tube and a depiction of the conversion of photons to an amplified electric signal. The is an original diagram with influences from a number of photomultiplier handbooks/data sheets.*[125]

Photomultiplier selection
The XP2020 PMT is commonly used in positron anihilation studies[43,120,126,127] but due to it's discontinuation, alternative options were explored. After several consultations with an expert at Hamamatsu in addition to other researchers in the field, the H1949-51 PMT was selected to be used for this research. This is a custom made hybridized instrument based on the on the R1828-01 model. A potential divider, magnetic shield and connecting socket have been incorporated. Its properties are very similar to that of the XP2020 as shown in Table 4.4. It should also be noted that this is perfectly compatible with the EJ232 scintillator (i.e full range of wavelengths covered). This PMT is now available on Hamamatsu store and advertised for fast-timing applications.

Table 4.4: *Property comparison between the commonly used XP2020 and the H1949-51. (*At optimal voltage).*

Property	**H1949-51**	**XP2020**
Spectral range (nm)	300 - 650	270 - 650
λ of Max. Emission (nm)	420	420
Rise Time (ns)	1.3	1.6
Gain *	2 $\times 10^7$	3×10^7

4.2.4 High voltage power supplies
Each electrical component of a photomultiplier tube (PMT) needs a voltage supply. To provide these voltages, a high voltage power supply is used to distribute the necessary voltage to each component via a potential divider. The required voltage for each component may vary and as such the potential divider needs to be set up with the correct arrangement of resistors. In this research, a dual high voltage power supply provided by Rehberg Electronic has been used. It has the ability to supply two channels with voltage up to 4 kV with a stability of 5 $\times 10^{-4}$ V. The stability is important, as the voltage supplied to the PMT affects the output of the PMT. This output is crucial for the timing measurement of PALS. This instrument is compact and also has the advantage of remote control usage by terminal commands and USB connection.

4.2.5 Signal discriminator
Time-to-amplitude converters
In order to correctly measure positron lifetimes, the output signals from the PMT must be differentiated from one another. If all signals are simply stored to memory then a large amount of the data is not useful. Post-processing of data to extract the desired signals (i.e a birth and annihilation signal) would be a lengthy process not to mention the increase in acquisition time. A general method of signal discrimination is to use time-to-amplitude (TAC) converters. A time window is set for which two pulses must enter the component for a measurement to be recorded. When a signal enters the component, a capacitor is charged. Once the next signal enters, the capacitor stops charging and a pulse is produced with an amplitude proportional to the charge on the capacitor.

4-fold coincidence unit

In this work, a relatively new instrument is used for discrimination called a 4-fold coincidence unit (CU). The CU can be set-up to detect signals above a certain threshold voltage and also whether multiple signals pass within a certain time window up to 2 μs. This thresholding allows for low voltage signals due to Compton scattering and digitizer noise to be ignored, which increases the useful count rate (see Section 4.3.4 for further details). A flow chart shown in Figure 4.2.6 outlines the basic functioning of the CU unit.

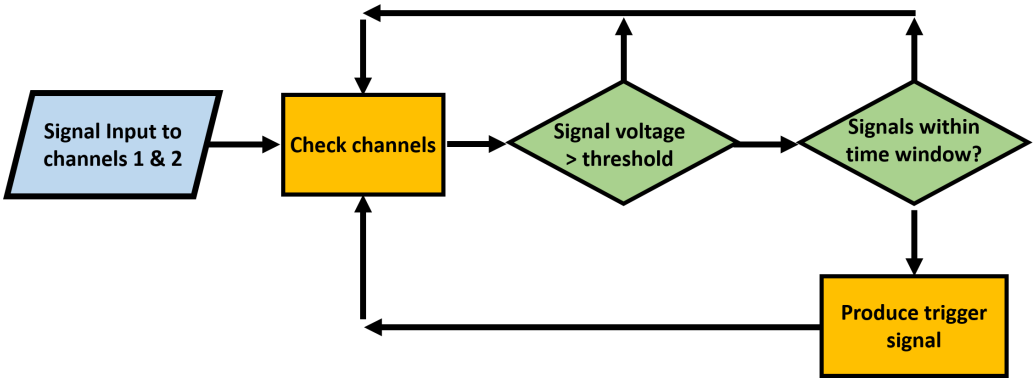

Figure 4.2.6: *Flowchart outlining the basic functionality of the discriminator unit. Electrical signals enter the instrument and if they meet the correct conditions, a trigger signal is outputted to the digitizer.*

The output signals from the detectors are split between the coincidence unit and the digitizer. When a coincidence event is detected, a trigger pulse is sent to the digitizer. This acts as a signal for the digitizer to record any immediate signals. Any signals which do not meet the criteria are ignored reducing false acquisitions. Figure 4.2.7 shows the the position of the CU in the PALS setup.

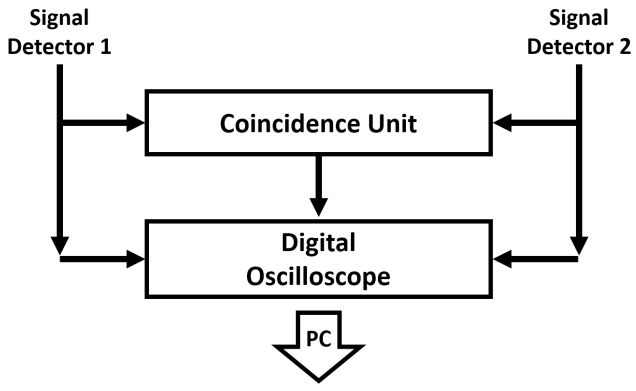

Figure 4.2.7: *The output signals from the detectors first pass through the coincidence unit. After discrimination, a trigger signal is sent to the digitizer to indicate that a lifetime measurement can be made. This pre discrimination increases acquisition speeds and reduces post processing steps.*

4.2.6 Digital oscilloscope

As PALS fundamentally measures several electrical signals, an oscilloscope is required for this purpose. Furthermore, a system capable of measuring signals rapidly is needed due to the scale of typical positron lifetimes ($\approx ns$) . In this research, digital oscilloscopes are used. Traditional PALS involved the use of analog sytems which requires extra electronics such as signal delays and time-to-amplitude converters[49]. Digital PALS reduces the number of electrical components as the signal amplitudes are recorded as a function of time and ouputed directly to a PC. Digital systems have been shown to perform to a similar level as analog systems so there is no loss in quality.[49] [120] The following defines some key features of a digitizer (Information obtained from the *Picoscope 6407 User Guide*[128]);

Channel Number: The number of signal channels available to use simultaneously.

Bit Resolution: How precisely the system converts the measured analog signal to a digital value. A computer stores values in a series of 1s and 0s (i.e. binary or in bits). The higher the bit resolution, the more precise the measurement. Effectively, the maximum number of bits that can be stored is equal to 2^n where n is the number of bits as shown in Table 4.5.

Table 4.5: *Technical comparison between the Picoscope 6407 digitizer and the DRS4 evaluation board.*

Resolution (bits)	Max stored values
1	1
2	4
4	16
8	256
16	65536

Bandwidth: The measure of a channel's ability to pass a signal without significant attenuation over a range of frequencies. A high bandwidth allows signals of a higher frequency to pass unaffected by attenuation.

Buffer Size: Data collected is initially stored on the digitizer, prior to being transferred to the PC. The buffer size is the memory available on the digitizer itself. A large buffer size is desired as this allows a large amount of data (i.e. measurements) to be stored before being transferred to the PC. This effectively reduces the "down-time" during data transfers which ultimately halt data collection for a period of time.

Sampling Rate: The number of measurements that can be acquired per second. When dealing with fast timing applications it is important to have a high sampling rate to provide an accurate representation of the signals being measured. Figure 4.2.8 shows how a low sampling rate can produce misleading results.

Picoscope 6407 High-Speed Digitizer

The initial digitizer used in this research was the PicoScope 6407 high speed digitizer supplied by Pico Technology. This is a compact 4 channel digitizer which connects to a PC via USB.

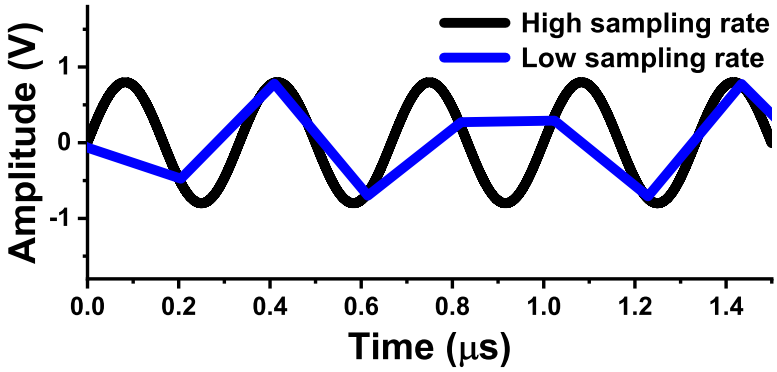

Figure 4.2.8: *A comparison between a high and low sampling rate for the same signal measurement.*

This digitizer comes with user friendly software aswell as software developmnent kits for several programming languages (MATLAB, C, C#, LabVIEW etc).

DRS4 Evaluation Board

An alternative, is the Domino Ring Sampler Evaluation Board version 4 (DRS4). This is a high speed digitizer prudcued at the Paul Sherrer Institute (PSI). This unit has some drawbacks such as buffer size but is suitable for most fast timing applications. PALS acquistion software has also been developed for the DRS4 board in the form of *QTPALS by Martin Petriska*[129]. The two digitizers used in this research are compared in Table 4.6.

Table 4.6: *Technical comparison between the Picoscope 6407 digitizer and the DRS4 evaluation board.*

Feature	**Picoscope 6407**	**DRS4 board**
Channels	4	8 plus 1 trigger channel
Bit resolution	8	16
Bandwidth (GHz)	1	0.95
Sampling rate (GS/s)	5.00 (**One channel**) 2.50 (**Two channel**) 1.25 (**Three/four channel**)	5.00 (**All channels**)
Buffer size (samples)	1,000,000,000	1024
Input voltage limits (V)	0.1	1

4.2.7 Summary

The total cost for the construction of the digital PALS system totalled £20,912.68. However, it can also be constructed for as low as £14,129.08 (Table 4.7).

Table 4.7: *Price breakdown for the PALS instrument built and used in this research.*

Component	Price (£)
Positron Source	3,620.40
Scintillators	480.65
PMTs	4,430.40
HV Supply	≈ 1,870
Coincidence Unit	≈ 1,688
Digitizer: PS6407	6,783.600
Digitizer: DRS4	1,040.23
Other Costs	≈ 1,000

4.3 PALS testing

This sections concerns necessary steps to perform prior to using PALS for experimental work. Photomultiplier output signals will shown and an example for the measurement of positron lifetime presented. Optimisation of components will be discussed and justified.

4.3.1 Photomultiplier tube outputs

For accurate lifetime measurements, the output signals from the photomultiplier tube should consist of a smooth signal pulse. To begin, the coincidence unit was set-up to record signals of any type regardless of amplitude or timing windows. On the CU this mode is called "ALL CHANNELS mode". When electrical signals enter the CU, a trigger pulse of fixed amplitude and width is sent to the digitizer which prompts the digitizer to store the data. Figure 4.3.1 shows an example of this for the detector labelled 'Detector 1'.

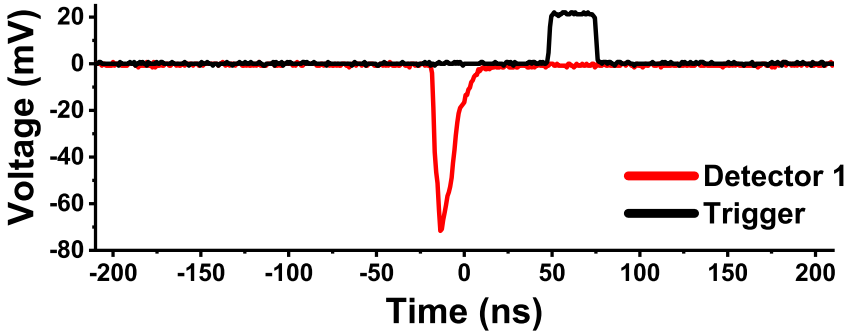

Figure 4.3.1: *An example trigger signal (black) and its corresponding output signal produced by Detector 1(red).*

The signals produced by detector 1 are as desired but this was not the case for detector 2. The signal from this detector was noisy and as such, several cable configurations were tested while keeping the settings the same. This involved repositioning of attenuators and switching cable connectors. Figure 4.3.2 shows four example signal tests.

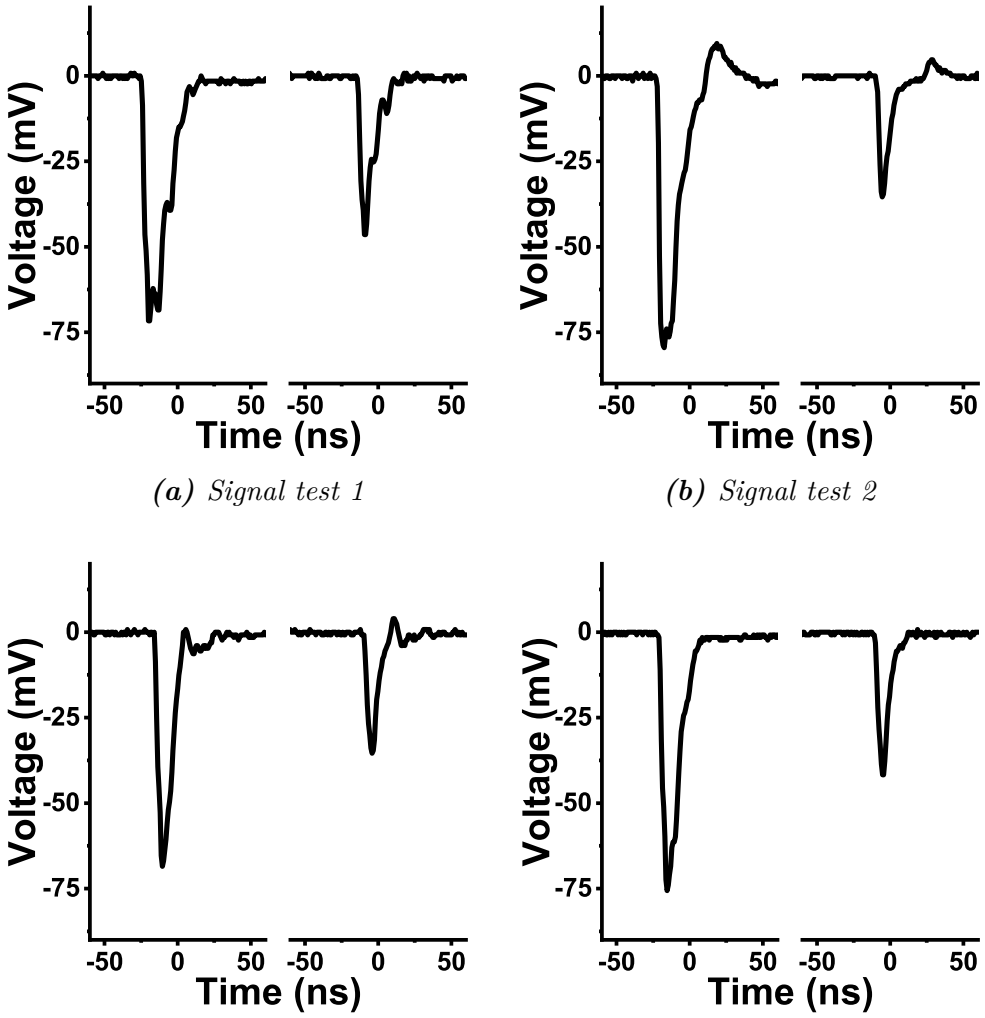

(a) Signal test 1 *(b) Signal test 2*

(c) Signal test 3 *(d) Signal test 4*

Figure 4.3.2: *Four examples from signal testing carried out. Each test represents a change in cable configuration or cable equipment. Ideally, a smooth signal is produced as shown in signal test 4.*

The noise observed in Signal tests (a) to (c) are most likely to signals reflecting inside cables as seen in other studies[130]. This is often a consequence of impedance mismatch although in this work, all components were quoted as 50 Ω impedance. A number of cable configurations were tested and it was found that the smoothest output (Figure 4.3.2 (d)) was produced when using RG174 BNC test leads supplied by Onecall along with the cable configuration shown in Figure 4.3.3. Attenuators and their respective attenuation level are shown in grey and red dots represent t-junction connectors.

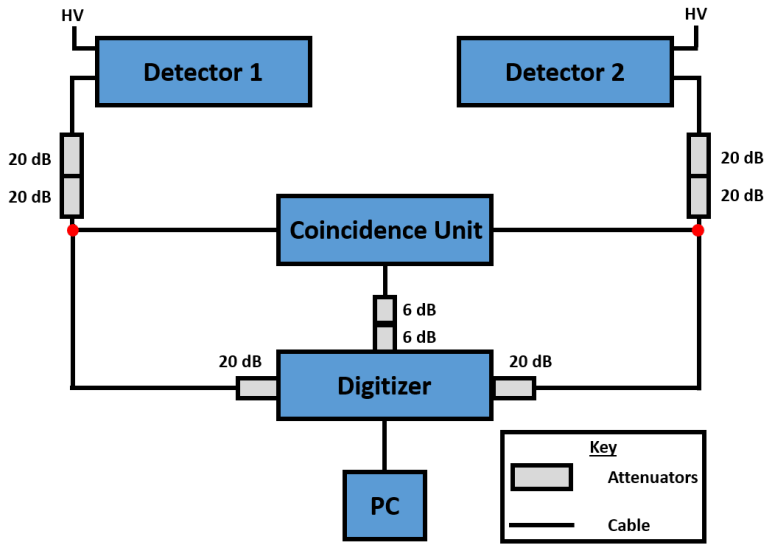

Figure 4.3.3: *The cable configuration used which produces the smoothest output signals. Attenuators are necessary to reduce the voltage supplied to the digitizer. The level of attenuation is labelled alongside each attenuator whilst red dots represent the position of t-junction connectors.*

4.3.2 Lifetime measurement

With both detectors producing smooth signals, the coincidence unit(CU) was adjusted to only produce a trigger signal when two input signals enter within a 50 ns window. The activity of the positron source is 1.85 MBq which in principle means the time between any two individual events is $\approx$ 500 ns and therefore a 50 ns window is suitable. An example recording of a positron birth and subsequent annihilation are shown in Figure 4.3.4. In black is the trigger produced by the CU, in green is the birth signal and in red is the annihilation. The amplitudes correspond to the energy of the gamma photons and hence the annihilation amplitude is smaller. Common sense may lead one to measure the positron lifetime as the time between the peaks of the signal but due to the nature of the signal produced, this is not the case. The decaying tail of the signal broadens in a non predictive manner and this causes difficulties in measuring the true signal peak value.

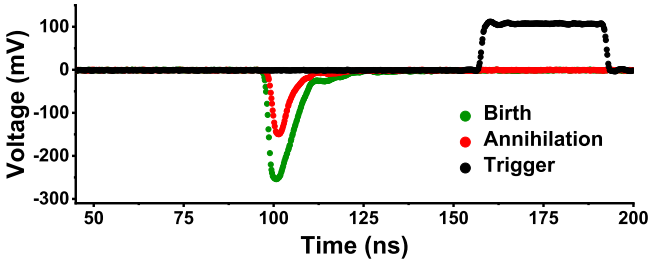

Figure 4.3.4: *The birth (red) and subsequent annihilation (green) of a positron in matter. The trigger signal (black) is used to prompt the digitizer to save the data. The two relevant signals are then sent to the PC and a positron measurement is made.*

A more accurate method of measurement is to use a constant fraction discrimination (CFD) level of the peak height. This is a fixed percentage of the amplitude on the rise of the signal. The rise is steep and stable opposed to the decay of the signal. An example of where the CFD level might be set is shown in Figure 4.3.5 for the same two signals show previously. Green and red show the CFD levels for their respective signal whilst black dashed lines show where the time-points for the lifetime measurement are located.

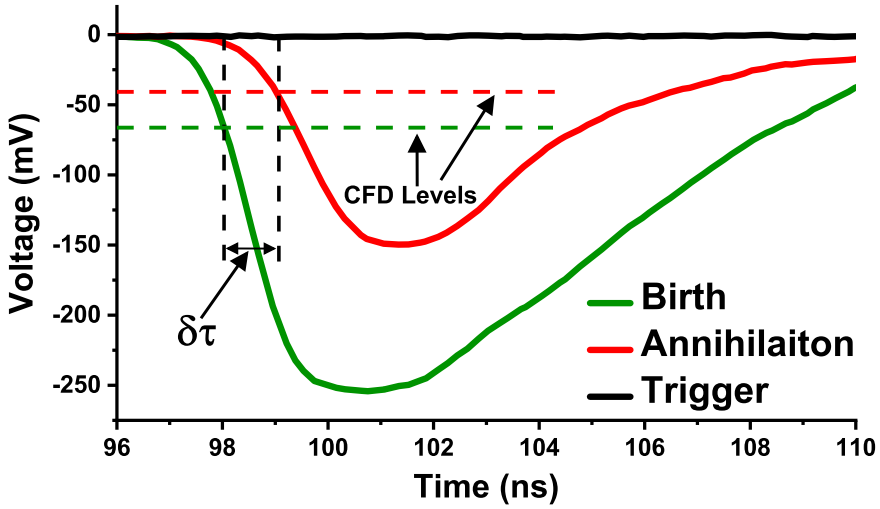

Figure 4.3.5: *A close up of the birth and annihilation signal. Constant fraction discriminator levels are shown by dashed lines. The lifetime measurement based on these levels is shown by $\delta\tau$. The difference in peak broadness causes the peak of the signal to be a poor measurement point.*

For a PALS spectrum to be produced, this measurement is made continuously until around 1 million counts are measured. For this measurement to be performed in an efficient and accurate manner, it is necessary to define the voltage of the birth and annihilation signals. The measurement can be then automated to measure lifetimes of signals with these specific voltages. In actuality, this is not a finite value but a distribution of voltages with peak positrons corresponding to 0.51 and 1.27 MeV for the annihilation and birth signals, respectively.

4.3.3 Voltage distributions

The output signals from PMT's produced correspond to the energies of gamma radiation as a result of a positron birth and subsequent annihilation. However, due to the nature of the prior scintillation, this energy produces a distribution of voltages. The range of these distributions are ultimately used to define the voltage "windows" in which an annihilation or birth signal will be contained. It is therefore important to optimise these distributions.

Evolution of output voltage distribution

To define the voltage windows correctly, the detector supply voltage needs to be optimized first. In general, as supply voltage is increased, the output voltage increases. The data sheet for the PMT's used in this work quote the optimal operating voltage to be 2500 V with a maximum operating voltage of 3000 V. Both detectors were set to supply voltages of 2000 V and increased in small steps. The evolution of detector output with increasing supply voltage is shown in Figure 4.3.6 for (a) Detector 1 and (b) Detector 2.

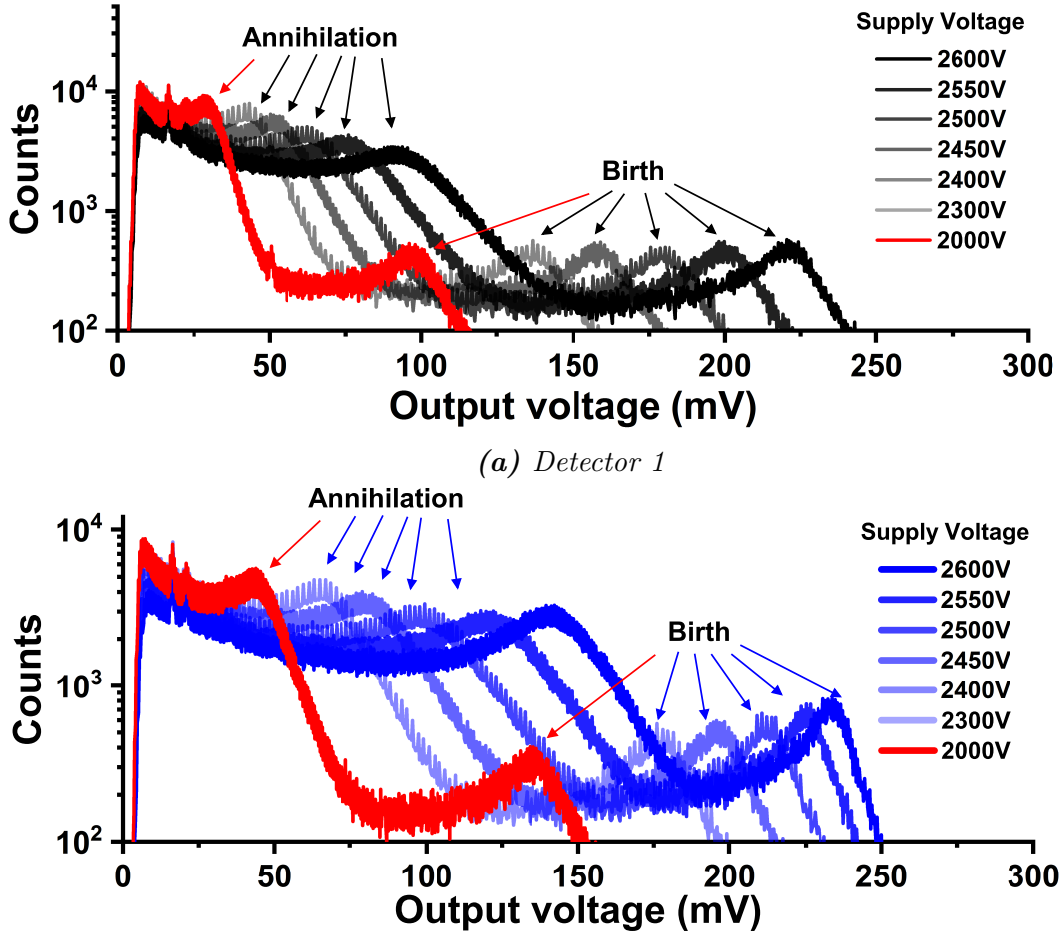

(a) Detector 1

(b) Detector 2

Figure 4.3.6: *The evolution of voltage output from detectors 1 and 2. As expected, the voltage increases with increased supply voltage. The two peaks correspond to birth and annihilation counts. The initial portion of the curve is attributed to Compton scattering.*

Peak-to-Peak distance

As supply voltage increases, the peak positions shift to the right because the PMT voltage gain increases. The distance between peaks also differs with an increase in supply voltage. To clearly distinguish the distributions, the largest peak-to-peak distance is preferred. The change in this distance is shown in Figure 4.3.7 where values have been determined by plotting Lorentzian fits and taking the peak position in Origin software. Detector 2 shows a maximum peak-to-peak distance at a supply voltage of $\approx$ 2475 V before decreasing beyond this value. This is roughly expected as the optimum supply voltage is quoted as 2500 V. Detector 1 however, continues to increase in peak-to-peak distance up to 2600 V. To avoid damaging the detector by approaching the maximum operating voltage, 2600 V is used as a suitable supply voltage.

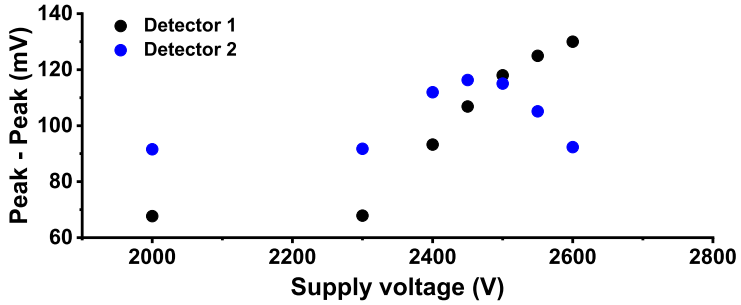

Figure 4.3.7: *The change in peak-to-peak distance with increasing supply voltage. The greatest distance is preferred to better distinguish between siganl types.*

Signal artefact

Each distribution shows a small spike at low output voltages ($<$ 20mV). To determine whether this is digitizer noise the supply voltage was set to 1000 V and voltage distributions recorded as shown in Figure 4.3.8). Two spikes occur with one corresponding exactly to one of the spikes seen in all distributions ($\approx$ 16 mV). The other is seen around 2 mV which does match up perfectly with that seen in Figure 4.3.6. However, it is safe to say these spikes will not cause any issues in lifetime measurements due to there positioning with respect to the voltage distributions.

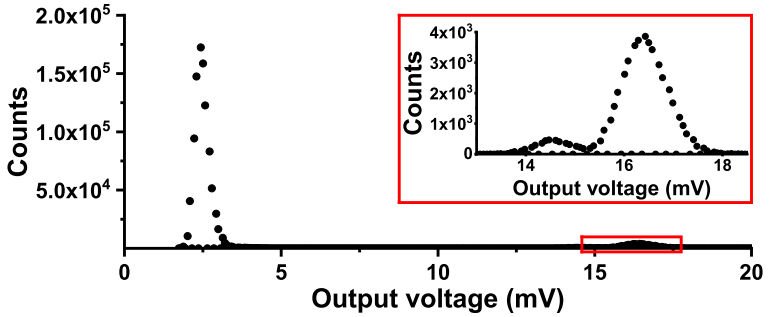

Figure 4.3.8: *The signals recorded for a very low supply voltage. A sharp peak is observed at $\approx$ 2.5 mV. The inset graph is a zoomed portion of the graph which shows two small peaks. These peaks match up with those seen in the distributions shown previously.*

With the supply voltages optimized, the process of removing unwanted counts at low output voltages (0 to 100 mV) will be shown . This can be achieved by voltage thresholding using the coincidence unit.

4.3.4 Voltage thresholding

Thresholding is a process where a cutoff point is applied to a measurement. An example of this is in image analysis where a pixel intensity is set as the threshold intensity. Any pixel with a lower value are set to 0 (black) and any above are set to 255 (white). An example of thresholding an image are shown in Figure 4.3.9 for (a) before and (b) after thresholding.

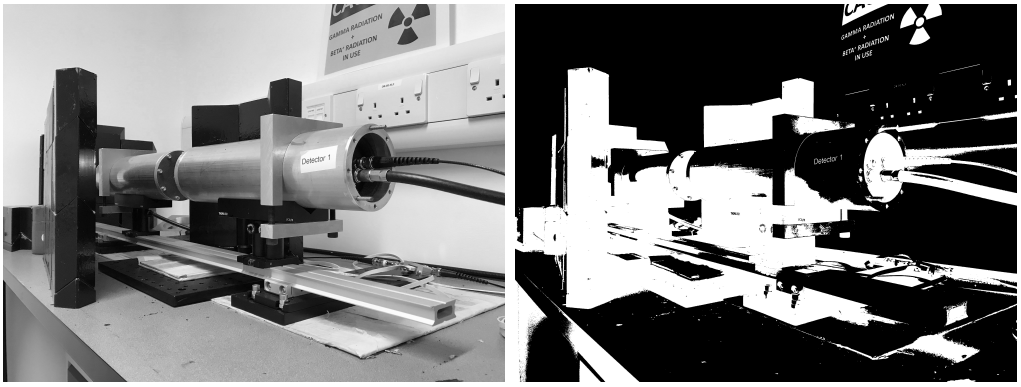

(a) ***(b)***

Figure 4.3.9: *An image of the PALS system used in this work (a) before and (b) after thresholding.*

For electronics, any value below the threshold voltage are ignored whereas high voltages are considered. For PALS, it is a necessary function in order to reduce the number on unwanted counts measured which ultimately improves the efficiency of the PALS acquisition. By measuring "useless" counts in addition to annihilation data, then the duration to obtain "useful" counts increases.

Threshold voltage distribution evolution

To begin, the coincidence unit is set to the lowest threshold level of 10 mV. It is also set to record all signals regardless of timing windows. The threshold voltage is gradually increased to 210 mV as shown in Figure 4.3.10. It can be seen that as the threshold level increases, the amount of Compton scattering is reduced. However, at a certain threshold level, this increase will begin to ignore useful measurements contained in the annihilation peak. This is shown clearly in Figure 4.3.10 (a) Detector 1 at a voltage level of 210 mV. Approximately half of the peak responsible for annihilation counts is lost.

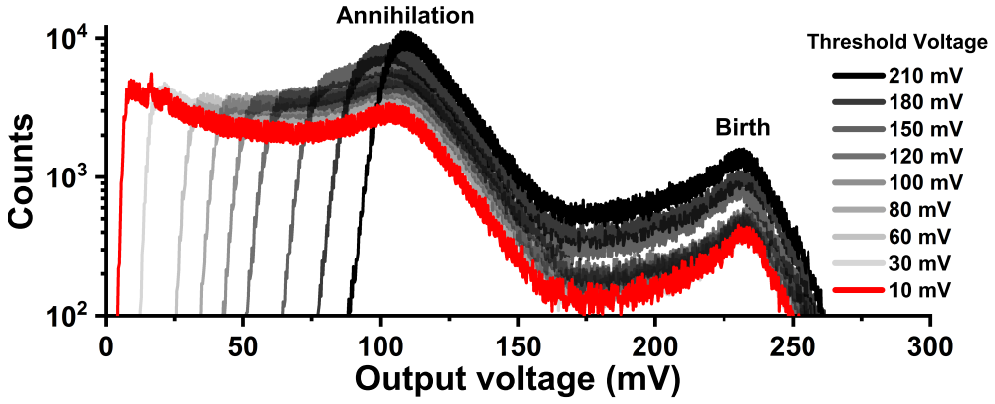

(a) Detector 1

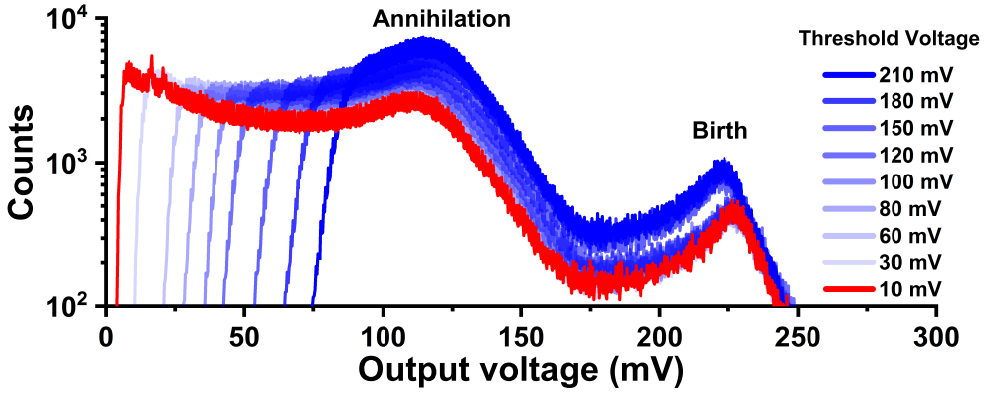

(b) Detector 2

Figure 4.3.10: *The effects on output voltages for detectors 1 and 2 as a consequence of increased threshold voltage. The aim is to reduce unwanted counts, mainly due to Compton scattering and improve acquisition efficiency.*

Calculation of lost counts

To determine the point at which thresholding begins to lose counts, we can use integration and peak fitting. Origin software was used to fit a Lorentzian function to the right-hand side of the peak. By generating a full Lorentzian, the expected useful counts in the left-hand side can be estimated. By subtracting the area of the useful counts from the area of the entire distribution, the number of counts due to Compton scattering can be determined in addition to any loss of counts due to thresholding. This is shown in Figure 4.3.11.

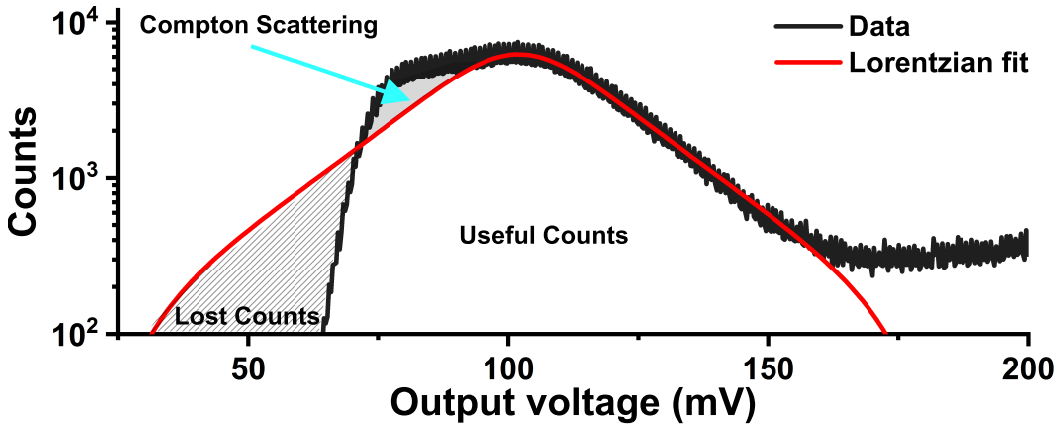

Figure 4.3.11: *An example of high thresholding which results in a loss of useful counts in addition to the decrease in Compton scattered counts.*

This process was applied to each distribution on both detectors and the results are shown in Figures 4.3.12 and 4.3.13. For both detectors it is seen that the number of Compton scattering counts per million decreases as expected with increased thresholding. The number of annihilation counts per million is also seen to increase.

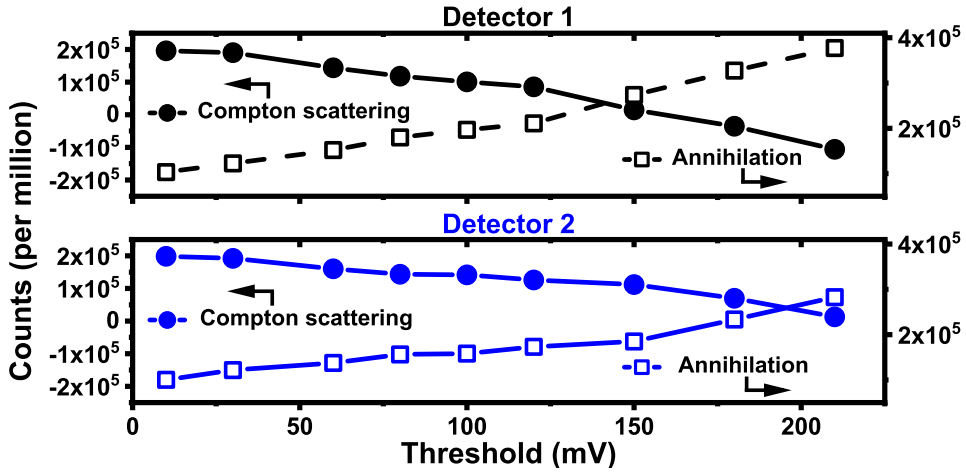

Figure 4.3.12: *Compton scattering and annihilation counts as a function of threshold. Compton scattering is reduced with increased thresholding whilst the number annihilation counts increases.*

It may be noted that the number of counts attributed to Compton scattering becomes negative but in actuality this is not the case. This is the point at which annihilation counts are starting to be lost. The number of gained counts is simply the difference between the number of useful and lost counts. The gained and lost counts are shown in Figure 4.3.13.

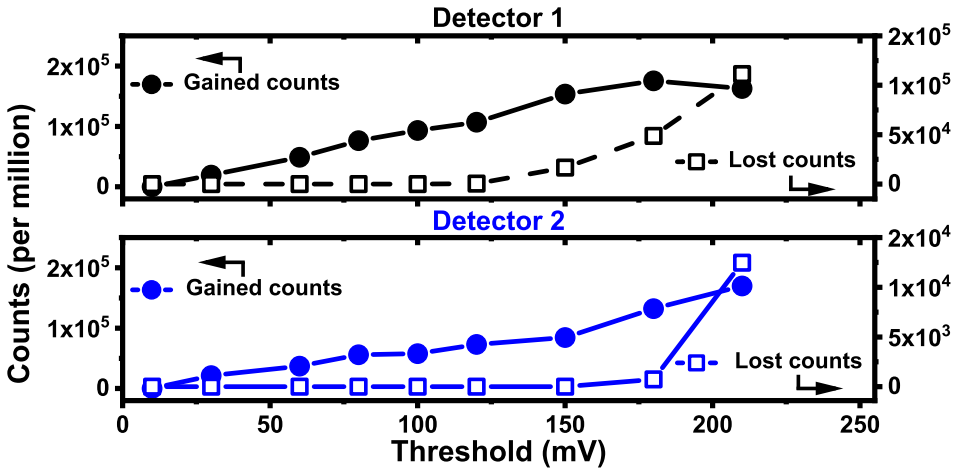

Figure 4.3.13: *Number of useful counts lost or gained with increased threshold voltage for detectors 1 and 2.*

It was decided that the point at which useful counts are lost, that this would be the threshold point. These were values 120 mV for for both detectors. The final output voltage distributions are shown in Figure 4.3.14.

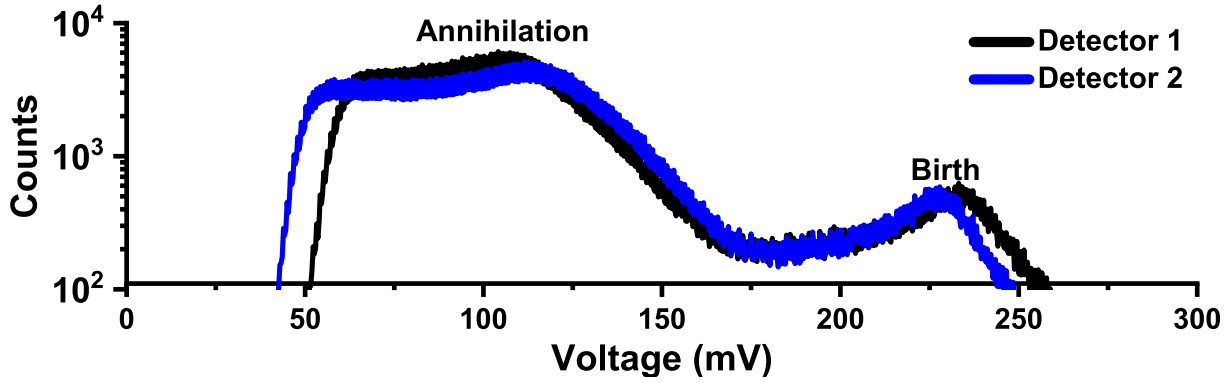

Figure 4.3.14: *The final optimised voltage distributions for detectors 1 and 2. Many unwanted counts have been removed whilst ensuring a loss of counts does not occur. This increases the rate of which useful counts are collected.*

4.3.5 Resolution optimization

An important feature of a PALS system is the timing resolution. This effectively determines how accurately lifetimes can be measured and the minimum lifetimes that can be measured. A common method of measuring this is by fitting a Gaussian to the rise in lifetime spectrum[131–133]. The resolution is then taken as the full-width at half maximum (FWHM) of this Gaussian distribution. Figure 4.3.15 illustrates this measurement for a lifetime spectra obtained for a silicone wafer sample using SPALS.

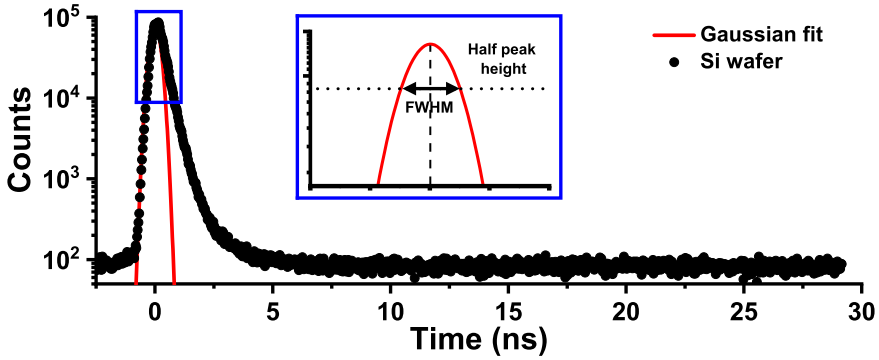

Figure 4.3.15: *Raw lifetime spectra of Si for a constant fraction discriminator level of 0.2. The Gaussian fit based on the FWHM of the rise of the spectra is shown. The FWHM represents the resolution of the PALS instrument.*

To improve the timing resolution, the constant fraction discriminator level can be adjusted.[134] Figure 4.3.16 shows the FWHM for a range of CFD levels. For this PALS instrument, the lowest FWHM was observed at a CFD level of 0.27 and this is used going forward which corresponds to a FWHM of 470 ± 26 ps. Although this is significantly higher than other instruments,[43,126,135,136] this resolution is suitable for studies in polymers where lifetimes are generally greater than 1.3 ns under standard conditions.[46,121,123,137]

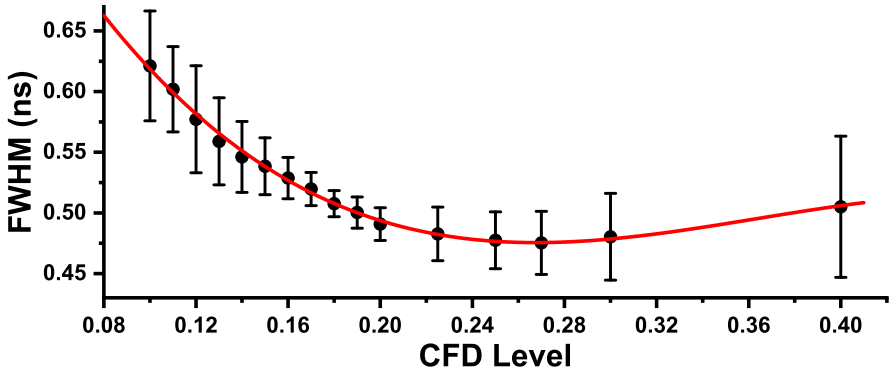

Figure 4.3.16: *The FWHM with increasing CFD level. The FWHM represents the resolution of the PALS system. The lowest value is the most desirable as small timing measurements become more reliable. The red curve represents a cubic polynomial fit. Error bars are standard error generated by Origin fitting software.*

4.4 Spectral acquisition and reference measurements

To ensure that measurements made using the PALS system in Sheffield (SPALS) are reliable, it is good practice to compare results to those obtained at another research institute. In this work, a sample of DGEBF-MXDA epoxy resin was prepared as per Section 2.2.2 and sent to The Reactor Institute at The University of Delft. At TU Delft, a high quality PALS system is in operation amongst other annihilation techniques. This section compares the results obtained using the Delft PALS system to those collected in Sheffield. Another sanity check has been performed by measuring the lifetimes in a PTFE sample (supplied by direct plastics). In addition, a sample of the aforementioned epoxy resin and a sample of PTFE are placed either side of the positron source and lifetimes measured simultaneously.

4.4.1 Minimum spectral counts

The number of counts (lifetime measurements) made ultimately affects the accuracy of the determined average lifetime from the spectra. To determine the minimum number of counts, an epoxy sample consisting of a mixture of DGEBF and DGEBA cured with MXDA was studied. The number of counts was increased from 50,000 to 2 million counts. Figure 4.4.1 shows both the orthopositronum lifetime and annihilation intensity with increasing PALS counts. The error in both is largest with the lowest amounts of counts as expected. Once 500,000 counts are measured the accuracy effectively stabilises.

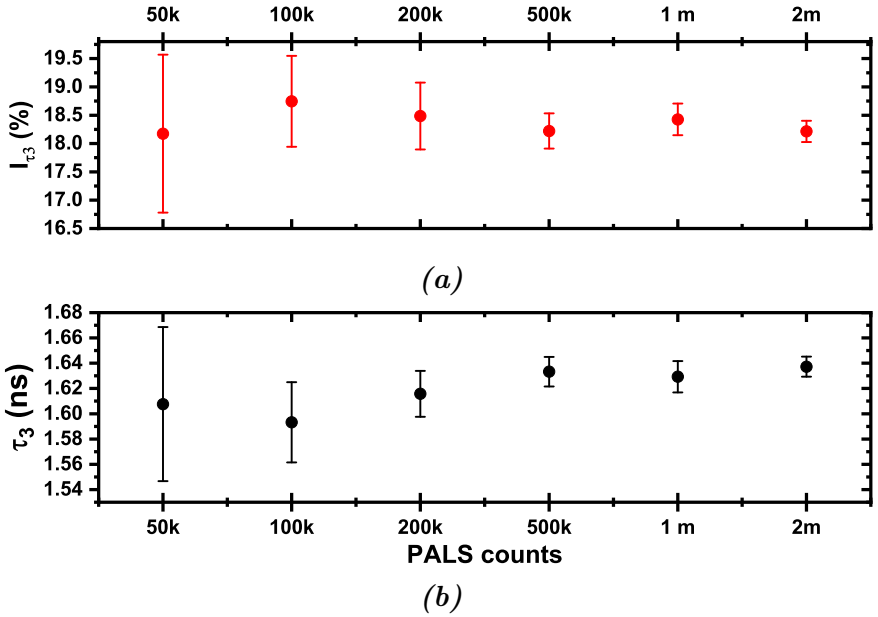

Figure 4.4.1: *The annihilation intensity and average orthopositronium lifetime as a function of total PALS counts measured. Standard error is shown using error bars. Error was generated in the program "LTPOLYMERS".*

The importance of the error in lifetime is better represented by the error in calculated free volume. Figure 4.4.2 shows the error in free volume as a function of PALS counts. The decrease in error is loosely described by an exponential decay. Increasing the number of counts from 50,000 to 500,000 corresponds to a drop in FV error of 10.13 to 1.96 Å^3. increasing to 2 million counts further decreases the error to 1.33 Å^3.

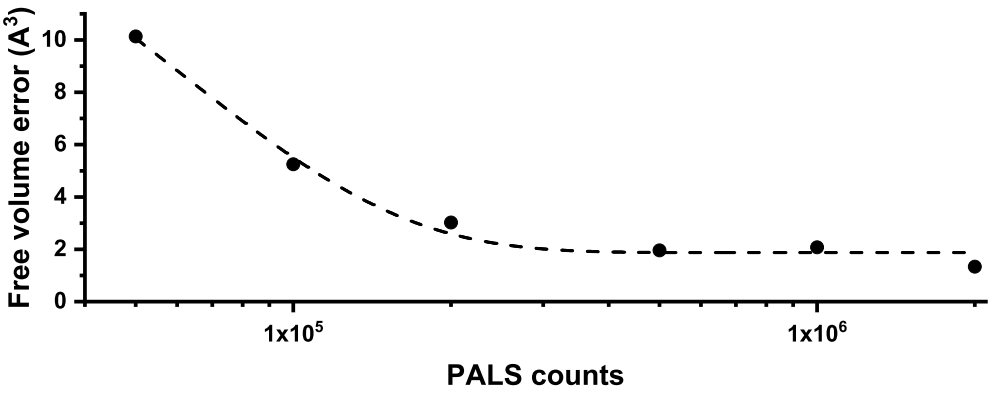

Figure 4.4.2: *Free volume error in an epoxy sample as a function of total PALS counts. The error decreases greatly from 50,000 to 500,000 counts but beyond this the improvement in measurement is minimal.*

Although this test has shown that 500,000 counts gives reasonable errors in lifetime measurements the majority of PALS measurements will be carried out using 1 million counts as most studies[43,46,112,132,135] measure from 1 - 5 million in traditional PALS. If a different number of measurements are recorded, this will be specified.

4.4.2 Comparison with TU Delft

Spectral background subtraction

As the results obtained by TU Delft were background subtracted before being received, a background subtraction was performed on the SPALS spectrum. 2 million counts were recorded using SPALS and a lifetime spectra obtained. In practice, the analysis performed throughout this thesis is performed using LTPOLYMERS which automatically subtracts the background but in order to directly compare results with TU Delft, the subtraction is included here. Both the original and subtracted spectra are shown in Figure 4.4.3.

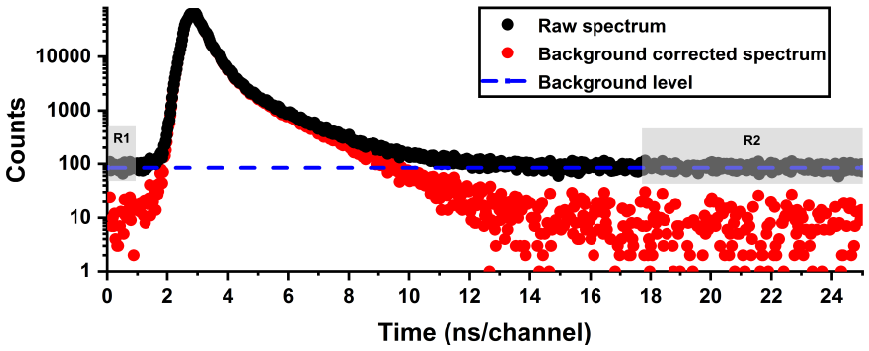

Figure 4.4.3: *The positron lifetime spectra for a sample of epoxy consisting of DGEBF and MXDA. In black shows the raw lifetime spectrum whilst in red is the background subtracted spectrum. The grey areas labelled R1 and R2 represent the regions used to determine the average background level. A blue dashed line shows the background level which is ultimately subtracted from the original (black) to produced the subtracted spectrum (red).*

The regions highlighted grey before the peak rise (R1) and to the far right of decay (R2) are used to calculate the background level. This level is simply determined as the average count value in these two regions. The dashed blue line shows the background level and the red spectra is the result of subtracting the level from the original raw spectrum.

Spectral comparison

Figure 4.4.4 shows two lifetime spectra for epoxy sample. The spectra in red is from data collected with the PALS system at TU Delft (acquired under the supervision of Dr Henk Schut). In black is the subtracted spectra collected in Sheffield for the same sample. The spectra are similar but some minor differences can be seen. The blue box zooms in on the rise of the spectra. A clear difference is seen on this scale and is due to a difference in instrument timing resolution. The resolution is determined by the FWHM which is described in Section 4.3.5. Ultimately, the system in Delft has a better timing resolution than the system in Sheffield. This was estimated to be 397 $\pm$ 13 ps by measuring the FWHM of the Delft spectra whilst the FWHM for SPALS was 470 $\pm$ 26 ps.

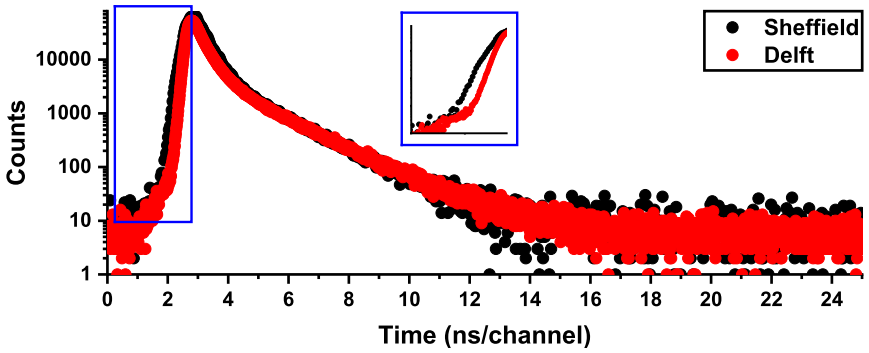

Figure 4.4.4: *The lifetime spectra acquired for a DGEBF-MXDA based epoxy resin. Background subtractions have been performed on both spectra. The time per channel resolution for the Delft and Sheffield PALS systems were 12.66 and 30 ps per channel respectively.*

Differences can also be seen in the background region (far right of Figure 4.4.4). This difference is most likely attributed to source activity differences. The source used in Delft had an activity of $\approx$ 1 MBq whereas the Sheffield system uses a source with activity of $\approx$ 1.8 MBq. This can be explained by the nature of background counts. These events are true coincidences in terms of two gamma photons being recorded within a specific time window although this is initially counter-intuitive. For example, a source of 1 MBq, should only logically emit 1 positron every 1 μs that is 1×10^6 counts divided by 1 second. Taking this into account and that an annihilation event should occur within 5 ns, then there should not be any overlapping events. However, the emission process is not deterministic and some positrons will be released in rapid succession. Reducing the activity will reduce the amount of false measurements. A smaller influence could be a reduction of background radiation at TU Delft. The PALS spectrometer is located inside an experimental hall which is heavily shielded and as a result, the background radiation inside the hall is reduced.

Summary of results

The lifetime results obtained for the epoxy sample using both systems are summarised in Table 4.8. Taking into account the errors of each measurements, the differences are significant. However, as all PALS measurements with this type of system are performed using the Sheffield system, this is not an issue as all measurements will be relative to one another. However, if measurements between researchers are to be compared then a reference measurement should also be measured to observe differences in results for differing PALS systems.

Table 4.8: *The lifetime (τ_i) and intensity (I_i) results for a DGEBF-MXDA based epoxy measured using two different PALS systems. The lifetime of parapositronium (pPs) is not shown as it was constrained to 0.125 ns.*

PALS System	τ_{e+} **(ns)**	τ_{oPs} **(ns)**	I_{pPs} (%)	I_{e+} %	I_{oPs} %
Delft	0.355 $\pm$ 0.001	1.534 $\pm$ 0.004	15.5 $\pm$ 0.2	58.1 $\pm$ 0.2	26.4 $\pm$ 0.1
Sheffield	0.366 $\pm$ 0.001	1.533 $\pm$ 0.028	13.04 $\pm$ 0.12	66.77 $\pm$ 0.17	20.19 $\pm$ 0.15

4.4.3 PTFE measurement

PALS was also performed on a PTFE sample and compared to literature values. The lifetime spectrum along with fitted lifetime components are shown in Figure 4.4.5. Four lifetime components are fitted as per the literature[138–140] and results are in agreement. However, literature values for lifetimes in PTFE vary significantly with τ_3 and τ_4 ranging between 1.2 - 2 and 2.5 - 4.5 ns respectively[96,138–140] . This reiterates the importance of performing reference measurements when comparing results obtained by other instruments.

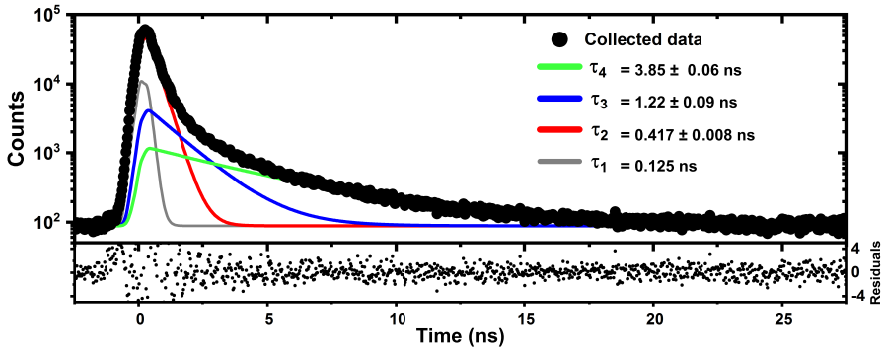

Figure 4.4.5: *The positron lifetime spectrum for a PTFE sample. Four lifetime components are fitted and shown. Standard errors are shown. Both lifetimes τ_3 and τ_4 are due to orthopositronium annihilation in free volume voids. Note: No background subtraction*

4.4.4 Two-material measurement

In addition to the PTFE measurement, a two-material measurement was made. One side of the positron source was covered by PTFE and the other side covered by epoxy. This means that two spectra are collected simultaneous but the result is a combination of the two. The arrangement is shown in Figure 4.4.6. Effectively both detectors behave as birth and annihilation detectors simultaneously.

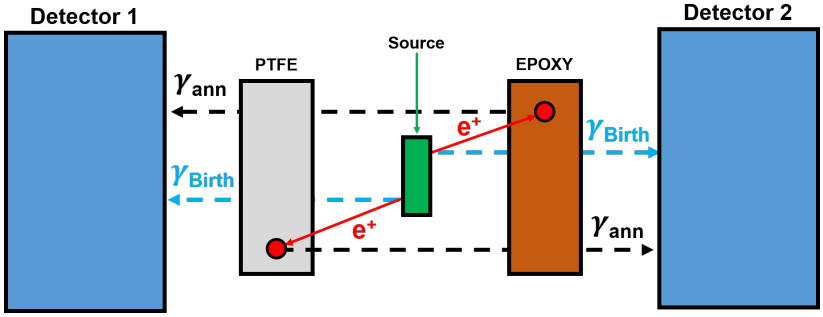

Figure 4.4.6: *The arrangement used for the two-material measurement. Each detector has the capability of detecting the birth and annihilaiton of positrons in either material. The resulting lifetime spectra is a combination of each materials spectrum and results in an average lifetime between the two. Note: image not to scale*

Lifetime spectra

Figure 4.4.7 shows the spectra for pure PTFE, PTFE - epoxy combination and pure epoxy. The PTFE-epoxy sample has a long lifetime which falls between pure PTFE and pure epoxy. It may seem an obvious result but this type of measurement was not seen in literature.

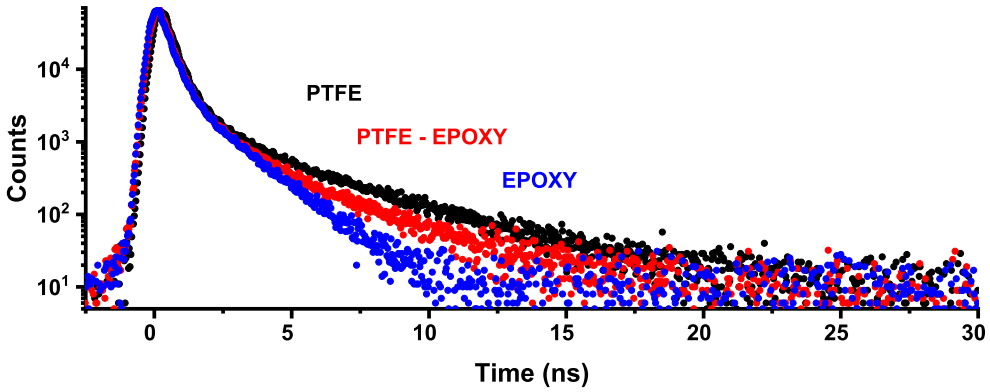

Figure 4.4.7: *The lifetime spectra for pure PTFE and epoxy in addition to a combination of the two. The resultant spectrum falls between the two pure samples.*

The closest example was a study by Madani *et al.* which measured lifetimes in PTFE-Silica composites.[138] They showed that $\tau_{oPs-long}$ lifetime decreased with increasing weight percent of silica. This is a similar result to that shown here. Table 4.9 is summary of results for the three measurements.

Table 4.9: *The lifetime (τ_i) and intensity (I_i) results for pure PTFE, pure epoxy and a measurement which involves both materials simultaneously (PTFE-EPOXY). PTFE has four lifetime components whereas the purt epoxy has three. Standard errors are shown which were produced in "LTPOLYMERS".*

Sample	τ_{oPs} **(ns)**	$\tau_{oPs-long}$ **(ns)**	I_{oPs} (%)	$I_{oPs-long}$ %
PTFE	1.221 ± 0.09	3.847 ± 0.004	9.02 ± 0.5	10.99 ± 0.3
PTFE-EPOXY	1.298 ± 0.1	3.214 ± 0.01	10.63 ± 0.3	7.36 ± 0.6
EPOXY	1.501 ± 0.02	-	18.974 ± 0.3	-

4.5 Conclusions

4.5.1 PALS components

This chapter presented the equipment required to construct the positron annihilation lifetime spectrometer (PALS) which is used throughout this research. Each component was discussed including the total pricing of the system. The PALS system is ultimately based on fast plastic scintillators coupled to photomultiplier tubes. A relatively new instrument was used for signal discrimination (4-fold coincidence unit) which is capable of performing timing and energy discrimination simultaneously. Two digitizers were used in this work. The Picoscope6407 by Picotech was used for initial signal testing and energy distribution measurements. The DRS4 evaluation board by PSI Tech was ultimately used for PALS acquisition in conjunction with acquisition software *QTPALS*.

4.5.2 PALS testing

After assembly, the PALS spectrometer was evaluated. Signal tests were performed in order to produce smooth PMT output signals in addition to optimisation of the output voltage distributions. The timing resolution was determined from the FWHM of the rise in lifetime spectra of a silicone wafer sample. The resolution was improved by adjusting the constant fraction discriminator level which determines which part of the PMT output signal will be used as a lifetime measurement point. The timing resolution achieved was 470 ± 26 ps which is suitable for the study of free volume in polymers. The minimum number of counts required per experiment was determined to be 500,000 counts.

4.5.3 Reference measurement

After optimisation of the spectrometer a measurement was made on an epoxy sample comprising of DGEBF resin and MXDA amine hardener and analysed at TU Delft, Netherlands as measure of reliability. Results produced were similar with Sheffield measuring a orthopositronium lifetime (τ_{oPs}) of 1.533 ± 0.028 ns with the Delft system showing a τ_{oPs} of 1.534 ± 0.004 ns.

4.5.4 Final remarks

The PALS system constructed here will be used the majority of traditional PALS measurements going forward. Future improvements for the PALS system are discussed in Chapter 6.

5

Diffusion and the relation to free volume

5.1 Chapter Introduction

The chapter concerns several methanol ingression experiments carried out for a range of epoxy-amine samples. All the samples were produced using the same batch of epoxy where possible as the epoxide equivalent weight can differ between batches. This was also the case for the hardeners used even though there is generally more consistency between batches of hardeners. For each study, the samples were produced simultaneously i.e. samples for diffusion, T_g and PALS measurements all came from the same cure. Each sample was immersed in methanol and its mass monitored over time. Generally, for the epoxy systems used here, this process takes several months. Samples which reached their ultimate ingression (constant mass) were removed and placed into an air environment to dry whilst further mass measurements were made. Full details of this experiment can be found in Section 2.5.1. Some studies underwent a second ingression cycles if egression mass became stable. The main results obtained from these experiments were the ultimate ingression (U_{ING}) and the diffusion coefficients for ingression (D_{ING}) and egression (D_{EGR}). U_{ING} is the maximum amount of methanol ingression in weight percent. (D_{ING}) and (D_{EGR}) are a measure of the rate of ingression and egression respectively. Each diffusion property will be compared to the glass transition temperature (T_g), free volume (FV) and fractional free volume (FFV). The aim was to determine whether free volume can be used as an indicator of material quality with respect to chemical resistance. As free volume is measured using PALS over several hours, this would be a great advantage over long term traditional gravimetric techniques such as ingression studies. An overview of each experimental study presented in this chapter is shown in Figure 5.1.1.

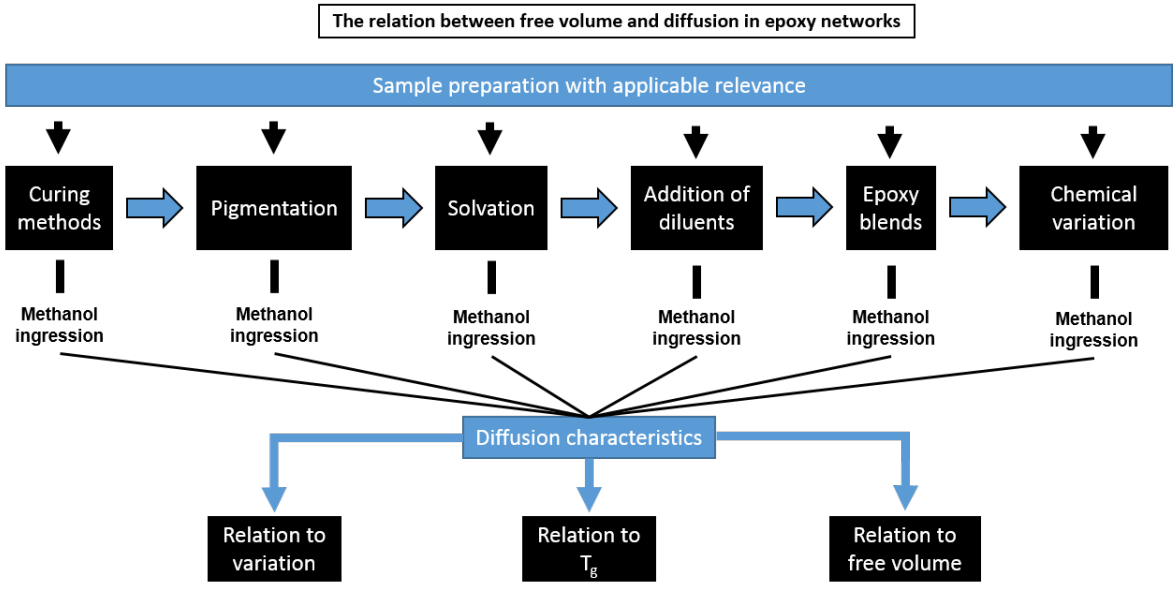

Figure 5.1.1: *An outline of the studies which are presented in Chapter 5.*

5.2 Pot-time and cure regime

5.2.1 Introduction

The first study of this chapter concerns the affects of varying the production method of epoxy samples on the diffusion and free volume properties. All samples consist of DGEBF epoxy resin cured with MXDA amine hardener. The time between initial mixing of the components and pouring into moulds pre-cure in this work is defined as the pot-time. The pot-time was increased from 0 to 3 hours and a pot-time which is varied depending on laboratory conditions (labelled VAR) is implemented. The significant changes in temperature and humidity are shown in Figure 5.2.2. Pot-time variation was was used in order to approximate sample viscosities prior to cure. In addition, for each pot-time two curing regimes are utilised which are referred to as the 'Sheffield' and 'Industrial cures'. Details of each cure are shown in Table 5.1 but effectively the Sheffield cure is hot and fast whilst the industrial cure is cooler and slower.

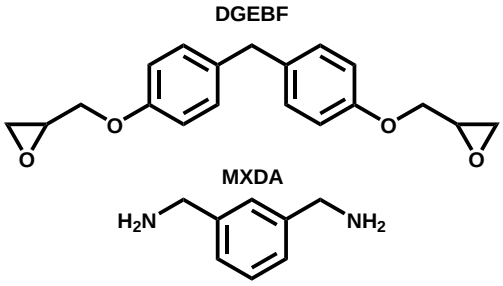

Figure 5.2.1: *The chemical structures of DGEBF and MXDA.*

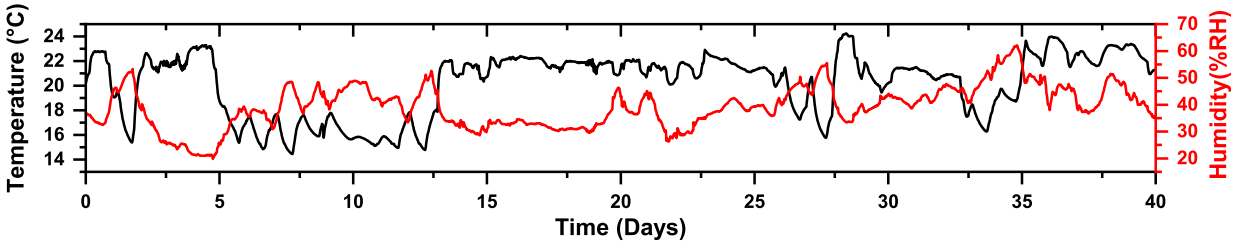

Figure 5.2.2: *The variation in temperature and humidity for the laboratory in Sheffield.*

Table 5.1: *The cure regimes for the Sheffield and industrial cure methods. S1 and S2 refer to stage 1 and stage 2 respectively.*

Cure	Stage 1	Stage 2	Environment
Sheffield	60 - 160 °C @ 1 °C min^{-1}	3 h @ 160 °C	S1 - Air, S2 - Air
Industry	24 h @ RT	16 h @ 80 °C	S1 - N2, S2 - Air

The reason for this study is to compare the affects on diffusion when more realistic methods (industrial cure) are implemented rather than those which are considered more ideal in terms of reaction conversion.[71,106] Figure 5.2.1 shows the structures of DGEBF and MXDA.

5.2.2 Diffusion characteristics

Diffusion curves

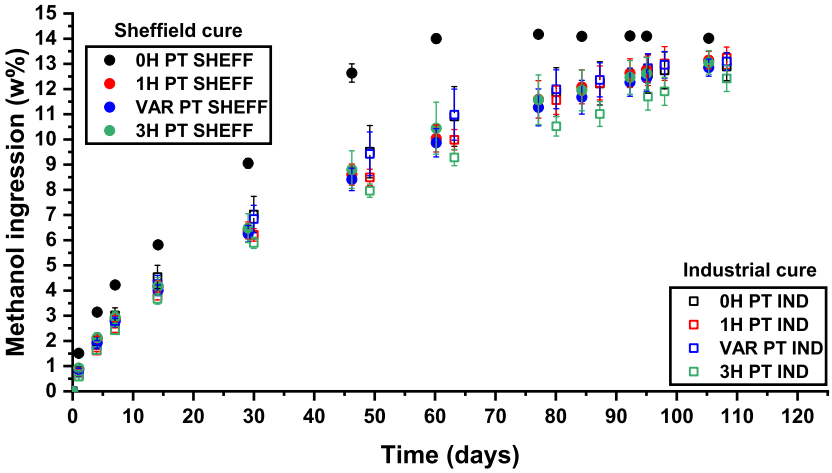

Figure 5.2.3: *The ingression of methanol monitored over time for DGEBF-MXDA epoxy resins. The Sheffield cure (solid circles) concerns epoxies prepared by curing at a temperature of 160 °C for 3 hours. The industrial cure concerns samples left at room temperature for 24 hours before post curing at 80 °C for 16 hours. The pot-time of samples were also adjusted and are labelled accordingly i.e. 1H PT represents a 1 hour pot-time. VAR PT refers to a pot-time which varies depending on laboratory conditions. In this work pot-time is defined as the time between mixing reactants to pouring into moulds. After pouring, the cure begins.*

The ingression of methanol in DGEBF-MXDA resins which were produced by different curing methods is shown in Figure 5.2.3. Visually, the majority of ingression curves are indistinguishable with the exception of the 0HPTSHEFF sample. In order to obtain more useful information, the Shen and springer model[76] shown by Equation 5.2.1 can be utilised.

$$\frac{M_t}{M_\infty} = \frac{4}{L}\sqrt{\frac{Dt}{\pi}} \tag{5.2.1}$$

Where (M_t), is the mass ingressed at a time (t), M_∞ is the ultimate uptake, (L) is the sample thickness and (D) is the diffusion coefficient. The ultimate uptake mass is achieved when the mass becomes stable indicating that ingression has ceased. However, the majority of these samples did not reach the ultimate ingression after 110 days. But, as the uptaken amount of methanol appears to be close to plateauing, the ultimate ingression has been estimated as shown in Figure 5.2.4 which is based on the ingression curve for the VAR PTSHEFF sample. In black are the measured methanol ingression in weight percentage. Based on these initial measurements, points leading to ultimate ingression are estimated as shown in red.

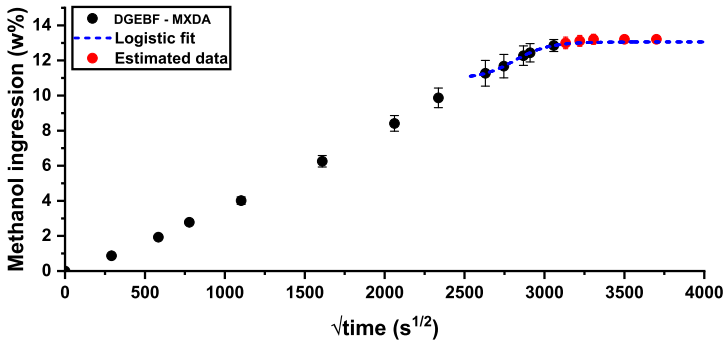

Figure 5.2.4: *The methanol ingression in DGEBF-MXDA thus far (red circles) along with estimated points (red circles) to a point of plateau based on an estimation obtained using a logistic fit (blue dashed line) in Origin.*

With the estimate for ultimate ingression, M_t/M_∞ can be plotted against the square root of time as shown in Figure 5.2.5. The linear region of each data set was fitted using Origin software in order to determine the gradient which can ultimately be used in Equation 5.2.1 to determine the diffusion coefficient.

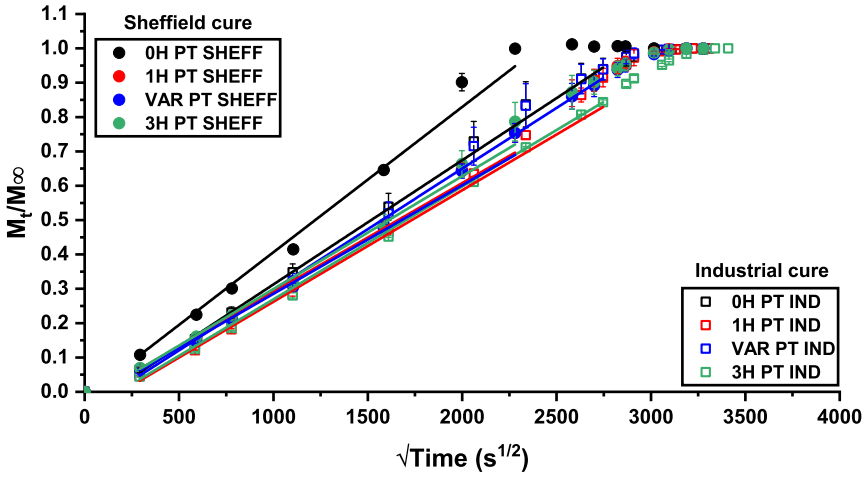

Figure 5.2.5: *Methanol ingression of DGEBF-MXDA epoxy samples with differing cure conditions (as described in Section 5.2.1). For this data, the maximum ingression (M∞) was estimated using a logistic fit. Fits are applied to the linear region of the curve and the gradient used to determine the diffusion coefficient for ingression (D_{ING}). Error bars represent the standard error of three samples.*

By plotting $\log(\frac{M_t}{M_\infty})$ against log(time), the type of diffusion can be determined (i.e. Fickian, sigmoidal etc.). According to the book 'Polymer Permeability'[141] the slope of the graph, n indicates the type of diffusion. An n value of 0.5 is Fickian, whilst values between 0.5 and 1 are considered non-Fickian. Figure 5.2.6 shows the $\log(\frac{M_t}{M_\infty})$ against log(time) for a typical DER354-MXDA sample cured under the "Sheffield" conditions. The slope and therefore the n value was found to be 0.59 which suggests that the diffusion in not Fickian.

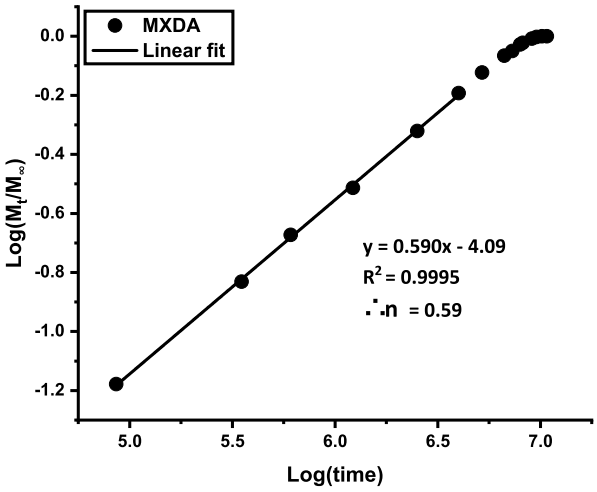

Figure 5.2.6: *The log of methanol ingression against log time for a typical MXDA-DER354 epoxy sample. A linear fit is shown by a solid line which is used to determine the type of diffusion.*

The affect of cure regime on diffusion

The diffusion properties for DGEBF-MXDA samples produced with different pot-times and cure regimes is shown in Figure 5.2.7. The ultimate ingression (in blue) is seen to be similar for all pot-times with the exception of a pot-time of zero when implementing the Sheffield cure method (solid bars). This can be explained by a combination of short pot-time and high curing temperature. A short pot-time means that minimal reaction between the epoxy and amine has occurred resulting in a relatively low viscosity prior to oven cure. On curing, the viscosity decreases further and rate of evaporation of the amine increases. The evaporation causes epoxy mixture to become amine deficient.
Increasing the pot-time of the mixture allows the reaction to begin, forming cross-links prior to curing. The amount of amine which is added to the gel phase of the mixture increase which in-turn increases the viscosity due to higher molecular weight. The increased viscosity and the amine bound to the gel phase hinders evaporation due to higher molecular weight and therefore the system will be closer to a stoichiometric ratio. As the industrial cure regime involves an initial room temperature dwell, the enhanced evaporation does not occur.

A similar trend is seen for the diffusion coefficient in that it is highest in the sheffield cure at zero pot-time before decreasing and stabilising at a pot-time of 1 hour. The diffusion coefficeint is lower in both 1H and VAR pot-times whilst a similar level is seen at 3 hours when comparing the Sheffield cure to the industrial method. A lower diffusion coeffiecent at 1H and VAR could be attributed to increased temperatures allowing for an increased reaction conversion[39,142]. This would mean more crosslinks are formed and ingression could be hindered[35,143,144]. A general indicator of reaction conversion is the glass transition temperature (T_g) and as such is measured here.

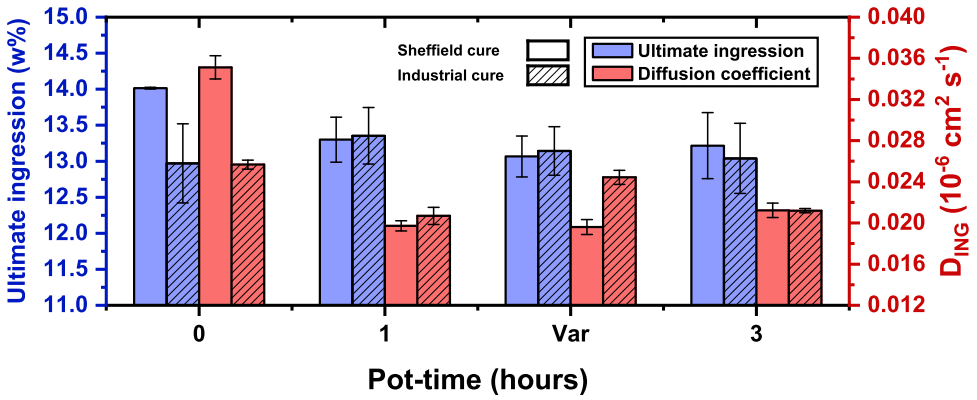

Figure 5.2.7: *The ultimate ingression (blue) and diffusion coefficient (red) for a number of DGEBF-MXDA epoxy samples with varying cure regimes. The solid bars represent the Sheffield cure regime whilst shaded bars correspond to industrial curing methods. Error bars represent the standard error of three samples. VAR refers to pot-times which are chosen with lab conditions considered.*

5.2.3 Diffusion and the glass transition temperature

T_g and cure regime

Figure 5.2.8 compares th T_g for DGEBF-MXDA epoxy samples cured with varied pot-times and cure regimes. The Sheffield (blue) results in a consistently higher T_g than the industrial method (red). The significant drop in T_g for a three hour pot-time is unexpected when considering marginal differences in cure.

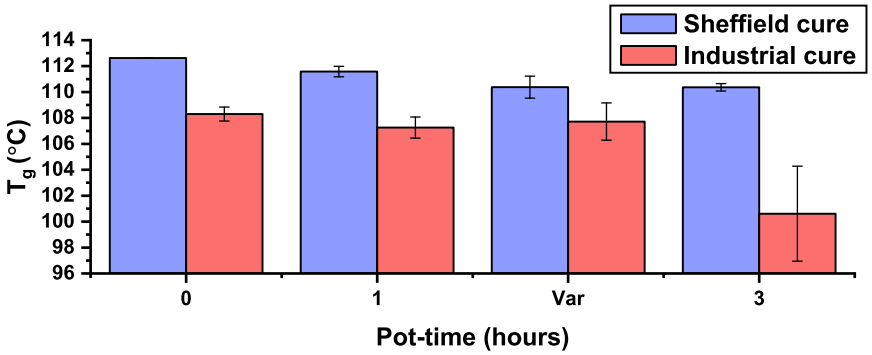

Figure 5.2.8: *The glass transition temperatures for DGEBF-MXDA epoxy samples prepared with various pot-times and differing cure regimes. Error bars represent the standard error of three samples.*

T_g and diffusion

The relationship between T_g and diffusion properties of the epoxy samples are shown in Figure 5.2.9 for (a) Sheffield and (b) industrial cures. For the (a) Sheffield cure, T_g is seen to generally increase with ultimate ingression. R^2 values suggest this is a good correlation (>0.9) but as three of the four points are clumped, the goodness of the correlation maybe false. T_g shows a slight upwards trend with ingression rate but this fit is shown to be poor

(R^2 <0.31). The (b) industrial cure shows no correlation between T_g and ultimate ingression and a slight upward trend is seen for D_{ING}.

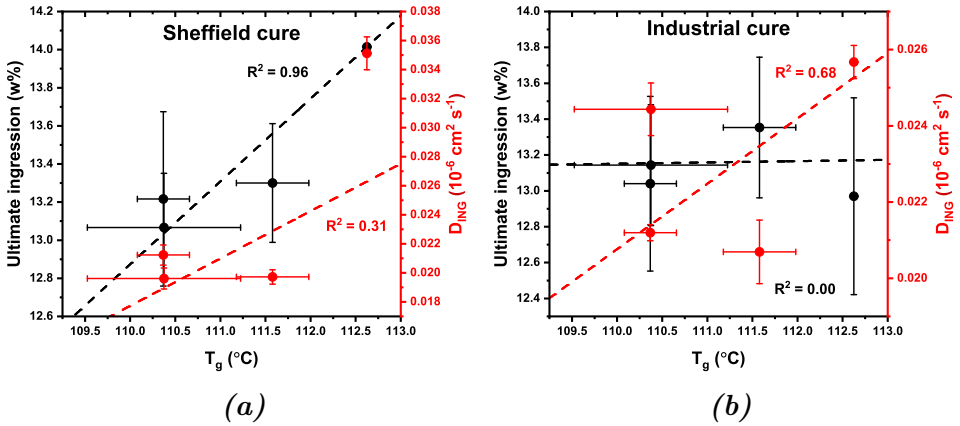

Figure 5.2.9: *A comparison of T_g with the ultimate ingression and diffusion coefficient for DGEBF-MXDA epoxies cured by (a) the Sheffield and (b) industrial cure methods. Linear fits are applied to data and R^2 values shown to indicate goodness of fit. Error bars represent the standard error of three samples in the y direction and two samples in the x direction.*

5.2.4 Diffusion and free volume

FV and cure regime

The free colume (FV) and fractional free volume (FFV) are shown in Figure 5.2.10 for DGEBF-MXDA samples cured under varied conditions. The free volume (blue), gradually increases with increasing pot-time for the Sheffield cure (solid bar). The industrial cure (shaded bar) shows an almost random FV with increased pot-time. The fractional free volume (red) shows no trent with increasd pot-time for the Sheffield cure. The FFV for industrial samples is seen to remain constant.

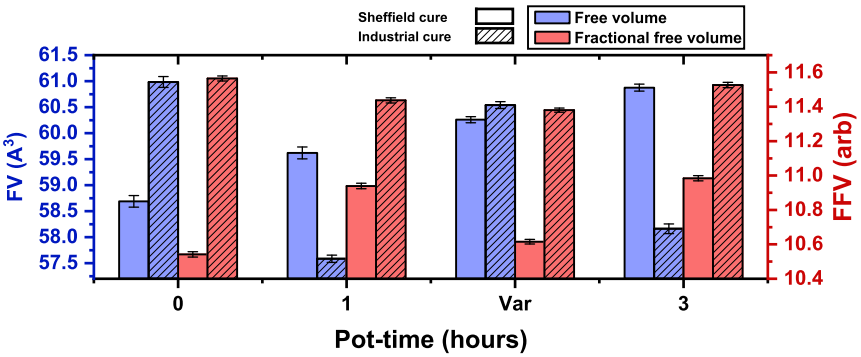

Figure 5.2.10: *The free volume (blue) and fractional free volume (red) for DGEBF-MXDA epoxy samples produced by different cure methods. Solid bars represent samples produced by the Sheffield cure regime whilst shaded bars correspond to the industrial cure method. Free volume properties were obtained by positron lifetime measurements using PALS Error bars represent the fitting errors generated in "LTPOLYMERS" software.*

FV and diffusion

Figure 5.2.11 compares free volume (FV) and fractional free volume (FFV) with the diffusion properties of the DGEBF-MXDA samples cured under varied conditions. The free volume for (a) samples produced using the Sheffield cure show a good (R^2 >0.9) downward trend with ultimate ingression whilst the relation with D_{ING} is poor (R^2 <0.5). The FV relation to diffusion for (b) shows D_{ING} increasing with FV in a highly correlated manner (R^2 2 >0.95). Ultimate ingression shows a weak downward trend with FV. The Ultimate ingression and D_{ING} for samples cured using the (c) Sheffield method decrease with increasing FFV but the both correlations are faily poor (R^2 < 0.6). The FFV shows no correlation with ultimate uptake or D_{ING} for samples cured by (d) industrial methods.

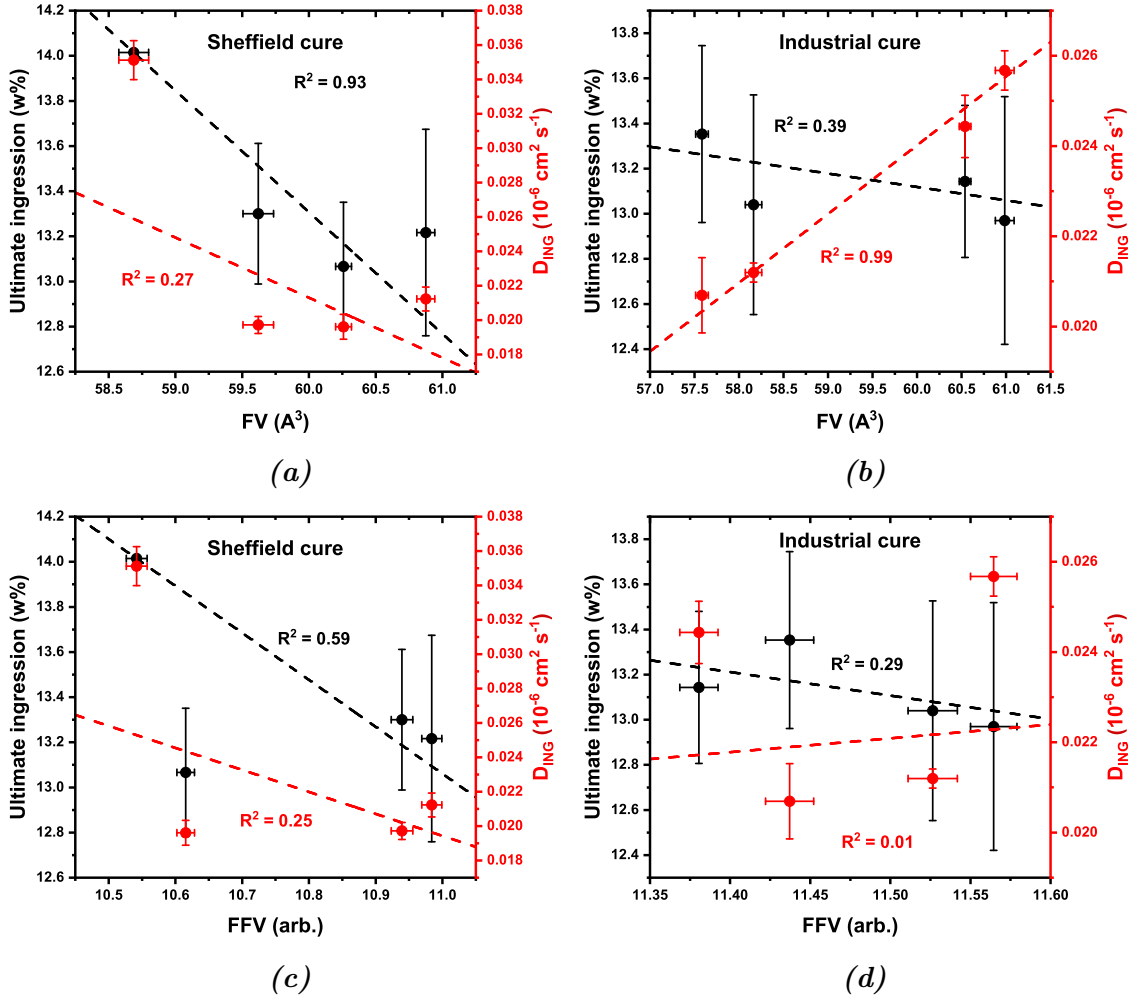

Figure 5.2.11: *The comparison between free volume measurements and diffusion properties of DGEBF-MXDA epoxy samples produced with varying curing method. The average free volume is compared with the ultimate ingression for (a) Sheffield and (b) industry cures. The Fractional free volume is also compared to diffusive properties for (c) Sheffield and (d) industry methods. Dashed lines represent linear fits with R^2 indicating goodness of fit. Y errors are standard errors of three samples whilst x errors are generated in the "LTPOLYMERS" software.*

5.2.5 Free volume and T_g

FV relation to T_g

The FV and FFV are compared with T_g values in Figure 5.2.12. For the samples produced using the (a) Sheffield cure , free volume decreases with increased T_g with a decent correlation level. No correlation is seen between FFV and the T_g. Samples produced using the (b) industrial method show no correlations between FV or FFV with T_g.

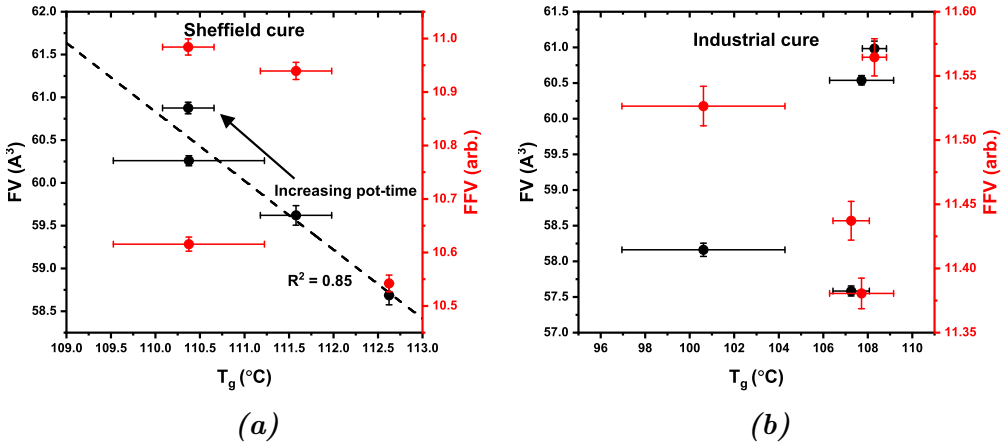

Figure 5.2.12: *A comparison of T_g with the free volume and fractional free volume for DGEBF-MXDA epoxies produced by (a) Sheffield and (b) industrial curing methods. Linear fits are shown by dashed lines with R^2 values indicating the goodness of fit. Y error bars represent errors generated from fitting lifetime data in "LTPOLYMERS" whilst x error bars represent that standard error of three samples.*

5.2.6 Conclusions

Epoxy samples consisting of DGEBF and MXDA were prepared by two curing methods. One referred to as the Sheffield cure was loosely based on an optimized cure schedule used in other work[71,106] which involves a relatively high cure temperature of 160 °C and a cure time of 3 hours (see Section 2.2.2 for details). The other method referred to as an industrial cure was implemented based on real world considerations. This was a 24 hour cure at room temperature followed by a 16 hour post-cure at 80 °C (see Section 2.2.6 for details.) For each method, four samples with varying pot-times were prepared and diffusion, T_g and free volume measurements were performed.

Affects on diffusion due to cure regime

The ultimate ingression for both Sheffield and industry cures were similar with increasing pot-time. The only difference was seen when samples were prepared without any pot-time and cured at 160 °C which resulted in an increased ultimate ingression from ≈ 13 to 14 %. It is expected that this increase is a consequence of amine evaporation during the oven cure which ultimately causes the system to be non-stoiciometric and the maximum number of possible cross-links is reduced.

The rate of ingression (D_{ING}) is high when there is no pot-time and a high temperature cure is used which could also be explained in the same manner as ultimate ingression. Increasing the pot-time to 1 hour causes a drop in ingression rate to a similar level to all of the industrially cured samples ($\approx$ 13%). Sheffield cured samples for a pot-time of 1 hour and varied pot-time, had lower ingression rates than the counterpart industrial samples. This could be due to more energy available in the in the higher temperature cure which increases the conversion of reaction.[39,145] As the only sample to show a considerable difference in diffusion properties was the sample which did not have a pot-time. This suggests that given just 1 hour for initial reactions to occur in the mixture is enough to increase the viscosity or bind sufficient amine to the system such that a near full reaction can be achieved.

The glass transition temperature

The glass transition temperature was measured for all samples as the tanδ peak obtained by dynamic mechanical analysis. Every sample cured using the industrial method resulted in a significantly lower T_g. The Sheffield samples had values between 110 and 112.5 °C whilst industrial samples were in the range of 100 and 108 °C . This is most likely attributed to a lack of high temperature to further increase the level of cross-linking[39,145,146] The samples cured using the hotter Sheffield cure method showed a good correlation between the ultimate ingression and T_g. There was no real correlation between T_g and the diffusion coefficient. The industrial cure had a reasonable correlation between T_g and D_{ING} based on R^2 values but the general spread in data was questionable. There was no correlation between T_g and ultimate ingression for industrial samples. All trends with T_g regardless of how poor the correlation showed an upward trend with diffusion properties. This is counter intuitive as an increase in T_g should indicate an increased reaction conversion[39,145]. This would lead to increased cross-links and increased ability to prevent ingression[143,144].

Free volume measurements

Samples cured using the Sheffield cure method resulted in free volume increasing gradually with increased pot-times. An increased pot-time was expected to improve the cross-linking in the epoxy network. The fractional free volume (FFV) fluctuated with increasing pot-time. Curing with the industrial method resulted in fluctuations in free volume whilst FFV was stable. The diffusion properties decreased with increasing free volume and FFV when using the Sheffield method which again, is a counter intuitive trend. Although only one of four correlations were considered good (R^2 >0.9), the general decrease in diffusion with increased free volume is still an interesting observation. Another interesting observation was that samples cured using the industrial method had an almost perfect (R^2 >0.99) positive correlation between FV and the diffusion coefficient. There were no other correlations with diffusion for the industrial cure.

A comparison of free volume and the T_g
A good correlation (R^2 >0.8) was seen between free volume and T_g for sample prepared using the Sheffield method. No other trends were seen between the T_g and either free volume or FFV for both curing methods.

5.2.7 Closing remarks
Although some trends were seen to be strongly correlating (based on R^2 values), no truly clear trends were seen that made logical sense. One thing which hasn't been taken into account thus far is how different the samples are and the difference between the results found. All chemistries are identical which, from positron beam studies shown in Chapter 3, probably means that only minor variations in free volume should be seen. Ultimately we can conclude, that curing at a higher temperature will result in a lower FFV and a higher T_g but the affects on diffusion are minimal as long as a pot-time of at least 1 hour (possibly lower) is implemented.

The industrial cure was implemented in order to study a more realistic cure regime for these epoxy networks. Another real-world consideration is the addition of pigments/fillers to the epoxy network. Whilst this is commonly done for aesthetic reasons (decorative paints), many studies have shown that this can increase mechanical performances[147,148] and improve chemical resistance in terms of ingression properties.[149]

5.3 Pigmentation of epoxy networks
5.3.1 Introduction
Resins used in several applications will often have pigments or fillers incorporated into the epoxy network.[147,150] The common reasons for pigmenting a network are to change the coating in an aesthetic manner (i.e. decorative paints) or to improve the mechanical properties of the material. Protective coatings can also have pigments amongst a number of components added to the epoxy-amine network. As such, this section studies the affects on diffusion due to the addition of pigments. Samples made for ingression will also have an identical sample produced for positrons annihilation lifetime spectroscopy (PALS) measurements and the free volume is determined. The diffusion and free volume results will be compared as will the thermomechanical properties (T_g) by means of dynamic mechanical analysis (DMA).
The materials used for this study are DGEBF epoxy resin mixed with MXDA amine which is cured as per Section 2.2.3. A barium sulphate pigment (referred to as barites or barytes) is incorporated into the network by vigorous mechanical mixing. Particles (sizes) of the pigment are essentially dispersed throughout the epoxy network. The size of the pigment has a mean diameter of 24.86 μm with 90% of particles less than 56.26 μm based on a study by Wang *et al*[151] The ratio between the epoxy and amine is determined with regards to number of epoxide and amine hydrogen equivalent weights (EEW and AHEW). This is kept at a stoichiometric ratio (1 epoxide : 1 amine hydrogen). Pigment is added in terms of weight percentage of the total mass (epoxy + amine + pigment) of the system and the structures of each material are shown in Figure 5.3.1. The pigment essentially dissolves in the epoxy

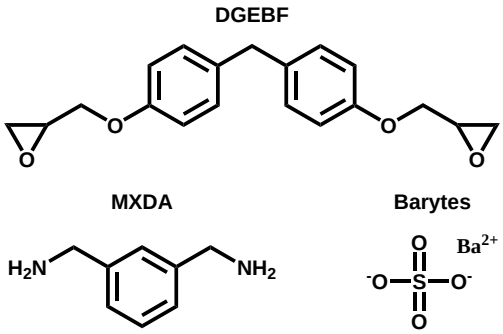

Figure 5.3.1: *The chemical structures of dyglycidyl ether of bisphenol F (DGEBF), m-Xylylenediamine (MXDA) and barium sulphate (Barytes).*

5.3.2 Diffusion characteristics

Diffusion curves

Diffusion measurements are made as described in Section 2.5.1 on four epoxy samples comprising of DGEBF resin and MXDA amine. Three of the samples have barytes pigment incorporated and are labelled in terms of weight percentage (w%). The ingression of methanol was monitored over time by mass measurements. The ingression curves for the four pigmented epoxies are shown in Figure 5.3.2 (a) along with their epoxy content mass (b)

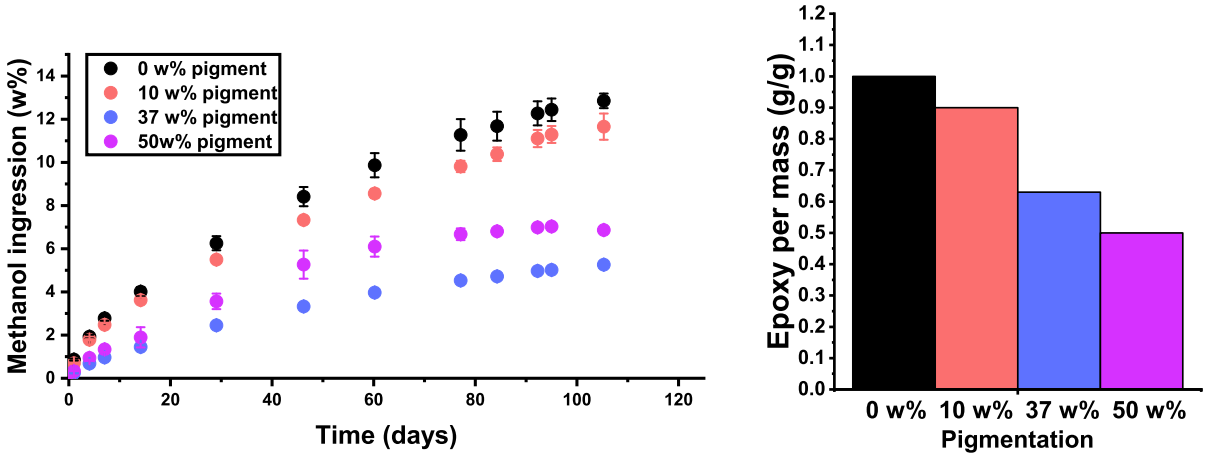

(a) *(b)*

Figure 5.3.2: *The (a) ingression of methanol into pigmented epoxy resins. Each sample consists of DGEBF resin cured with MXDA with varying amounts of barytes pigment. (b) the amount of epoxy per unit mass for each sample. The pigmentation amount is given in terms of weight percentage (w%). Errors bars given represent the standard error of three samples.*

The samples consisting of pure epoxy (black) has the greatest amount of ingression with a 10 w% addition of pigment resulting in a marginal decrease in ingression. Increasing to 37 pc pigment causes ingression to be hindered greatly dropping from $\approx$ 12.5 to 5 %.

Increasing the pigmentation to 50 w% has a slightly higher amount of ingression than 37 w% but significantly lower than 10 w% or a pure epoxy sample. The ultimate ingression has been reached in samples 37 and 50 w% pigmentation but sample 10 w% and the pure epoxy have not reached this point yet. Therefore, the ultimate ingression has been estimated based on the current ingression characteristics as described in Section 5.2.2. This is done to produce a graph of M_t/M_∞ plotted against the square root of time. From these plots, the ingression diffusion coefficient can be determined as described in Section 5.2.2.

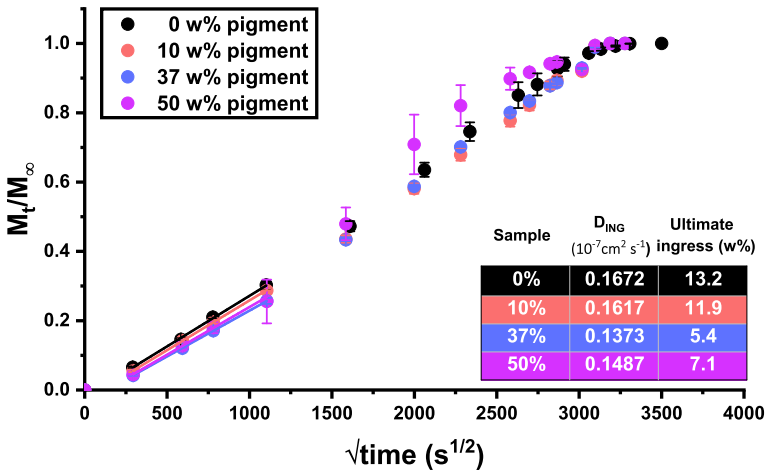

Figure 5.3.3: *The methanol ingression curves for pigmented epoxy networks. Each sample comprises of DGEBF-MXDA with different weight percentages (w%) of barium sulphate (barytes) incorporated to the network. By plotting the M_t/M_∞ against root time means the gradients of a linear fit can be used to determine the diffusion coefficient of ingression using. The regions used for linear fitting are shown as solid lines. Error bars represent the standard error of three samples.*

Diffusion properties and affects of pigment

Figure 5.3.4 shows the ultimate ingression, D_{ING} and the epoxy mass per mass (g/g) for the pigmented networks. The epoxy content is simply determined by the amount of epoxy per gram of each sample. For example, the sample containing 10 w% pigment has 90 w% of epoxy (epoxy-amine) substance. Therefore, the amount of epoxy in the sample equals 0.9 grams per gram of sample. Both diffusion properties have similar trends with respect to increasing pigment content. The rate of ingression is shown to decrease marginally when increasing the pigmentation to 10 w%. A large drop from ≈ 0.16 to 0.135×10^{-8} cm ^{2} s^{-1} occurs when increasing to 37 %. The ultimate ingression also drops from ≈ 12 to 5.5 w%. The rate then increases to $\approx 0.15 \times 10^{-8}$ cm ^{2} s^{-1} for a pigmentation level of 50 w%. The epoxy content in gram per gram is shown to show that the amount of epoxy available does not directly correlate to diffusion. As the pigment is an inorganic mineral, methanol should not penetrate it. Therefore the majority of ingression should be due to the epoxy network. As a direct trend is not seen between epoxy content and pigmentation, this suggests that on some level, the interaction between the epoxy network and the pigment affect the ability to prevent methanol ingression.

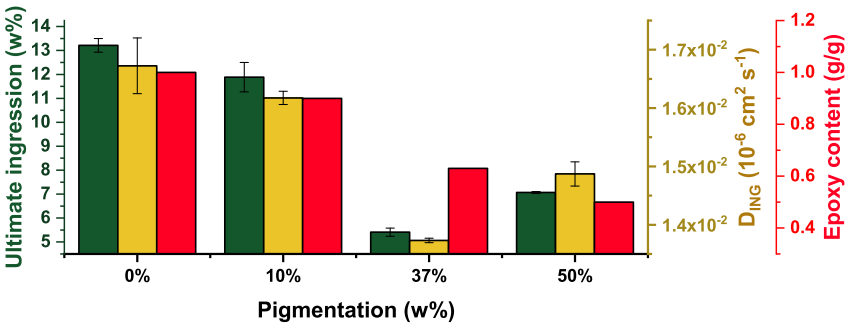

Figure 5.3.4: *The ultimate ingression, diffusion coefficient and the epoxy content for each pigmented epoxy network. Each network consists of DGEBF-MXDA-Barytes pigment. Error bars represent the standard error of three samples.*

5.3.3 Diffusion and glass transition

T_g and pigmentation

T_g for each pigmentation network were measured as the peak of the tanδ peak obtained by dynamic mechanical analysis (DMA). Figure 5.3.5 shows the variation in T_g with weight percentage of pigmentation for each epoxy sample. The T_g varies between 106 and 113 °C and there is no trend between T_g and pigmentation.

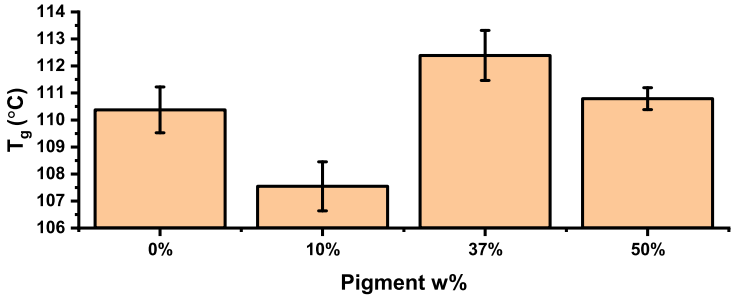

Figure 5.3.5: *The glass transition temperature (T_g) determined by dynamic mechanical analysis for epoxy resins containing different amounts of barytes pigment. Error bars represent the standard error of two measurements.*

T_g and diffusion

The T_g is compared with the ultimate ingression and ingression coefficient in Figure 5.3.6. Both diffusion properties show a downward trend. The correlation between Ultimate ingression and T_g is relatively poor ($R^2 < 0.5$) whilst T_g and D_{ING} show a good correlation ($R^2 > 0.9$). As shown in other studies,[145] the T_g is a good measure of reaction conversion and within a sample series, increased T_g implies a higher conversion. This means that more crosslinks form and the network is more tightly packed which would hinder the mobility of ingressors such as methanol. This should also reflect in free volume measurements as space between cross-links will also decrease.[35,143,144]

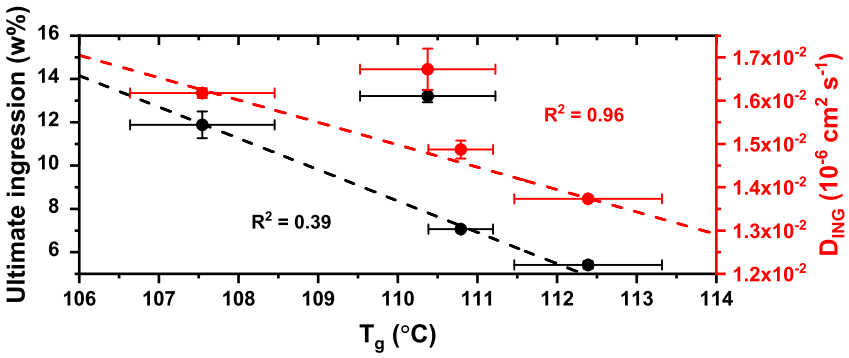

Figure 5.3.6: *The ultimate ingression and diffusion coefficents compared with T_g of pigmented epoxy networks which consist of DGEBF-MXDA-Barytes pigment. Error bars represent the standard error of three samples.*

5.3.4 Diffusion and the free volume

FV and pigmentation

The free volume (FV) and fractional free volume (FFV) are compared with pigmentation in Figure 5.3.7. The T_g - FV relation is reasonable (R^2 >0.8) whilst the T_g - FFV relation with FFV is good (>0.9).The FV and FFV decreased with increased pigmentation, which could be due to epoxy-pigment interactions, but it could also be a consequence of positrons annihilating within pure pigment. It was shown in Section 4.4.4 when two materials are measured simultaneously, the resulting lifetime spectra, and therefore the free volume measurement, is an average of the two materials. However, as the pigment is non-polymeric, it is expected that the lifetime spectra from the pigment would be narrow due to a lack of free volume annihilations and therefore would not affect the free volume determination.

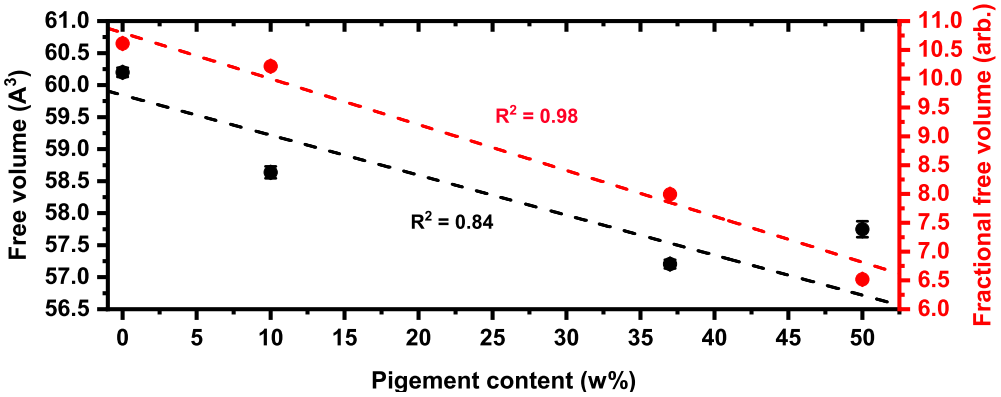

Figure 5.3.7: *The free volume and fractional free volume compared with the pigmentation amount in DGEBF-MXDA epoxy samples. Dashed lines represent linear fits with R^2 values indicating the goodness of correlations. Error bars represent standard errors based on errors generated in "LTPOLYMER" software.*

FV and diffusion

Figure 5.3.8 shows how the (a) free volume (FV) and (b) fraction free volume (FFV) relate to the ultimate ingression and diffusion coefficient. Free volume is shown to increase with both the ultimate ingression and D_{ING} in a meaningful fashion (R^2 >0.9). The FFV generally trends upwards with the ultimate ingression and D_{ING} but the correlations are poor and reasonable respectively (R^2 < 0.39 and >0.69). These trends follow theory of increasing free volume will cause ingression to be more favourable due to increased space for molecular mobility.

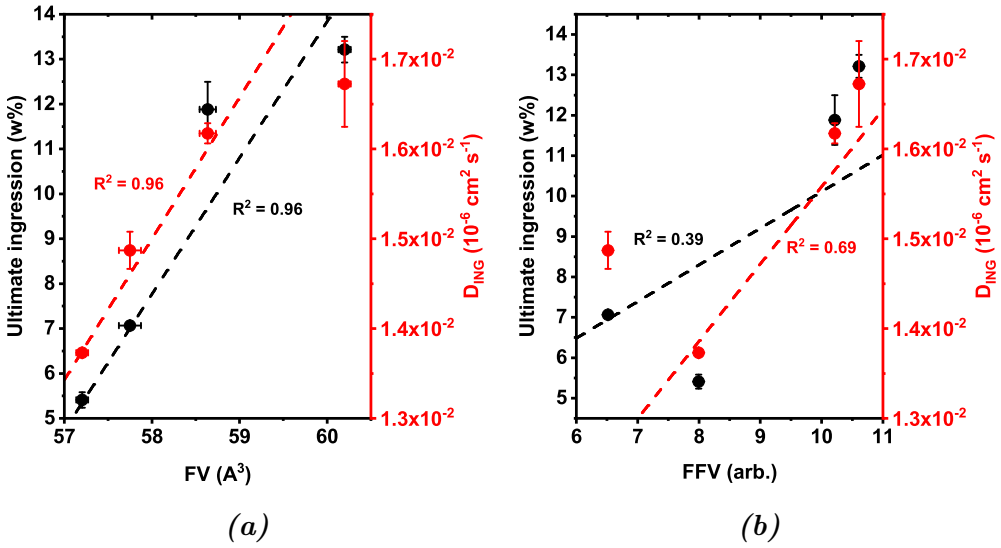

Figure 5.3.8: *The diffusion properties compared to free volume measurements for DGEBF-MXDA epoxies which are pigmented with barytes pigment. The ultimate ingression and the diffusion coefficient are compared with (a) free volume (FV) and (b) fractional free volume (FFV). Dashed lines represent linear fits with R^2 values indicating the quality of correlation. Y error bars represent the standard error of three samples whilst x error bars are from errors generated in the fitting routine carried out in "LTPOLYMERS" software.*

Pigment lifetime measurement attempt

To determine whether this decrease in FV is due to epoxy-pigment interaction, the free volume of the pure pigment should be determined. Generally, two identical solid pieces are required for PALS measurements which surround the positron source. As such, the production of pure pigment samples was attempted by pressing barytes powders into circular pellets of approximately 1 cm in diameter using a hydraulic press, with pressure applied up to 4000 psi at which the sample were held for 30 seconds. Although it was possible to produce discs of pigment, these were incredibly fragile and during positioning of the discs for PALS, they ultimately failed. Figure 5.3.9 shows (a) the top and side views of the formed discs and (b) the resulting powder due failure.

(a) ***(b)*** ***(c)***

Figure 5.3.9: *(a) The discs of barytes formed by pressuring powders in a steel disc mould and (b) the powder formed on moving the discs. For PALS, two identical samples are required and need to be positioned around the positron source. During positioning, small stresses are applied to samples and the fragile nature of the discs causes failure. (c) The positron source buried in barytes pigment inside a sample tube. It was placed between the PALS detectors, and a measurement made.*

The resulting powder was compacted into a sample tube and the positron source placed on top. More powder was then added on top of the source and gently pressed. A PALS measurement was made with the idea that the majority of positrons will still annihilate within the powder. The resulting spectra is compared to the 10 w% pigment sample in Figure 5.3.10. It can be seen that the lifetime spectra is much narrower in the pure pigment than in the epoxy-pigment mixture. Blue lines represent the exponential for corresponding to the orthopositronium lifetime component (τ_{oPs}) for pure pigment (dashed) and a DGEBF-pigment sample of 10 w%(solid). As oPs represents annihilations in free volume, it is interesting to see a small amount of oPs annihilations for the pure pigment. This could be due to the surrounding sample tube or annihilations occurring in the thin polymeric film, which surrounds the radioactive material. At this point, it is difficult to determine whether the changes in FV and FFV with increasing levels of pigments are due to epoxy-pigment interactions or just because of a higher amount of non-polymeric material. However, it should be noted that the study of PTFE-DER354 samples (Section 4.4.4) concerns two polymers, which contain free volume whereas the pigment is inorganic. Therefore the pigment should not contain free volume which would not affect the free volume portion of the lifetime spectra which would imply that any changes to FV, are a consequence of epoxy-pigment interaction.

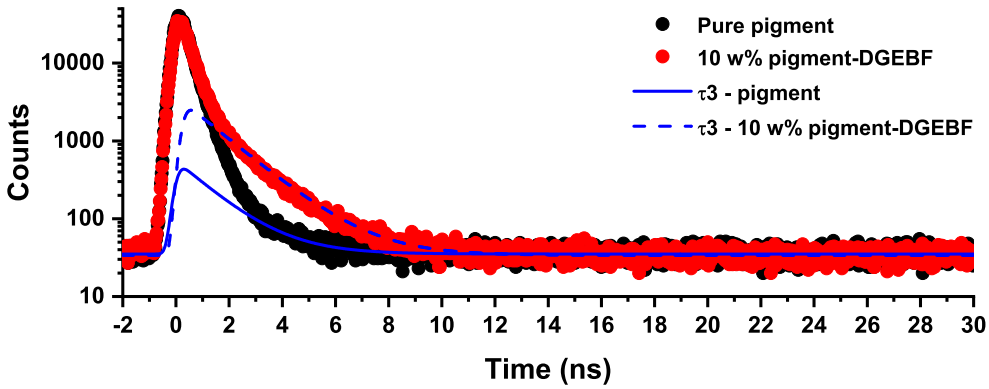

Figure 5.3.10: *The positron annihilation lifetime spectra for pure barytes pigment (black) compared to DGEBF-barytes sample with 10 w% pigment. The blue dashed and solid lines show the fitted orthopositronium lifetime componets (τ_3) for DGEBF-pigment and pure pigment samples.*

5.3.5 FV and T_g

FV relation to T_g

The comparison of T_g with the free volume (FV) and fractional free volume (FFV) for the pigmented epoxies is shown in Figure 5.3.11. Both FV and FFV shows a general downward trend but the correlation is poor as indicated by R^2 values (< 0.5). Generally a decrease in FV is expected to correlate to increasing T_g as this implies the reaction conversion is increasing within this sample set which results in more cross-links and a reduction if free volume.

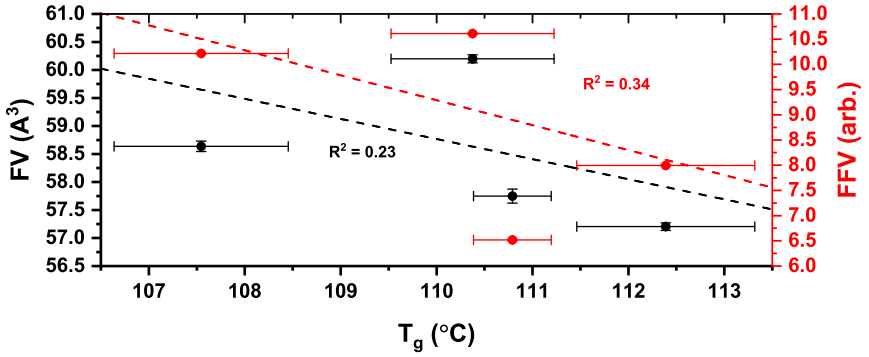

Figure 5.3.11: *The glass transition temperature, compared with the free volume and fractional free volume for pigmented epoxy samples. Each sample consists of DGEBF-MXDA and varying weight percentages of barytes pigment. Dashed lines represent linear fits generated in Origin software with R^2 values indicating the goodness of the correlation. Y error bars represent the standard error of three samples whilst x error bars represent the standard error of two samples.*

5.3.6 Conclusions

Affects of pigmentation

The addition of barytes pigment to epoxy networks comprising of DGEBF-MXDA resulted in the hindrance of methanol ingression. Increasing the amount of pigmentation seemingly caused a drop in the ultimate ingression and the diffusion coefficient up. This was true up to a pigmentation amount of 37 w% and when increased to 50 w%, the ultimate ingression and diffusion coefficient increased. It could be considered that that decrease in diffusion exhibited in samples containing 10 and 37 w% pigment is due to the amount of epoxy present in the sample. The inorganic pigment shouldn't uptake solvent which means increasing the pigmentation reduces the amount of material which can uptake solvent. Following this theory, it would be expected that increasing the pigment further would further reduce the ingression but as shown with the 50 w%, the ingression increases. This might be because at this level of pigmentation, the epoxy-amine network is highly swollen and would allow for easier ingression of methanol.

Free volume measurements

Free volume measurements were measured by positron annihilation lifetime spectrosocpy (PALS) for the pigmented networks. Both the free volume and fractional free volume decreased with increasing pigmentation. Some studies have suggested that fillers/pigments can "fill" free volume voids[123] but due to the mean pigment size of barytes ($\approx$58 μm) compared to free volume ($\approx$ nm), this is not the case. The correlation between FV and FFV were considered reasonable and good respectively when taking the R^2 values into consideration which were obtained by linear fitting. In an attempt to determine whether this decrease in FV is due epoxy-pigment interaction or a consequence of pure pigment having a lower average lifetime, PALS was performed on pigment discs and it was seen that the lifetime distribution was much narrower.

The ultimate ingression and diffusion coefficient increased with increased free volume. The correlations for both were considered high by R^2 values obtained through linear fitting ($R^2 > 0.95$). The relation between FFV and the diffusion properties showed the same trend as FV but the correlations were much weaker ($R^2 < 0.7$). These results add to the theory that an increasing free volume causes the ingression of penetrators to be more favourable[15].

T_g

The glass tranistion temperature showed variations between 107.5 and 112.4 °C but the changes did not correlate to increasing pigment. The T_g did correlate well with the diffusion coefficient in that a higher T_g resulted in a lower D_{ING} value. The same trend was seen when comparing T_g to ultimate ingression but the correlation was poor. Within a sample series, it can be expected that increasing T_g would hinder the ingression of methanol. This is because an increase in T_g implies that a higher degree of reaction occurs which therefore means a higher number of crosslinks.[39,145] A higher number of cross-links ultimately causes the network to be more tightly packed, reducing free volume and hindering the ingression of methanol.

A comparison of trends in FV and T_g

Significant changes in diffusion properties showed a high correlation in that a decrease in free volume corresponded to a decrease in the ultimate ingression and the rate of ingression. Whilst the T_g also showed some correlations in that, a decrease in T_g resulted in a decrease in ingression, this correlated in a poorer manner than FV relations. This suggests that both measurements can be used to infer ingression properties of pigmented systems but changes in diffusion are detected in a more sensitive manner when measuring free volume by means of positron annihilation. As PALS is a non-destructive technique, this is a desirable ability.

5.3.7 Closing remarks

This section presented diffusion, T_g and free volume measurements for pigmented samples of epoxy resins. The affects of the amount of pigmentation on the diffusion, T_g and free volume were shown. This information is useful in the field of protective coatings as many applications incorporate pigments into chemical formulations generally to increase mechanical properties. Future work should consider a range of pigments and metal particles to study how interfacial interactions affect the free volume and whether these changes are correlative with T_g surfaces. Another common necessity in protective coatings is to reduce the viscosity. This can be achieved by incorporating diluent epoxies or solvents into the formulation. The next section concerns the affects of solvent addition on the diffusion, T_g and free volume whilst Sections 5.5 and 5.6 will investigate the affect of epoxy diluents.

5.4 Solvated epoxy networks

5.4.1 Introduction

This section concerns epoxy samples which were prepared such that xylene is locked into the network as described in Section 2.2.5. Solvents are added to epoxy resins in order to reduce the viscosity of the epoxy pre-application/cure. This is because some application methods such as spray coating would not be possible with high viscosities. The solvent evaporates after application but it is expected that a fraction of solvent will remain in the coating. The samples prepared here have different amounts of xylene incorporated to the network and are studied with regards to diffusion, glass transition temperature and free volume.

5.4.2 Methanol diffusion

Diffusion cycle 1

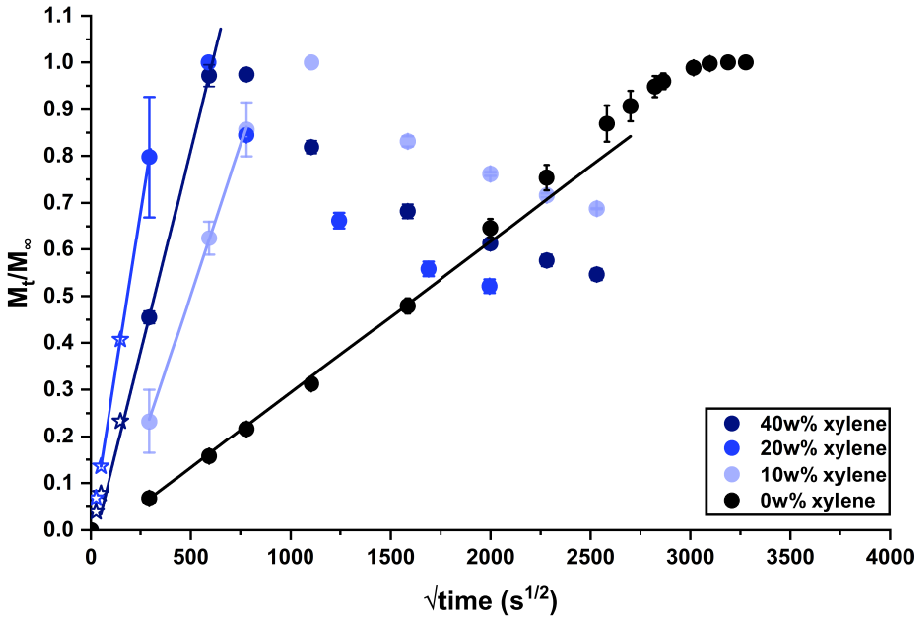

Figure 5.4.1: *The ingression curves for epoxy resin samples consisting of DGEBF mixed with different levels of xylene in weight percentage which were then cured with MXDA. Solid and dashed lines represent the gradients used for the determination of ingression and egression diffusion coefficients respectively. Error bars represent standard error of three samples.*

Figure 5.4.1 shows the ingression curves for three epoxy samples with different amounts of xylene incorporated. It can be seen that the ingression (solid circles) is rapid, reaching ultimate ingression for all samples (containing xylene) in less than 700 $s^{1/2}$ (5.6 days). This rapid ingression rate could be due to the trapped xylene swelling the epoxy-amine network, which exhibits plasticisation behaviour. This causes the glass transition temperature to decrease significantly, that leads to improve polymer chain mobility, which in turn promotes the diffusion of small molecules through the network. behaves as a plasticiser which reduces the Tg causing increased polymer mobility.[24,29] All xylene containing samples then show a decrease in mass whilst the pure epoxy continued before plateauing.

The mass loss did not visually appear to be due to physical degradation and was expected to be due to loss of xylene after the ingression of methanol. To prove this, gas chromatography was performed on samples of the fluid in which the epoxies were immersed.

Gas chromotography

In order to obtain useful information by means of gas chromatography, a series of reference standards need to be measured. As such, four samples containing a mixture of methanol and o-xylene with concentrations of 0.2, 0.5, 1 & 2 % with respect to xylene were prepared. Figure 5.4.2 shows the elution time for the different concentrations of the xylene isomer, o-xylene. The sharp peak at approximately 6 minutes corresponds to methanol which accounts for at least 98 % of each solution. The smaller peak at approximately 7.6 minutes correspond to o-xylene.

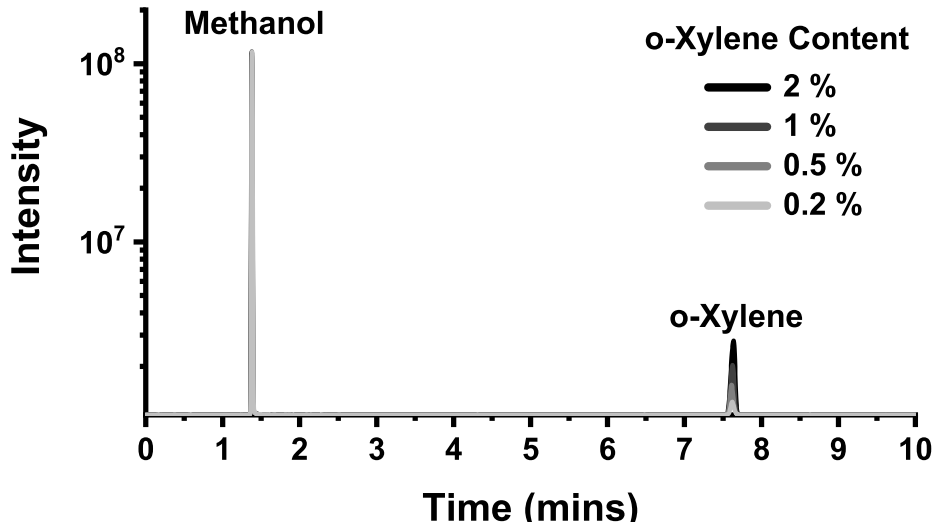

Figure 5.4.2: *Retention times obtained using gas chromatography for four samples containing differing concentrations of xylene with respect to methanol.*

Comparison of unknown samples with reference standards

Two samples (S1 and S2) were taken from ingression jars which contained solvated epoxy resins. The elution times obtained by gas chromotography are compared to the reference standards are shown in Figure 5.4.3. A small peak in S1 and S2 corresponds to the o-xylene peak shown in the reference measurement but there are also two peaks at shorter retention times ($\approx$ 6.1 and 6.5 minutes). A large peak corresponding to methanol was seen at 1.6 minutes again but is outside the chosen x scale. The peaks between 6 and 6.6 minutes are assumed to be isomers of xylene (m and p xylene).

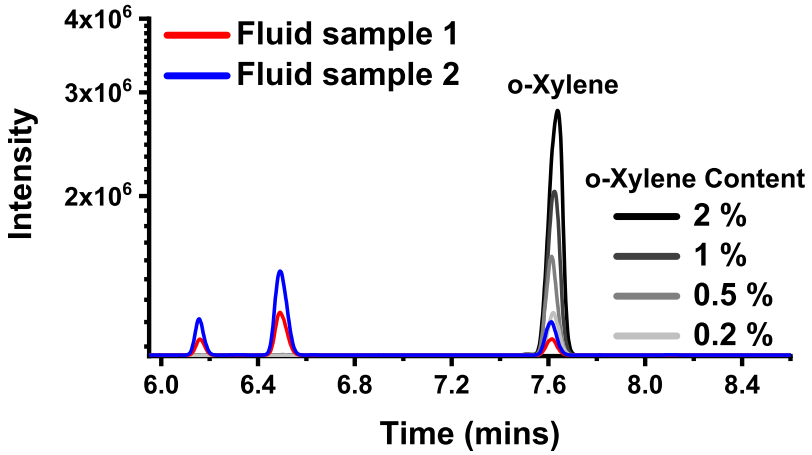

Figure 5.4.3: *Retention times of the methanol-xylene reference samples in comparison to two samples taken from the ingression fluid of a solvated epoxy samples obtained by gas chromatography. A large peak at 1.6 minutes is also seen which corresponds to methanol but is outside the chosen x-scale.*

To confirm that the two peaks to the left of the o-xylene peak are isomers, a solution of cleaning grade xylene was measured which contains all three isomers of xylene. The retention times for S1 and S2 are compared to the mixed xylene sample in Figure 5.4.4. It can be seen that the peaks at shorter retention times occur in the reference samples and as such we can suggest that isomers p, m & o-xylene are all present in the ingression fluid samples. In general, o-xylene has the longest elution time, owing to its larger kinetic radius. p-xylene is generally found to have the shortest elution time[152–154]. Based on this literature, Figure 5.4.4 is labelled to relate each peak to each of the isomers.

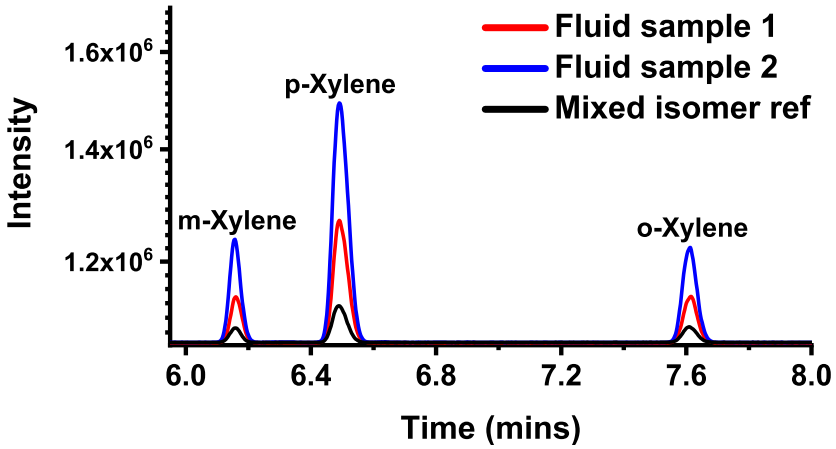

Figure 5.4.4: *Retention times of the three xylene isomers obtained by gas chromatography. The labelling of isomers is estimated from literature values in which the majority of results show retention times in this order i.e. $m \rightarrow p \rightarrow$ o-xylene. The data labelled mixed xylene isomers is a solution containing all three isomers which was used as a reference.*

Estimation of xylene concentration in unknown samples

The concentrations of xylene in the unknown samples can be estimated by comparing the area underneath each retention peaks. Figure 5.4.5 shows the peak area against xylene concentrations. A linear fit (red dashed lines) has been applied to the known xylene concentrations (black circles) and the unknown samples (open circle, red and blue triangles) have been positioned on the fitted line with respect to their peak areas. The xylene concentration is estimated as the corresponding point on the dashed red line. This was found to be 0.113 and 0.246 % for S1 and S2 respectively.

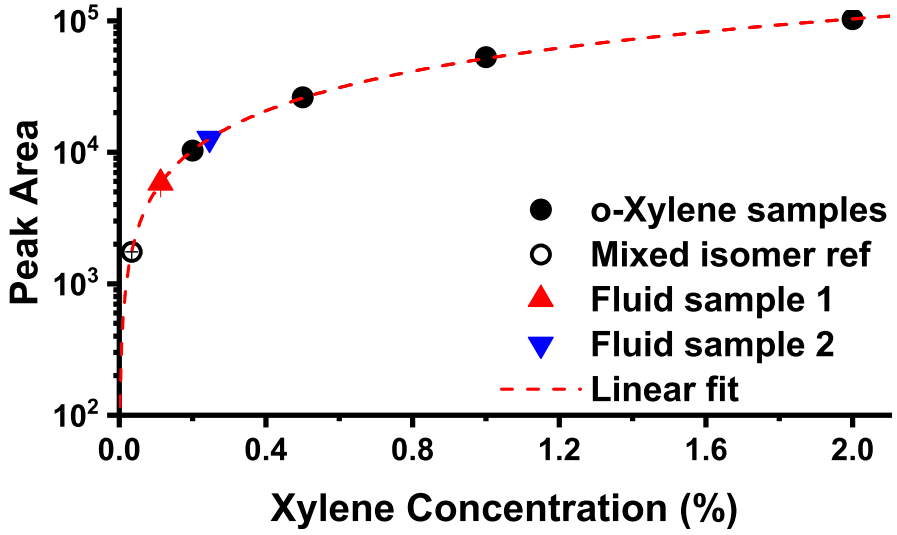

Figure 5.4.5: *The are of the retention peaks obtained by gas chromatography. A linear fit (red dashed line) is applied to the samples with known concentrations (black circles). The areas of the unknown samples (triangles) is then correlated to the linear fit to determine their concentrations. The open circle data point is the mixed xylene isomers samples.*

Following the detection of xylene, the samples were removed from methanol and egression is monitored by mass measurements overtime.

Egression curves

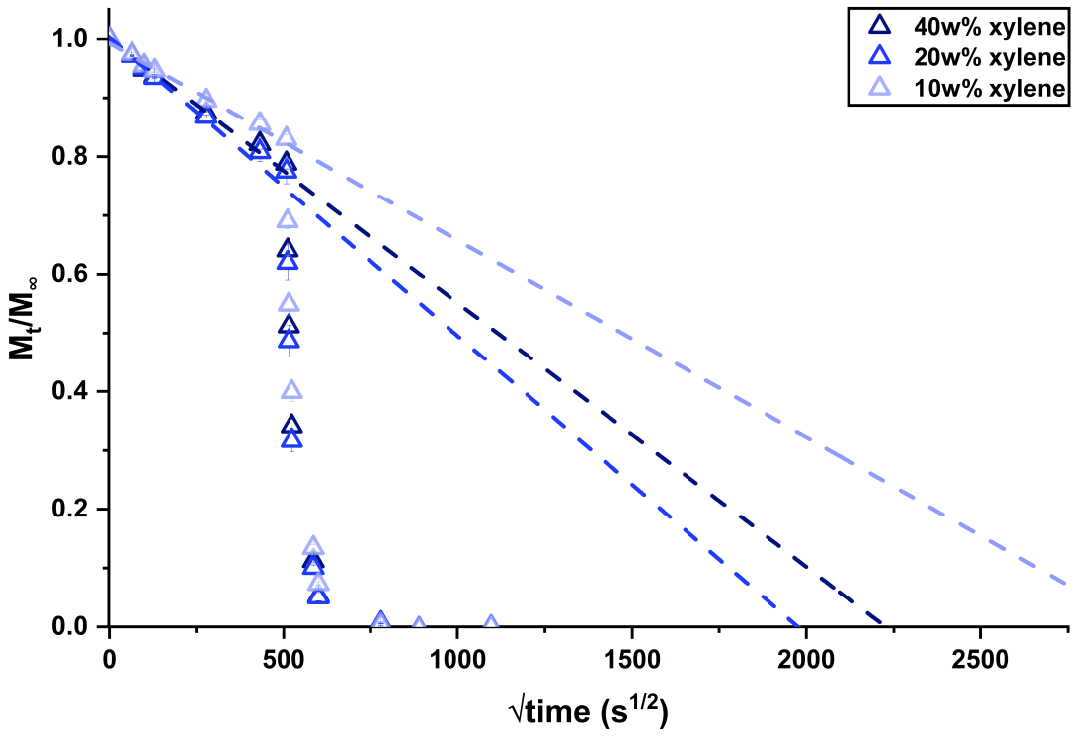

Figure 5.4.6: *The egression of methanol for epoxy samples comprising of DGEBF resin and MXDA amine. Each sample has different weigh percentages of xylene incorporated to the network. Dashed lines represent linear fits applied to short egression times (< 400 $s^{1/2}$) which are used to determine egression coefficients. A large drop is seen at ≈ 500$s^{1/2}$ which is due to samples being placed in an oven at 80°C to drive off xylene and methanol. Error bars represent the standard error of three samples.*

Figure 5.4.6 shows the egression curves for the three epoxy samples containing different amounts of xylene. The samples were left in air for around 3 days (≈ 500 $s^{1/2}$), before being placed in an oven at 80°C (large drop in M_t/M_∞). This was done in order to remove all methanol and any remaining xylene to prepare for new ingression studies. Linear fits (dashed lines) are applied at short ingression times and are used to determine egression diffusion coefficients.

Diffusion summary

Figure 5.4.7 shows the diffusion properties for each sample. The ultimate ingression is similar for all three samples with the 20 w% sample marginally lower. The ingression rate for 40 and 10 w% are similar with 20 w% being considerably higher in both ingress and egression rates. Whilst it is not understood why the 20 w% has a larger increase in ingression rate than the other two xylene containing samples, the increase when comparing all solvated samples to a neat epoxy (DGEBF) can be rationalised. The xylene locked into the epoxy network has a Van der Waals volume of 122 A^3. This inevitably causes the network to swell and T_g decreases. This decrease causes the polymer chains to be more mobile which allows

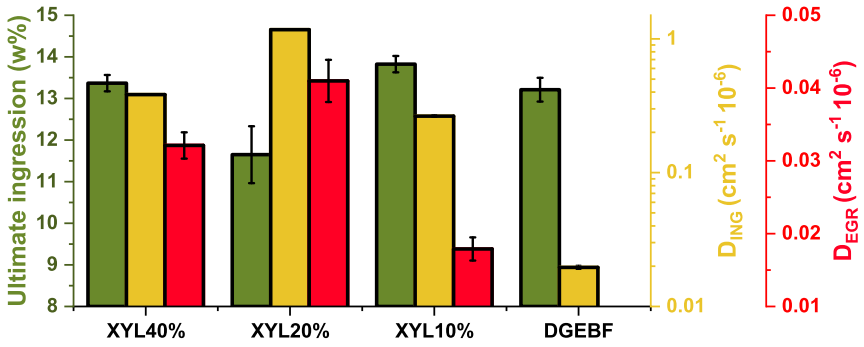

Figure 5.4.7: *The diffusion properties for DGEBF epoxy samples cured with MXDA which contain different amounts of xylene. Error bars show standard error of three samples.*

the methanol to more easily ingress into the sample. As methanol ingresses, the xylene simultaneously egresses and once the ultimate ingression of methanol is reached, mass losses are seen as the remaining xylene diffuses out of the network. This is likely due to the epoxy being plasticised further by the methanol, which increases molecular mobility. As methanol diffuses into the network, xylene also diffuses out.

5.4.3 Diffusion - T_g relation

Relation to xylene content

Figure 5.4.8 shows the expected decrease in T_g with increasing xylene content in the epoxy network. The T_g decreases in an exponential growth fashion as indicated by the blue dashed line. Based on this fit, the T_g for the 10 w% sample is estimated as the experimental T_g was not measured.

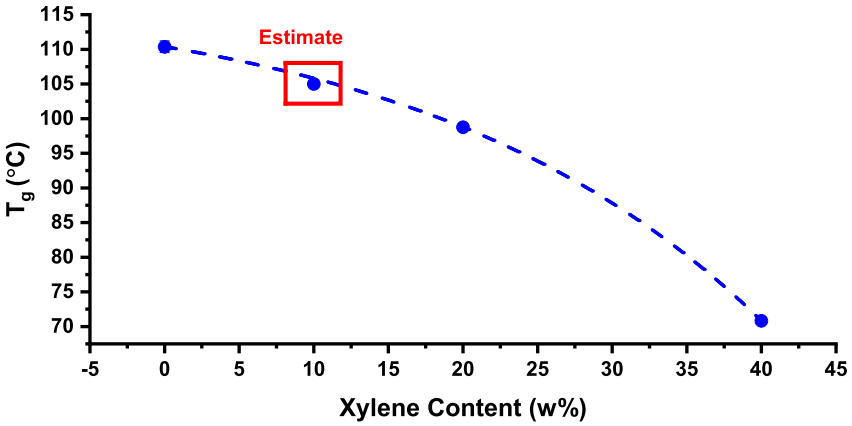

Figure 5.4.8: *The glass transition temperature for DGEBF-MXDA samples with different amounts of xylene in weight percent. A dashed blue line represents an exponential grow fit performed using Origin software. The data point highlighted by a red box is an estimated T_g as per Section 5.4.3.*

T_g and diffusion

Figure 5.4.9 compares the T_g to the diffusion properties. The ingression rate is much lower for the 0 w% xylene sample than any of the xylene containing epoxies. This difference is emphasised by the need for a log scale. The 20 w% xylene sample shows the highest ingression rate whilst 10 and 40 w% are similar. The ultimate ingression is similar for all samples except the 20w% which is lower by ≈ 1.56 - 2.17 w%. It should be noted that the value for ultimate ingression is estimated for the 0 w% sample based on the trend of ingression thus far (similar to the estimate in Section 5.2.2. These results show no trend between xylene content and the glass transition temperature. From these results we can conclude that any amount of xylene incorporated into the epoxy network causes the rates ingression and egression to greatly increases.

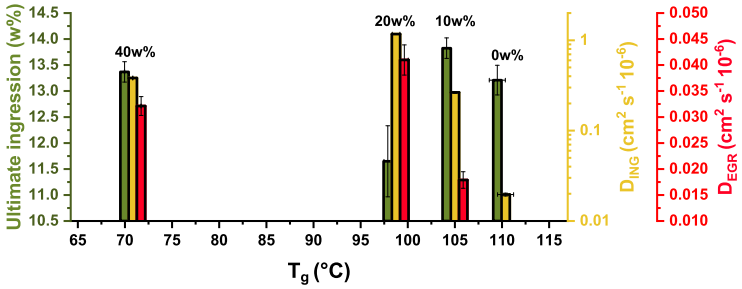

Figure 5.4.9: *Diffusion properties for samples of DGEBF-MXDA which contain different amounts of xylene. Error bars represent the standard error of three samples.*

5.4.4 Free volume and diffusion

Free volume relation to Xylene content

Figure 5.4.10 compares the xylene content with both free volume and fractional free volume (FFV). Free volume and fractional free volume increase in an almost exponential fashion. A study by Karbowski *et al*[155] shows positron lifetime measurements in benzene, which are longer than the lifetime measurements made for DER354-MXDA samples presented in this work. As xylene contains a benzene ring, it could be suggested that the lifetime measurements will be affected by annihilation within xylene.

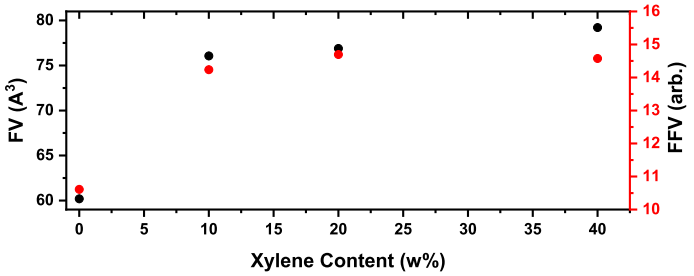

Figure 5.4.10: *The free volume (FV) and fractional free volume (FFV) for DGEBF-MXDA networks containing different amounts of xylene in terms of weight percentage. Error bars represents the standard error of three samples.*

Karbowski *et al*[155] presented oPs lifetimes from 17 sources, which was on average 2.75 ± 0.119 ns. Assuming that benzene has a similar oPs lifetime to that of xylene, we can estimate the lifetime of a sample containing different weight percentages of xylene and epoxy. Figure 5.4.11 shows the measured and estimated lifetimes as a function of time. The estimated values are shown to increase with xylene content whereas the actual values show an initial increase to ≈ 1.8 ns and remains constant. To fully understand the effects of xylene, PALS measurements are needed on xylene in future.

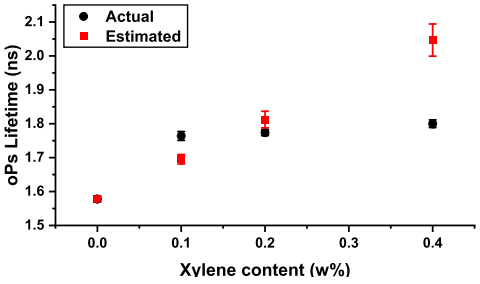

Figure 5.4.11: *The measured and estimated orthopositronium lifetimes for DER354-MXDA epoxy samples which contain differing amounts of xylene.*

Correlations

The relationship between free volume (FV) and fractional free volume (FFV) with diffusion properties is shown in Figure 5.4.12. Boxes highlight the pure and solvated epoxy networks. The ultimate uptake shows no correlation with FV or FFV with three of the four samples showing similar ultimate uptake values of 13-14 w%. The rate of ingression increases greatly with the addition of solvent and this is increase is also seen in free volume. It is interesting to see that there is a large increase in free volume for the initial addition of xylene but further addition does not correspond to increased free volume. In FFV a trend is seen but locally within the solvated epoxy networks. The inset image highlights this with increasing FFV corresponding to increased egression and ingression.

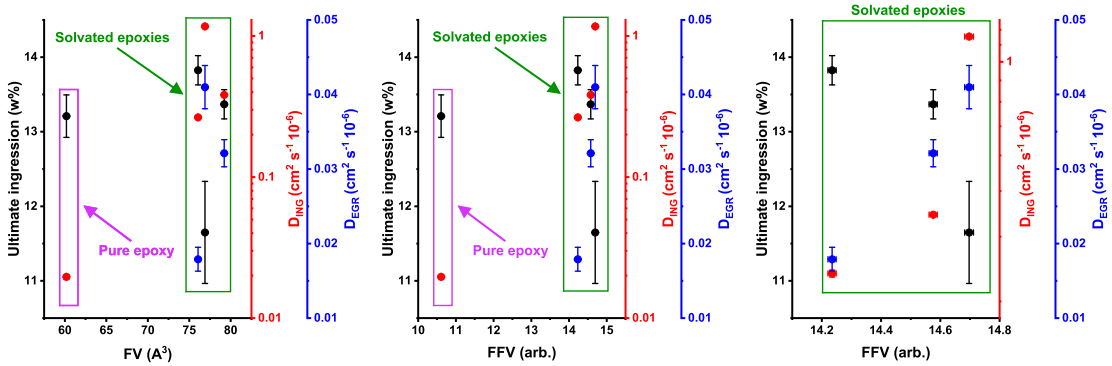

Figure 5.4.12: *The free volume (FV) and fractional free volume (FFV) compared to the ultimate ingression, ingress and egress diffusion coefficients for epoxies containing xylene.*

5.4.5 T_g and free volume relation

T_g, FV and FFV

Figure 5.4.13 shows how FV and FFV vary with T_g for epoxy samples containing different amounts of xylene. FV and FFV show a slight decrease with increased T_g where solvent is involved but a huge difference is seen when solvent is removed.

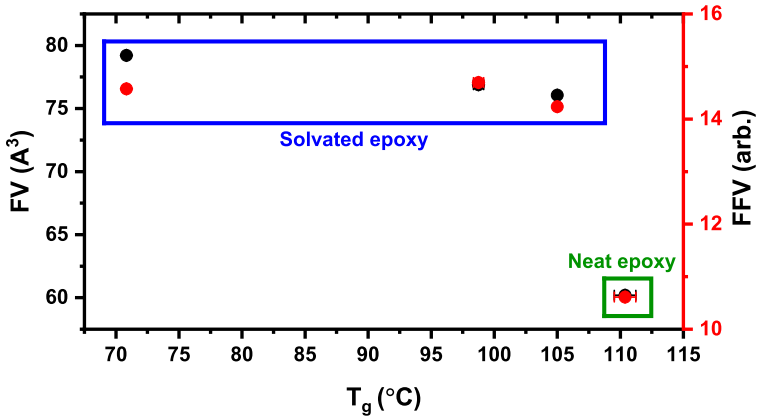

Figure 5.4.13: *Free volume (FV) and fractional free volume (FFV) compared to relevant T_g values. Blue and green boxes highlight epoxy samples containing solvent and pure epoxy respectively.*

Comparison of diffusion trends

Figure 5.4.14 compares the correlations of T_g and free volume with diffusion properties. The T_g does not show any clear trend with any of the diffusion properties.

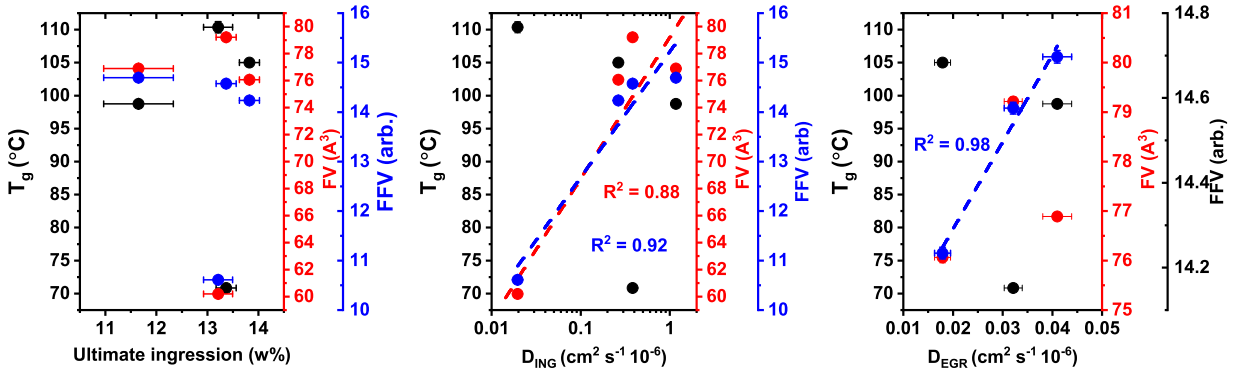

Figure 5.4.14: *The diffusive characteristics compared to free volume for DGEBF-MXDA epoxy samples which contain different levels of xylene. Error bars represent the standard error of three samples.*

Ingression cycle 2

After the solvated samples were dried in the oven, they were re-immersed into methanol and mass measurements were made over time again. Figure 5.4.15 shows the ingression of methanol thus far in terms of weight percentage. The second cycle (solid circles) exhibits a slower ingression rate than the first cycle (open circles). This is probably due to the lack of xylene swelling and plasticising the network. The rate of the standard neat epoxy sample (0 w% xylene) is lower than all the solvated samples but it cannot be determined whether this difference is due to the solvated samples being previously swollen or due to the curing method. The neat sample was cured at the standard higher temperature of 160 °C whereas the solvated samples were cured up to 135 °C. The reduced cure temperature could result in a less cross-linked network increasing the amount of free volume.

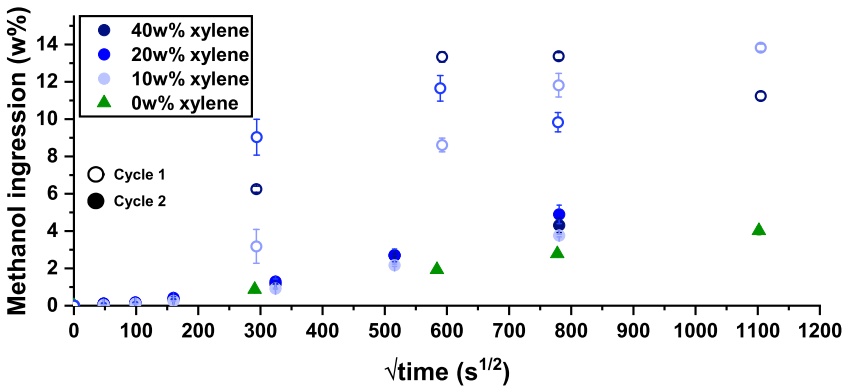

Figure 5.4.15: *The methanol ingression curves for solvated epoxy samples comprising of DGEBF resin, MXDA harderner and xylene solvent. The first ingression cycle (open circles) exhibits a much quicker rate of ingression than the second cycle (solid circles). The second cycle was carried out following oven drying of the samples. 0 w% xylene is shown by green triangles and is shown to have the lowest rate of ingression. Error bars represent standard errors of three samples.*

5.4.6 Conclusions

Affects of solvation on diffusion

In comparison to the pure DGEBF-MXDA sample, the addition of xylene to the DGEBF-MXDA epoxy network caused a large increase in the ingress diffusion coefficient (D_{ING}) whilst the ultimate ingression was only reduced by 2 w% for a xylene concentration of 20 w%. The increased D_{ING} did not correlate to increasing xylene concentration and was slightly random. All three xylene containing samples experienced a drop in mass at $\approx$ 750 $s^{1/2}$ which was not visibly due to physical degradation. Gas chromatography was performed on the methanol fluid (post ingression study) and three xylene isomers were found with a concentration between 0.1 and 0.25 %. This confirms the loss in mass of the xylene samples on ingression. The xylene is expected to have largely swollen the network due to its large VdW volume of 122 A^3 and in combination with lowering the T_g, this allows for enhanced ingression capabilities The release of xylene cane be explained in terms of Fickian diffusion in that the concentration gradient between the xylene and methanol causes xylene to move from a region of high to relatively low concentration.

After ingression studies, the xylene containing samples were place in the air for 3 days before being placed in an oven at 80 °C to remove remaining xylene and methanol. The mass losses in the initial 3 days were used to determine the diffusion coefficient of egression (D_{EGR}). The D_{EGR} was shown to be lowest for a xylene content of 10 w% with a D_{EGR} value of 0.0179 × 10 cm^2 s^{-1}. The D_{EGR} then increased to 0.04098 × 10 $cm^2 s^{-1}$ for the 20 w% sample before decreasing to 0.03212 × 10 $cm^2 s^{-1}$ in the 40 w% sample.
A second ingression cycle has begun and so far the ingression curves of the solvated samples are more similar to that of neat epoxy. The rate of ingression appear marginally higher than that of pure epoxy but it is not understood whether this is due to a lower cure temperature, the swelling of the network or a combination of the two.

The glass transition temperature

The glass transition temperature (T_g) was seen to decrease in an almost exponential fashion. The addition of xylene causes the T_g to drop from 110 °C in pure epoxy to ≈ 70 °C for a solvation of 40 w%. Decreasing T_g due to solvation has been shown in other studies[99,156] and could be attributed to plasticisation which weakens dipole-dipole interactions. A decrease in T_g related somewhat to increased ingression properties (D_{ING}, D_{EGR} and ultimate ingression). As T_g decreased, diffusion increased in an exponential fashion with increased xylene content. However, the 20 w% samples exhibited the highest rate of diffusion in both ingress and egress studies whilst showing the lowest ultimate ingression.

Free volume measurements

The free volume and fractional free volume (FFV)were measured the solvated epoxies using positron annihilation lifetime spectroscopy (PALS). Both free volume and FFV increased in an almost exponential fashion with increased xylene content. When free volume increased from ≈ 60 A^3 (pure epoxy) to between 75 and 80 A^3 (solvated epoxy), the diffusion of methanol was enhanced. A similar trend was observed in the FFV. It is interesting to see that the addition of 10 w% xylene greatly increases the free volume but further increases do not. The same observation is noted for FFV when looking at the overall data but focusing on the solvated samples did reveal that increasing rates of diffusion did correspond to small increases in FFV. This could suggest that the increased solvation produces a larger number of voids whilst the average size remains similar. However, the FFV was only seen to increase from ≈ 14.2 to 14.7 and is potentially a coincidental trend. The free volume increased in an exponential fashion with reducing T_g.

A comparison of trends between free volume and T_g

The ultimate ingression lacked any real trends with either T_g, free volume or fractional free volume (FFV). The diffusion coefficient of ingression (D_{ING}) increased when a decrease in T_g occurred but this was not in a correlative manner. The free volume and fractional free volume did show a trend with D_{ING} in that an increase in free volume correlated well with increased D_{ING}. Only egression of solvated samples was compared to T_g, free volume and FFV due to the pure epoxy not undergoing egression studies at this time. For the solvated samples, egression did not correlate to T_g or free volume but did show a strong positive correlation with FFV.

5.4.7 Closing remarks

This section presented diffusion, T_g and free volume measurements for xylene solvated epoxy networks. The results were compared to one another and trends observed. Ultimately it was seen that the addition of solvent enhanced the capabilities of methanol ingression with T_g and free volume results correlating to this enhancement. The results for the 20 w% xylene were seen to be strange in that the diffusion characteristics differed considerably when compared to a higher and lower xylene content. The FFV was shown to correlate strongly with the ingression rate of methanol whilst no trend was apparent for T_g. It should be noted that due to xylene egression during the ingress of methanol, this method of diffusion analysis is not adequate and membrane permeation studies would be preferable. These results are useful to the field of protective coatings as many applications incorporate solvents into epoxy networks in order to reduce the viscosity of coating application methods. Where the addition of solvents are not possible (due to coating end use), diluent epoxies can be incorporated. As such, the next two sections discuss the affects of diluent epoxies on the diffusive properties of the produced network.

5.5 Unifunctional diluent epoxy incorporation

5.5.1 Introduction

This section presents methanol ingression and free volume results for epoxy samples comprising of DGEBF epoxy cured with MXDA amine. Each sample has a unifunctional epoxy content in terms of EEW% as described in Section 2.2.4. The unifunctional epoxy used in this work is phenyl glycidyl ether (PGE). The chemical structure is shown in Figure 5.5.1. Due to its functionality, the number of chain ends should increase and in theory this should increase the free volume of the network[8].

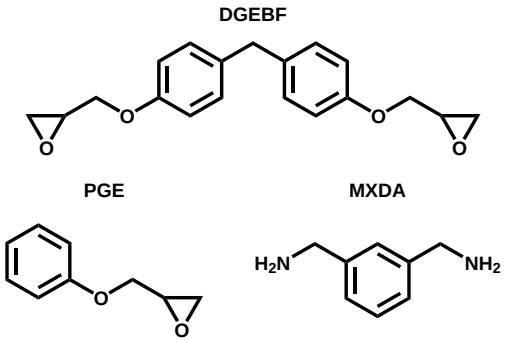

Figure 5.5.1: *The chemical structures of the diglycydyl ether of bisphenol F (DGEBF), phenyl glycidyl ether (PGE) and m-xylenediamine (MXDA).*

5.5.2 Methanol diffusion

5.5.3 Diffusion cycle 1

Figure 5.5.2 shows the ingression curves for epoxy samples comprising of DGBEF resins cured with MXDA and contain different amounts of the unifunctional epoxy PGE with respect to epoxide equivalent weight percentage (EEW%). This is denoted by the legend on the graph.

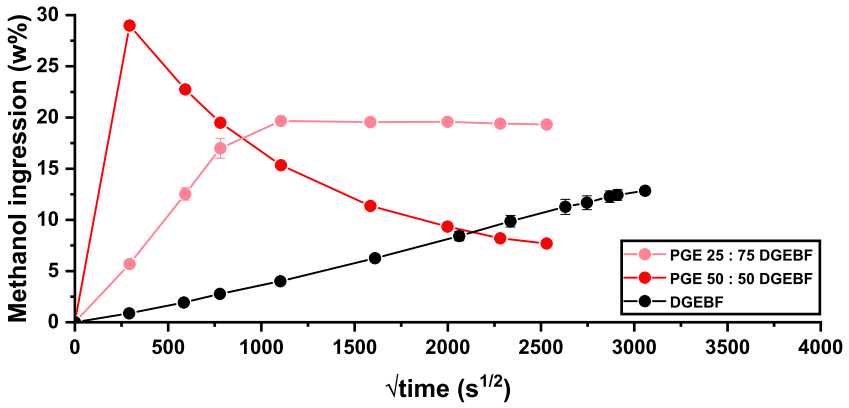

Figure 5.5.2: *The ingression of methanol in epoxies comprising of DGEBF resin cured with MXDA which contain differing levels of the unifunctional epoxy PGE. The amount of PGE is with respect to the epoxide equivalent weight percentage as compared to DGEBF. Connected lines are shown as a guide for the reader. Error bars represent the standard error of three samples but are barely visible due to the size of the date point.*

When PGE is introduced to the epoxy network, the ability to prevent the ingression of methanol is greatly reduced as shown by the PGE 25 : 75 DGEBF sample. Increasing the PGE EEW contribution to 50 % causes the rate of ingression to increase further, to the point that the data before reaching the ultimate ingression was missed and so from the point of 1 day ($\approx$ 300 $s^{1/2}$) it can not be determined if this is a point at which mass is increasing or decreasing. After 500 s $^{1/2}$ it can be said that the mass begins to drop which is normally a sign of physical degradation. However, none of the three samples of PGE 50:50 DGEBF showed any visual degradation. It could be postulated that the incorporation of PGE into the epoxy network causes the formation of oligomers to occur similar to those depicted in Figure 5.5.3. These oligomers add to the sol-fraction in the network and would be extracted during the ingression of methanol.

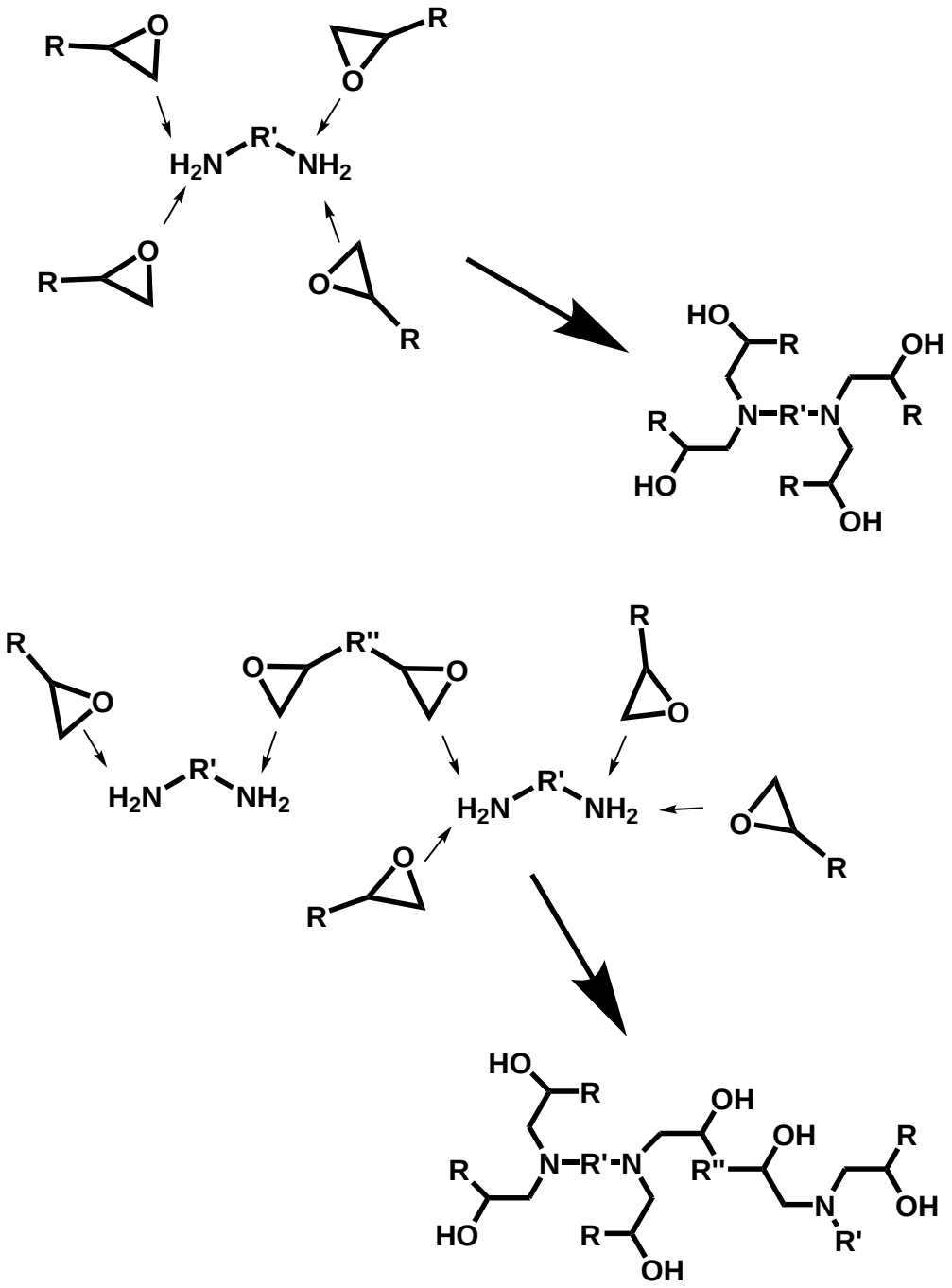

Figure 5.5.3: *Two examples of possible oligomer formation during the reaction between phenyl glycidyl ether (PGE), Diglycidyl ether of bisphenol F (DGEBF) and m-xylenediamine (MXDA). As PGE is unifunctional, it can cause small terminated epoxies to form. An increase in PGE into the network results in a higher number of oligomers. Small arrows represent the direction of functional reactions and the large arrows point to the resulting molecule.*

Diffusion cycle 1

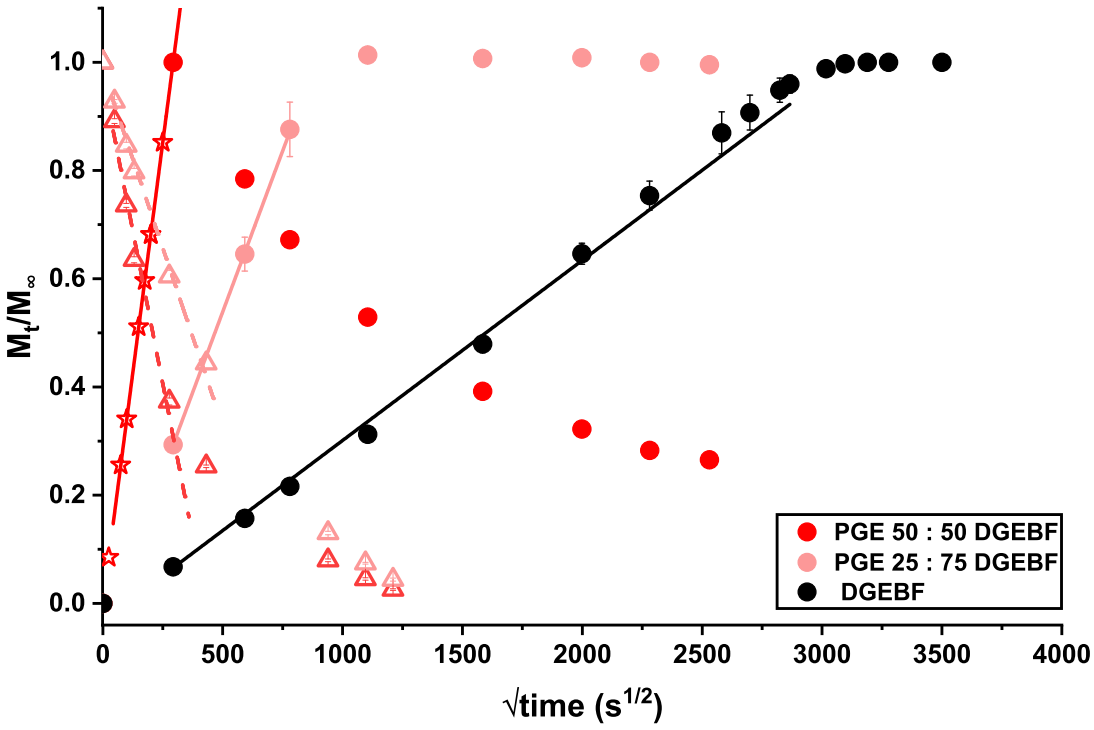

Figure 5.5.4: *The first ingression (solid circles) and egression (hollow triangles) curves for DGEBF-MXDA samples with different PGE content levels. The solid and dashed lines show the linear regions used to determine ingression and egression diffusion coefficients respectively. Error bars represent standard error calculated for three samples. The hollow stars represent the estimated ingression at $\sqrt{time}$ values below 500 $s^{1/2}$. The initial ingression occurred within 1 day. M_t/M_∞ represents the mass over time with respect to the mass at ultimate uptake.*

The ingression curves in terms of M_t/M_∞ are shown in Figure 5.5.4 for the first methanol diffusion cycle for the DGEBF-MXDA epoxies containing different amounts of PGE. In black, the ingression curve of the DGEBF sample is shown based on the estimation of the ultimate uptake (similar to Figure 5.2.4 Section 5.2.2). Linear fits are applied at short diffusion times for both ingression (solid lines) and egression (dashed lines). However, as DGEBF did not reach its ultimate methanol ingression within the time constraints of this thesis, egression studies were not possible. From the linear fits, diffusion coefficients can be determined using the Shen and Springer model outlined in Section 1.3.5.

Diffusion summary

Figure 5.5.5 summarises the diffusion properties from diffusion cycles 1 and 2 (where possible). Cycle 2 begins immediately after a stable mass has been reached in cycle 1 at which point the samples are removed from methanol, weighed and placed into a clean empty glass staining jar in an upright position and masses were monitored over time.

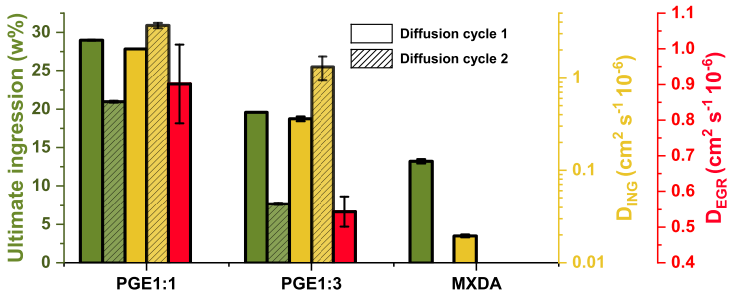

Figure 5.5.5: *The ultimate methanol ingression and diffusion coefficients for DGEBF-MXDA epoxy samples with different PGE EEW% content. Diffusion cycles 1 (solid) and cycle 2 (shaded) are shown. Cycle 1 involves samples being immersed in methanol until the ultimate uptake is reached. Following this, samples are removed and left in air at room temperature until mass decreases to a stable level. Cycle 2 follows cycle 1 and is an identical repeat. Error bars represent the calculated standard error of three samples.*

The diffusion coefficients for ingression and egression were determined using Shen and Springer's[76] simplified model of diffusion as described in Section 1.3.5. Ultimate ingression increased with increasing amounts of PGE from 13.2 to 28.9 w%. The ingression rate described by the ingression diffusion coefficient (D_{ING}) greatly increased from 0.0196 to 0.361 $\times$ cm^2 s^{-1} when 25 EEW% was added to the epoxy network. A further increase was seen when increasing the PGE EEW% from 25 to 50. The drastic increase is emphasised by the use of a log scale in order to clearly see the pure epoxy's ingression rate. The rate of ingression was seen to increase between cycles 1 and 2 for both PGE containing samples with a greater increase in the 50 EEW% sample. The ultimate ingression saw a decrease in both PGE containing samples but in contrast to ingression rate, the difference was larger in the 25 EEW% that in 50 EEW%.

The ingression cycles 1 and 2 are shown in Figure 5.5.6 for the PGE50:50DGEBF sample. In the second cycle, mass measurements were made frequently within the first day of ingression ($<$ 300 s$^{1/2}$). A similar maximum ingression was reached in both cycles but based on the mass measurements of cycle two it is likely that the rate of ingression in cycle 1 is an underestimate. Both exhibit a decrease in mass beyond 500 s$^{1/2}$ but at different rates. The second cycle loses mass at a much slower rate than cycle 1. As with cycle 1, cycle 2 showed no obvious signs of physical degradation. This mass loss could still be due to oligomers within the network which remained after the first egression. The change in rate of mass loss maybe due to a reduction of oligomers locked in the network.

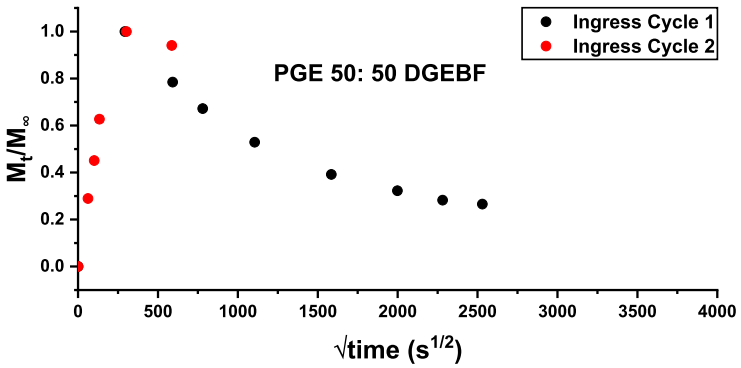

Figure 5.5.6: *The methanol ingeression curve for cycles 1 and 2 for the epoxy sample comprising of DGEBF and PGE resin in a 50:50 ratio in terms of EEW% which were cured with the amine harderener MXDA. Both cycles exhibit a mass loss at similar times which usually implies physical degradation. This was not clearly the case and could be due to the extraction of oligomers during methanol ingression. Error bars represent the standard error of three samples.*

5.5.4 Diffusion - Glass transition temperature relation

Relation to PGE content

Figure 5.5.7 shows the change in T_g with increasing EEW% of PGE into the epoxy network. T_g is seen decreases significantly with increasing EEW PGE in a strong linear fashion ($R^2 > 0.9$).

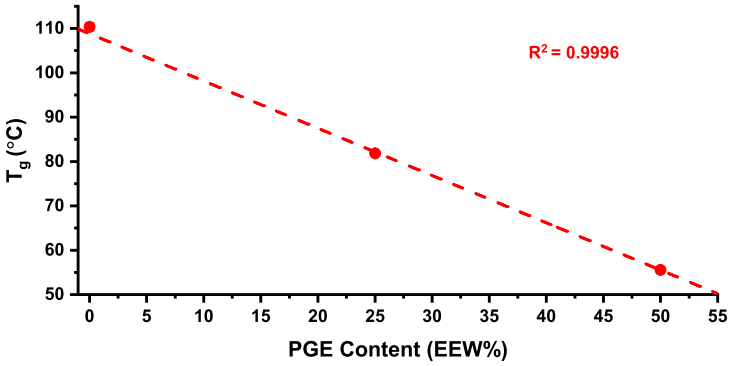

Figure 5.5.7: *The glass transition temperature with increasing PGE EEW% in samples DGEBF-MXDA epoxy samples. A linear fit (dashed line) shows a meaningful correlation ($R^2 > 0.9$) between PGE content and T_g. Standard errors are included based on 2 sample measurements but error bars are smaller than the data point size.*

Figure 5.5.8 shows that as T_g increases, the resistance to methanol ingression also increases i.e. ultimate uptake and diffusion coefficients decrease. This is an expected observation as when the sol-fraction is extracted, stresses occur throughout the network which is compensated by the addition of solvent.

T_g and diffusion

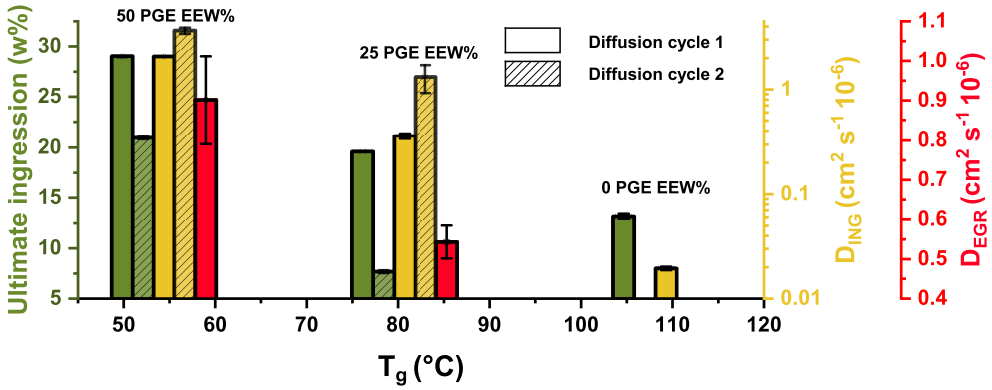

Figure 5.5.8: *The ultimate methanol ingression and diffusion coefficients in relation to T_g for each DGEBF-MXDA epoxy with different PGE EEW% content. The PGE EEW% content is noted above each set of results. Diffusion cycles 1 (solid) and cycle 2 (shaded) are shown. Cycle 1 involves samples being immersed in methanol until the ultimate uptake is reached. Following this, samples are removed and left in air at room temperature until mass decreases to a stable level. Cycle 2 follows cycle 1 and is an identical repeat. Error bars represent the calculated standard error of three samples.*

5.5.5 Free volume and diffusion

The ultimate goal is to determine whether trends between free volume measurements obtained using PALS and diffusion are present. As such, this section presents FV and fractional free volume (FFV) results and compares them to diffusion.

Correlations

Figure 5.5.9 shows the relationship between ultimate ingression (UT) and the diffusion coefficient for ingression and egression (D_{ING} and D_{EGR}). As FV and FFV increases, each diffusion property is seen to increase in a linear fashion as shown by dashed lines which represent linear fits. R^2 values are shown to indicate the goodness of fit but this value could be misleading due to few data points but is a good indicator of the general trend. From these results, we can suggest that where diffusion becomes favourable, free volume is shown to increases. For these PGE containing systems, this could be explained by the increased number of dangling chain ends.

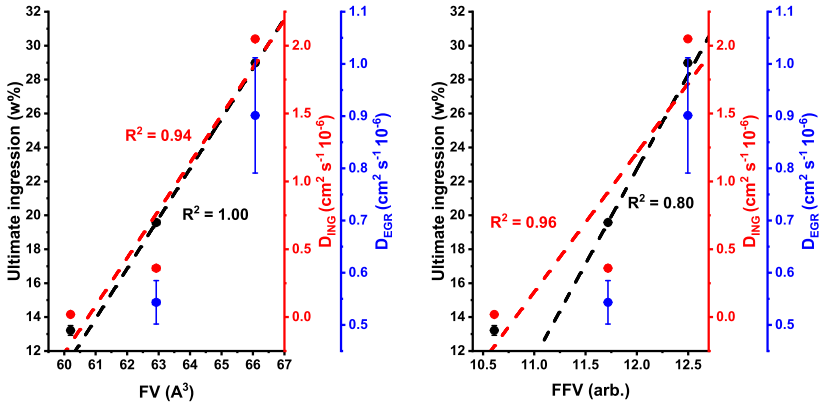

Figure 5.5.9: *(a) Free volume (FV) and (b) fractional free volume (FFV) in relation to diffusion properies of DGEBF-MXDA epoxy samples with different levels of PGE EEW% content. Shown is the ultimate ingression and diffusion coefficients (ingression and egression). Standard errors are shown by error bars. Linear fits show the trend of FV and diffusion properties.*

5.5.6 Glass transition temperature and free volume relation

T_g, FV and FFV

The relationship between free volume properties (FV and FFV) and T_g are shown in Figure 5.5.10. Both FV and FFV show a downward linear correlation to T_g. The correlation goodness is shown by high R^2 (above 0.9) values for the respective fits as indicated by colour. This is not unexpected as literature has previously shown free volume and T_g to be related.[157] An increase in T_g suggests that the the mechanical properties are improved. In epoxy networks, this is normally due to increased cross-link density which should also relate to a reduction in free volume.

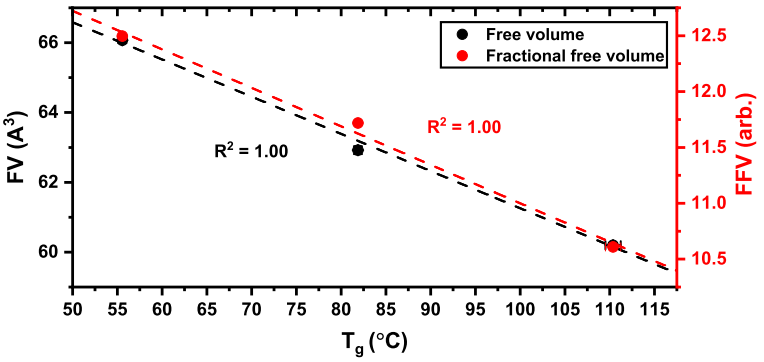

Figure 5.5.10: *Free volume (FV) and fractional free volume (FFV) in relation to glass transition temperature (T_g). A linear fit is shown which indicates a good correlation between FV, FFV and T_g ($R^2 > 0.9$). Standard errors are represented by error bars where larger than the data point size.*

5.5.6.1 Comparison of diffusion trends

To compare which property (T_g or FV) correlates to diffusion more strongly, each diffusion property has been plotted against each as shown in Figure 5.5.11. The ultimate ingression and D_{ING} both show similarly strong correlations to FV and T_g. This is depicted by the R^2 values.

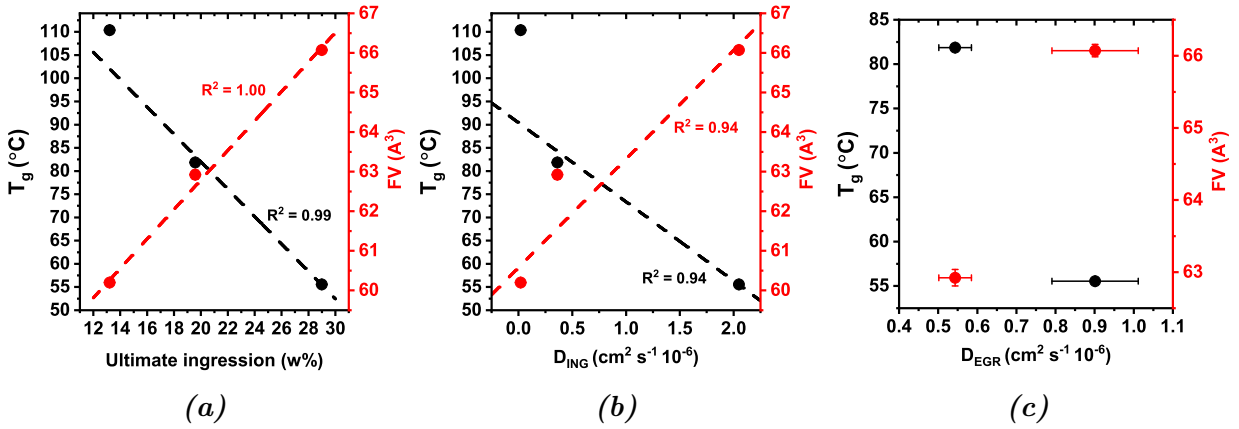

Figure 5.5.11: *A comparison of diffusion trends for glass transition temperatrue (T_g) and free volume (FV). Diffusion trends are shown for (a) The ultimate ingression and diffusion coefficients of (b) ingression and (c) egression coefficient. Standard errors are shown using error bars. Linear fits are applied to compare trends in terms of R^2 values.*

5.5.7 Conclusions

Addition of PGE

The addition of PGE to the DGEBF-MXDA epoxy network caused diffusion to be accelerated and enhanced. With increased amounts of PGE, the ultimate uptake and diffusion coefficients (D_{ING} and D_{EGR}) increased in an almost exponential fashion. Increasing the PGE content to 50 EEW% saw the mass begin to decrease. This was not visually clear to be due to physical degradation and is postulated to be due to oligomer formation and subsequent extraction of the sol. After a stable mass was achieved, samples were removed from methanol and dried in an air environment and egression studies began. Egression had similar trends to that of ingression in that an increase in PGE content resulted in increasing egression rates. Once the egression mass stabilised, PGE containing samples were re-immersed in methanol for a second cycle of ingression studies. The same trend was seen in terms of increasing PGE content resulted in an increase in D_{ING} and ultimate ingression. The second ingression cycle yielded a lower ultimate ingression but higher D_{ING} than the first cycle. The second ingression cycle also saw a loss in mass for the 50 EEW% PGE sample but the mass loss occurred at a slower rate. This loss could still be attributed to sol extraction with the decrease in rate of loss being due to less sol in in the network following the first ingression cycle.

The glass transition temperature

The glass transition temperature (T_g) decreased in a linear fashion with increased PGE content. This could be expected as the formation of cross-links is limited due to PGE creating points of termination throughout the networks. As T_g decreases, the diffusion properties are seen to increase substantially.

Free volume measurements

Diffusion properties increased in a linear fashion with free volume and fractional free volume (FFV). The relation between ultimate ingression and free volume was considered a perfect correlation based on an $R^2 = 1.00$. The relation between free volume and D_{ING} was shown to be a good correlation ($R^2 > 0.9$). The egression coefficient also increased with increasing free volume but as only two of the samples underwent egression, a linear fit was not applied. The relationship between FFV and diffusion was similar to that of free volume except with D_{ING} shown to correlate better than ultimate ingression ($R^2 = 0.96$ and 0.8 respectively.)

A comparison of the Tg and free volume

The T_g decreased linearly in a near perfect manner ($R^2 > 0.99$) with increasing ultimate ingression whilst free volume increased linearly with an R^2 value of 1. The same trends were seen when T_g and free volume were compared with D_{ING} except the R^2 values were slightly lower ($R^2 = 0.94$ in both cases). Similar trends were seen when compared to D_{EGR} but fitting was not performed due to lack of data. These results suggest that in this case, free volume and glass transition temperature are affected in the same manner.

5.5.8 Closing remarks

This study showed how the incorporation of the unifucnctional epoxy PGE influences the diffusive nature of methanol in the polymer network. The diffusion results showed that PGE greatly disrupts the network and enhances the diffusive nature of methanol. The T_g and free volume were seen to strongly correlate to diffusion with an increased ingression corresponding to an increase in free volume whilst T_g decreased. PGE was incorporated into the network as epoxy diluents are used in industry to decrease viscosities as an alternative to solvents. In actuality, the levels of PGE used in this study are probably much higher than those used in real world scenarios. Here, the PGE content was increased in an attempt to induce free volume by increasing dangling chain ends[8]. The next study is based around another epoxy diluent but is bi-functional and linearly chained.

5.6 Linear chain epoxy incorporation

5.6.1 Introduction

This section concerns an ingression study of methanol in epoxy resins with the incorporation of a bi-functional linear chained epoxy. The epoxy samples comprise of DGEBF and MXDA with different amounts of butanediol diglycidyl ether (BDDGE). The amount of BDDGE incorporation is in EEW % and amounts studies were 0, 25, 50 and 100% where 100 % is an epoxy made purely of MXDA and BDDGE. Diffusion properties are presented and related to the glass transition temperature and the free volume properties of the material.

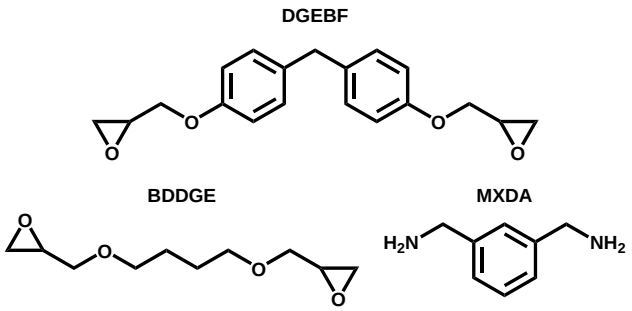

Figure 5.6.1: *The chemical structures of the materials used in this section. Diglycidyl ether of bisphenol F (DGEBF), Butanediol glycydyl ether (BDDGE) and myxlenediame (MXDA) are shown.*

5.6.2 Methanol diffusion

5.6.2.1 Diffusion cycle 1

Figure 5.6.2 shows the ingression curve for epoxy samples comprising of DGEBF resin cured with MXDA amine. Each sample contains different levels of BDDGE in terms of epoxide equivalent weight percentage (EEW%) relative to DGEBF EEW%. This is represented as a ratio of between BDDGE and DGEBF i.e BDDGE 1:1 DGEBF corresponds to 50 EEW% of each epoxy resin.

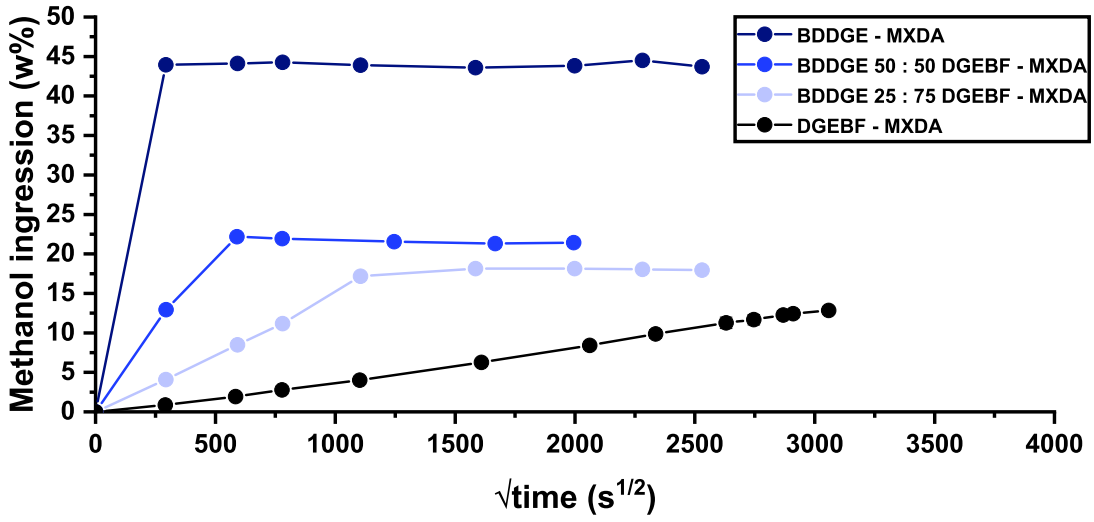

Figure 5.6.2: *The ingression of methanol into epoxy resins comprising of DGEBF-MXDA and different amounts of BDDGE in terms of EEW%. Connected lines are shown as a guide for the reader. Error bars represent the standard error of three samples but a barely visible due to the data point size.*

Samples made purely with DGEBF (black circles) exhibit the lowest rate of ingression of methanol in comparison to DGEBF-BDDGE mixtures. As the amount of BDDGE in the network increases, the maximum ingression also increases. The rate of ingression in the pure BDDGE sample occured in less than a day so the exact time to reach this maximum ingression is not accurate.

Diffusion properties

The weight percent of solvent ingression over time is a good representation of diffusion properties but it is common to determine coefficients of diffusion in terms of ingression and egression.[106] This can be determined by plotting M_t/M_∞ against the square root of time. A linear fit can be applied at short ingression times and used as per the Shen and Springer equation (shown in Section 1.3.5) to determine the coefficients of diffusion. The new ingression curves are shown in Figure 5.6.3 including the egression of BDDGE containing epoxy samples.

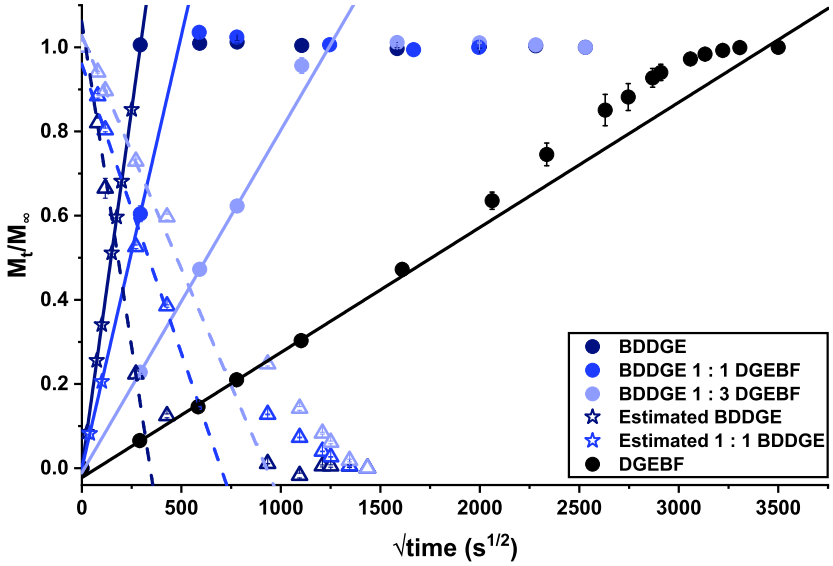

Figure 5.6.3: *The ingression curves for the first cycle of methanol diffusion. Ingression (solid circles) and egression (hollow triangles) is shown for different amounts of BDDGE content in terms of epoxide equivalent weight percentage. Linear fits are shown which are used to determine the ingression (solid lines) and egression (dashed lines) coefficients. Hollow stars represent estimated values during regions in which ingression was too rapid to record. As previously mentioned, the DGEBF ingression curve was produced based on an estimation for the ultimate value of methanol ingression. Standard errors are shown using error bars and are determined based on three individual sample measurements.*

Diffusion summary

Figure 5.6.4 presents the diffusion properties obtained from the methanol ingression curves for cycles 1 and 2 (where possible). Ultimate uptake is seen to decrease (VALUE RANGE) between cycles 1 and 2 for each sample. D_{ING} is seen to increase between each cycle with differences between cycles increasing with increased BDDGE content.

Egression is seen to decrease with decreasing BDDGE content. A second egression cycle was not possible for the BDDGE sample due to sample degradation. Diffusion properties are presented on a logarithmic scale due to significant differences between DGEBF and the BDDGE containing networks. Egression properties are not present for the DGEBF sample as the sample is still yet to reach ultimate ingression.

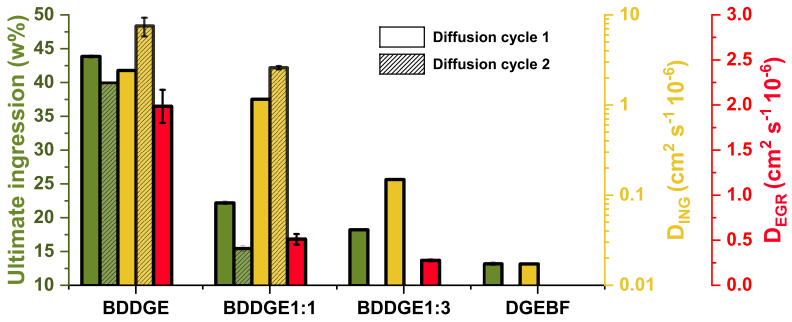

Figure 5.6.4: *The diffusion results for DGEBF-MXDA based resins with differing levels of BDDGE EEW% content. Solid and shaded bars signify diffusion cycles 1 and 2 respectively. Standard error is represented by error bars which were calulcated based on the measurements of three sample (except BDDGE which was 2 samples due to degradation of the sample.)*

5.6.3 Diffusion - glass transition temperature relation

Relation to BDDGE content

Figure 5.6.5 shows the relationship between glass transition temperature and BDDGE EEW% content. The T_g decreases in a strong linear fashion and in a highly correlative manner ($R^2 > 0.9$). This trend is somewhat expected due to the linear nature of the structure of BDDGE. This causes BDDGE to be a flexible material. Whilst the DGEBF benzene rings add strength to the network, BDDGE causes a reduction.

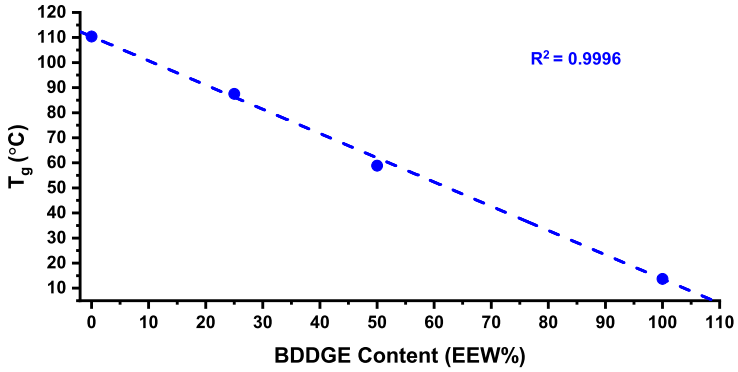

Figure 5.6.5: *The glass transition temperature for DGEBF-MXDA epoxy resins containing different amounts of BDDGE in terms of epoxide equivilent weight (EEW) percentage. A linear fits is shown along with R^2 values. Standard error bars represent standard errors based on three sample measurements.*

Tg and diffusion

Figure 5.6.7 shows diffusion properties as a function of T_g. As T_g increases, the ultimate uptake and diffusion coefficients are seen to decrease. The worst performing sample in terms of preventing egression is the pure BDDGE sample. This can likely be attributed to having a T_g of 13.73 °C which means at room temperature the materials behaviour is rubber(i.e. above T_g). This means that swelling is more favourable and therefore more solvent can ingress and at a higher rate. A logarithmic scale emphasis the huge differences in the rate of ingression between samples. It is expected that the sample produced purely with DGEBF would also see a similar trend in terms of egression. The DGEBF sample has a higher T_g than BDDGE due to the phenolic rings contained in DGEBF. These rings contained in the polymer's backbone increase steric hindrance. As the amount of BDDGE is increased, the resulting network comprises of less phenolic epoxy causing the chain stiffness to decrease and therefore diffusion is more favourable.

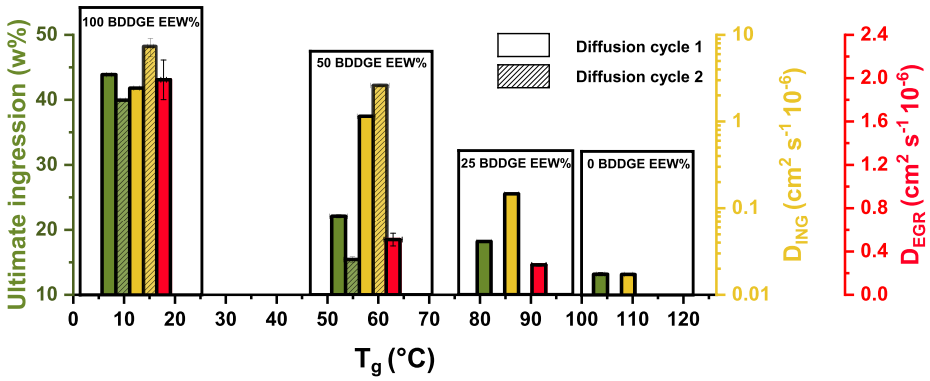

Figure 5.6.6: *Diffusion properties of BDDGE containg DGEBF-MXDA resins (as labelled). Diffusion cycles 1 and 2 are signified by solid and shaded bars respectively. Standard errors are shown using error bars which are caluclated from from individual sample measurements (2 samples for BDDGE due to degradation.)*

5.6.4 Free volume and diffusion

Correlations

Figure 5.6.7 shows how free volume and fractional free volume compare with diffusion. Ultimate uptake (UT), D_{ING} and D_{EGR} are seen to increase overall with FV. However, at FV of $\approx$ 58 A^3, significant differences in all diffusion properties are seen. A large FV does coincide with the largest change in diffusive properties. An exponential decay has been fitted reasonably well but without sufficient data, this relationship cannot be confirmed to be reliable. FFV shows a similar trend but in an opposing manner. As FFV increases, diffusion appears to be hindered. This implies that the total amount of free volume decreases but the size of the voids on average (i.e FV) have a larger effect on diffusion. An exponential decay has been fitted reasonably well but again, the lack of data means this relationship cannot be confirmed to be reliable.

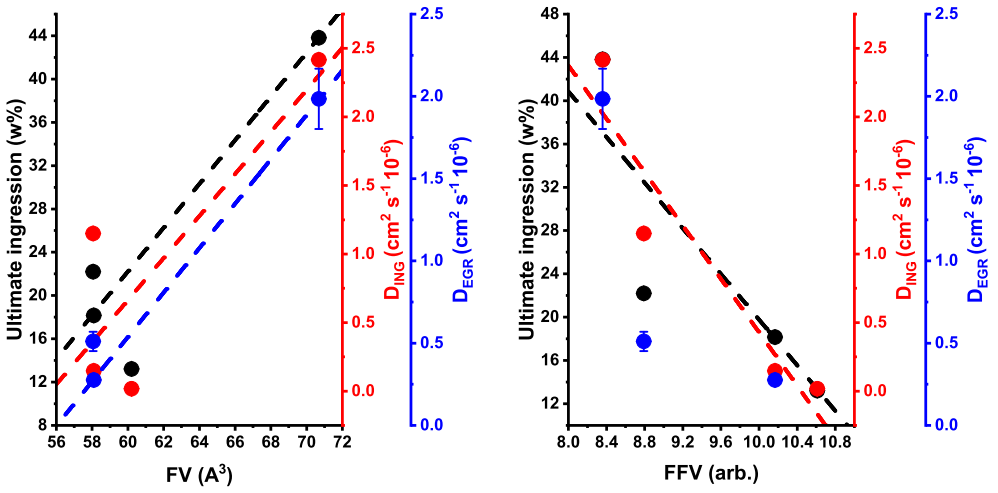

Figure 5.6.7: *Diffusion properties of for samples of DGEBF-MXDA containing different amounts of BDDGE EEW % in relation to (a) free volume (FV) and (b) fractional free volume (FFV). Dashed lines represent exponential/linear fits. Standard errors are shown using error bars and are a result of three individual sample measures (except BDDGE which has two due to degradation.)*

5.6.5 Tg and free volume relation

Tg, FV and FFV

Figure 5.6.8 shows how free volume and fractional free volume relate to T_g. There is no trend present between FV and T_g although a linear fit is shown which is poorly fitted. The FFV does shows a reasonable relationship with T_g in that it increases with increased T_g. However, this relationship is counter intuitive. As FFV is a measure of the total free volume of a material, it would be expected to decrease with increased with T_g. The high FV at the lowest T_g can be explained by mobility of the network. The T_g of this polymer was around 12 °C and therefore at room temperature, polymer chains are mobile. This mobility in conjunction with an increased amount of linear chains is expected to induce free volume. It is possible that FV exhibits a significant decrease in FV but the data for the region between 20 and 60 °C was not collected.

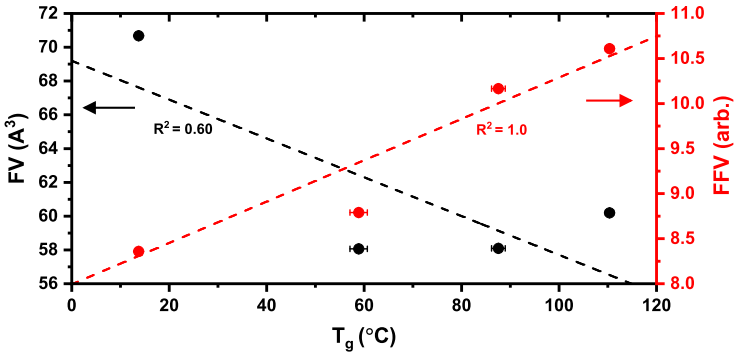

Figure 5.6.8: *Free volume (FV) and fractional free volume (FFV) in comparison to the glass transition temperature (T_g). Dashed lines represent linear fits produced in origin software with their respective R^2 values. Error bars represent standard error based on the average of three samples.*

Comparison of trends

Figure 5.6.9 shows how T_g and FV relate to each of the diffusive properties measures. As T_g decreases, each diffusive property is seen to increase in a reasonably linear fashion. FV is only seen to change when a large change in diffusion occurs. The trends in egression only show three data points due to one sample not undergoing egression measurements.

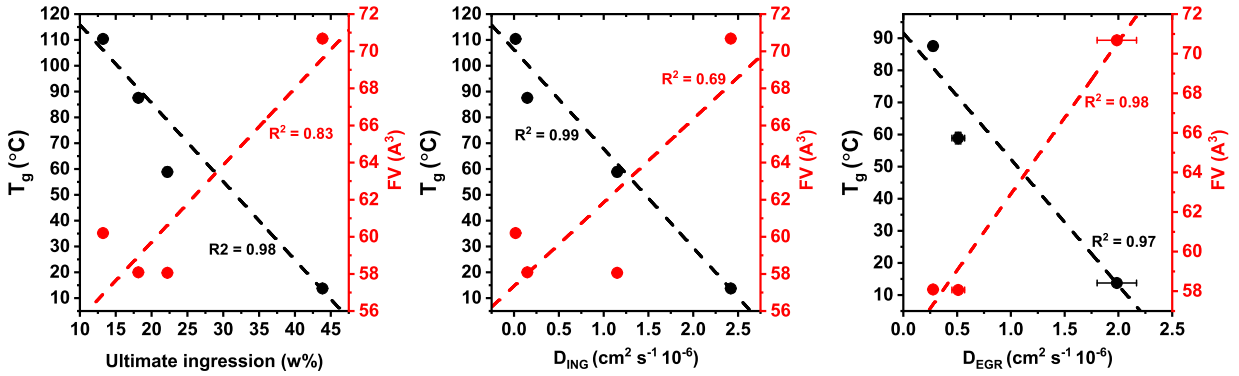

(a) *(b)* *(c)*

Figure 5.6.9: *The diffusive characteristics compared to free volume for DGEBF-MXDA epoxy samples which contain different amount of the linear chained epoxy BDDGE. Dashed lines represent linear fits with R^2 values shown. Error bars represent the standard error of three samples.*

5.6.6 Conclusions

This section presented the results of diffusion of methanol in epoxies comprising of DGEBF-MXDA and differing levels of the bi-functional linear chained epoxy butanediol dyglycidyl ether (BDDGE) in terms of EEW%. The ultimate uptake, D_{ING} and D_{EGR} were determined and compared to the BDDGE content and the respective glass transition temperature. The free volume (FV) and fractional free volume (FFV) were also compared to diffusion. It was shown that T_g had a reasonable linear relation with each property in that an increase in T_g resulted in a decrease in diffusion. FV did not show a strong relation to diffusion and when significant changes to diffusion were measured, this change was not reciprocated by the free volume. Only for the highest levels of diffusion did FV increase.

5.6.7 Closing remarks

This section in addition to Section 5.5, concerned diffusion, T_g and free volume measurements made for epoxy diluents which are used to lower the viscosity for coating application methods. Effectively, epoxy blends were prepared in both studies involving PGE and BDDGE. The next section also involves epoxy blends but ones which are considered in model epoxy networks[106,158]

5.7 DGEBF and A epoxy blends

5.7.1 Introduction

The section concerns diffusion and free volume measurements of several epoxy blend samples. These samples comprise of diglycidylether of bisphenol F and A (DGEBF and DGEBA) which were cured with m-xylyldiamine (MXDA). The amount of DGEBF was increased in terms of epoxide equivalent weight percentage (EEW%). These two resins show very different free volumes which correlate somewhat to their diffusive properties. As such, this study measures free volume and diffusion of blends of DGEBF and DGEBA.

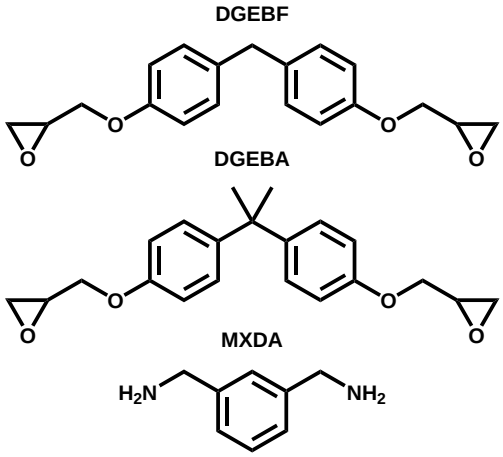

Figure 5.7.1: *The chemical structures of the epoxy resins diglycidyly ether of bisphenol F and B (DGEBF and DGEBA) along with the amine harderner m-xylydiamine (MXDA) which is used as a curing agent.*

5.7.2 Methanol diffusion

5.7.3 Ingression Cycle

Figure 5.7.2, shows the ingression of methanol in weight percentage over time for a number of epoxy blend samples. Each sample consists of DGEBF and DGEBA resins cured with MXDA with differing epoxide equivalent weight percentage (EEW%). The samples in shades of red represent ratios which are weighted more towards DGEBA wheras blue shaded data concerns epoxy blends weighted towards DGEBF. As it is difficult to assess the data as a whole, subfigures have been included.

Figure 5.7.2 (b) compares the ingression curves of DGEBF and DGEBA in addition to a 50 EEW% mixture. DGEBF exhibits the lowest rate of uptake. It is interesting that the 50 EEW% mixtures shows an even higher rate of ingression as well as a higher ultimate uptake of methanol.

Figure 5.7.2 (c) shows the variation of ingression for blends which move away from the mixture which is evenly split between DGEBF and A. With the addition of DGEBA to DGEBF, the ingression of methanol increases in terms of rate. However this does not occur in a predictable manner. This is shown by a reduction in DGEBF showing an increase in the rate of ingression initially with the 90 EEW% sample but this trend does not continue. An 80 EEW% contribution of DGEBF results in higher ingression rates than a 50 EEW % exhibits.

Figure 5.7.2 d shows the variation in ingression for epoxy blends which are weighted towards DGEBA (<50EEW %). Adding 10 EEW% of DGEBF results in a significant reduction in rate of ingression and is expected to also result in a reduced ultimate ingression based on the nature of the curve. Increasing to 20 EEW% results in an increase in ingresison rates as does increasing further to 30 and 50 EEW%. As with the results shown in Figure 5.7.2 (a) there is no apparent trend in terms of increasing DGEBF content.

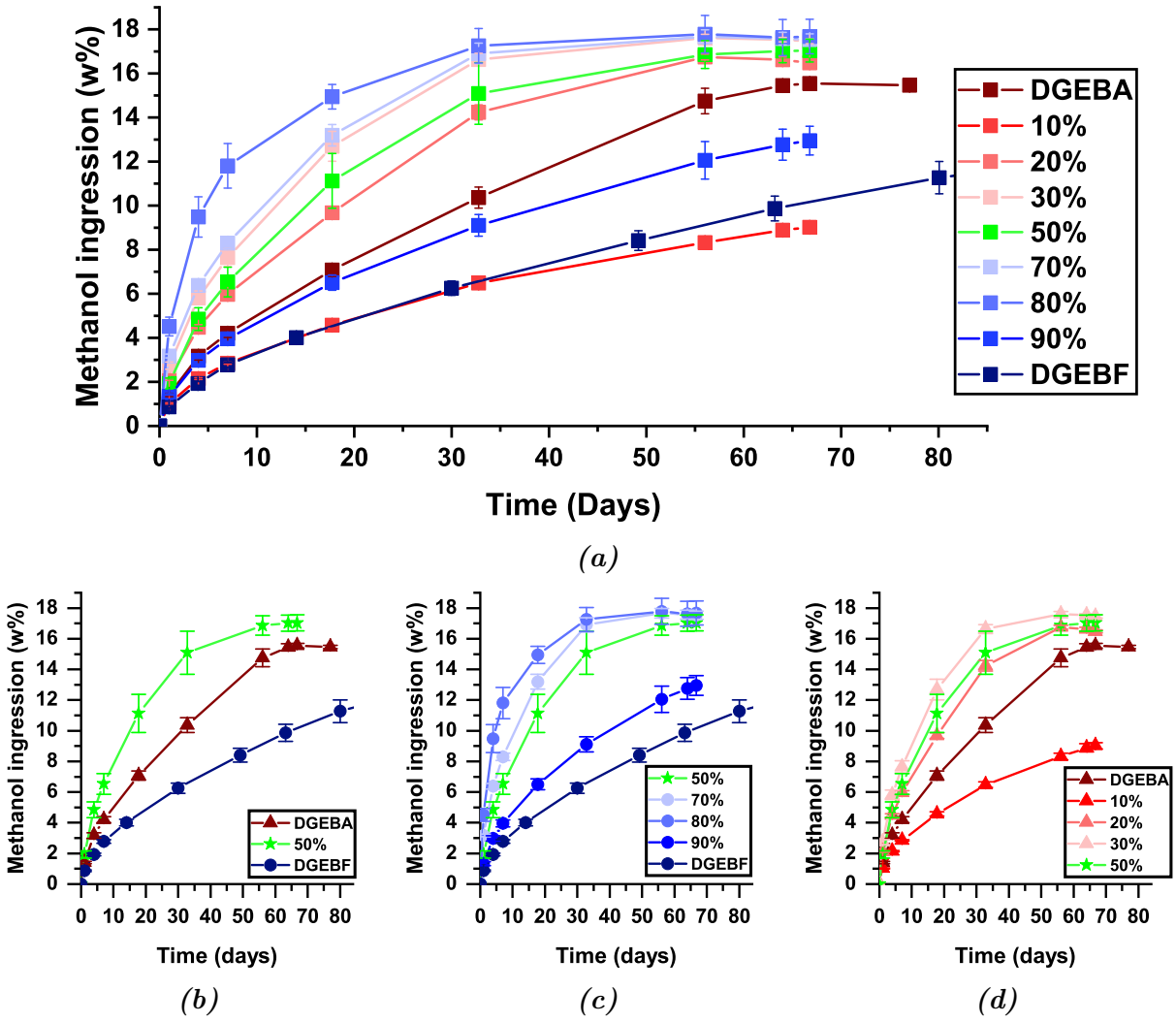

Figure 5.7.2: *(a) The ingression of methanol in weight percentage over time for a number of epoxy blend samples. Each sample consists of DGEBF and DGEBA resins cured with MXDA. The blends were formulated in terms of DGEBF epoxide equivalent weight percentage (EEW%) i.e. 10 EEW % refers to a sample which consists of 10 EEW% DGEBF and 90 EEW% DGEBFA. The formulation also kept the ratio of epoxide to amine hydrogen at 1:1. (b) The comparison between pure DGEBF, pure DGEBA and a 50 EEW% blend of each (c) Ingression curves for samples increasing from 50 EEW% to a pure DGEBF (d) Ingression curves for samples decreasing from 50 EEW % to pure DGEBA. Error bars for all figures represent the standard error of three samples. Connected lines are included as a guide for the reader.*

Ingression cycle

For this study, the Shen and Springer method is utilised in order to determine diffusion coefficients (see Section 1.3.5 for details). The Ingression curves in terms of M_t/M_∞ against $\sqrt{time}$ time for the epoxy blends are shown in Figure 5.7.3. Three of the epoxy blends did not reach their ultimate ingression (10, 90 and DGEBF samples), these were estimated in a similar manner to that shown in Section 5.2.2.

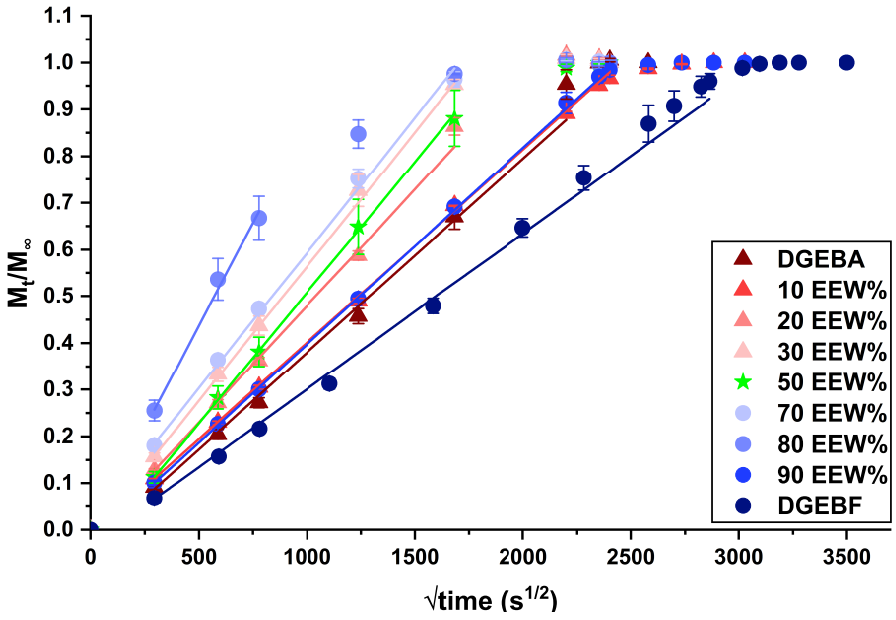

Figure 5.7.3: *Methanol ingression curves for several epoxy samples. Each sample is a mixture of DGEBF and DGEBA resins cured with MXDA. The samples were prepared based on epoxide equivalent weight percentages (EEW%) and are labelled as such. Linear fits were applied at short ingression times (<1000 $s^{1/2}$). Standard error is shown using error bars.*

Figure 5.7.3 shows methanol ingression curves for several blends of DGEBF and DGEBA resins. Each sample is labelled with respect to it's DGEBF epoxide equivalent weight percentage (EEW %). Each sample was immersed in methanol and its mass recorded over time until a the mass became constant. In the cases where a constant mass has not been reached, the final data points have been estimated (10, 90 and DGEBF samples). From this graph, the diffusion coefficients for ingression and egression (D_{ING} and D_{EGR}) can be determined.. For this study, D_{EGR} will not be included as masses are still decreasing. Instead egression rate will be presented in w% s^{-1}.

Diffusion summary

Figure 5.7.4 shows the results for ultimate uptake, D_{ING} and the egression rate for each epoxy resin blend. Blue boxes are included to clearly separate each set of data. The ultimate uptake and D_{ING} are higher in DGEBA than DGEBF. As such it might be expected diffusion properties for blended epoxy samples would lie somewhere between the values for the two pure epoxies. In actuality, this was not the case.

Decreasing the DGEBF content to 90 EEW%, ultimate uptake was unaffected. Decreasing DGEBF content further to 80 EEW% did see the ultimate ingression increase by 4.5 w%. Decreasing further from 80 to 20 EEW % resulted in a marginal decrease in ultimate uptake ($\approx$ 1.2 w %) . Strangely, dropping to just 10 EEW% saw a large decrease in ultimate ingression, to a level even lower than that of pure DGEBF. Increasing the DGEBF content from 0 to 30 EEW % sees the ingression rate gradually increase from 0.034 to 0.075 $\times$ 10^{-6} cm^2 s^{-1}. An increase to 50 EEW% sees a marginally decrease before increasing to 0.11 $\times$ 10^{-6} cm^2 s^{-1} for a DGEBF content of 70 and 80 EEW%. A significant decrease in ingression rate is seen for 90 EEW% DGEBF content before further decreasing to 0.02 $\times$ 10^{-6} cm^2 s^{-1} in the pure DGEBF epoxy sample. A similar trend is seen for the rate of egression (red) although egression data is not available for the pure epoxy samples at present.

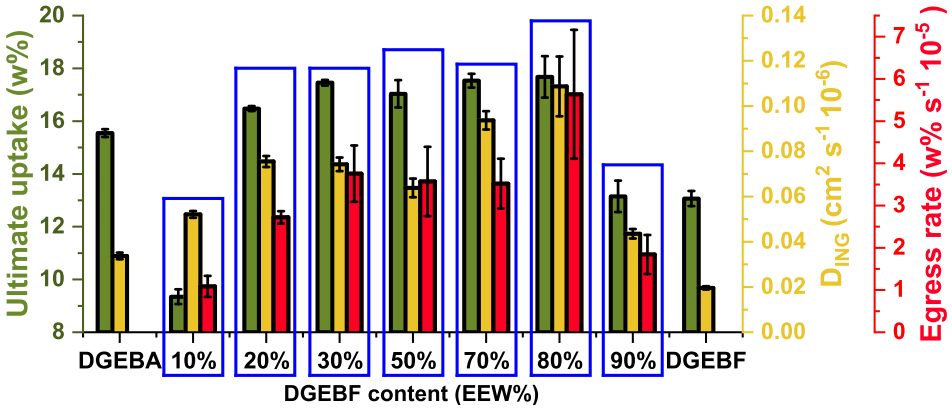

Figure 5.7.4: *The diffusion properties for epoxy blends determined by methanol ingress and egress studies. Results for the ultimate ingression (green), the diffusion coefficient of ingression (yellow) and the egress rate (red). Each sample consists of a mixture of DGEBA and DGEBF resins cured with MXDA amine. Each mixture is formulated based on the epoxide equivalent weight percentage (EEW%) where an EEW% of 50 means the number of epoxide groups between DGEBA and DGEBF are equal to one another. The ultimate uptake in samples 10, 90 EEW% and DGEBF were estimated in order to calculate* D_{ING}*. Error bars represent the standard error of three measurements. Blue boxes are intended to segregate each sample for easier reading.*

During the production method (full details in Section 2.2.4), samples are heated and thoroughly mixed together. This was done in order to incorporate the high viscosity DGEBA with the DGEBF resin. The samples are then left to cool before adding amine (MXDA here) as a higher temperature would increase the rate of reaction. During this cooling process a level of phase separation between the two epoxies might have occurred. Separation of the epoxy resins would form a cross-linked network on reaction with amine which would have regions of differing chemistries i.e. DGEBF-MXDA connected to regions of DGEBA-MXDA. Where these regions combine could be large interfaces which could explain why the poorest performance, in terms of preventing the ingression of methanol, occurs near the midpoint of blends as this would see the greatest differential in networks.

Change in ingression rate

Some samples exhibit a change in ingression rate before plateuing as shown in Figure 5.7.5 which is the ingression curve for DGEBA. A linear fit is shown by a solid line for root times below 1000 whilst the dashed line represents the linear fit beyond this time. This sort of behaviour is most like sigmoidal diffusion[63]. The inset of Figure 5.7.5 shows the $\log(\frac{M_t}{M_\infty})$ against log(time) and the slope of the linear fit. With the n value = 0.57 and the shape of the general ingression profile suggests that this is sigmoidal behaviour[141]. Most samples showed a change in the ingression rate as seen in Figure 5.7.6. It can be expected that the rate of change decreases as the ultimate ingression is approached but an increase is more unexpected. The pure DGEBA (0 EEW%) and a 20 EEW% showed significant increase in the rate of ingression.

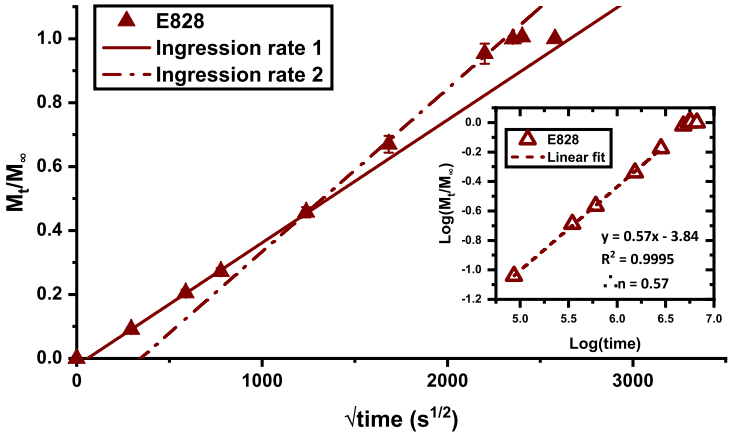

Figure 5.7.5: *The ingression curve for a DGEBA resin cured with MXDA. A linear fit is applied over two ranges to emphasise the change in rate of ingression (solid and dashed lines). The inset figure is the log($\frac{M_t}{M_\infty}$) vs log (time). The slope of this graph can be used to determine the type of diffusion.*

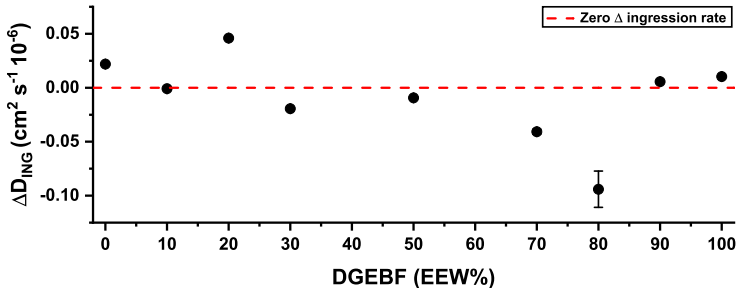

Figure 5.7.6: *The change in the ingression diffusion coefficient (D_{ING}) when comparing ingression at short times to those at later times. A positive or negative change in D_{ING} means that the rate of ingression is increasing or decreasing respectively. A decrease in ingression is expected as ultimate ingression is reached but an increase in rate is unexpected. A dashed line represents no change in D_{ING}. Error bars represent the standard error of three samples.*

5.7.4 Tg and free volume

Tg and DGEBF EEW

The glass transition temperature (T_g) was determined using dynamic mechanical anlaysis (DMA) for all the epoxy blend samples. The T_gs are shown as a function of DGEBF EEW% in Figure 5.7.7. The results are somewhat random but generally a decrease in T_g is seen when increasing the DGBEF content form 0 to 70 EEW%. Beyond this point the glass transition temperture increases. The Flory - Fox equaiton can be used to deterimne the expected T_g based on a mixture of epoxies[159]. Using this model, the T_g of a 50/50 mixture of DGEBA (0 EEW%) and DGEBF (100 EEW%) is estimated to be $\approx$ 114 °C. Clearly, this is not the case with the 50/50 resulting in the second lowest T_g and a T_g that is lower than either of the pure epoxies. This suggest an incompatibility between the DGEBA and DGEBF epoxies. It could be postulated that the diffusion here is dependent on the amount of interface available in the network. For a high DGEBF and low DGEBA content, the system consists of mainly a DGEBF-MXDA matrix with isoloated pockets of DGEBA-MXDA. Between the two network regions (matrix and pockets), there is interpenetrative phase separation with a high amount of interface[160,161]. This increased interface enhances diffusion through the epoxy network. An example of this effect in literature is shown by Schwahn *et al*[162] where they showed separation between polystyrene (PS) and deutero PS of high molecular weight ($M_w = 10^6$ dalton).

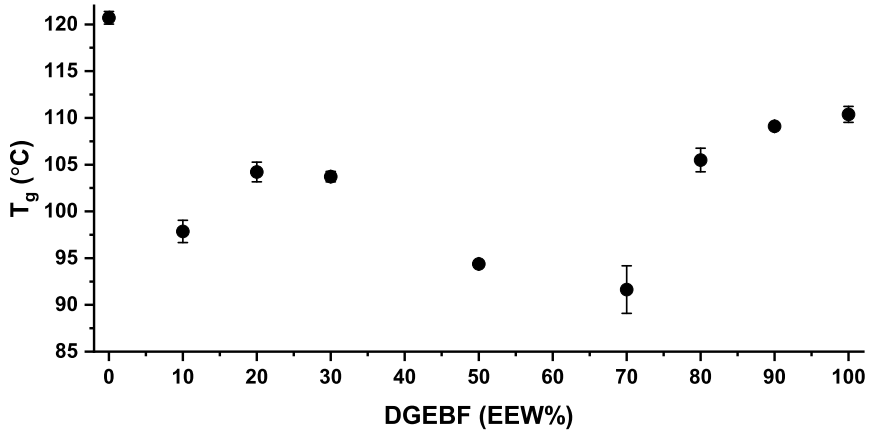

Figure 5.7.7: *The glass transition temperatures of epoxy blends consisting of DGEBF and DGEBA resins cured with MXDA. T_g was determined using the tanδ peak measured by dynamic mechanical analysis. Error bars represent the standard error between two samples.*

Free volume and DGEBF content

Figure 5.7.8 shows the the variation of free volume (FV) and fractional free volume (FFV) with increasing levels of DGEBF in the epoxy blend. Unlike T_g, both FV and FFV exhibit a predictable trend with increasing levels of DGEBF. If the previous discussion concerning inter-facial regions is relevant, then these free volume measurements are of interest. Diffusion is highest near the point at which the postulated amount of interface would be highest. This implies that the accelerated diffusion is governed by the inter-facial regions between the two epoxy networks. In this work it has been shown that an increase in free volume in many instances correlates to increased diffusion. It has also been shown that a combination of materials results in an average free volume somewhere between the two individual free volume measurements of either material. With this in mind, and the results shown in Figures 5.7.7 and 5.7.8, we can suggest that PALS is measuring the free volume within the bulk of both DGEBA and DGEBF based regions and an average result is produced which is insensitive to these inter-facial regions. Small angle x-ray and neutron scattering (SAXS and SANS) along with free volume depth profiling using mono-energetic positron spectroscopy (MEPS) should be utilised to investigate these hypotheses.

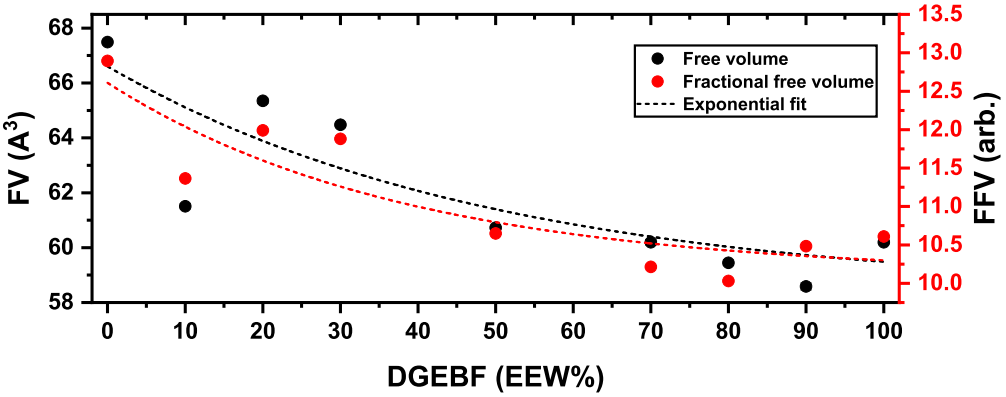

Figure 5.7.8: *The free volume (FV) and fractional free volume (FFV) of epoxy blends comprising of DGEBF-DGEBA resins cured with the amine MXDA. PALS Measurements were obtained using positron annihilation lifetime spectroscopy (PALS). Epoxy blends were formulated with regards to the content of DGEBF resin in terms of epoxide equivilent weight percentage (EEW%). Exponential fits are shown by dashed lines. Standard errors were generated in "LTPOLYMERS" software but are not visible due to ehre small size.*

Free volume - diffusion results

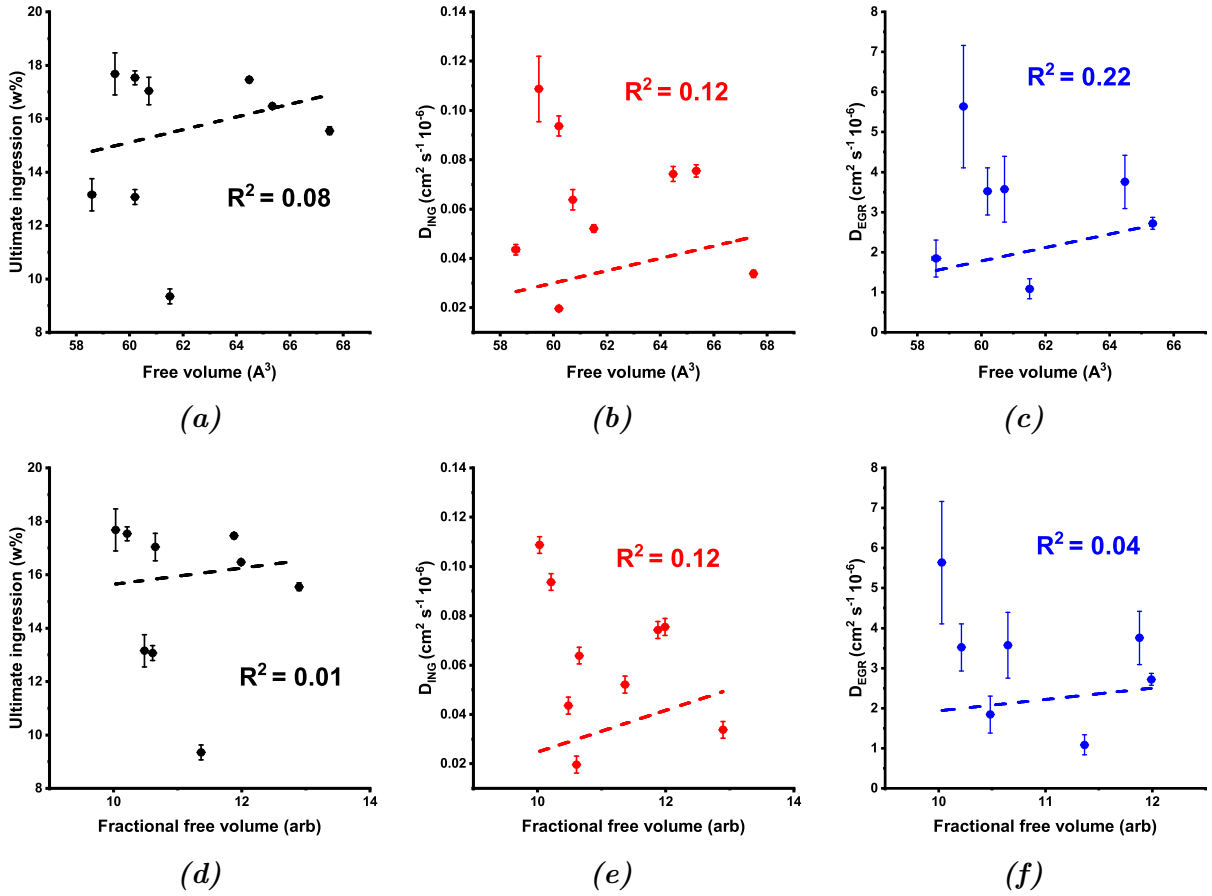

Figure 5.7.9: *The diffusive properties of methanol in several epoxy resin blends. (a) - (c) compares the measured free volume with the Ultimate Ingressions, D_{ING} and D_{EGR} respectively. (d) - (f) compares the fractional free volume with the Ultimate Ingression, D_{ING} and D_{EGR} respectively. The free volume and fractional free volume were measured using positron annihilation lifetime spectroscopy. The epoxies consist of differing ratios of DGEBF and DGEBA resins which are oven cured with MXDA amine. Dashed lines represent linear fits applied using origin software along with their respective R^2 values. Error bars represent the standard error of three samples where visible.*

Figure 5.7.9 shows the diffusive properties of all the epoxy blends presented in this section and compares the to the free volume (FV) and fractional free volume (FFV) which were determines using positron annihilation lifetime spectroscopy (PALS). Both FV and FFV are plotted against respective values of the ultimate ingression, the ingression diffusion coefficient (DING) and the egression rate. Whilst there linear fits show a marginal upwards trend, there is no correlation between diffusion and either FV or FFV which is emphasised by the low R^2 values.

Free volume - Tg relation

Figure 5.7.10 shows the FV and FFV for the epoxy blends against the T_g. Whilst a general upwards trend is seen the correlation is poor (R^2 <0.5).

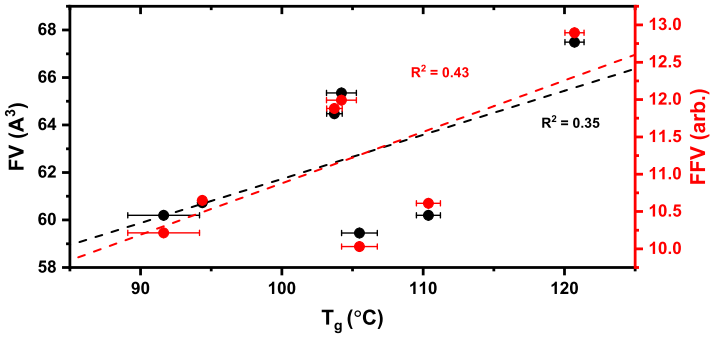

Figure 5.7.10: *The free volume (FV) and fractional free volume (FFV) compared to the corresponding glass transition temperature (T_g) for a number of epoxy blends. Epoxy samples comprised of DGEBF-DGEBA and are cured using MXDA. Error bars shown represent the standard error of three samples.*

Correlations

The T_g and FV are plotted against diffusion properties in Figure 5.7.11. The (a) ultimate ingression appears to be fairly random with respect to T_g but when applying a linear fit to the data set a reasonable R^2 value was calculated. This trend does make sense in that a lower T_g material will be more flexible which allows for easier ingression of methanol as chains are more easily swollen. The free volume shows no correlation with the ultimate ingression. The (b) diffusion coefficient for ingression (D_{ING}) increases with decreasing T_g whilst the relation to FV is random. The (c) egression rate also decreases with decreasing T_g whilst FV correlates in a random manner which is emphasised by the R^2 values.

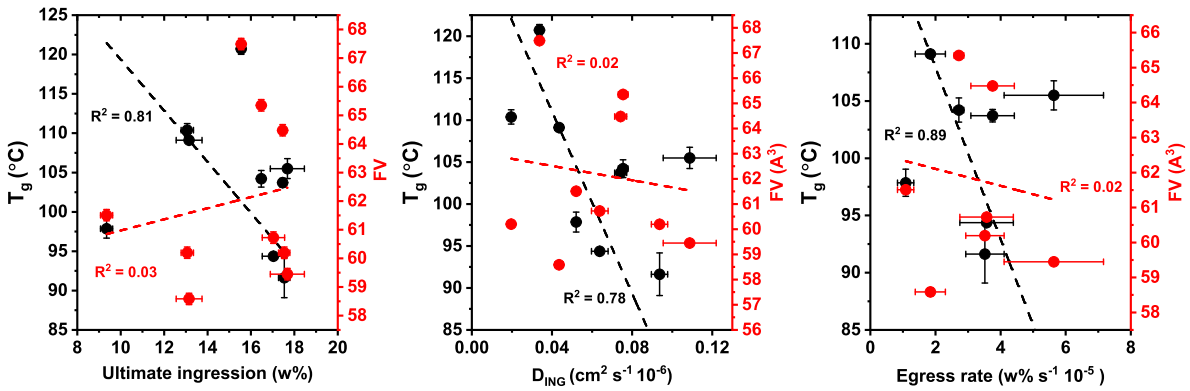

Figure 5.7.11: *The relation between the diffusive properties of epoxy blends and how they relate to T_g and free volume (FV). The diffusive properties presented are (a) the ultimate ingression, (b) the ingression diffusion coefficient (D_{ING}) and (c) the egression rate.*

5.7.5 Conclusions

Increasing DGEBF content

Epoxy blends were prepared consisting of DGEBF and DGEBA resins cured with MXDA. Pure DGEBF has a higher ultimate ingression and ingression rate than pure DGEBF but on increasing the DGEBF content, unusual results were observed. Ultimate uptake and diffusion rates increase before becoming somewhat stable at DGEBF content of 30 EEW%. When levels above 80 EEW% DGEBF content, diffusion decreased to levels similar to that of pure DGEBF. It is assumed that some phase separation occurs between the epoxies during cure or just prior. Swelling observations were also indicated by changing ingression rates for some blends.

The glass transition temperature

The glass transition measured as a function of DGEBF content produces some interesting results. Rather than gradually decreasing from the T_g of pure DGEBA to pure DGEBF, it decreased to values lower than either pure T_g values. This could be an indication of phase separation between the epoxies and the formation of inter-facial regions between DGEBA and DGEBF regions. T_g was lowest near the midpoint which could be due to the maximum amount of interface being present at this point. The T_g showed reasonable correlations with the ultimate ingression in addition to the rates of ingression and egression in that a decrease in T_g corresponded to higher and quicker diffusion. As T_g decreases, swelling of the network is more favourable due to the increase in polymer mobility.

Free volume measurements

In contrast to T_g, free volume produced predictable results in that the free volume gradually decreased from a value corresponding to DGEBA to a level which corresponds to a free volume value for pure DGEBA. However, no trends were present when comparing either free volume or fractional free volume to diffusion with the highest R^2 value being 0.22.

A comparison of Tg and free volume

The glass transition temperature was shown to correlate well with diffusion rates, in that a decreased T_g correlated to increased rates of diffusion. Free volume on the other hand did not. These trends suggest that inter-facial regions may be present between the two epoxies which enhances the diffusion of methanol through the system. As free volume measures the bulk, the average free volume of the two pure epoxies is measured with respect to the fraction of each epoxy. With this in mind, bulk PALS measurements are insensitive to growth in the inter-facial regions and therefore insensitive to changes in the diffusive nature of systems of this type.

5.7.6 Closing remarks

This study has arguably presented the most interesting results thus far and merits further investigation. It is strongly recommended that in order to carry out a more conclusive study of the relationship between free volume, glass transition temperature and diffusion in epoxy blends, advanced experimental techniques such as mono energetic positron spectroscopy (MEPS), small angle x-ray and neutron scattering should be considered.

All studies presented in this chapter have been focussed on how relatively local changes (increase pigment, cure conditions, solvent content etc.) to the material affect the glass transition temperature, free volume and how this in turn corresponds to diffusion measurements. The final study in this chapter concerns how changing the chemistry of DGEBF based resins by hardener variation affects, once again, the T_g free volume and how this relates to diffusion.

5.8 Harderner variation

5.8.1 Introduction

Thus far, studies have presented results based on production methods, increasing the level of an additional single component. In reality, a plethora of materials are used in the field of protective coatings and as such, the effects of changing the chemistry of resins, is shown. A number of sample were produced using DGEBF resin with several curing amines. Some of which were prepared by adjusted methods and by other colleagues which, where necessary, will be indicated. All samples underwent methanol ingression studies and diffusion properties determined. The glass transition temperature, free volume and fractional free volume are compared with these diffusive properties and conclusions drawn. The chemical structures of the various chemicals used in this section are shown in Figure 5.8.1

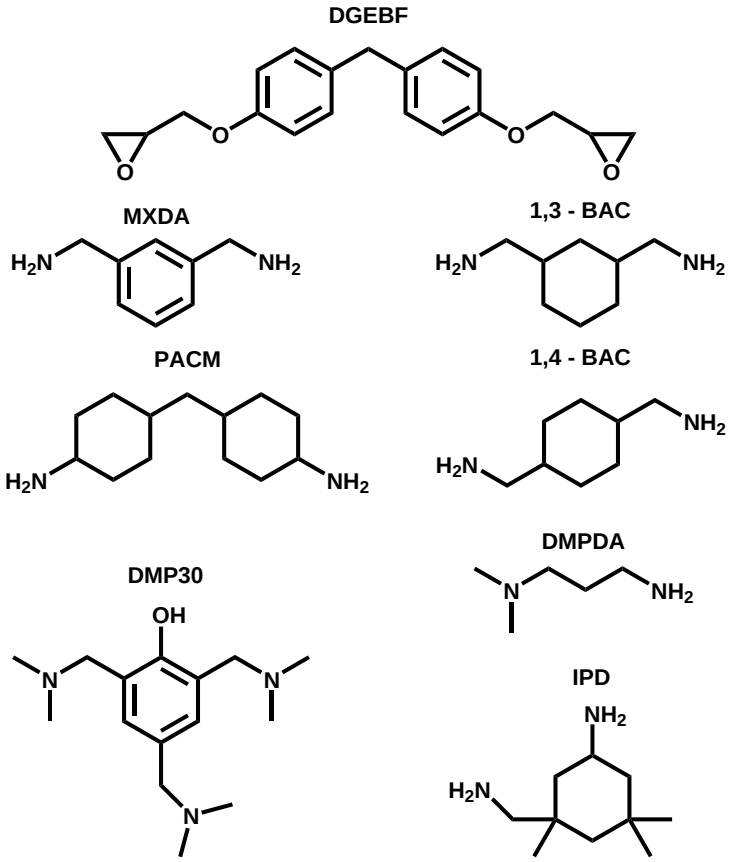

Figure 5.8.1: *The chemical structures of materials used in this section. The epoxy resin DGEBF is reacted with each of the seven amines shown.*

5.8.2 Sample set - 1

Diffusion of methanol

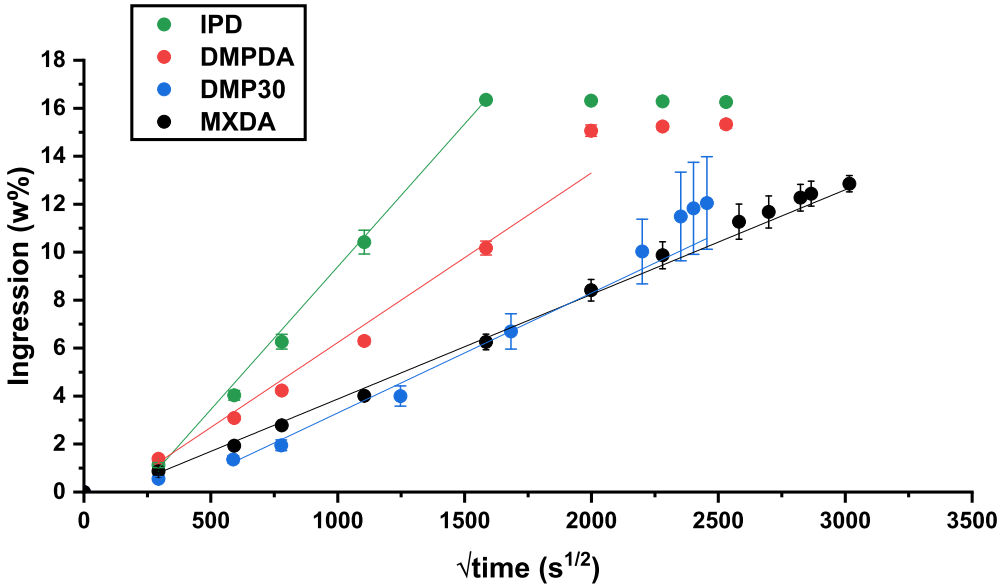

Figure 5.8.2: *Methanol ingression over time for DGEBF based epoxies cured with different amine as labelled. Linear fits are applied to determine the rate of ingression. Error bars shown represent the standard error of three samples.*

The ingression of methanol in epoxy samples consisting of DGEBF resin cured with four amines is shown in Figure 5.8.2. IPD shows the highest rate of ingression and highest ultimate uptake (assuming unlikely changes in ingression for DMP30 and MXDA). DMPDA shows a lower rate of ingression than IPD and a slightly lower ultimate uptake. It also seems that DMPDA experiences a change in the ingression rate beyond 1750 $s^{1/2}$. DMP30 and MXDA show the lowest rates of ingression and it can be assumed the lowest ultimate uptakes. DMP30 starts with a slower rate of ingression which then increases between 750 and 1500 $s^{1/2}$. Solid lines represent regions used to determine ingression rate. The results are summarised in Figure 5.8.3

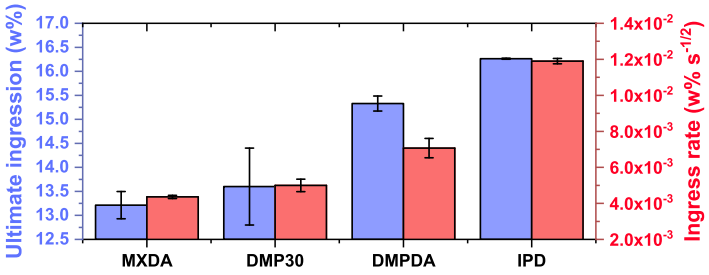

Figure 5.8.3: *The ultimate and rate of ingression of methanol in DGEBF based epoxy samples cured with different amines. Error bars represent the standard error of three samples.*

Free volume and the glass transition temperature

The glass transition temperature, free volume and fractional free volume are shown in Figure 5.8.4 for the amine varied epoxy samples. MXDA exhibits the lowest T_g with a slight increase for DMPDA. The T_g for DMP30 and IPD are higher and fiarly similar to one another. MXDA has the lowest free volume whilst DMP30 and DMPDA are slightly higher. DMPDA has a higher free volume than DMP30 whilst IPD has a significantly higher free volume than the other three amines. IPD also has the highest FFV by some margin, whilst MXDA, DMP30 and DMPDA have similar FFV.

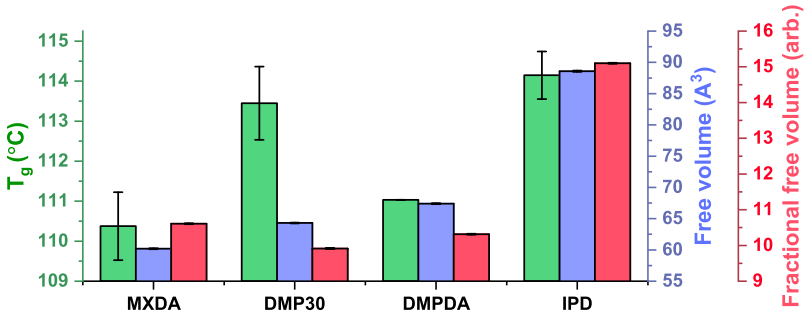

Figure 5.8.4: *The glass transition temperature, free volume and fractional free volume for DGEBF based epoxy samples cured with different amines. Error bars represent the standard error of two samples for T_g results whilst FV and FFV are based on errors generated in the program "LTPOLYMERS".*

5.8.3 Sample set 2

Another set of DGEBF based resins were cured with amines but this was carried out by colleague, Stephen Knox. Samples for diffusion studies were in the form of epoxy coatings ($\approx$ 300 μm thickness) drawn down onto glass microscope slides. Samples were cured under nitrogen at 160 °C as described in Section 2.2.2. Along side these coatings, thicker samples (2mm thickness) were cured using the same materials intended for PALS measurements.

Diffusion properties

The diffusion properties for these samples are shown in Figure 5.8.5.

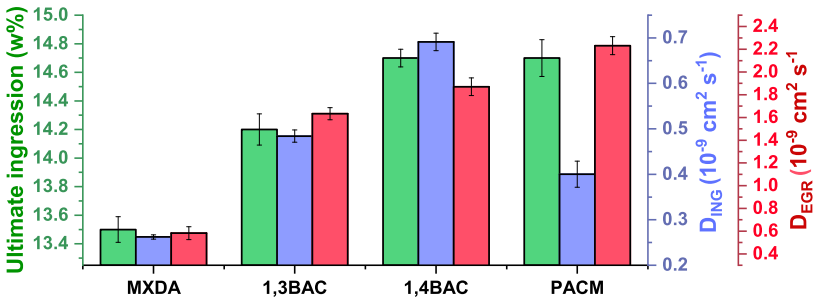

Figure 5.8.5: *The diffusion properties of DGEBF resins cured with different amines on glass microscope slides. Error bars represent the standard error of three samples. These results were measured by Stephen Knox.*[71,106]

Free volume and the glass transition temperature

The T_g, free volume and fractional free volume (FFV) are shown for the DGEBF epoxies cured with different amines by S Knox in Figure 5.8.6. MXDA shows the lowest T_g of the four amines. 1,3 and 1,4 BAC have similar T_gs which are considerably higher than MXDA. PACM has the highest T_g. The free volume is lowest for MXDA by a significant margin whilst 1,3 and 1,4 BAC are considerably higher but similar to one another. PACM has the highest level of free volume . PACM also has the highest fractional free volume (FFV). 1,4 BAC has a lower FFV than PACM but considerably higher than 1,3BAC. MXDA has the lowest FFV out of the four samples.

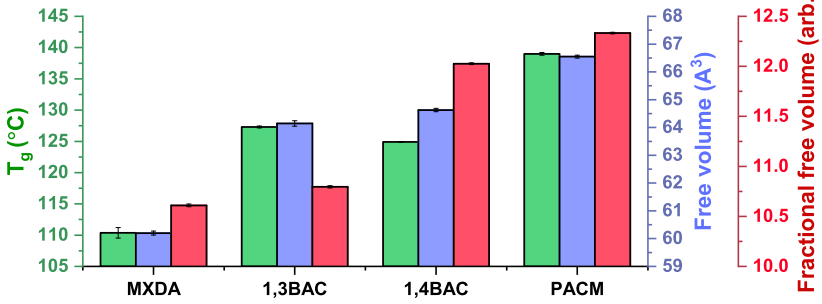

Figure 5.8.6: *The glass transition temperature, free volume and fractional free volume for epoxy resins consisting of DGEBF resin cured with various amines. Error bars represent the error of three samples. S Knox produced the samples 1,3BAC, 1,4BAC and PACM. Free volume and fractional free volume were measured by positron annihilation lifetime spectroscopy.*

5.8.4 Free volume and relation to diffusion

Sample set - 1

Figure 5.8.7 shows the (a) free volume and (b) the fractional free volume in comparison to diffusion for DGEBF epoxy samples cured with different amines. Linear fits were applied to data and R^2 values determined to indicate the quality of correlations. The (a) free volume increases with increased ultimate ingression with a reasonable correlation. As free volume increases the rate of ingression also increases with an R^2 value showing that the correlation is strong ($R^2 = 1$). The (b) fractional free volume shows similar trends to that of free volume with Ultimate ingression and rate of ingression increasing with increased FFV. A similarly strong correlation is shown for the FFV - ingress rate relation.

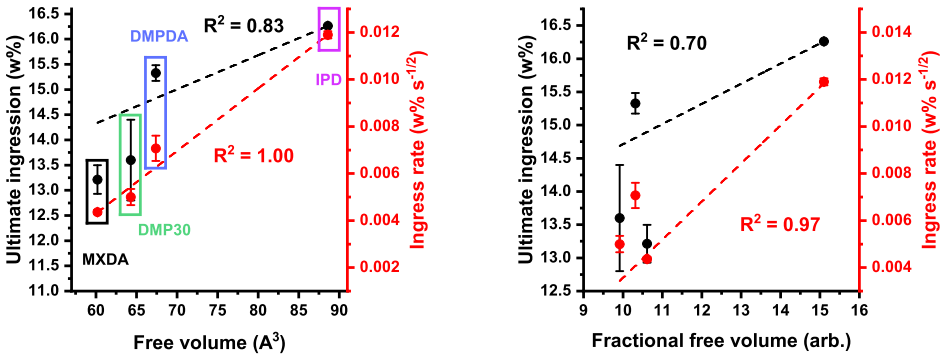

Figure 5.8.7: *The (a) free volume and (b) fractional free volume compared with diffusion properties for samples of DGEBF cured with different amines. Dashed lines represent linear fits whilst R^2 values indicate to quality of correlation. Error bars represent the standard error of three samples.*

Sample set - 1

The diffusion properties for samples cured on glass slides are compared to free volume properties of the corresponding thicker samples in Figure 5.8.8. As (a) free volume increases, the ultimate ingression, and rates of egression and ingression are seen to increase. The correlation is good for both ingression and D_{ING} whilst the correlation for D_{EGR} is near perfect. As (b) fractional free volume (FFV) increases all three diffusion properties increase. The correlation between FFV and ultimate ingression is good whilst the relations with both diffusion coefficients is average.

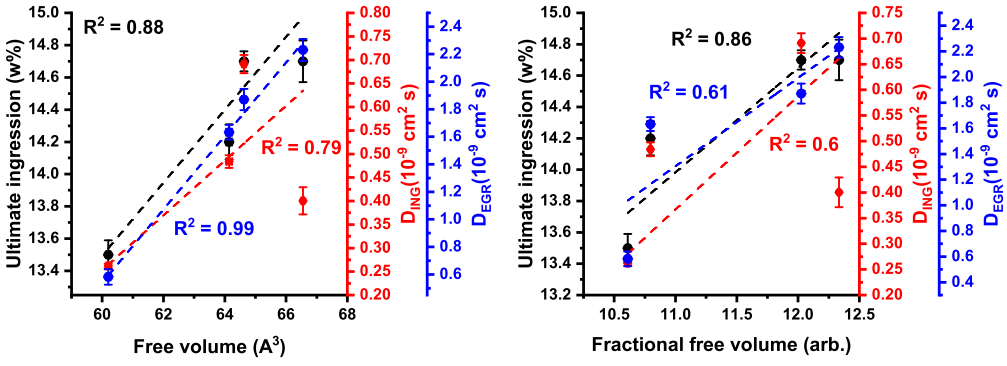

Figure 5.8.8: *The (a) free volume and (b) fractional free volume for samples of epoxy consisting of DGBEF and various amines. The error bars represent the standard error of three samples. Diffusion measurements and epoxy production was carried out by S Knox.*

5.8.5 Free volume and its relation to Tg

Figure 5.8.9 compares the T_g to the diffusion properties for both sets of DGEBF-amine varied samples. The general trends shown in both (a) and (b) are that as T_g increases, each diffusive property also increases. The R^2 values are reasonable to very good which implies that the trends are reliable.

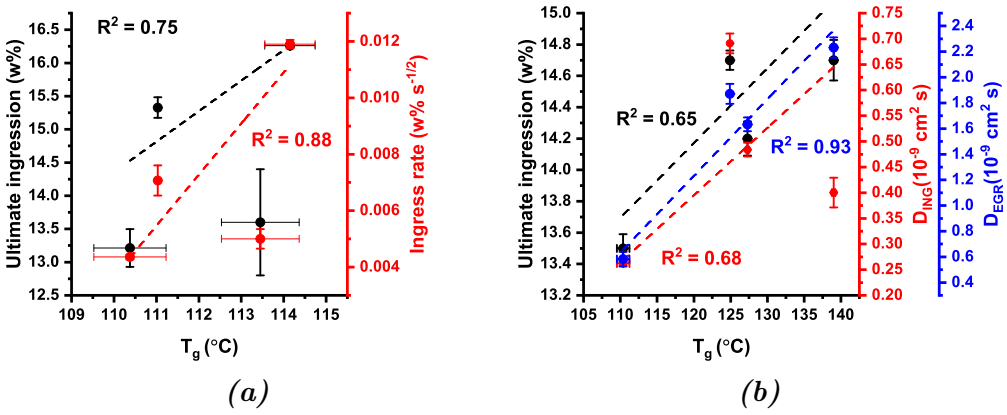

Figure 5.8.9: *A comparison between T_g and diffusion properties for DGEBF - amine varied samples. (a) Thick free standing samples (b) Coatings applied to glass for diffusion studies as prepared by S Knox. The error bars represent the standard error of three samples in the y direction whilst the x error is the standard error of two samples.*

Figure 5.8.10, compares the T_g to free volume properties for all DGEBF-amine samples. It is evident that there is no trend between the T_g and free volume for this sample set. Linear fits are shown by dashed lines with R^2 values emphasising the poorness of fit ($R^2 \approx 0$).

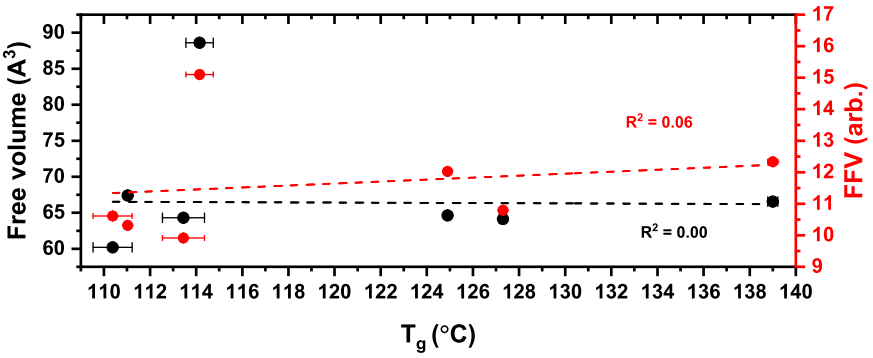

Figure 5.8.10: *The free volume and fractional free volume compared to all T_g values for epoxy resins comprising of DGEBF with varied amine. Error bars represent the standard error of two samples in the x direction whilst free volume errors are generated in "LTPOLYMERS" software.*

5.8.6 Conclusions

Several epoxy samples comprising of DGEBF resin cured with various amines were studied with regards to diffusion, glass transition temperature (T_g) and free volume. One set of samples were produced as described in Section 2.2.2. whilst another were produced with similar cure conditions but were thin and coated onto glass slides (produced by S Knox).

Free volume and diffusion

In both sets of samples, free volume and fractional free volume (FFV) correlated to an increase in diffusion properties. In sample set 1, a high correlation ($R^2 > 0.95$) was seen when comparing both free volume and FFV to the rate of ingression. When comparing free volume and FFV with the ultimate ingression, reasonable correlations were observed ($R^2 > 0.7$). For sample set 2, an increase in free volume and FFV corresponded reasonably well ($R^2 > 0.7$) with increasing ultimate ingression. The diffusion coefficient for ingression (D_{ING}) was shown to increase with increasing free volume and FFV with R^2 values of 0.79 and 0.6 respectively. The diffusion coefficient of egression D_{EGR} increased with increasing free volume in a near perfect manner (R^2 >0.99) it increased with an average correlation (R^2 >0.6) when compared with FFV.

Tg and diffusion

The glass transition temperature (T_g) generally increased with an increase in diffusion for both sample set. The correlations had R^2 values greater than 0.68 and a maximum of 0.93. This trend is fairly counter intuitive when considering the relations alone in terms of using T_g as an indicator for conversion of reaction. However, it must be taken into consideration that when comparing different chemistries, the relationship between T_g and conversion of reaction should not be taken into account. The trends between T_g and diffusion should probably be taken as a coincidence.

T_g and free volume
Free volume was compared for all samples with the T_g. No trends were seen which was highlighted by R^2 values of 0.00 and 0.06 when comparing T_g to free volume and FFV respectively.

Closing remarks
This section compared how amine variation affects the diffusive nature of methanol in epoxy samples based on DGEBF epoxy. Free volume measurements obtained by means of PALS were compared to the diffusion and trends noted. As free volume or fractional free volume increased, the rates of diffusion and the ultimate ingression also increased. Relations between T_g and diffusion were seen but subsequently ignored. The next section of this chapter will discuss some key findings of all the studies presented.

5.9 Chapter summary
This section will discuss the different studies undertaken and concisely present the key findings of this chapter.

5.9.1 Experimental design
The ultimate goal of this chapter was to compare diffusion to both T_g and free volume in a number of epoxy resin samples. To give the overall investigation some applicably relevant results, a number of experiments were designed. The affects of curing were studied by comparing a real world cure regime to that of a more optimised one. The affects of additional components were studied such as pigmentation and solvation of the epoxy network as this is usual practice in many protective coatings. Diluent epoxies were added to the DGEBF-MXDA network since these are sometimes added to coating where solvents cannot be utilised. A blend of the the resins DGEBA and DGEBF were prepared and study due to their significantly different free volume and diffusion characteristics when between the epoxies when solely prepared with MXDA. Finally, changing the chemistry in terms of amine variation was carried out as up until that point, chemistries were similar within the previous studies.

5.9.2 Key findings
Cure conditions
This study showed that as long as the epoxy amine mixture is left at room temperature for 1 hour (maybe less), effectively the maximum performance in terms of chemical resistance, is achieved. No true correlations were seen when comparing diffusion to either T_g or free volume properties.

5.9.3 Pigmentation
The addition of the pigment barytes caused a reduction in diffusion. Although each sample had reduced epoxy available to uptake methanol, this was not solely the case for reduced ingression. Once pigmentation reached 50 w%, the diffusion increased which indicates an epoxy-pigment effect on ingression. Free volume and fractional free volume were shown to decrease as pigmentation increased. It was also generally seen that as free volume increased, so did the diffusion of methanol. As T_g increased so did the diffusion of methanol. An increase in T_g also corresponded to a decrease in free volume although this correlation was weak.

5.9.4 Solvated epoxies

Xylene was added to the epoxy network which caused diffusion to increase significantly. After ultimate ingression was reached, the samples began to decrease in mass which was attributed to xylene diffusing out of the coating (indicated by gas chromatography). The T_g decreased exponentially with the addition of xylene whilst free volume and FFV increased significantly with solvation. Ultimately, it was concluded that when solvent is present in the network, methanol diffusion is enhanced. The second ingression cycle shows signs that ingression is greatly reduced if xylene is removed by drying.

5.9.5 Diluent epoxies

Uni-functional and bi-functional epoxies PGE and BDDGE were mixed with DGEBF prior to reacting with amines. PGE caused an increase in methanol diffusion and also saw mass loss of the sample with the highest concentration. The mass loss is expectedly due to an increased sol-fraction in the network which is extracted on methanol ingression. BDDGE also caused diffusion to increase which is most-likely due its long linear chained structure. Both epoxies saw diffusion increase with decreased T_g and increased free volume. The T_g and free volume were highly correlated with free volume decreasing with increased T_g.

5.9.6 Epoxy blends

Epoxy samples consisting of different amounts of DGEBF and DGEBA resins resulted in increased diffusion as blend ratios approached 50:50. No real trend was seen when between T_g and blend ratio although the lowest T_g was seen at a 50:50 blend. Free volume decreased in a loosely exponential manner with increasing levels of DGEBF. Diffusion did not show any correlations with free volume or FFV. It was shown that diffusion increased with a decrease in T_g. No true correlation was seen between free volume and T_g.

5.9.7 Amine variation

Epoxy samples based on DGEBF were prepared with a number of different amines and diffusion measured. Free volume was shown to highly correlate to the majority of diffusion properties. As free volume increased, the ultimate ingression and diffusion rates increased in a linear fashion. This was the case for free standing and drawn down samples. The diffusion appeared to correspond to increasing T_g but ultimately the T_g is not expected to correlate to diffusion when comparing different samples. There was no correlation between the T_g and free volume.

5.9.8 Closing remarks

An overall observation from this chapter is that both T_g and free volume have the capability to sense the chemical resistance of an epoxy material. In some cases, neither show any change or non nonsensical changes which correspond to diffusion. In several instances both T_g and free volume change accordingly to diffusive properties but only free volume measurements by PALS were able to detect changes in chemical resistance between samples of greatly differing chemistries. This observation, in addition to the non destructive nature of free volume measurement, suggest that PALS can be utilised to determine the chemical resistance of epoxy resins and in a much shorter time scale to traditional gravimetric ingression experiments.

6

Conclusions and fundamental observations

This last chapter will consider the original aims and objectives of the research and direct the reader to relevant sections of the thesis for further details. Following this, some key observations will be noted based on different aspects of the work. Some current work and suggestions for continuation will be presented.

6.1 PALS in Sheffield

A key aspect of the work presented in this thesis was the successful assembly of a digital positron annihilation lifetime spectroscopy (PALS) system. This process was pivotal to the PhD project as a whole as the majority of study considered free volume measurements. There were many setbacks which do not fit in with the reading of a thesis which will hopefully become available in a technical manual elsewhere.
In the grand scheme of the field of positron annihilation studies, the instrument assembled in this work is by no means a huge feat. A positron source and high performing system can be purchased and set-up within a few months for a substantial fee. In this work it was not intended to push the boundaries of PALS technology to the next level but instead to give an informed, relatively simple outline of how a system can be built for a low cost whilst having the ability to access useful information in terms of free volume measurements in polymers. This objective was achieved and the University of Sheffield can now venture further into the field of positron annihilation.

PALS in Sheffield is currently capable of measuring free volume and fractional free volume in polymers with it's timing resolution of 470 ± 26 ps but several improvements can be made in terms of instrument resolution and efficiency. New fast plastic scintillators have been released since the beginning of this study such as the EJ-232Q model from Eljen technology. This scintillating material has timing characteristics which are more than twice as fast as the EJ232 used here. Additionally, further optimisation of the constant fraction discriminator level can be performed with regards to photomultiplier supply voltage which should improve the instrument resolution. Scintillator geometry adjustments and the improvement of acquisition methods can also have an effect. The next logical step in terms of improving efficiency is the addition of more PMTs as the digitiser used in this work can accommodate two more. A heated chamber has already been produced in the laboratory which, with simple modification could be implemented to the PALS assembly and thermal studies carried out. The design for the sample chamber is shown in Figure 6.1.1 (a) and a schematic of the 4-detector PALS (b).

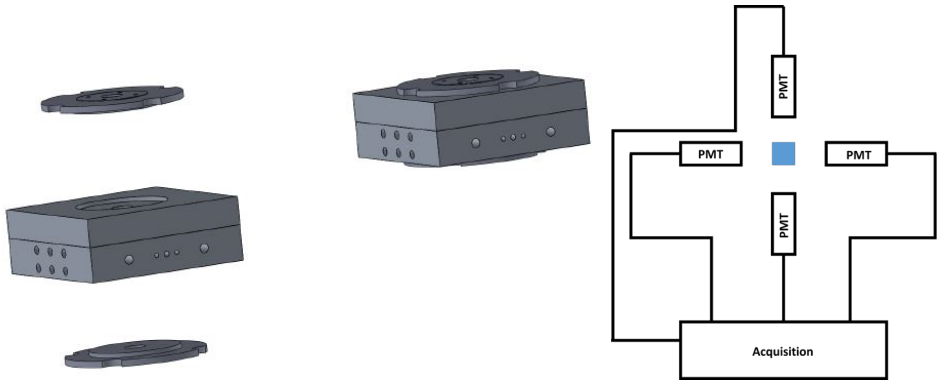

Figure 6.1.1: *Future improvement of PALS could involve the implementation of an already produced (a) heated cell chamber for thermal PALS studies and (b) the addition of extra detectors to improve spectral acquisition times.*

Large amounts of data were collected from mono energetic positron spectroscopy (MEPS) and as such, there is still a lot to gain; notably free volume distributions. This work has presented free volume in terms of an average free volume and fractional free volume. Analytical techniques exist which allow the lifetime spectra collected through PALS to be deconvoluted into lifetime distributions and, hence in the case of ortho-positronium, free volume distributions.

Figure 6.1.2 shows the free volume distributions for DGEBF cured with the amines 1,3 - BAC and MXDA for an implantation energy of 10 keV. The average free volumes are noted in the inset table. Up until this point, only the average free volume had been indicated by free volume measurements but the results shown for distributions reveal that the 1,3-BAC based epoxy has a broader distribution of free volume showing a proportion of smaller voids than that seen in MXDA. Whilst the peaks of distributions are in similar positions, 1,3-BAC is weighted to the right hand side which accounts for the higher average free volume.

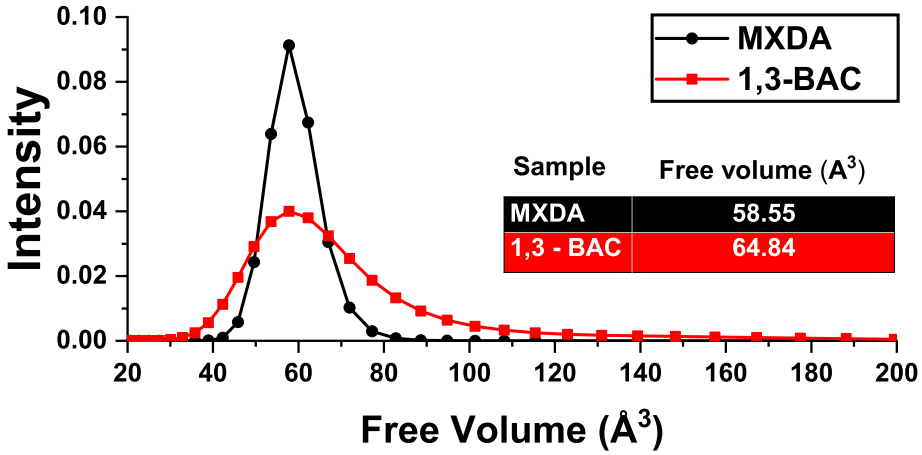

Figure 6.1.2: *Free volume distributions in DGEBF epoxy samples cured with MXDA (black) and 1,3-BAC (red). Distributions were produced using the MATLAB program MELT.*

The shape of the distribution could be attributed to isomerism found in 1,3-BAC. Figure 6.1.3 shows computational modelling carried out by Stephen Knox. The modelling yields results concerning distances between nitrogens (blue). Table 6.1 summarises the distances (N-N) for MXDA, cis and trans 1,3-BAC. MXDA is shown to have an N-N distance of 7.3 A^3 whilst the 1,3 BAC isomers have values of 7.59 and 6.85 A^3 respectively. The average of the two based on their relative amounts is 7.41 A^3. The fact that 1,3-BAC has both a lower and higher N-N distance than MXDA could be responsible for the higher and lower free volume voids shown in Figure 6.1.2. Additionally, the average value being marginally higher than MXDA could also account for the large average free volume in 1,3 BAC. This is based on the idea that there is a larger distance between the functional groups which ultimately react with epoxide groups. This would result in a greater distance between cross-links and therefore a larger free volume.

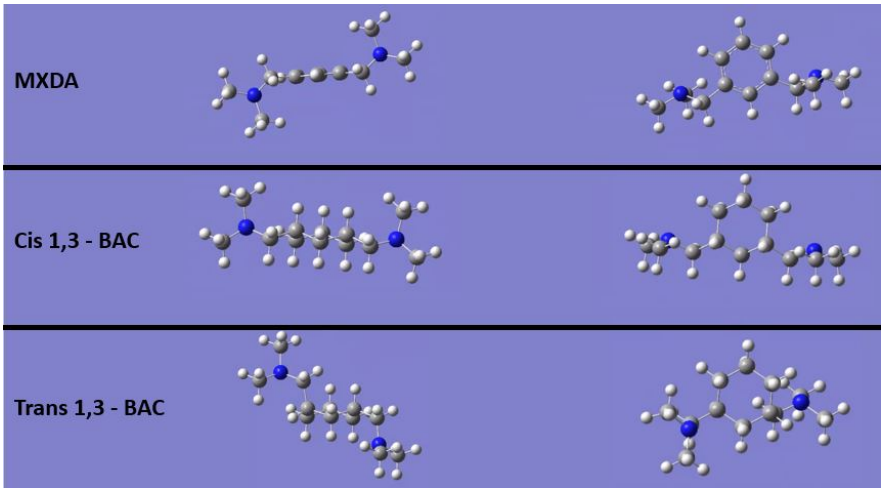

Figure 6.1.3: *Computational modelling showing the structure of MXDA and the two regioisomers of 1,3-BAC which were obtained using GaussView 5.0.8 by Stephen Knox.*

Table 6.1: *The distance between nitrogens in MXDA and the two regioisomers cis and trans 1,3-BAC.*

Amine	**N-N distance (Å)**	
MXDA	7.30	
cis 1,3 - BAC	7.59	7.41
trans 1,3 - BAC	6.85	

6.2 Observations in free volume and diffusion.

6.2.1 Chemical changes

Another key aim of this research was to measure free volume in epoxy resins and observe how it was affected by changes to the chemistry and production of the epoxy network. Ultimately it was shown that where chemistries are similar, and no external factors are involved (solvation, temperature, pressure etc.) free volume is also similar which was shown in Section 5.2.1.

Where cure conditions were changed, the free volume only varied by 2 - 3 A^3. Significant changes in free volume occur when the chemistry differs, as was shown by MEPS (Figure 6.2.1a) and supported by PALS (Figure 6.2.1b) when measuring free volume in DGEBF epoxies cured with MXDA, PACM and BAC. It can only be assumed at this point that the variation in values of free volume are attributed to MEPS concerning free volume near the surface whilst PALS is a bulk measurement.

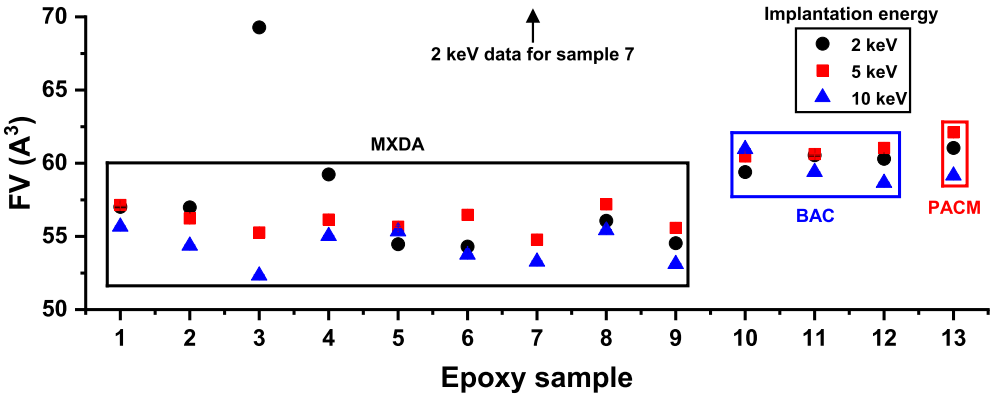

(a) Free volume at implantation energies 2, 5 and 10 keV for all epoxy samples. Coloured boxes highlight the amines which correspond to the contained data points.

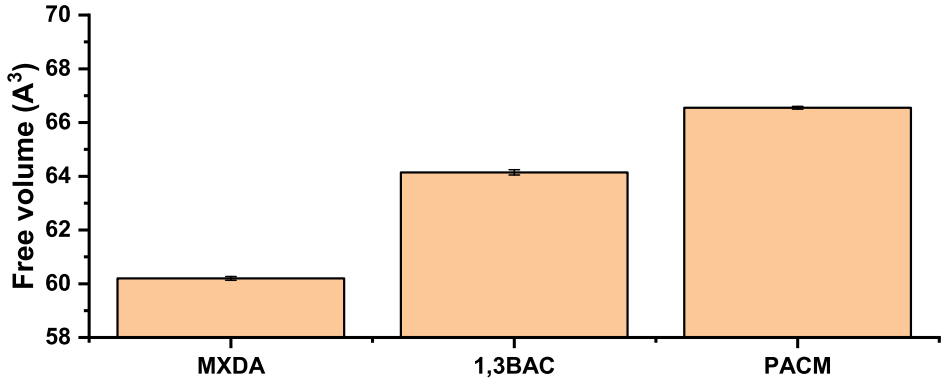

(b) The average free volume values for DGEBF epoxy cured with the three amines MXDA, 1,3-BAC and PACM. Error bars represent the standard error of three samples.

Figure 6.2.1

Free volume changes were observed for similar chemistries when other factors were involved. This was shown by pigmentation and solvation studies in Sections 5.3 and 5.4. Increased pigmentation correlated reasonably well with small changes in free volume in that it was reduced. However based on the lifetime spectra obtained for pigment powder, this free volume reduction is likely a consequence of combined lifetime spectra. When the epoxy network was solvated by xylene, a large increase in free volume was observed but this increase did not increase with further xylene addition.

As this research concerns protective coatings with regards to chemical resistance, diffusion studies were performed. Curing conditions were shown to have a minimal effect on the ability to prevent ingression as long as a pot-time of at least 1 hour (possibly lower but not studied here). It is expected that the molecular weight increases sufficiently in this time to prevent the evaporation of amine during cure. When pot-time is eliminated completely then evaporation is more favourable which results in a non-stoichiometric ratio between amine hydrogens and epoxide groups. This causes the number of cross-links to reduce and ingression is enhanced. As with free volume, diffusion was only noticeably affected when chemistry was changed or external factors involved.

It was shown that free volume on numerous occasions was related to diffusion in that increased free volume would correspond to increased ingression. Similar trends were seen for the glass transition temperature; in most cases T_g was more sensitive to changes in diffusive properties. One key difference between T_g and free volume in terms of sensing diffusion is observed on changing the chemistry. T_g is a good indicator of reaction conversion for similar chemistries but when comparing T_g between differing chemistries, only information on thermomechanics is obtained. Free volume however, appears to be most sensitive to changes in diffusion when the chemistries are significantly different. Figure 6.2.2 shows the comparison of the ingression rate for each study with both free volume and the glass transition temperature. Whilst not perfect, the ingression rate tends to increase with increasing free volume. The glass transition temperature on the other hand sometimes shows an increasing ingression rate and other times the opposite trend is seen. However, it should be noted that overall a low T_g results in high ingression rates whereas the highest FV does not correspond to the highest ingression rate.

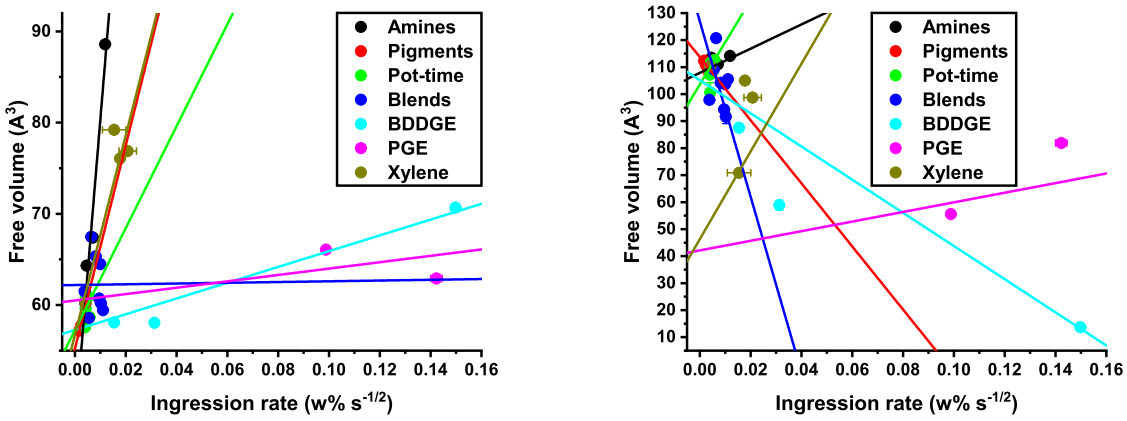

Figure 6.2.2: *(a) The free volume and (b) glass transition temperature compared to the ingression rate for each study. Linear fits are shown by solid lines. Error bars represent the standard error of three samples.*

When studying the effects on diffusion and free volume in epoxy blends of DGEBA and DGEBF, unusual results were obtained. Diffusion was shown to become greater as the mixtures moved further away from either pure DGEBA or DGEBF. This increased diffusion correlated to decreasing T_g whereas free volume measurements were only sensitive to the addition of DGEBF to DGEBA or vice versa in that the result in free volume similar to the average of two separate free volumes. Free volume showed no correlation to diffusion which leads to speculation that weak inter-facial regions exist in the network between regions of DGEBA-MXDA and DGEBF-MXDA. Further study is required in the field of x-ray and neutron scattering possibly in conjunction with positron beam studies before solid conclusions can be drawn.

6.3 Future work

As with much research, this work has considerable room for further work in several areas. Many studies have been presented in this work but they were largely carried out under ambient conditions, which do not represent a number of locations where the materials in question would be used. Also, whilst studies angled towards more applicable materials (i.e. pigmented and solvated epoxies) were performed, real world materials are formulations that contain several components. Therefore, the effects of each component in a single formulation on the diffusion properties and free volume is not understood. Furthermore, diffusion results were compared to free volume measurements made in a dry state. Therefore, the evolution of free volume during the diffusion and drying processes is unknown for these materials. With these points in mind, some suggestions for the continuation of work are;

a) PALS studies during diffusion

An interesting study would be to observe the evolution of free volume during the diffusion and also the effects of drying the samples. This would require quicker PALS acquisition times especially for diffusion time less than 24 hours. A receptacle would need to be designed for the solvent and sample, which would surround the positron source. PALS testing of the receptacle would be required in order to observe the effects the spectra.

b) Environmental effects

Data that is more useful could be obtained from experiments carried out in conditions, which would represent different parts of the world (i.e. India and Norway) in terms of temperature, humidity and ultraviolet radiation. Temperature studies could be performed during diffusion studies whilst variations to all three conditions could be made prior to diffusion studies. Furthermore, the previously mentioned heated cell could be used to measure free volume at different temperatures and potentially varied humidity.

c) The study of realistic formulations

PALS and diffusion studies of a wide range of formulations could help pinpoint which components are more effective on the diffusive nature of solvents and how this in turn corresponds to free volume. Before this can be carried out, the effects on the PALS spectra due to the addition of pigments, solvents and other additives is needed to determine whether results collected would be reliable.

Bibliography

[1] McCrum, N. G., Buckley, C. P., and Bucknall, C. B. *Principles of polymer engineering*. Oxford University Press, 2nd edition, (1997).

[2] Young, R. J. and Lovell, P. A. *Introduction to Polymers, Third Edition*. CRC Press, (2011).

[3] Baird, D. G. and Collias, D. I. *Polymer processing : principles and design*. Wiley, New Jersey, second edi edition, (2014).

[4] Flory, P. J. *Journal of the American Chemical Society* **63**(11), 3083–3090 nov (1941).

[5] Stockmayer, W. H. *The Journal of Chemical Physics* **12**(4), 125 dec (1944).

[6] Pascault, J. P., Sautereau, H., Verdu, J., and Williams, R. J. J. *Thermosetting Polymers*. Plastics engineering. Taylor & Francis, New York, (2002).

[7] Ellis, B. *Chemistry and Technology of Epoxy Resins*. Springer Netherlands, Dordrecht, (1993).

[8] Zee, M., Feickert, A. J., Kroll, D., and Croll, S. *Progress in Organic Coatings* **83**, 55–63 jun (2015).

[9] Van der Waals, J. *Over de Continuiteit van den Gas-en Vloeistoftoestand (On the Continuity of the Gas and Liquid State)*. PhD thesis, University of Leiden, (1873).

[10] Bartky, W. *The Astrophysical Journal* **70**, 194 oct (1929).

[11] Haring, M. M. *Journal of Chemical Education* **19**(5), 249 may (1942).

[12] Utracki, L. A. and Sedlacek, T. *Rheologica Acta* **46**(4), 479–494 oct (2006).

[13] Letcher, T. M. *Thermodynamics, Solubility and Environmental Issues*. Elsevier B.V., 1st editio edition, (2007).

[14] Auras, R. A. In *Thermodynamics, Solubility and Environmental Issues*, 343–368. Elsevier (2007).

[15] Jackson, M., Kaushik, M., Nazarenko, S., Ward, S., Maskell, R., and Wiggins, J. *Polymer* **52**(20), 4528–4535 (2011).

[16] Budd, P. M., McKeown, N. B., and Fritsch, D. *Journal of Materials Chemistry* **15**(20), 1977 (2005).

[17] Ebnesajjad, S. In *Chemical Resistance of Engineering Thermoplastics*, chapter Introducti, xiii–xxv. William Andrew Publishing jan (2016).

[18] Ramesh, N. and Duda, J. L. *Korean Journal of Chemical Engineering* **17**(3), 310–317 may (2000).

[19] Consolati, G., Kansy, J., Pegoraro, M., Quasso, F., and Zanderighi, L. *Polymer* **39**(15), 3491–3498 jul (1998).

[20] Recio, R., Lozano, Á. E., Prádanos, P., Marcos, Á., Tejerina, F., and Hernández, A. *Journal of Applied Polymer Science* **107**(2), 1039–1046 jan (2008).

[21] Drake, A. C., Lee, Y., Burgess, E. M., Karlsson, J. O. M., Eroglu, A., and Higgins, A. Z. *PLOS ONE* **13**(1), 1 – 15 jan (2018).
[22] Yang, B., Huang, W. M., Li, C., and Chor, J. H. *European Polymer Journal* **41**(5), 1123–1128 may (2005).
[23] Yong, A. X. H., Sims, G. D., Gnaniah, S. J. P., Ogin, S. L., and Smith, P. A. *Advanced Manufacturing: Polymer & Composites Science* **3**(2), 43–51 apr (2017).
[24] Jadhav, N. R., Gaikwad, V. L., Nair, K. J., and Kadam, H. M. *Asian Journal of Pharmaceutics* **3**(2), 82 – 89 (2009).
[25] Zhang, Y., Adams, R. D., and Da Silva, L. F. *International Journal of Adhesion and Adhesives* **50**, 85–92 apr (2014).
[26] Zeleznak, K. and Hoseney, R. *Cereal Chemistry Back Issues* **64**(2), 121 – 124 (1987).
[27] Royall, P. G., Craig, D. Q., and Doherty, C. *International journal of pharmaceutics* **192**(1), 39–46 dec (1999).
[28] Patial, B. S., Thakur, N., and Tripathi, S. K. In *AIP Conference Proceedings*, volume 1591, 770–772. American Institute of Physics Inc., feb (2014).
[29] Honary, S. and Orafai, H. *Drug Development and Industrial Pharmacy* **28**(6), 711–715 jan (2002).
[30] Cheng, M.-L. and Sun, Y.-M. *Journal of Polymer Science Part B: Polymer Physics* **47**(9), 855–865 may (2009).
[31] Neway, B., Hedenqvist, M. S., and Gedde, U. W. *Polymer* **44**(14), 4003–4009 jun (2003).
[32] Lincoln, J. E., Morgan, R. J., and Shin, E. E. *Journal of Polymer Science Part B: Polymer Physics* **39**(23), 2947–2959 dec (2001).
[33] Silverstein, M. S., Cameron, N. R., and Hillmyer, M. *Porous Polymers*. John Wiley and Sons, Hoboken, NJ, USA, jan (2011).
[34] Wool, R. P. and Sun, X. S. In *Bio-Based Polymers and Composites*, chapter 7, 202–255. Academic Press jan (2005).
[35] Krongauz, V. V. *Journal of Thermal Analysis and Calorimetry* **102**(2), 435–445 nov (2010).
[36] Patil, P. N., Rath, S. K., Sudarshan, K., Dutta, D., Patri, M., and Pujari, P. K. **1313**, 298 (2010).
[37] Yu, W. C. and Sung, C. S. P. *Macromolecules* **21**(2), 365–371 mar (1988).
[38] Pascault, J. P. and Williams, R. J. J. *Journal of Polymer Science Part B: Polymer Physics* **28**(1), 85–95 jan (1990).
[39] Min, B.-G., Stachurski, Z., and Hodgkin, J. *Polymer* **34**(23), 4908–4912 jan (1993).
[40] Dlubek, G., Pionteck, J., Sniegocka, M., Hassan, E. M., and Krause-Rehberg, R. *Journal of Polymer Science Part B: Polymer Physics* **45**(18), 2519–2534 sep (2007).
[41] Dlubek, G., Wawryszczuk, J., Pionteck, J., Goworek, T., Kaspar, H., and Lochhaas, K. H. *Macromolecules* **38**(2) (2004).
[42] Jeffrey, K. and Pethrick, R. A. *European Polymer Journal* **30**(2), 153–158 feb (1994).
[43] Kumar, H., Kumaraswamy, G., Ravikumar, H., and Ranganathaiah, C. *Polymer International* **54**(10), 1401–1407 (2005).
[44] Chen, H., Hung, W.-s., Lo, C.-h., Huang, S.-h., Cheng, M.-l., Liu, G., Lee, K.-r., Lai, J.-y., Sun, Y.-m., Hu, C.-C., Suzuki, R., Ohdaira, T., Oshima, N., and Jean, Y. C.

Macromolecules **40**(21), 7542–7557 (2007).
[45] Dlubek, G., Stejny, J., and Alam, M. A. *Macromolecules* **31**(14), 4574–4580 (1998).
[46] Liao, K.-S., Chen, H., Awad, S., Yuan, J.-P., Hung, W.-S., Lee, K.-R., Lai, J.-Y., Hu, C.-C., and Jean, Y. C. *Macromolecules* **44**(17), 6818–6826 sep (2011).
[47] Van Horn, J. D., Chen, H., Jean, Y. C., Zhang, W., and Jaworowski, M. R. *Journal of Physics: Conference Series* **618**(1), 1–6 jun (2015).
[48] Bečvář, F., Čížek, J., Procházka, I., and Janotová, J. *Nuclear Instruments and Methods in Physics Research Section A: Accelerators, Spectrometers, Detectors and Associated Equipment* **539**(1-2), 372–385 feb (2005).
[49] Bečvář, F., Čížek, J., and Procházka, I. *Applied Surface Science* **255**(1), 111–114 oct (2008).
[50] Tao, S. J. *The Journal of Chemical Physics* **56**(11), 5499 (1972).
[51] Eldrup, M., Lightbody, D., and Sherwood, J. *Chemical Physics* **63**(1-2), 51–58 (1981).
[52] Yampolskii, Y. P. *Russian Chemical Reviews* **76**(1), 59–78 jan (2007).
[53] Mohammadi-Jam, S. and Waters, K. *Advances in Colloid and Interface Science* **212**, 21–44 oct (2014).
[54] White, R. P. and Lipson, J. E. *Macromolecules* **49**(11), 3987–4007 (2016).
[55] Crank, J. *The mathematics of diffusion*. Clarendon Press, Oxford, 2nd ed. edition, (1975).
[56] Jansen, K. M., Zhang, M. F., Ernst, L. J., Vu, D. K., and Weiss, L. *Microelectronics Reliability* **107**, 113596 apr (2020).
[57] Hajiagha, S. and Karimi, M. In *Proceedings of the International Conference on Intelligent Textiles*, 125–126, (2010).
[58] Billing, C. and Bentz, A. In *Performance of Protective Clothing: Second Symposium*, 226–235. ASTM International (1988).
[59] Dung, V. B. and Van Thien, D. *Journal of Physics: Conference Series* **537**(1), 012011 sep (2014).
[60] Allen, G. *Comprehensive polymer science and supplements*. Elsevier, (1996).
[61] De Kee, D., Liu, Q., and Hinestroza, J. *The Canadian Journal of Chemical Engineering* **83**(6), 913–929 may (2008).
[62] Hansen, C. M. *European Polymer Journal* **46**(4), 651–662 apr (2010).
[63] De Kee, D., Liu, Q., and Hinestroza, J. *The Canadian Journal of Chemical Engineering* **83**(6), 913–929 may (2005).
[64] Crank, J. *The Mathematics of Diffusion*. Clarendon Press, Oxford, second edi edition, (1975).
[65] Shankar, V. *Polymer* **22**(6), 748–752 jun (1981).
[66] Long, F. A. and Richman, D. *Journal of the American Chemical Society* **82**(3), 513–519 feb (1960).
[67] Richman, D. and Long, F. A. *Journal of the American Chemical Society* **82**(3), 509–513 feb (1960).
[68] Rossi, G. and Mazich, K. A. *Physical review. A, Atomic, molecular, and optical physics* **44**(8), R4793–R4796 oct (1991).
[69] Mazich, K. A., Rossi, G., and Smith, C. A. *Macromolecules* **25**(25), 6929–6933 dec (1992).

[70] Rossi and Mazich. *Physical review. E, Statistical physics, plasmas, fluids, and related interdisciplinary topics* **48**(2), 1182–1191 aug (1993).
[71] Knox, S. *A Fundamental Understanding of the Factors Controlling the Chemical Performance of Model Polymer Networks*. PhD thesis, University of Sheffield, (2018).
[72] Hui, C. Y., Wu, K. C., Lasky, R. C., and Kramer, E. J. *Journal of Applied Physics* **61**(11), 5129–5136 jun (1987).
[73] Neogi, P. *Diffusion Polymers*. (1996).
[74] Van Krevelen, D. and Te Nijenhuis, K. In *Properties of Polymers*, chapter 7, 189 – 227. Elsevier, Amsterdam (2009).
[75] Lapuerta, M. and Canoira, L. *Biofuels for Aviation* , 47–84 jan (2016).
[76] Shen, C.-H. and Springer, G. S. *Journal of Comosite Materials* **10**, 2 – 20 (1976).
[77] Charlton, M. and Humberston, J. *Positron Physics*. (2001).
[78] Anderson, C. D. *Physical Review* **43**(6), 491– 494 mar (1933).
[79] Blackett, P. M. S. and Occhialini, G. P. S. *Proceedings of the Royal Society A: Mathematical, Physical and Engineering Sciences* **139**(839), 699–726 mar (1933).
[80] Berko, S. and Pendleton, H. N. *Annual Review of Nuclear and Particle Science* **30**, 543 – 581 (1980).
[81] Mohorovičić, S. *Astronomische Nachrichten* **253**(4), 93–108 (1934).
[82] Ruark, A. E. *Physical Reviw Letters* **68**(11-12), 278 (1945).
[83] Deutsch, M. *Physical Review* **82**(3), 455–456 may (1951).
[84] Rich, A. *Reviews of Modern Physics* **53**(1), 127 – 165 (1981).
[85] Nath Mondal, N. In *AIP Conference Proceedings*, volume 1970, (2018).
[86] Cassidy, D. B., Canter, K. F., Sherer, R. E., Klinkowstein, R. E., and Hughey, B. C. *Nuclear Instruments and Methods in Physics Research B* **195**(3-4), 442–448 (2002).
[87] Sabelova, V., Krsjak, V., Petriska, M., and Slugen, V. *Proceedings of the 19th International Conference on Applied Physics of Condensed Matter* , 302 (2013).
[88] Brandt, W., Berko, S., and Walker, W. W. *Physical Review* **120**(4), 1289–1295 nov (1960).
[89] Hughes, A. E., Mayo, S., Yang, Y., Markley, T., Smith, S. V., Sellaiyan, S., Uedono, A., Hardin, S. G., and Muster, T. H. *Progress in Organic Coatings* **74**(4), 726–733 (2012).
[90] Unterweger, M., Hoppes, D., Schima, F., and Coursey, J. *NIST Standard Reference Database 120* (2003).
[91] Andres, C. *Some effects on polymers of low-energy implanted positrons*. PhD thesis, (2008).
[92] Pethrick, R. A. *Progress in Polymer Science* **22**(1), 1–47 (1997).
[93] Fong, C., Dong, A. W., Hill, A. J., Boyd, B. J., and Drummond, C. J. *Phys. Chem. Chem. Phys.* **17**(27), 17527–17540 (2015).
[94] Jean, Y. C. *Microchemical Journal* **102**, 72–102 (1990).
[95] Choudalakis, G. and Gotsis, A. *Current Opinion in Colloid & Interface Science* **17**(3), 132–140 jun (2012).
[96] He, C., Suzuki, T., Hamada, E., Kobayashi, H., Kondo, K., Shantarovich, V. P., and Ito, Y. (2016).
[97] Wang, Y. Y., Nakanishi, H., Jean, Y. C., and Sandreczki, T. C. *Journal of Polymer*

Science Part B: Polymer Physics **28**(9), 1431–1441 aug (1990).

[98] Gidley, D. W., Peng, H.-G., and Vallery, R. S. *Annual Review of Materials Research* **36**(1), 49–79 aug (2006).

[99] Masoumi, S. and Valipour, H. *Modelling and Simulation in Materials Science and Engineering* **24**(3), 035011 mar (2016).

[100] Chenze, Q., Chunqing, L., Minfeng, Z., Baoyi, W., and Jian, Z. *Journal of Physics: Conference Series* **225**(1), 012044 apr (2010).

[101] Salgueiro, W., Somoza, A., Goyanes, S., Rubiolo, G., Marzocca, A., and Consolati, G. *Materials Science Forum* **363-365**, 349–351 apr (2001).

[102] Suzuki, T., Oki, Y., Numajiri, M., Miura, T., Kondo, K., and Ito, Y. *Polymer* **34**(7), 1361–1365 jan (1993).

[103] Huang, F., Huang, J., Gao, Y., Zhou, Y., and Du, L. *The Blends of a Silicon-Containing Arylacetylene Resin and an Acetylene-Functional Benzoxazine*. Elsevier, jan (2011).

[104] Kroutilová, I., Matějka, L., Sikora, A., Souček, K., and Staš, L. *Journal of Applied Polymer Science* **99**(6), 3669–3676 mar (2006).

[105] Yu, J. W., Jung, J., Choi, Y.-M., Choi, J. H., Yu, J., Lee, J. K., You, N.-H., and Goh, M. *Polymer Chemistry* **7**(1), 36–43 dec (2016).

[106] Knox, S. T., Wright, A., Cameron, C., and Fairclough, J. P. A. *Macromolecules* **52**(18), 6861–6867 sep (2019).

[107] Escobar Galindo, R., van Veen, A., Alba Garcıéa, A., Schut, H., and De Hosson, J. *Acta Materialia* **48**(18-19), 4743–4747 dec (2000).

[108] Dong, A. W., Fong, C., Waddington, L. J., Hill, A. J., Boyd, B. J., and Drummond, C. J. *Physical Chemistry Chemical Physics* **17**(3), 1705–1715 dec (2015).

[109] Procházka, I., Cížek, J. ., Melikhova, O., Kuriplach, J., Konstantinova, T. E., and Danilenko, I. A. *J. Phys.: Conf. Ser* **265**, 12020 (2011).

[110] Shen, Z., Guo, L., Zhang, W., Jin, S., Cao, X., Long, Y., and Wei, Y. *Materials* **11**(9), 1523 aug (2018).

[111] Hugenschmidt, C., Bauer, A., Böni, P., Ceeh, H., Eijt, S. W. H., Gigl, T., Pfleiderer, C., Piochacz, C., Neubauer, A., Reiner, M., Schut, H., and Weber, J. *Applied Physics A* **119**(3), 997–1002 jun (2015).

[112] Liao, M.-H. and Chen, C.-H. *AIP Advances* **3**(4), 042108–1 – 042108–8 apr (2013).

[113] Ruiz-Ripoll, M. L., Schut, H., Van Dijk, N. H., Alderliesten, R. C., Van Der Zwaag, S., and Benedictus, R. *Journal of Physics: Conference Series* **262**(1), 012052 jan (2011).

[114] Jean, Y. C., Mallon, P. E., and Schrader, D. M. *Principles and Applications of Positron & Positronium Chemistry*. World Scientific Publishin Co. Pte. Ltd., (2003).

[115] Cao, H., Zhang, R., Sundar, C. S., Yuan, J.-P., He, Y., Sandreczki, T. C., Jean, Y. C., and Nielsen, B. *Macromolecules* **31**(19), 6627–6635 sep (1998).

[116] Delft Research Team. *The Delft intense slow positron beam 2D-ACAR facility for analysis of nanocavities and quantum dots*. PhD thesis, (2002).

[117] Valkealahti, S. and Nieminen, R. M. *Applied Physics A Solids and Surfaces* **35**(1), 51–59 sep (1984).

[118] Leo, W. R. *Techniques for Nuclear and Particle Physics Experiments : a How-to Approach*. Springer Berlin Heidelberg, 2nd edition, (1994).

[119] Zaitseva, N., Glenn, A., Mabe, A., Carman, M., Hurlbut, C., Inman, J., and Payne,

S. *Nuclear Instruments and Methods in Physics Research Section A: Accelerators, Spectrometers, Detectors and Associated Equipment* **889**, 97–104 may (2018).

[120] Nissilä, J., Rytsölä, K., Aavikko, R., Laakso, a., Saarinen, K., and Hautojärvi, P. *Nuclear Instruments and Methods in Physics Research Section A: Accelerators, Spectrometers, Detectors and Associated Equipment* **538**(1-3), 778–789 (2005).

[121] Zaleski, R. and Wawryszczuk, J. *Nukleonika* **55**(1), 73–78 (2010).

[122] Park, C. H., Lee, A., Kim, R., and Moon, J. H. *Science and Technology of Nuclear Installations* **2014**, 1–6 (2014).

[123] Patil, P. N., Sudarshan, K., Sharma, S. K., Maheshwari, P., Rath, S. K., Patri, M., and Pujari, P. K. *Chemphyschem : a European journal of chemical physics and physical chemistry* **13**(17), 3916–22 dec (2012).

[124] Einstein, A. *American Journal of Physics* **33**(5), 367 (1905).

[125] K, H. P. K. *Photomultiplier Tubes: Basics and Applications*. 3rd edition, (2007).

[126] Procha, I. *Nuclear Instruments and Methods in Physics Research Section A: Accelerators, Spectrometers, Detectors and Associated Equipment* **450**, 325–337 (2000).

[127] Rytso, K., Aavikko, R. Ã., Laakso, A., Saarinen, K., and Hautoja, P. *Nuclear Instruments and Methods in Physics Research Section A: Accelerators, Spectrometers, Detectors and Associated Equipment* **538**, 778–789 (2005).

[128] Bronks, J. *Technical Report, https://www.picotech.com/download/manuals/ps6407.en-1.pdf* (2011).

[129] Petriska, M., Sojak, S., and Slugeň, V. *Journal of Physics: Conference Series* **505**(1), 012044 apr (2014).

[130] Petschke, D. and Staab, T. E. *SoftwareX* **9**, 183–186 jan (2019).

[131] Tuomisto, F. and Makkonen, I. *Reviews of Modern Physics* **85**(4), 1583–1631 nov (2013).

[132] An, R., Chen, B., Liu, Y.-F., Ye, B.-J., Kong, W., and Ritt, S. *Chinese Physics C* **38**(5), 056001 may (2014).

[133] Wagner, A., Anwand, W., Attallah, A. G., Dornberg, G., Elsayed, M., Enke, D., Hussein, A. E. M., Krause-Rehberg, R., Liedke, M. O., Potzger, K., and Trinh, T. T. *Journal of Physics: Conference Series* **791**(1), 012004 jan (2017).

[134] Myllylä, R. *Nuclear Instruments and Methods* **148**(2), 273–274 jan (1978).

[135] Winberg, P., Eldrup, M., and Maurer, F. H. J. *The Journal of chemical physics* **136**(24), 244902 (2012).

[136] Shukla, A., Peter, M., and Hoffmann, L. *Nuclear Instruments and Methods in Physics Research Section A: Accelerators, Spectrometers, Detectors and Associated Equipment* **335**(1-2), 310–317 oct (1993).

[137] Shantarovich, V. P., Bekeshev, V. G., Pastukhov, A. V., Davankov, V. A., Krasil'nikova, O. K., Belousova, E. V., Kevdina, I. B., Filimonov, M. K., and Gustov, V. W. *Journal of Physics: Conference Series* **618**(1) (2015).

[138] Madani, M. M., Macqueen, R. C., and Cranata, R. D. *Journal of Polymer Science Part B: Polymer Physics* **34**, 2767–2770 (1996).

[139] Kerr, D. *Canadian Journal of Physics* **52**(11), 935–939 (1974).

[140] Sawada, S.-i., Yabuuchi, A., Maekawa, M., Kawasuso, A., and Maekawa, Y. *Radiation Physics and Chemistry* **87**, 46–52 jun (2013).

[141] Comyn, J. *Polymer Permeability*. Springer Netherlands, (1985).
[142] Heba, F., Mouzali, M., and Abadie, M. J. M. *Journal of Applied Polymer Science* **90**(10), 2834–2839 dec (2003).
[143] Daenicke, J., Schubert, D. W., Hedenqvist, M., Linde, E., Sigl, T., and Horch, R. E. In *AIP Conference Proceedings*, volume 2055, 080004. AIP Publishing LLC, jan (2019).
[144] Wu, Y., Joseph, S., and Aluru, N. R. *The Journal of Physical Chemistry B* **113**(11), 3512–3520 mar (2009).
[145] Hale, A., Macosko, C. W., and Bair, H. E. *Macromolecules* **24**(9), 2610–2621 apr (1991).
[146] Carbas, R., da Silva, L., Marques, E., and Lopes, A. *Journal of Adhesion Science and Technology* **27**(23), 2542–2557 dec (2013).
[147] Hussein, S. I., Abd-Elnaiem, A. M., Asafa, T. B., and Jaafar, H. I. *Applied Physics A* **124**(7), 475 jul (2018).
[148] Wang, Z., Zhang, F., Song, N., and Ni, L. *Polymers and Polymer Composites* **16**(4), 257–262 may (2008).
[149] Vosgien Lacombre, C., Bouvet, G., Trinh, D., Feaugas, X., Touzain, S., and Mallarino, S. *Journal of Materials Science* **53**(3), 2253–2267 feb (2018).
[150] Horwath, J. C., Schweickart, D. L., Garcia, G., Klosterman, D., Galaska, M., Schrand, A., and Walko, L. C. In *Conference Record of the 2006 Twenty-Seventh International Power Modulator Symposium*, 189–191. IEEE, may (2006).
[151] Wang, G., Du, H., and Zhang, Z. *Journal of Petroleum Science and Engineering* **159**, 773–782 nov (2017).
[152] *https://www.sigmaaldrich.com/technical-documents/articles/analytical-applications/gc/gc-analysis-of-xylene-isomers-g006241.html* .
[153] Nimkar, N., Zarad, S., and Suraliwala, M. *International Journal of Innovatice Research in Science and Engineering* **2**(8), 49 – 56 (2016).
[154] Alegretti, A. P., Thiesen, F. V., and Maciel, G. P. *Journal of Chromatography B* **809**(1), 183–187 sep (2004).
[155] Karbowski, A., Fedus, K., Służewski, K., Bruzdowska, J., and Karwasz, G. In *Proceedings of the 12th International Workshop on Positron and Positronium Chemistry*, volume 132, 1466 – 1469, (2017).
[156] Eriksson, M., Goossens, H., and Peijs, T. *Nanocomposites* **1**(1), 36–45 feb (2015).
[157] White, R. P. and Lipson, J. E. G. *Macromolecules* **49**(11), 3987–4007 jun (2016).
[158] Yang, L., Hristov, H. A., Yee, A. F., Gidley, D. W., Bauchiere, D., Halary, J. L., and Monnerie, L. *Polymer* **36**(21), 3997–4003 jan (1995).
[159] Fox, T. G. and Loshaek, S. *Journal of Polymer Science* **15**, 371–390 (1955).
[160] Keddie, J. L., Jones, R. A. L., and Cory, R. A. *Faraday Discussions* **98**(0), 219 jan (1994).
[161] Kawana, S. and Jones, R. A. L. *Physical Review E* **63**(2), 021501 jan (2001).
[162] Schwahn, D., Hahn, K., Streib, J., and Springer, T. *The Journal of Chemical Physics* **93**(11), 8383–8391 dec (1990).